

Estimation of Fracture Toughness of Cast Stainless Steels during Thermal Aging in LWR Systems

AVAILABILITY OF REFERENCE MATERIALS IN NRC PUBLICATIONS

NRC Reference Material

As of November 1999, you may electronically access NUREG-series publications and other NRC records at NRC's Library at www.nrc.gov/reading-rm.html. Publicly released records include, to name a few, NUREG-series publications; *Federal Register* notices; applicant, licensee, and vendor documents and correspondence; NRC correspondence and internal memoranda; bulletins and information notices; inspection and investigative reports; licensee event reports; and Commission papers and their attachments.

NRC publications in the NUREG series, NRC regulations, and Title 10, "Energy," in the *Code of Federal Regulations* may also be purchased from one of these two sources.

1. The Superintendent of Documents

U.S. Government Publishing Office
Mail Stop IDCC
Washington, DC 20402-0001
Internet: bookstore.gpo.gov
Telephone: (202) 512-1800
Fax: (202) 512-2104

2. The National Technical Information Service

5301 Shawnee Rd., Alexandria, VA 22312-0002
www.ntis.gov
1-800-553-6847 or, locally, (703) 605-6000

A single copy of each NRC draft report for comment is available free, to the extent of supply, upon written request as follows:

Address: **U.S. Nuclear Regulatory Commission**
Office of Administration
Publications Branch
Washington, DC 20555-0001
E-mail: distribution.resource@nrc.gov
Facsimile: (301) 415-2289

Some publications in the NUREG series that are posted at NRC's Web site address www.nrc.gov/reading-rm/doc-collections/nuregs are updated periodically and may differ from the last printed version. Although references to material found on a Web site bear the date the material was accessed, the material available on the date cited may subsequently be removed from the site.

Non-NRC Reference Material

Documents available from public and special technical libraries include all open literature items, such as books, journal articles, transactions, *Federal Register* notices, Federal and State legislation, and congressional reports. Such documents as theses, dissertations, foreign reports and translations, and non-NRC conference proceedings may be purchased from their sponsoring organization.

Copies of industry codes and standards used in a substantive manner in the NRC regulatory process are maintained at—

The NRC Technical Library

Two White Flint North
11545 Rockville Pike
Rockville, MD 20852-2738

These standards are available in the library for reference use by the public. Codes and standards are usually copyrighted and may be purchased from the originating organization or, if they are American National Standards, from—

American National Standards Institute

11 West 42nd Street
New York, NY 10036-8002
www.ansi.org
(212) 642-4900

Legally binding regulatory requirements are stated only in laws; NRC regulations; licenses, including technical specifications; or orders, not in NUREG-series publications. The views expressed in contractor-prepared publications in this series are not necessarily those of the NRC.

The NUREG series comprises (1) technical and administrative reports and books prepared by the staff (NUREG-XXXX) or agency contractors (NUREG/CR-XXXX), (2) proceedings of conferences (NUREG/CP-XXXX), (3) reports resulting from international agreements (NUREG/IA-XXXX), (4) brochures (NUREG/BR-XXXX), and (5) compilations of legal decisions and orders of the Commission and Atomic and Safety Licensing Boards and of Directors' decisions under Section 2.206 of NRC's regulations (NUREG-0750).

DISCLAIMER: This report was prepared as an account of work sponsored by an agency of the U.S. Government. Neither the U.S. Government nor any agency thereof, nor any employee, makes any warranty, expressed or implied, or assumes any legal liability or responsibility for any third party's use, or the results of such use, of any information, apparatus, product, or process disclosed in this publication, or represents that its use by such third party would not infringe privately owned rights.

Estimation of Fracture Toughness of Cast Stainless Steels during Thermal Aging in LWR Systems

Manuscript Completed: June 2015
Date Published: May 2016

Prepared by: Omesh K. Chopra
Argonne National Laboratory
Argonne, IL 60439

Appajosula S. Rao, NRC
Technical Monitor and Project Manager

NRC Job Code Number V6455

ABSTRACT

Cast austenitic stainless steel (CASS) materials are used extensively in reactor coolant pressure boundary systems as well as core support structure and reactor internals. However, these materials have a duplex structure consisting of austenite and ferrite phases and are susceptible to thermal aging embrittlement during reactor service. In addition, the prolonged exposure of these materials to neutron irradiation changes their microstructure and microchemistry, which can degrade their fracture properties even further. This report is a revision of NUREG/CR-4513, Rev. 1, ANL-93/22 (August 1994); it revises the procedure and correlations used for predicting the change in fracture toughness and tensile properties of CASS components due to thermal aging during service in light water reactors at 280–330°C (535–625°F). The updated correlations are based on the current fracture toughness database for CASS materials aged up to 100,000 h at 290–350°C (554–633°F). The methodology for estimating fracture properties has been extended to cover CASS materials with a ferrite content of up to 40%. The correlations for estimating the change in tensile stress, including the Ramberg/Osgood parameters for strain hardening, are also described. The fracture toughness J-R curve, tensile stress, and Charpy-impact energy of aged CASS materials are estimated from material composition. The mechanical properties of a specific CASS material are estimated from the extent and kinetics of thermal embrittlement. Embrittlement is characterized in terms of room temperature Charpy-impact energy. The extent or degree of thermal embrittlement at “saturation” (i.e., the minimum impact energy that can be achieved for a material after long-term aging) is determined from the chemical composition of the material. Charpy-impact energy as a function of the time and temperature of reactor service is estimated from the kinetics of thermal embrittlement, which are also determined from the chemical composition. Data on the initial impact energy and tensile flow stress of the unaged material are required for these estimations. The fracture toughness J-R curve for the material is then obtained by correlating room temperature Charpy-impact energy with fracture toughness parameters. The values of J_{Ic} are determined from the estimated J-R curve and flow stress. A common “predicted lower-bound” J-R curve for CASS materials of unknown chemical composition is also defined for a given grade of steel, range of ferrite content, and temperature. In addition, guidance is provided for evaluating the combined effects of thermal and neutron embrittlement of CASS materials used in the reactor core internal components.

CONTENTS

ABSTRACT	iii
CONTENTS	v
LIST OF FIGURES.....	vii
LIST OF TABLES	xi
EXECUTIVE SUMMARY	xiii
ACKNOWLEDGMENTS	xvii
ABBREVIATIONS AND ACRONYMS.....	xix
NOMENCLATURE.....	xxi
1 INTRODUCTION.....	1
2 THERMAL EMBRITTLEMENT OF CAST STAINLESS STEELS	7
2.1 Mechanism of Thermal Embrittlement	7
2.2 Distribution and Morphology of Ferrite in CASS Materials	11
2.2.1 Ferrite Morphology.....	11
2.2.2 Ferrite Content.....	13
2.2.2.1 Measured Ferrite	15
2.2.2.2 Estimated Ferrite	16
2.3 Kinetics of Thermal Embrittlement	18
2.4 Extent of Thermal Embrittlement	26
2.4.1 Charpy-Impact Energy	26
2.4.2 Effect of Trace Nb Content.....	32
2.4.3 Fracture Toughness J-R Curve	33
2.4.3.1 Potential Effects of Reactor Coolant Environment	41
2.4.3.2 Potential Effects of High Loading Rate.....	43
2.5 Methodology for Estimating Thermal Embrittlement of CASS Materials.....	44
3 ASSESSMENT OF THERMAL EMBRITTLEMENT	49
3.1 Estimation of Thermal Embrittlement of CASS Materials of Known Composition and Service Condition – Service Time Values	49
3.2 Estimation of the Thermal Embrittlement of CASS Materials of Unknown Composition: Lower-Bound Values.....	54
3.3 Screening Criteria for Susceptibility of CASS Materials to Thermal Embrittlement	56
3.4 Estimation of Tensile Flow Stress.....	63
4 USE OF METHODOLOGY IN ASME CODE, SECTION XI.....	69
4.1 Current Editions of the ASME Code Section XI	71
5 COMBINED EFFECTS OF THERMAL AND NEUTRON EMBRITTLEMENT	73
5.1 Fracture Toughness of Irradiated Austenitic Stainless Steels	74

5.1.1	Fracture Toughness J_{IC}	76
5.1.2	Fracture Toughness J-R Curve	78
5.1.2.1	Irradiation Conditions	78
5.1.2.2	Material Type	78
5.1.2.3	Test Temperature	80
5.1.2.4	Test Environment.....	81
5.1.2.5	Irradiation Temperature	82
5.2	Lower-Bound Fracture Toughness Curve	83
5.3.1	Methodology for Incorporating Irradiation Effects on CASS Materials including the Combined Effects of Thermal and Neutron Embrittlement.....	88
5.3.1.1	Threshold Neutron Dose for Irradiation Effects	88
5.3.1.2	Potential Effects of Thermal and Neutron Embrittlement.....	89
6	SUMMARY	91
7	REFERENCES.....	95
APPENDIX A:	MATERIAL INFORMATION.....	A-1
APPENDIX B:	J-R CURVE CHARACTERIZATION	B-1
	Data Analysis Procedure	B-2
	Data Qualification	B-5
APPENDIX C:	EXPERIMENTAL AND ESTIMATED CHARPY-IMPACT DATA FOR AGED CASS MATERIALS.....	C-1
APPENDIX D:	REFERENCES.....	D-1
APPENDIX E:	PREVIOUS DOCUMENTS IN SERIES	E-1

LIST OF FIGURES

1.	Time-temperature curve for the formation of various phases in CASS materials.	8
2.	Deformation twins in a Charpy-impact specimen of CF-8 material aged for 30000 h at 350°C and tested at 290°C.....	9
3.	Pseudo binary diagram for Fe-Ni-19%Cr alloy.....	11
4.	Microstructure along the axial and circumferential sections of centrifugally cast CF-8 and CF-3 stainless steel pipes showing equiaxed grain structure.....	12
5.	Microstructure along axial section of a check valve from the decommissioned Shippingport reactor showing columnar grains.	12
6.	Ferrite content and morphology of vanes of a static cast CF-3 pump impeller and along a circumferential section of regions near the inside and outside diameter of centrifugally cast CF-3 and CF-8 pipes.....	14
7.	Plots of measured ferrite content and values for various CASS materials calculated by using Hull's equivalent factor.	16
8.	Plots of measured ferrite content and values for various CASS materials calculated using the ASTM A800/A800M methodology.	17
9a.	Plots of ferrite content calculated by using Hull's equivalent factor and those estimated from the ASTM A800/A800M methodology for various CASS materials.	18
9b.	Plots of ferrite content for various CASS materials calculated by using Hull's equivalent factors and those determined from the EMA formula developed by EdF.	19
10.	Plots of ferrite content for various CASS materials estimated by using the ASTM A800/A800M methodology and those determined from the EMA formula developed by EdF.....	19
11.	Arrhenius plots for the formation of the G phase and a reduction in impact energy.	21
12.	Decrease in Charpy-impact energy for various heats of CASS materials aged at 400°C.....	22
13.	Correlation between RT Charpy-impact energy at saturation and the material parameter ϕ for CASS materials.....	27
14.	Comparison of the updated (chain-dash line) and original (solid line) correlation between the RT Charpy-impact energy at saturation and material parameter ϕ	29
15.	Measured values of saturation RT Charpy-impact energy for CF-3, CF-8, and CF-8M CASS materials and those estimated from (a) the material parameter ϕ , (b) the material composition and ferrite content, and (c) the lower of these two values.....	30

16.	Correlation between RT Charpy-impact energy at saturation and the ferrite content for CF-3, CF-8, and CF-8M materials.	31
17.	Fracture surface of Charpy-impact specimen of Heat 4331 aged for 700 h at 400°C and tested at room temperature.	32
18.	Ductile-to-brittle transition curves for Charpy-impact specimens of thermally aged Heats 4331 and 75 of CF-8M material.....	33
19a.	Correlation between RT Charpy-impact energy and coefficient C at RT for CF-3, CF-8, CF-3M, and CF-8M CASS materials.....	33
19b.	Correlation between RT Charpy-impact energy and coefficient C at 290–320°C for CF-3, CF-8, CF-3M, and CF-8M CASS materials.....	34
20.	Distribution of the J-R curve exponent for various grades of thermally aged and unaged CASS materials at (a) room temperature and (b) 290–325°C.	36
21.	Correlation between the RT Charpy-impact energy and exponent n of the power-law J-R curve at RT and 290°C for CF-8M materials.	37
22.	Distribution of ferrite content in CASS grades of (a) CF-8, (b) CF-8A, (c) CF-8M, and (d) CF-3 piping material in Westinghouse PWRs.....	40
23.	Fracture toughness J-R curves for sensitized Type 304 SS in simulated BWR coolant at 288°C and three different displacement rates.	41
24.	Fracture toughness J-R curve data for thermally aged Heat 68 of CF-8M plate at 54°C.....	42
25.	Fracture toughness J-R curves for thermally aged CF-3M at 0°C and quasi-static and dynamic loading rates.....	43
26.	Flow diagram for estimating mechanical properties of thermally aged CASS materials in LWR systems.	44
27.	Predicted and measured fracture toughness J-R curves for unaged materials (a) CASS at 290–320°C and (b) wrought austenitic SSs at various temperatures.	45
28.	Estimated and experimental values of coefficient C of the J-R curve for static-cast CF-3 plate during thermal aging.	50
29.	Estimated and experimental values of coefficient C of the J-R curve for static-cast CF-8 plate during thermal aging.	50
30.	Estimated and experimental values of coefficient C of the J-R curve for static-cast CF-8M plate during thermal aging.	50
31.	Estimated and experimental values of coefficient C of the J-R curve for centrifugally cast CF-8 pipe during thermal aging.....	51

32.	Experimental and estimated fracture toughness J-R curves at RT and 290°C for an ANL heat of a static cast CF-8 plate.	51
33.	Experimental and estimated fracture toughness J-R curves at RT and 290°C for an ANL heat of a static cast CF-3 plate.	51
34.	Experimental and estimated fracture toughness J-R curves at RT and 290°C for an ANL heat of a centrifugally cast CF-8 pipe.	52
35.	Experimental and estimated fracture toughness J-R curves at RT and 290°C for an ANL heat of a static cast CF-8M plate.	52
36.	Experimental and estimated fracture toughness J-R curves at RT and 290°C for an ANL heat of a static cast CF-8M plate.	53
37.	Experimental and estimated fracture toughness J-R curves at RT and 290°C for an EdF heats of a static cast CF-8M plate (Ht. DI) and a 50° elbow.	53
38.	Experimental and estimated fracture toughness J-R curves at RT and 290°C for a MHI heat of a static cast CF-8M pipe.	53
39.	Correlation between saturation RT Charpy-impact energy and ferrite content.	54
40.	Estimated lower-bound J-R curves at RT for static-cast CASS materials with ferrite contents of >25–30%, >20–25%, and >15–20%.	57
41.	Estimated lower-bound J-R curves at 290–320°C for static-cast CASS materials with ferrite contents of >25–30%, >20–25%, and >15–20%.	58
42.	Estimated lower-bound J-R curves at RT for centrifugally cast CASS materials with ferrite contents of >25–30%, >20–25%, and >15–20%.	59
43.	Estimated lower-bound J-R curves at 290–320°C for centrifugally cast CASS materials with ferrite contents of >25–30%, >20–25%, and >15–20%.	60
44.	Saturation J at a 2.5 mm crack extension as a function of the ferrite content for static-cast CF-3, CF-8, and CF-8M CASS materials.	61
45.	Saturation J at a 2.5 mm crack extension as a function of the ferrite content for centrifugally cast CF-3, CF-8, and CF-8M CASS materials.	62
46.	Flow stress ratio R_f of aged CF-3, CF-8, and CF-8M materials at RT and 290°C as a function of the normalized aging parameter.	64
47.	Comparison of the lower-bound J-R curve at 290°C for aged static-cast CF-8M material estimated by using the NUREG/CR-4513, Rev. 1, expressions, with the SAW data used to develop ASME Section XI, Subsection IWB-3640 evaluations.	69
48.	Comparison of the lower-bound J-R curve at 290°C for aged static-cast CF-8M material estimated by using the updated expressions, with the fracture toughness of SAW data used to develop ASME Section XI, Subsection IWB-3640 evaluations.	71

49.	Comparison of the lower-bound J-R curve at 290°C for aged centrifugally cast CF-8M estimated by using the updated expressions, with the fracture toughness of SAW data used to develop ASME Section XI, Subsection IWB-3640 evaluations.	71
50.	Change in fracture toughness J_{Ic} as a function of neutron exposure for LWR irradiated austenitic SSs.....	77
51.	Fracture toughness J_{Ic} as a function of neutron exposure for SSs.....	78
52.	Change in fracture toughness J_{Ic} for a select data set as a function of neutron exposure for LWR irradiated austenitic SSs.	79
53.	Fracture toughness J-R curves for sensitized Type 304 SS, weld HAZ materials of Type 304 and 304L SS, and CF-8M steel in high-purity water at 289°C.	80
54.	Fracture toughness J_{Ic} of irradiated austenitic SSs and welds as a function of test temperature.....	80
55.	Fracture toughness J-R curves for irradiated specimens of Type 304L SAW HAZ in air and NWC BWR environment.	81
56.	Fracture toughness J-R curves for thermally aged and irradiated CF-8M steel.....	82
57.	Change in initiation toughness J_{Ic} of (a) wrought austenitic SSs and (b) CASS materials and weld metals as a function of neutron exposure.....	84
58.	Plots of fracture toughness J_{Ic} values as a function of neutron dose for (a) austenitic SS welds, (b) CASS materials, and (c) austenitic SS HAZ.	85
59.	Coefficient C of the J-R curve as a function of neutron dose for CASS materials. Solid line represents the lower-bound C values proposed in NUREG/CR-7027.....	87
60.	Fracture toughness $J_{2.5}$ values as a function of neutron dose for CASS materials.	88
61.	Comparison of the fracture toughness J_{Ic} , coefficient, and $J_{2.5}$ value obtained in air and LWR environment at 290–320°C of CF-3, CF-8, and CF-8M materials in the unaged and aged as well as unirradiated and irradiated conditions.....	90

LIST OF TABLES

1.	Screening criteria for thermal-aging susceptibility of CASS CF-3, CF-8, and CF-8M materials.	5
2.	Chemical composition, ferrite content, and kinetics of thermal embrittlement for various heats of CASS materials.	24
3.	Primary circuit piping CASS material in Westinghouse plants.	39
4.	The lower-bound J-R curve at RT and 290–320°C for aged CASS materials.	56
5.	Updated screening criteria for thermal-aging susceptibility of CASS CF-3, CF-8, and CF-8M materials.	63
6.	LWR core internal components made of CASS materials and maximum neutron dose after 60 years of service.	74
7.	Fracture toughness J-R curve data on irradiated CASS CF-3, CF-8, and CF-8M materials in air and LWR environments.	86

EXECUTIVE SUMMARY

Cast austenitic stainless steels (CASSs) used in reactor pressure-boundary components — such as valve bodies, pump casings, primary coolant piping, and some reactor core internal components of light water reactors (LWRs) — suffer a loss in fracture toughness due to thermal aging after many years of service at temperatures in the range of 280–320°C (≈535–610°F). Thermal aging of CASS materials at these temperatures causes an increase in hardness and tensile strength and a decrease in ductility, impact strength, and fracture toughness of the material. The Charpy transition curve also shifts to higher temperatures. In addition, for CASS materials used in reactor core support structures and core internals components, exposure to neutron irradiation for extended periods leads to further degradation of their fracture properties due to radiation hardening and radiation-induced segregation (RIS). In such instances, a fracture mechanics methodology, such as linear-elastic fracture mechanics (LEFM) or elastic-plastic fracture mechanics (EPFM) is needed for analyzing structural integrity and developing inspection guidelines. Therefore, an assessment of the degradation of mechanical properties due to thermal and irradiation embrittlement is required to evaluate the performance of CASS components during prolonged exposure to service temperatures and environments.

Investigations at Argonne National Laboratory (ANL) and elsewhere have shown that thermal embrittlement of CASS components can occur during the reactor design lifetime of 40 years. Different grades and heats of CASS materials exhibit varying degrees of thermal embrittlement. In general, the low carbon (low C) CF-3 materials are the most resistant to thermal embrittlement, and the Mo-bearing, high C CF-8M materials are the least resistant.

Embrittlement of CASS materials can result in brittle fracture associated with cleavage and/or twinning of the ferrite phase and separation of the ferrite/austenite phase boundary. The amount of cleavage increases with increases in the degree of thermal embrittlement or decreases in test temperature. At high temperatures (>500°C), twinning appears to play an important role in brittle failure of ferrite. The thermal aging of CASS materials at temperatures <500°C (<932°F) leads to (a) the formation of a Cr-rich α' phase by spinodal decomposition and by precipitation and growth of α' , and (b) the nucleation and growth of additional phases such as α' , Ni- and Si-rich G phase, $M_{23}C_6$ carbides, and γ_2 austenite. The formation of the α' phase provides the strengthening mechanisms that increase strain hardening and local tensile stress. Consequently, the critical stress level for brittle fracture is attained at higher temperatures. Predominantly brittle failure occurs when either the ferrite phase is continuous (e.g., in CASS material with a high ferrite content) or the ferrite/austenite phase boundary provides an easy path for crack propagation (e.g., in high-C grades of cast steel with large phase-boundary carbides). Consequently, the amount, size, and distribution of the ferrite phase in the duplex structure along with the presence of phase-boundary carbides are important parameters in controlling the degree or extent of thermal embrittlement.

NUREG/CR-4513, Rev. 1, presented a procedure and correlations for estimating the Charpy-impact energy and fracture toughness J-R curve of CASS components under LWR operating conditions from material information readily available in certified material test records (CMTRs). In this report, the procedure and correlations have been updated by using a much larger fracture toughness database for thermally aged CASS materials. The applicability of the methodology has also been extended to materials with a ferrite content of up to 40%. In addition, for CASS materials used in the reactor core support structure and core internals components, guidance is provided for evaluating the combined effects of thermal and neutron embrittlement. The procedure for estimating the change in tensile stress, including the Ramberg/Osgood parameters for strain hardening, is also presented.

The fracture toughness of a specific CASS material is estimated from the extent and kinetics of thermal embrittlement. The extent of thermal embrittlement (i.e., the degradation of mechanical properties) is characterized by the room-temperature (RT) Charpy-impact energy. A correlation for the extent of thermal embrittlement at “saturation” (i.e., the minimum impact energy that would be achieved for the material after long-term aging) is given in terms of the chemical composition. The extent of the change in RT Charpy-impact energy as a function of the time and temperature of reactor service is estimated from the extent of change in RT Charpy-impact energy at saturation and from the correlations describing the kinetics of embrittlement, which are also given in terms of chemical composition.

The fracture toughness J-R curve for the material is then obtained from the correlation between the fracture toughness parameters and the RT Charpy-impact energy. The tensile yield and flow stresses and Ramberg/Osgood parameters for tensile strain hardening are estimated from the flow stress of the unaged material and the kinetics of embrittlement. The fracture toughness J_{Ic} and tearing modulus can then be determined from the estimated J-R curve and tensile flow stress. A common lower-bound J-R curve for CASS materials of unknown chemical composition is also defined for a given material specification, ferrite content, and temperature.

The differences between the methodology presented in this report and that described in NUREG/CR-4513, Rev. 1, are as follows:

- (i) For CF-8M materials, the correlation between the RT Charpy-impact energy and material parameter ϕ has been revised.
- (ii) For CF-8M materials, the correlations between the RT Charpy-impact energy and coefficient C of the J-R curve at RT and 290–320°C have been extended to include CASS materials with a ferrite content of up to 40%.
- (iii) The correlations between the RT Charpy-impact energy and exponent “n” of the J-R curve at RT and 290–320°C have been revised.
- (iv) The minimum fracture toughness J-R curve for centrifugally cast CASS materials, has been revised.
- (v) New lower-bound curves that correlate the saturation RT Charpy-impact energy with ferrite content for CF-3, CF-8, and CF-8M materials are presented.
- (vi) Guidance is provided for estimating the lower-bound fracture toughness curves for CASS materials used in the reactor core support structures and core internals components.

These updated expressions for estimating fracture toughness of CASS materials during reactor service have the following impact on the criteria proposed by NRC for determining the susceptibility of various categories of CASS components to thermal aging embrittlement. Based on the casting process and whether the materials contains low Mo (0.5 wt.% max.) or high Mo (2.0–3.0 wt.%), the proposed criteria specify the ferrite content above which the material would be susceptible to thermal embrittlement.

- The criteria for low-Mo CF-3 and CF-8 materials have not changed. All centrifugally cast materials and static cast materials containing $\leq 20\%$ ferrite are not susceptible to thermal embrittlement. Only static cast materials containing $>20\%$ ferrite are potentially susceptible.

- The criteria for CF-8M materials depend on whether the material contains ≥ 10 wt.% Ni.
 - The criterion for static cast CF-8M materials containing $< 10\%$ Ni has not changed. Static cast materials with $\leq 14\%$ ferrite are not susceptible and with $> 14\%$ ferrite are potentially susceptible.
 - The criterion for centrifugally cast CF-8M materials containing $< 10\%$ Ni has been revised. The threshold value of ferrite content has been decreased from 20% to 19% ferrite. Centrifugally cast materials with $\leq 19\%$ ferrite are not susceptible and with $> 19\%$ ferrite are potentially susceptible to thermal embrittlement.
 - The criterion for static cast CF-8M materials containing $\geq 10\%$ Ni has been revised. The threshold value of ferrite content has been decreased from 14% to 11% ferrite. Static cast materials with $\leq 11\%$ ferrite are not susceptible and with $> 11\%$ ferrite are potentially susceptible to thermal embrittlement.
 - The criterion for centrifugally cast CF-8M materials containing $\geq 10\%$ Ni has been revised. The threshold value of ferrite content has been decreased from 20% to 13% ferrite. Centrifugally cast materials with $\leq 13\%$ ferrite are not susceptible and with $> 13\%$ ferrite are potentially susceptible to thermal embrittlement.

The methodology presented in this NUREG/CR report is only applicable to service times that are equivalent to 10,000 h at 400°C. This corresponds to

- ≥ 125 effective full power years (efpy) at 290°C for CF-8/CF-3 materials,
- ≥ 30 efpy at 320°C for CF-8/CF-3 and ≥ 15 efpy for CF-8M materials used within primary pressure boundary components, and
- ≥ 15 efpy at 350°C for CF-8/CF-3 materials used in the reactor core internals.

Additional long-term aging data are needed to estimate fracture properties for longer service times. Furthermore, this methodology may not be applicable for CF-8M materials with more than a trace amount of Nb, particularly for materials containing $> 15\%$ ferrite. The methodology also does not consider the effect of reactor coolant environment on fracture toughness. Limited data indicate significant effect of environment, particularly at low temperatures (e.g., shutdown water chemistry at 54°C). In addition, the existing fracture toughness data on LWR-irradiated CF-3 and CF-8 materials is inadequate to accurately establish the lower-bound J-R curves for these materials as a function of neutron dose.

ACKNOWLEDGMENTS

The author thanks Sébastien Sallet of EdF for providing valuable information and helpful discussions. The author also thanks Tim Griesbach of Structural Integrity Associates, Inc. (SIA) for his comments and help in obtaining relevant data.

ABBREVIATIONS AND ACRONYMS

AMP	aging management program
APFIM	atom probe field ion microscopy
ASME	American Society of Mechanical Engineers
ASTM	American Society for Testing and Materials
AWS	American Welding Society
B&W	Babcock and Wilcox
BWR	boiling water reactor
C	Carbon
CASS	cast austenitic stainless steels
CE	Combustion Engineering
CEA	control element assembly
CEGB	Central Electricity Generating Board
CMTR	certified material test record
Cr	Chromium
CRGT	control rod guide tube
CT	compact tension
CTOD	crack tip opening displacement
CW	cold-worked
DO	dissolved oxygen
dpa	displacement(s) per atom
EdF	Electricité de France
efpy	effective full power year(s)
EMA	Etude des Matériaux (EDF formula for ferrite content prediction)
EPFM	elastic-plastic fracture mechanics
EPRI	Electric Power Research Institute
Fe	Iron
FN	ferrite number
FRA	Framatome (now Areva)
GE	General Electric
GF	George Fischer
GMAW	gas metal-arc weld
GTAW	gas tungsten-arc weld
HAZ	heat-affected zone
JAPEIC	Japan Power Electric Engineering and Inspection Corp.
JNES	Japan Nuclear Energy Safety Organization
J-R	J-integral resistance
ksi	kilo pounds per square inch
LEFM	linear-elastic fracture mechanics
LPCI	low-pressure core injection
LTCP	low-temperature crack propagation

LWR	light water reactor
MEA	Materials Engineering Associates, Inc.
MHI	Mitsubishi Heavy Industries
Mn	Manganese
Mo	Molybdenum
MRP	Materials Reliability Program
MWe	megawatt(s)-electric
N	Nitrogen
Nb	Niobium
NDT	nil-ductility transition
Ni	Nickel
NP	National Power
NPP	nuclear power plant
NRC	U.S. Nuclear Regulatory Commission
NWC	normal water chemistry
P	Phosphorous
PFM	probabilistic fracture mechanics
ppb	part(s) per billion
ppm	part(s) per million
PWR	pressurized water reactor
RIS	radiation-induced segregation
RT	room temperature (25°C)
S	Sulfur
SANS	small-angle neutron scattering
SAW	submerged arc weld
SCC	stress corrosion cracking
SE(B)	single-edge bend
Si	Silicon
SIA	Structural Integrity Associates, Inc.
SMAW	shielded metal arc weld
SS	stainless steel
TEM	transmission electron microscopy
TG	transgranular
Ti	Titanium
TWI	The Welding Institute
WH	Westinghouse

NOMENCLATURE

a	crack length
C	coefficient of the power-law J-R curve
Cr _{eq}	chromium equivalent for the material
C _V	room temperature “normalized” Charpy-impact energy; i.e., Charpy-impact energy per unit fracture area at any given service and aging time (J/cm ²). The fracture area for a standard Charpy V-notch specimen (ASTM Specification E 23) is 0.8 cm ² . The value of the impact energy in J has been divided by 0.8 to obtain the “normalized” impact energy in J/cm ² .
C _{Vint}	initial room temperature “normalized” Charpy-impact energy of a material; i.e., unaged material (J/cm ²)
C _{Vsat}	room temperature “normalized” Charpy-impact energy of a material at saturation. It represents a “quasi-saturation” value of RT (i.e., 25°C) impact energy achieved by the material after long-term aging, primarily due to spinodal decomposition of the ferrite. The impact energy continues to decrease further during aging, but at much slower rate.
da	increment in crack length
dJ	increment in J integral
E	elastic modulus
F	ferrite content
J	J integral, a mathematical expression used to characterize the local stress-strain field at the crack tip region (parameter J represents the driving force for crack propagation)
J _d	deformation J integral
J _{lc}	value of J near the onset of crack extension
J _M	modified J integral
ksi	kilo pound per square inch
K	stress intensity factor
K _{lc}	critical stress intensity factor
K _{Jc}	equivalent critical stress intensity factor
m	constraint factor for the power-law J-R curve
M	constraint factor, which relates J to the crack tip opening displacement (CTOD)
MPa	mega Pascal
n	exponent of the power-law J-R curve
n ₁	Ramberg-Osgood parameter
Ni _{eq}	nickel equivalent for the material
P	aging parameter; i.e., the log of the time of aging at 400°C
Q	activation energy for the process of thermal embrittlement (kJ/mole)
R	gas constant
R _f	the ratio of the tensile flow stress of aged and unaged CASS ($\sigma_{faged}/\sigma_{funaged}$)
R _y	the ratio of the tensile yield strength of aged and unaged CASS ($\sigma_{yaged}/\sigma_{yunaged}$)
t	time (h)
T	tearing modulus or temperature

α	shape factor of the curve for the change in room-temperature Charpy-impact energy with the time and temperature of aging
α_1	Ramberg-Osgood parameter
β	half the maximum change in room temperature Charpy-impact energy
γ	gamma phase (i.e., austenite)
δ_c	ferrite content calculated from the chemical composition of a material (%)
Δa	crack extension
ϵ	strain
ϕ	material parameter
σ	stress
σ_f	flow stress, defined as the average of yield and ultimate strength
σ_0	an arbitrary reference stress
σ_u	ultimate strength
σ_y	yield strength
θ	aging behavior at 400°C; i.e., the log of the time to achieve the β reduction in impact energy at 400°C
ν	Poisson ratio

In this report, all values of impact energy were normalized with respect to the actual cross-sectional area of the Charpy-impact specimen. Thus, for a standard Charpy V-notch specimen per ASTM Specification E 23 (i.e., 10 × 10-mm cross section and 2-mm V notch), the impact energy value in J was divided by 0.8 cm² to obtain the impact energy in J/cm². The impact energies obtained for sub-size specimens were normalized with respect to the actual cross-sectional area, and appropriate correction factors were applied to account for size effects. Similarly, impact energies from other standards, such as the 2.5-mm U-notch specimens used for the Charpy VSM values in Switzerland or the 5-mm U-notch specimens used for the KCU values in France, were converted to a Charpy V-notch value by appropriate correlations.

SI units of measurements are used in this report. Conversion factors for measurements in British units are as follows:

<u>To Convert from</u>	<u>To</u>	<u>Multiply by</u>
in.	mm	25.4
J*	ft-lb	0.7376
kJ/m ²	in.-lb/in. ²	5.71015
kJ/mole	kcal/mole	0.239

* When the impact energy is expressed in J/cm², first multiply by 0.8 to obtain the impact energy of an ASTM standard Charpy V-notch specimen in J.

1 INTRODUCTION

Austenitic stainless steels (SSs) are used extensively as structural alloys in light water reactor (LWR) systems, including reactor core internal components, because of their excellent ductility, high notch toughness, corrosion resistance, and good formability. In addition, cast austenitic stainless steel (CASS) materials are used in LWR systems for reactor pressure-boundary components, such as valve bodies, pump casings, primary coolant piping, and some reactor core internal components. Although austenitic SSs are completely austenitic in the wrought condition, CASS materials or welded SSs have a duplex structure consisting of austenite and ferrite phases. The ferrite phase provides additional benefits; it increases tensile strength and improves resistance to stress corrosion cracking (SCC).

However, CASS materials, because they have a duplex structure, are susceptible to thermal embrittlement after extended operation at reactor operating temperatures for core internals,^{1–32} typically 282°C (540°F) for boiling water reactors (BWRs), 288–327°C (550–621°F) for pressurized water reactor (PWR) primary coolant piping, and 343°C (650°F) for PWR pressurizers. In addition, exposure to neutron irradiation for extended periods changes the microstructure (radiation hardening) and microchemistry (radiation-induced segregation or RIS) of wrought and cast austenitic SSs and degrades their fracture properties.^{33–47} In such instances, a fracture mechanics methodology, such as linear-elastic fracture mechanics (LEFM) or elastic-plastic fracture mechanics (EPFM), is needed for analyzing structural integrity and developing inspection guidelines. EPFM involves the J integral-resistance (J-R) curve approach where failure is caused by plastic deformation. The J integral is a mathematical expression used to characterize the local stress-strain field at the crack tip region (parameter J represents the driving force for crack propagation), and the J-R curve characterizes the resistance of the material to stable crack extension. The fracture toughness of such materials is represented by fracture mechanics parameters such as J_{Ic} , the value of J near the onset of crack extension, and T, the tearing modulus, which characterizes the slope of the J-R curve:

$$T = \frac{dJ}{da_{Ic}} \frac{E}{\sigma_f^2}, \quad (1)$$

where the first term represents the slope of the J-R curve at a_{Ic} , E is the elastic modulus, a is the crack length, and σ_f is the flow stress defined as the average of the yield strength (σ_y) and ultimate strength (σ_u). The LEFM methodology is used where failure involves negligible plastic deformation. The fracture toughness of such materials is represented by parameter K_{Ic} (i.e., critical stress intensity factor, a plane strain fracture toughness measure), which characterizes the resistance of the material to unstable crack extension. Since J_{Ic} and K_{Ic} have different units, it is often convenient to represent J_{Ic} in terms of a parameter K_{Jc} , which has the units of the stress intensity factor and is determined from the J_{Ic} value using the relationship:

$$K_{Jc} = (E' J_{Ic})^{1/2}, \quad (2)$$

where the normalized elastic modulus is given by $E' = E/(1 - \nu^2)$, E is the elastic modulus, and ν is the Poisson ratio. Only in cases where LEFM is applicable, is K_{Jc} equal to the critical stress intensity.

The fracture toughness of austenitic SSs has been divided into three broad categories.⁴⁸ Category III corresponds to materials with a high toughness and with J_{Ic} that is above 150 kJ/m² (857 in.-lb/in.²). In these materials, fracture occurs after stable crack extension at stresses well

above the yield strength. Category II corresponds to materials with intermediate toughness and with J_{Ic} in a range of 30–150 kJ/m² (171–857 in.-lb/in.²). In Category II materials, fracture occurs by stable or unstable crack extension at stress levels close to the yield strength. Category I corresponds to low-toughness materials with J_{Ic} of <30 kJ/m² (<171 in.-lb/in.²), and fracture occurs below the yield strength with little or no stable crack extension.

Unirradiated and unaged wrought SSs and CASS materials fall in Category III. For these materials, the fracture toughness J_{Ic} values for Type 304 and 316 SS at temperatures up to 125°C (257°F) vary between 169 and 1660 kJ/m² (965 and 9479 in.-lb/in.²), with a median value of 672 kJ/m² (3,837 in.-lb/in.²).⁴⁸ The J_{Ic} values at 400–550°C (752–1022°F) are approximately 35% lower, with a median value of 421 kJ/m² (2404 in.-lb/in.²). Fracture in such high-toughness materials is by the nucleation and coalescence of microvoids and is characterized by dimpled fracture morphology. Typically, CASS materials also exhibit ductile fracture at temperatures up to 550°C (1022°F), but their fracture toughness is lower than that of the wrought SSs. The fracture toughness of CASS material is affected by the density and morphology of second-phase inclusions in the material, and it varies with the casting method. For example, static cast products have a slightly lower fracture toughness than the centrifugally cast pipes.

Extensive studies have been conducted on the thermal embrittlement of CASS materials at Georg Fischer Co. (GF),¹ Westinghouse (WH),² The Welding Institute (TWI),⁶ Framatome (FRA),^{7–9} Electric Power Research Institute (EPRI),¹⁰ Argonne National Laboratory (ANL),^{12–18} Central Electricity Generating Board* (CEGB),²¹ Electricité de France (EdF),^{22–27} Mitsubishi Heavy Industries (MHI),^{28–31} and Japan Nuclear Energy Safety Organization (JNES).³² In the ANL study, a procedure and correlations were developed for estimating the Charpy-impact energy and fracture toughness J-R curve of CASS components under LWR operating conditions from material information readily available in certified material test records (CMTRs). The methodology for estimating the fracture toughness of aged CASS materials was described in NUREG/CR-4513, Rev. 1.¹⁶ The ANL estimation scheme is applicable to Grades CF-3, CF-3A, CF-8, CF-8A, CF-3M, and CF-8M of CASS materials within American Society for Testing and Materials (ASTM) Specification A351 for austenitic castings for pressure-retaining parts and Specification A451 for centrifugally cast austenitic SS pipes for high-temperature service. The fracture toughness of a specific CASS material is estimated from the extent and kinetics of thermal embrittlement.

The extent of thermal embrittlement (i.e., the degradation of mechanical properties) is characterized by the room temperature (RT), “normalized” Charpy-impact energy (C_V or Charpy-impact energy per unit fracture area). A correlation for the change in RT Charpy-impact energy at “saturation” (i.e., the minimum Charpy-impact energy that would be achieved for the material after long-term aging) is given in terms of the material chemical composition. The extent of the change in RT Charpy-impact energy as a function of the time and temperature of reactor service is estimated from the change the RT Charpy-impact energy at saturation and the correlations describing the kinetics of embrittlement. The kinetics of embrittlement are given in terms of the material composition and the initial Charpy-impact energy, C_{Vint} , of the material in the unaged condition. If C_{Vint} is not known, a typical value of 200 J/cm² (118 ft-lb) is assumed.

The fracture toughness J-R curve for the material is then obtained from the correlation between the fracture toughness parameters and RT Charpy-impact energy. A common lower-bound J-R curve for CASS materials of unknown chemical composition is also defined for a given material specification, ferrite content, and temperature. Tensile yield and flow stresses and Ramberg/Osgood parameters for tensile strain hardening are estimated from the flow stress of

*The British electricity industry from 1957 to 1990 when it was privatized.

the unaged material and the kinetics of embrittlement.¹⁸ Examples of estimating mechanical properties of CASS components during reactor service is presented. The significant features of the methodology proposed in NUREG/CR-4513, Rev. 1,¹⁶ are as follows:

- The correlations are based on a database consisting of about 80 compositions of CASS materials and of mechanical-property data (mostly Charpy V-notch impact energy) on materials aged up to 58,000 h at 290–350°C (554–662°F).
- The saturation RT impact energy C_{Vsat} is estimated from two different correlations. In general, the two methods result in comparable estimates for most materials. However, for a few heats one or the other set of expressions results in estimates that are more accurate. It is likely that minor differences in the composition and microstructure of the ferrite caused by differences in the production heat treatment and possibly in the casting process influence C_{Vsat} values. These factors are difficult to quantify from the existing database. To ensure that the estimates are either accurate or conservative for all heats of CASS materials within ASTM Specification A351, the lower of the two estimated values is used for estimating the fracture properties.
- Separate correlations are proposed for estimating the saturation RT impact energy C_{Vsat} for low-Mo (maximum 0.5 wt.%) CF-3 and CF-8 materials and high-Mo (2.0 to 3.9 wt.%) CF-8M materials; also, for the latter, separate correlations are proposed for materials containing <10 wt.% Ni and those containing ≥10 wt.% Ni.
- Separate correlations are also proposed for estimating fracture toughness J-R curves for static cast and centrifugally cast materials; the fracture toughness of the latter is considered superior.
- The methodology also includes correlations for estimating the yield and flow stresses and Ramberg/Osgood parameters for tensile strain hardening of aged CASS materials from the initial tensile properties and the kinetics of thermal embrittlement.

The criteria used in developing the NUREG/CR-4523, Rev. 1, correlations ensure that the estimated mechanical properties are either accurate or somewhat conservative for compositions of CASS materials within ASTM Specification A351. The correlations do not consider the effects of metallurgical differences that can arise from differences in production heat treatments or casting processes; therefore, they may be conservative for some CASS materials. Mechanical properties are expressed in SI units (see Nomenclature for units of measure and for conversion factors for British units). However, the methodology in NUREG/CR-4513, Rev. 1, has the following limitations.

1. The correlations may yield nonconservative estimates of the fracture toughness J-R curve for compositions of static-cast CF-8M steel that are very sensitive to thermal aging. These compositions consist of static-cast CF-8M materials for which the estimated value of the RT Charpy-impact energy C_{Vsat} is less than 25 J/cm² (15 ft-lb). Typically, these compositions contained 25% or more ferrite. The thermal embrittlement data on CASS materials that were available at the time NUREG/CR-4513, Rev. 1, was published were not adequate for accurately establishing the correlations between the RT Charpy-impact energy and fracture toughness parameters for C_{Vsat} values less than 25 J/cm².
2. Furthermore, the methodology is not applicable for CASS materials that may contain a significant amount of Nb content (i.e., more than 0.05 wt.%). An acceptable level of Nb content was not defined in NUREG/CR-4513 Rev. 1. The ASTM Specification A351 for CF-8M cast material also does not specify a maximum amount of Nb in the casting; but typically, these materials contain less than 0.05 wt.% Nb.

3. For CASS materials used in reactor core support structures and core internal components, the combined effect of thermal aging and neutron irradiation embrittlement was also not discussed in the NUREG/CR-4523, Rev. 1, report.

The results of NUREG/CR-4513, Rev. 1, indicate that the lower-bound fracture toughness of thermally aged CASS materials is similar to that of submerged arc welds (SAWs) of austenitic SSs. Based on these results, the NRC staff accepted the use of the SAW flaw evaluation procedures in IWB3640 of Section XI of the American Society of Mechanical Engineers (ASME) Code (the 1989 edition of the Section XI Code) to evaluate flaws in thermally aged CASS materials (with a ferrite content of less than 25%).⁴⁹ The NRC staff recognized that since this conclusion is based on the lower-bound fracture toughness of aged CASS materials, in some instances, utilities might estimate component-specific fracture toughness by using procedures developed by ANL on a case-by-case fracture mechanics flaw evaluation.

In addition, based on the results of NUREG/CR-4513, Rev. 1, the industry proposed screening criteria in EPRI TR-106092 to determine if a specific component should be inspected due to its potential susceptibility to thermal aging.⁵⁰ The EPRI report uses a deformation J value of 255 kJ/m² (1450 in.-lb/in.²) at a crack depth of 2.5 mm (0.1 in.) (i.e., J_{2.5} value) to differentiate between a nonsignificant and a potentially significant reduction in fracture toughness for fully aged CASS material. Flaw tolerance evaluations, described in Appendices A and B of EPRI TR-106092 demonstrate that a material toughness of 255 kJ/m² adequately protects against a loss of structural integrity in CASS components.

The NRC staff reviewed the EPRI TR-106092 report and other industry submittals addressing thermal embrittlement of CASS materials and developed a position for managing the degradation of fracture properties of thermally aged CASS materials.⁵¹ The staff found that Appendices A and B of the EPRI report provide an acceptable justification that 255 kJ/m² is an acceptable screening value to use in differentiating between a nonsignificant and a potentially significant reduction in fracture toughness of aged CASS components. The staff compared the J_{2.5} values taken from the saturated lower-bound J-R curves as well as the J_{2.5} values from the experimental data with the screening value of 255 kJ/m² in order to develop screening criteria for determining the susceptibility of various categories of CASS components to thermal aging. Table 1 presents the criteria that are based upon the Mo content, casting process, and ferrite content of the material. The same screening criteria for thermal embrittlement of CASS materials have also been proposed by industry.⁴³ The criteria are applicable to all primary pressure boundary components constructed from SA-351 Grades CF-3, CF-3A, CF-8, CF-8A, and CF-8M, with service conditions above 250°C (482°F). Alternately, components can be considered as "potentially susceptible" without considering such screening. The details of the criteria are as follows:⁵¹

- For high Mo static castings, materials with ferrite levels >14% are considered potentially susceptible to thermal embrittlement. Materials with ferrite content ≤14% have adequate fracture toughness (i.e., the J_{2.5} values are above 255 kJ/m²).
- For high Mo centrifugal castings, materials with ferrite levels >20% are considered potentially susceptible, and those with ≤20% ferrite have adequate fracture toughness.
- For low Mo static castings, materials with ferrite levels >20% are considered potentially susceptible to thermal embrittlement. However, as discussed later, the J_{2.5} values for CASS materials with up to 40% ferrite are well above the screening value of 255 kJ/m².
- For low Mo centrifugal castings, none of the CASS materials are considered susceptible to thermal embrittlement. The J_{2.5} values are well above 255 kJ/m² for all materials.

Table 1. Screening criteria for thermal-aging susceptibility of CASS CF-3, CF-8, and CF-8M materials (Ref. 51).

Mo Content (wt.%)	Casting Method	Ferrite Content (%)	Susceptibility Determination
High (2.0–3.0)	Static	≤14	Not susceptible
		>14	Potentially susceptible
	Centrifugal	≤20	Not susceptible
		>20	Potentially susceptible
Low (0.5 max.)	Static	≤20	Not susceptible
		>20	Potentially susceptible
	Centrifugal	All	Not susceptible

The NRC staff position⁵¹ also recognized that for reactor vessel internal components fabricated from CASS materials, the concurrent exposure to high neutron fluence levels can result in a combined effect wherein the service-degraded fracture toughness is reduced from the levels predicted independently for either thermal aging or neutron irradiation alone. Therefore, reactor vessel internal components that are determined to be subject to thermal embrittlement require additional consideration of the neutron fluence of the component to determine the full range of degradation mechanisms applicable for the component.

The component-specific evaluation looks first at the neutron fluence of the component. If the neutron fluence exceeds 1×10^{17} n/cm² (E>1 MeV), a mechanical loading assessment would be conducted for the component.⁵¹ This assessment will determine the maximum tensile loading on the component during ASME Code Level A, B, C and D conditions. A supplemental inspection is not required for the component if the loading is compressive or low enough to preclude fracture of the component. Failure to meet this criterion would require continued use of the supplemental inspection program.

If the neutron fluence is less than 1×10^{17} n/cm² (E>1 MeV), an assessment would be made to determine if the affected component(s) are bounded by the screening criteria in Table 1. In order to demonstrate that the screening criteria are applicable to reactor vessel internal components, a flaw tolerance evaluation specific to the reactor vessel internal components would be required similar to that provided in EPRI TR-106092.⁵¹ If the material is determined to be "potentially susceptible," then a supplemental examination is required on those susceptible components determined to be limiting from the standpoint of thermal aging susceptibility (e.g., Mo content, δ -ferrite content, casting process, and operating temperature), and cracking susceptibility (applied stress level, operating time and environmental conditions). No inspections or evaluations are required if the material is determined not susceptible. The threshold neutron dose above which an assessment of the neutron embrittlement and its effect on component design is needed has been updated in Section 5.3.1.1 of this report.

The NRC staff further proposed⁵¹ that if a particular heat of CASS material is found or assumed "potentially susceptible" and subject to plausible degradation (e.g., thermal fatigue), aging management can be accomplished through volumetric examination or a plant/component-specific flaw tolerance evaluation. The volumetric examination should be performed on the base material of the heat, with the scope of the inspection covering the portions determined to be limiting from the standpoint of the applied stress level, operating time and environmental considerations. Alternately, a plant/component-specific flaw tolerance evaluation using the specific geometry and stress information can be used to demonstrate that the thermally embrittled material has adequate toughness.

Furthermore, based on Lee et al.,⁴⁹ flaws detected in CASS components should be evaluated in accordance with the applicable procedures of IWB-3500 in Section XI of the ASME Code. If the delta ferrite content does not exceed 25%, then flaw evaluation would be in accordance with the principles associated with IWB-3640 procedures for SAW, disregarding the Code restriction of 20% delta ferrite in IWB-3641(b)(1) (of the 1989 edition of the Code). If the material is "potentially susceptible," and the delta-ferrite content exceeds 25%, then flaw evaluation would be on a case-by-case basis using fracture toughness data supplied by the licensee, such as that published by Jayet-Gendrot, et al.²⁴

Since the time NUREG/CR-4513 Rev. 1 was published and the NRC staff developed a position for managing the degradation of the fracture properties of thermally aged CASS materials, the industry has also published a few topical reports describing a methodology for managing the structural integrity of CASS components during LWR service. EPRI 1016236 provided a preliminary methodology for the flaw tolerance evaluation, which when used in concert with inspection techniques being developed by EPRI can be used for the long-term management of CASS piping in the nuclear industry.⁵² The EPRI 1024966 report applies a probabilistic fracture mechanics (PFM) methodology for the evaluation of depths of part-circumferential cracks in fully aged CASS piping that would fail with a given probability when specified loads are applied.⁵³ The PFM method relies on the key elements of a deterministic analysis but also incorporates the inherent uncertainties in these parameters. The methodology is based on the data and correlations developed in NUREG/CR-4513, Rev. 1,¹⁶ for fracture toughness and NUREG/CR-6142¹⁸ for tensile properties.

The EPRI 1024966 report also provides a technical basis for management of thermal aging and reliability of CASS piping in PWRs. The results indicated that CASS piping components are highly flaw-tolerant, even in the thermally aged condition. ASME Code Case N-838 was also developed based on the PFM methodology for evaluating the effects of thermal aging and uncertainties in the CF-8M CASS piping material properties. The technical basis for the flaw tolerance evaluation of CASS piping to support the Code Case is presented in a Materials Reliability Program (MRP) report, MRP-362.⁵⁴ The combined effects of thermal and neutron embrittlement of CASS materials for PWR and BWR core internals are also discussed in industry reports MRP-276⁵⁵ and BWRVIP-234,⁵⁶ respectively.

In this report, the methodology presented earlier in NUREG/CR-4513, Rev. 1, has been updated. The revised methodology is applicable to CASS materials containing up to 40% ferrite and for operating times equivalent to only 10,000 h at 400°C. This corresponds to

- ≥ 125 effective full power years (efpy) at 290°C for CF-8/CF-3 materials, and
- ≥ 30 efpy at 320°C for CF-8/CF-3 and ≥ 15 efpy for CF-8M materials used within primary pressure boundary components, and
- ≥ 15 efpy at 350°C for CF-8/CF-3 materials used in the reactor core internals.*

The combined effects of thermal and neutron embrittlement on the loss of fracture toughness of these materials have also been included. The lower-bound value of fracture toughness — defined in terms of the J_{IC} , C (i.e. the coefficient of the power law J-R curve), or the J value at a 2.5-mm crack extension — due to thermal and neutron embrittlement is expressed in terms of the neutron dose. The details regarding the various CASS materials and the associated Charpy-impact energy, tensile property and fracture toughness J-R curve information included in the database evaluated for this study are compiled and tabulated in Appendix A.

* A higher temperature is used to include gamma-heating effect.

2 THERMAL EMBRITTLEMENT OF CAST STAINLESS STEELS

It has been known that binary Fe-Cr alloys and ferritic SSs are susceptible to severe embrittlement when exposed to temperatures in the range of 300 to 500°C (572 to 932°F).⁵⁷⁻⁵⁹ The potential for significant embrittlement of CASS duplex materials, has been confirmed by studies at ANL¹²⁻¹⁸ and elsewhere^{1,2,6-10,21-32} on materials that were aged at temperatures of 285 to 450°C (545 to 842°F) for times up to 118,000 h (≈13.5 yr). The results indicate that thermal aging of CASS materials (ASTM Specification A-351 for Grades* CF-3, CF-3A, CF-8, CF-8A, and CF-8M) at 250–350°C (482–662°F) (a) increases their hardness and tensile strength; (b) decreases their ductility, impact strength, and fracture toughness; and (c) shifts the Charpy transition curve to higher temperatures. Different grades and heats of CASS exhibit varying degrees of thermal embrittlement. The low-carbon (low-C) CF-3 materials are the most resistant to thermal embrittlement, and the Mo-bearing, high-C CF-8M materials are the least resistant. Ferrite morphology has a strong effect on the degree or extent of embrittlement, whereas small changes in the material composition significantly alter the kinetics of embrittlement. In addition, as the results of studies on the kinetics of thermal aging demonstrate, thermal embrittlement of CASS materials can occur during the initial 40-year license period for power reactor operation.¹²

2.1 Mechanism of Thermal Embrittlement

Fracture of the 300 series austenitic SSs occurs essentially by nucleation, growth, and coalescence of microvoids, which results in a dimpled fracture morphology, regardless of the test temperature.⁴⁸ The heat-to-heat variability is due to the differences in the density and morphology of inclusions such as carbides, calcium aluminates, and manganese sulfides, which serve as nucleation sites for void formation. The large inclusions or inclusion clusters aligned in the working direction fail early in the deformation process, thereby resulting in poor fracture toughness. In relatively tough materials, microvoids nucleate away from the primary fracture plane, and significant plastic deformation is required for void coalescence.

A similar fracture behavior is also observed in unaged CASS materials; fracture occurs by microvoid coalescence. In CASS materials, voids nucleate preferentially within the ferrite phase, or at inclusions and phase boundaries.^{20,22,48} The overall fracture toughness is controlled by the density and morphology of the second phase particles and to some extent by the volume fraction of ferrite.

Furthermore, in materials with a duplex structure, the ferrite phase exhibits a ductile-to-brittle-transition temperature. The plastic straining capacity of ferrite is substantially decreased at low temperatures. However, the ferrite is ductile at RT and higher temperatures. Therefore, in the unaged condition, CASS materials exhibit a ductile dimpled fracture. The transition temperatures of unaged materials are relatively low. The differences in the transition temperature for the various unaged heats and grades of CASS materials are due to the amount of ferrite and the differences in the mechanism of brittle fracture. The high-carbon CF-8 or CF-8M materials have a higher transition temperature than CF-3 materials because of the presence of phase boundary carbides. The carbides weaken the boundaries and lead to premature phase boundary separation with little or no strain hardening.¹²

*The CF-3A and CF-8A grades represent materials with a high tensile strength. The chemical composition of these grades is further restricted within the composition limits of CF-3 and CF-8 in order to obtain a ferrite/austenite ratio that results in higher ultimate and yield strengths. In this report, they are considered equivalent to CF-3 and CF-8 grades.

The available data indicate that the fracture toughness of wrought austenitic SSs is strongly influenced by specimen orientation.³⁹ Fracture toughness J-R tests on Type 304 control-rod and Type 304L top guide materials irradiated to 4.7–12.0 displacements per atom (dpa) in a BWR show lower fracture toughness in the longitudinal direction (T-L orientation)* than in the L-T orientation. The lower fracture toughness along the T-L orientation is attributed to the presence of stringers. These stringers consisted of long, narrow particles oriented in the rolling direction that result in a long, narrow quasi-cleavage structure that is parallel to the crack plane and thereby accelerates crack advance. When stringers are aligned parallel to the crack propagation direction T-L (or C-L) orientation, tear ridges are nucleated ahead of the crack front, and the coalescence of these torn ridges results in premature crack advance without extensive plastic deformation.³⁹ When stringers are normal to the crack propagation direction (i.e., L-T or L-C orientation), microvoids are very deep and equiaxed, which blunts the advancing crack tip, and significant plastic deformation is needed for failure.

The available data also indicate that CASS materials suffer from thermal embrittlement of the ferrite during service at 300–450°C (572–842°F) and that the ductile-to-brittle transition temperatures shift higher.^{12–18,48} The time-temperature curves for the formation of various phases in thermally aged CASS materials⁴ are shown in Fig. 1. The results indicate that at temperatures above 550°C (1020°F), the embrittlement is largely due to the formation of the sigma phase, and that below 500°C (930°F), the precipitation of the α' phase leads to embrittlement. The formation of carbides and the chi phase influences mechanical properties in the 500–600°C (930–1110°F) temperature range. At reactor operating temperatures of 280–370°C (535–698°F), thermal aging of CASS materials leads to:

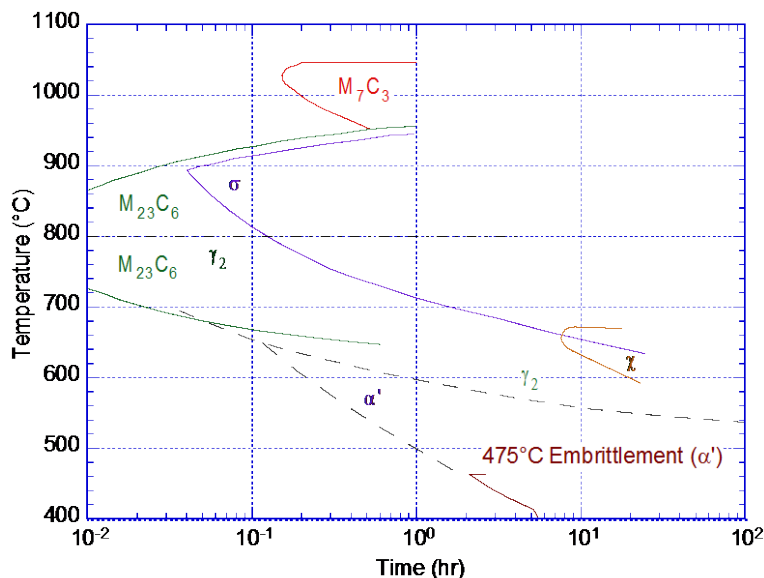


Figure 1. Time-temperature curve for the formation of various phases in CASS materials (Ref. 4).

- (a) spinodal decomposition of the ferrite into high-Cr α' and low-Cr α regions;

*The first letter represents the direction perpendicular to the plane of the crack, and the second letter represents the direction of crack advance. For plates, L = longitudinal or rolling direction and T = transverse direction (i.e., perpendicular to the rolling direction but not across the plate thickness). For pipes, L = longitudinal or axial direction, and C = circumferential direction (across the wall).

- (b) nucleation and growth of the high-Cr α' phase;
- (c) precipitation of a Ni- and Si-rich G phase, $M_{23}C_6$, and γ_2 (austenite); and
- (d) additional precipitation and/or growth of existing carbides at ferrite/austenite phase boundaries.^{5,60-67}

Another mechanism that can cause such behavior is a decrease in the ferrite content of CASS materials aged at temperatures above 400°C, particularly CF-8M materials. The metallographic data on CF-8 and CF-8M materials indicate significant precipitation of phase boundary carbides and/or growth of existing carbides during thermal aging, particularly at 450°C. The precipitation of Cr-rich carbides is always accompanied by a decrease in the ferrite content.⁴ The depletion of Cr destabilizes the ferrite phase, leading to ferrite-to-austenite transformation along the phase boundary. The growth of austenite into the ferrite grain occurs as cellular precipitation, along with the carbides.⁴ Such transformations can result in an increase in Charpy-impact energy.

A study at EdF on the evolution of thermally aged CASS materials using Charpy U-notch impact test specimens indicates that at RT, the brittle transgranular fracture of ferrite takes place primarily by cleavage; some twinning is also observed in highly embrittled material.²² Multiple cleavage of ferrite islands is observed throughout the material. All the cleavage facets are parallel to each other, regardless of the geometry of the individual islands. The percent of cleavage increases with increases in the degree of thermal embrittlement or with decreases in test temperature. At higher temperatures, although cleavage of the ferrite is reduced, twinning appears to play an important role in brittle failure of ferrite. The ferrite/austenite phase boundary exhibits a jagged appearance, with very fine lines and straight deformation bands within the ferrite islands (most likely slip bands and twins).²² Figure 2 shows deformation twins in a Charpy-impact specimen of CF-8 material aged for 30,000 h at 350°C and tested at 290°C. The fracture behavior of the austenite also changes from a dimple fracture to shear fracture. The presence of a completely embrittled ferrite skeleton promotes the low-energy failure mode of ductile shearing or tearing of the austenite ligaments between the islands of ferrite.⁹ Typically, in unaged duplex materials, cavities initiate from the cleavage cracks in the ferrite and not from matrix-inclusion decohesions.

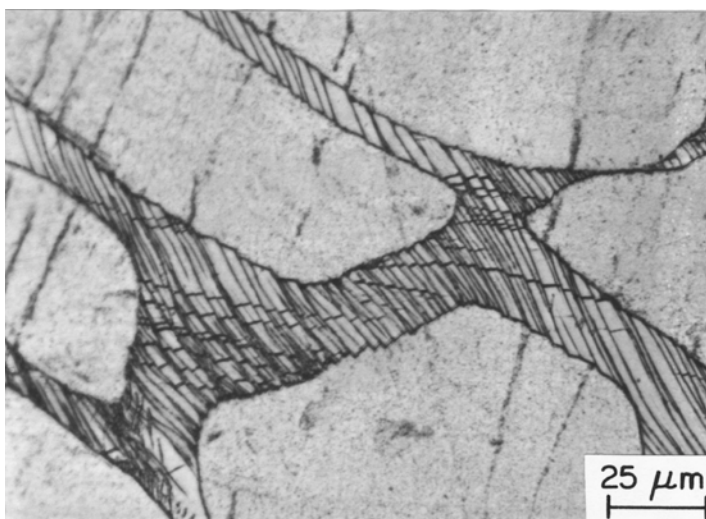


Figure 2.
Deformation twins in a Charpy-impact specimen of CF-8 material aged for 30000 h at 350°C and tested at 290°C (Ref. 12).

Another study on microstructural characterization and fracture behavior of unaged and aged CF-8M material at RT using Charpy V-notch and fracture toughness CT specimens also showed

similar failure mechanisms.⁶⁸ At RT, a fully ductile dimple fracture is observed for unaged material and material aged up to 40,000 h at 300°C (572°F). Ductile dimple fracture and brittle cleavage facets are observed for material aged up to 10,000 h at 350 and 400°C (662 and 752°F). In addition to these two fracture modes, ferrite/austenite phase boundary separation is also observed in materials aged at 450°C (842°F). Phase boundary separation is generally observed in high-C CASS materials aged at high temperatures (i.e., 400 or 450°C). Fractographic evaluation of both Charpy V-notch and fracture toughness CT specimens shows similar fracture modes for aged CF8M material. The only difference is that in the CT specimens, longer aging times are needed before brittle cleavage fracture is observed. Although only RT (i.e., 25°C) tests were conducted in this study, tests at higher temperatures are expected to show a larger fraction of ductile dimple fracture and less brittle fracture.

Thus, severely embrittled CASS materials generally exhibit large areas of brittle transgranular fracture of ferrite, linked by ductile shearing or tearing of the austenite ligaments. The degree of embrittlement and, thus, the toughness of the material are controlled by the amount of brittle fracture. CASS materials with poor toughness and impact strength exhibit a greater fraction of brittle fracture. For some CASS materials, although a fraction of the material may fail in a brittle fashion, the surrounding austenite provides ductility and toughness. Such materials have adequate toughness even after long-term aging. A predominantly brittle failure occurs when either the ferrite phase is continuous (e.g., in cast material with a large ferrite content) or the ferrite/austenite phase boundary provides an easy path for crack propagation (e.g., in high-C grades of cast steel with large phase-boundary carbides). For CF-8M materials with lacy ferrite morphology, ferrite contents of about 10% or more can provide a continuous ferrite phase.* Consequently, the amount, size, and distribution of the ferrite phase in the duplex structure and the presence of phase-boundary carbides are important parameters in controlling the degree or extent of thermal embrittlement.

Cleavage of ferrite occurs when the local tensile stress reaches the critical cleavage fracture stress. At low temperatures, (i.e., high values of yield strength), cleavage cracks nucleate in the ferrite in the plastic zone near the notch tip at loads that are below general yielding. At high temperatures (i.e., low values of yield stress), strain hardening is needed to raise the local tensile stress to the cleavage fracture stress. Ductile fracture results when strain hardening is not sufficient to raise the tensile stress to the critical value. The relationship between the degree of cleavage fracture and toughness, however, is complex since cleavage cracks can be initiated by several mechanisms (e.g., dislocation pile-up, cracking of carbide or nitride particles, and cracking of twin intersections). Each mechanism requires a unique stress level. Thus, for the same degree of cleavage fracture, the toughness may vary in different CASS materials.

The time-temperature curves for the formation of various phases and the change in the impact strength of thermally aged CASS materials,³ indicate that at temperatures above 550°C (1022°F), the embrittlement is largely due to formation of the sigma phase, and that below 500°C (932°F), precipitation of the α' phase leads to embrittlement. Furthermore, the time-temperature transformation curves for Fe-Cr alloys indicate that the α' phase is not stable at 550°C (1022°F). At 550°C, the Fe-Cr alloys are embrittled after aging for >10 h owing to the formation of the sigma phase.⁴ Consequently, the fracture toughness of embrittled CASS materials can be recovered virtually completely by annealing for 1 h at 550°C (1022°F) and water quenching. This short heat treatment dissolves the α' phase and prevents formation of sigma phase.¹² The dissolution of α' has been confirmed by microstructural studies.⁵

* Per private communications with Mr. M. Guttman, EdF, Research and Development, Department MMC, 77818 Moret sur Loing, France, in January 1986.

2.2 Distribution and Morphology of Ferrite in CASS Materials

2.2.1 Ferrite Morphology

The degree and kinetics of thermal embrittlement of CASS materials are controlled primarily by the amount, size, and distribution of the ferrite phase, and to some extent by the presence of carbides or nitrides at the phase boundaries. These material parameters in turn depend on the chemical composition of the materials and the manufacturing process. Differences in the thermal aging behavior have been observed in CASS materials produced by different foundries, suggesting that the material composition and ferrite content are not the only parameters that are relevant for thermal aging; manufacturing parameters may also be important.²⁵

The pseudo binary diagram for Fe-Ni-19%Cr system is shown in Fig. 3. Duplex SSs with high Cr contents solidify into a primary δ ferrite phase. Such materials generally have lathy ferrite morphology. These materials are most sensitive to thermal aging. Materials that solidify in the $\delta+\gamma$ regime exhibit vermicular and interdendritic lacy ferrite morphology. In both cases, during cooling of the solidified material, if the concentrations of the γ -forming elements such as C, N, Mn, and Ni, are sufficient, a fraction of the δ -ferrite transforms to γ -austenite by solid-state δ to γ transformation. Furthermore, if the cooling rate between 900 and 600°C (1652–1112°F) is slow, δ ferrite can transform to the brittle sigma (σ) phase, and $M_{23}C_6$ carbides can also precipitate at the δ/γ phase boundaries, both of which lead to degradation of the mechanical properties of the material.²⁵ Therefore, the manufacturing processes require that the casting must be annealed at around 1100°C (2012°F) followed by a rapid quench to avoid the formation of these deleterious precipitates.

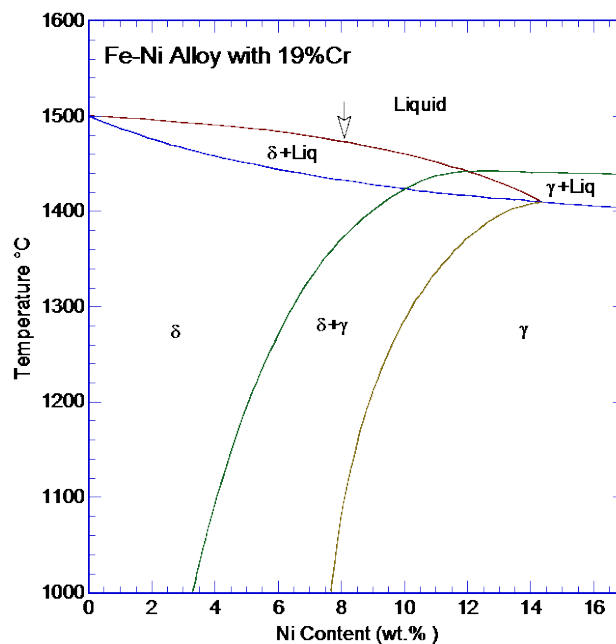


Figure 3. Pseudo binary diagram for Fe-Ni-19%Cr alloy (Ref. 25).

Typically, the structure of the core of large sand-cast CASS components consists of equiaxed grains, and the surface regions contain columnar grains, elongated in the direction of the temperature gradient. Steeper temperature gradients result in smaller and more elongated columnar grains.²⁵ Examples of equiaxed and columnar grain structures are shown in Figs. 4 and 5, respectively.

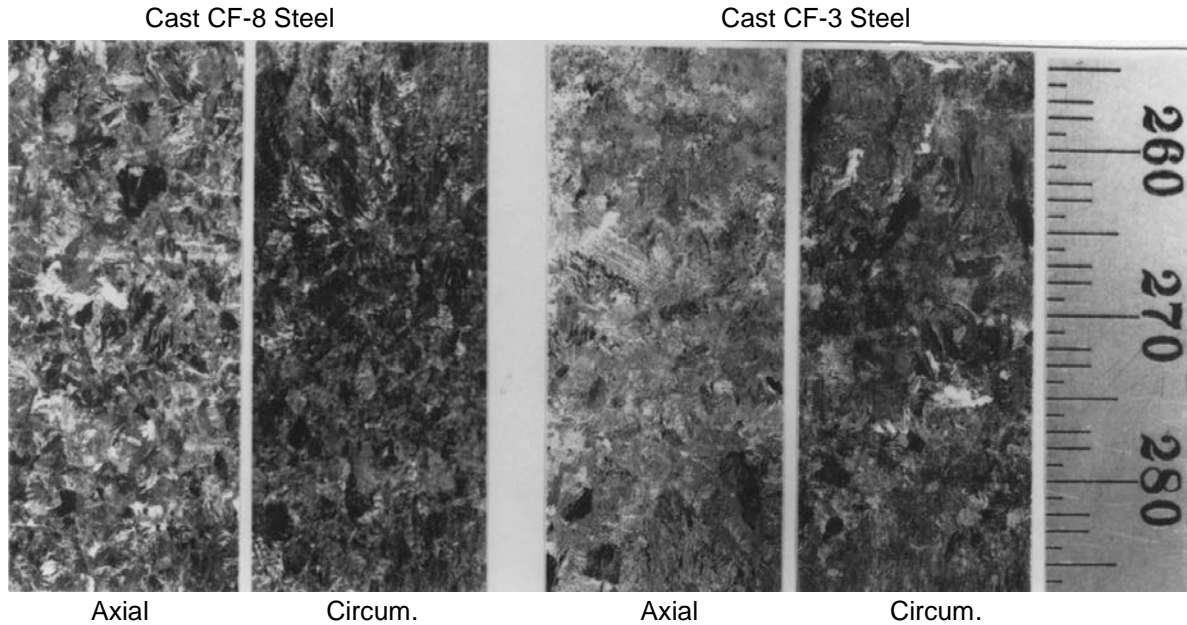


Figure 4. Microstructure along the axial and circumferential sections of centrifugally cast CF-8 and CF-3 stainless steel pipes showing equiaxed grain structure.



Figure 5. Microstructure along axial section of a check valve from the decommissioned Shippingport reactor showing columnar grains.

The effect of manufacturing process on the thermal embrittlement of CASS materials has been investigated by Massoud et al.²⁵ The manufacturing process for castings involves solidification of the material from a liquid state at around 1500°C (2732°F), followed by a homogenizing heat treatment of the solid at 1050–1150°C (1922–2102°F) and water quenching. The homogenizing treatment allows any brittle phases such as σ phase that may have precipitated during solidification to dissolve. It also establishes the ferrite-austenite ratio in the material and the partitioning of the alloying elements in the two phases. Consequently, the homogenizing treatment may be important for thermal embrittlement of the material during reactor service.

The results of the parametric study of the manufacturing process parameters conducted by Massoud et al.²⁵ indicate that the microstructural changes in the ferrite by spinodal decomposition during thermal aging at temperatures between 250 and 400°C are very sensitive to the initial state of the ferrite in the as-quenched condition. Any manufacturing process

parameter that improves the homogeneity of the ferrite solid solution such as long homogenizing heat treatments and rapid quench, delay the beginning of the ferrite decomposition, which results in a more aging-resistant CASS material. The significant results from the EdF study are as follows:

- The solidification rate affects the morphology of the ferrite-austenite microstructure and the characteristics of the toughness transition curve but does not seem to affect the aging behavior of the steel. The size and spacing of the ferrite phase increase with a decrease in cooling rate. Material with the low cooling rate has a high upper shelf Charpy-impact energy.
- An increase in the homogenizing treatment temperature increases the ferrite content of the material and the chemical composition within each phase. Consequently, it affects the aging behavior of the steel. The fracture toughness of CASS materials treated at a high temperature (which consequently have a high ferrite content) decreases sooner than the fracture toughness materials treated at a low temperature. However, the overall thermal embrittlement behavior depends on two mechanisms that counter each other. In CASS materials with higher ferrite content, the extent of thermal embrittlement is greater than it is in materials with low ferrite content. However, the ferrite in high-ferrite materials is less sensitive to thermal embrittlement because its Cr content is lower. Although the materials treated at low temperatures have low ferrite content and aging effects on them start late, they are more sensitive to thermal embrittlement. This behavior is discussed further in Section 2.3.
- The homogenizing treatment holding time and the quenching rate affect the beginning of the decomposition of the ferrite and consequently the overall kinetics of aging.

The ferrite morphology of the various CASS materials varies with the ferrite content, chemical composition, and size of the casting. Figure 6 shows examples of the ferrite morphology and ferrite content in centrifugally cast CF-3 and CF-8 pipes and a static cast CF-3 pump impeller. Studies conducted at ANL on 30 heats of CF-3, CF-8, and CF-8M CASS materials showed that globular ferrite morphology was observed for materials containing <5% ferrite.¹² Some differences in morphology were observed for the different grades of CASS materials containing >5% ferrite. The CF-8 and CF-8M materials had a lacy morphology while the CF-3 cast materials showed a mixture of lacy and acicular ferrite.

2.2.2 Ferrite Content

Significant variations in ferrite content within a CASS component have been observed in hot-leg elbow and crossover-leg elbow removed from the Ringhals reactor.⁶⁹ The material of the elbows is ASTM Specification 351 CF-8M steel, and the ferrite content, determined from the modified Schaefer diagram,⁷⁰ is 20.1 for the hot-leg elbow and 19.8% for the crossover-leg elbow. Test rings were cut from the two elbows, and the ferrite content measured with a ferrite meter at the inside surface at three different heights of the ring, as well as through the thickness of the ring. Around 700 measurements were made, and the results show that the ferrite content in the actual components varies significantly. The ferrite content of the hot-leg elbow varies from 3.0% to 22.5%, with an average of 13.3% \pm 4.2% ferrite; that of the crossover-leg elbow from 1.5% to 15.0%, with an average of 9.8% \pm 3.4% ferrite. The results also indicate that for both elbows, the measured average ferrite contents are comparable with the values estimated from the material chemical composition by using Hull's equivalent factors⁷¹ or the ASTM A800/A800M methodology.^{72,73}

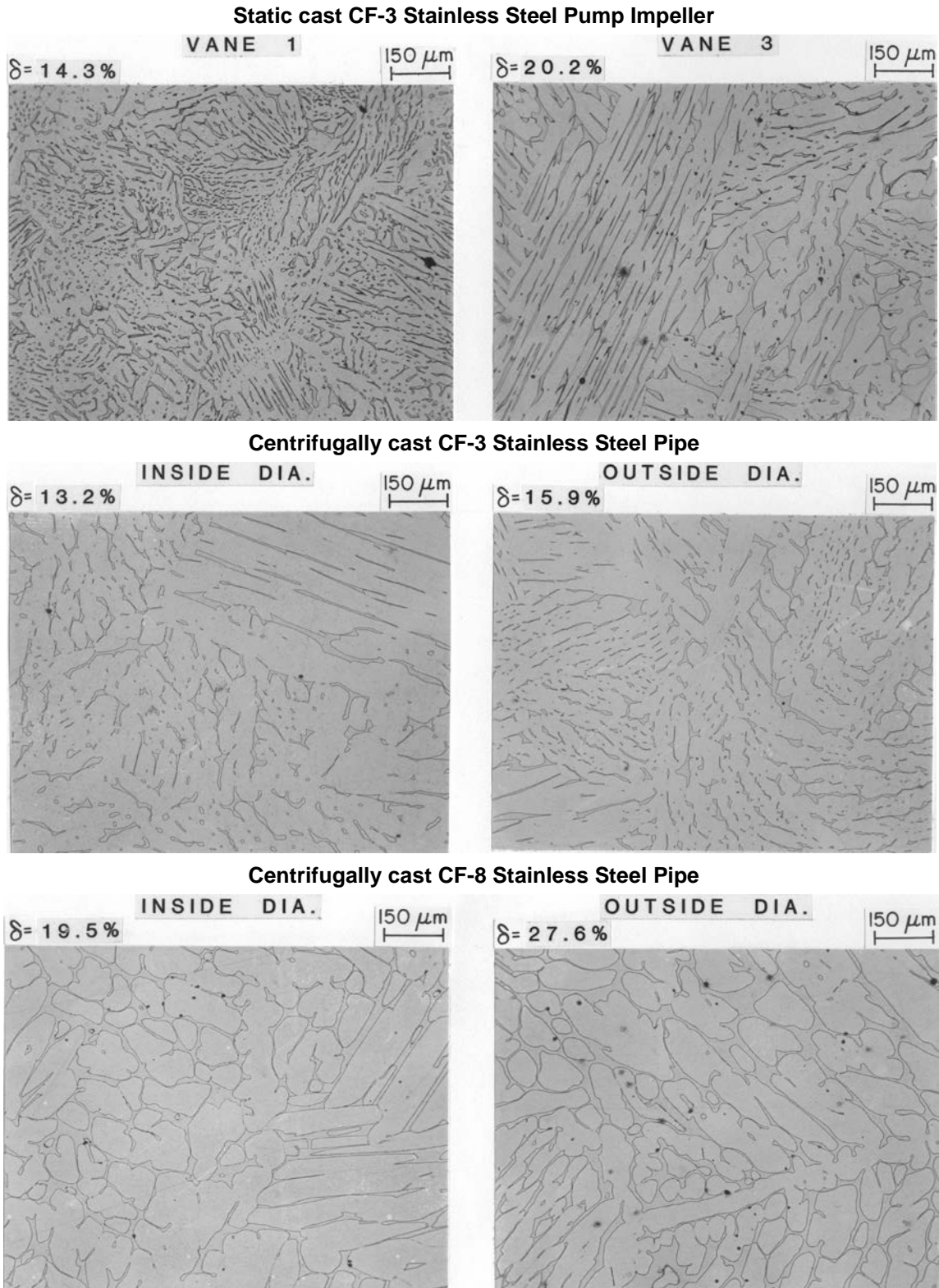


Figure 6. Ferrite content and morphology of vanes of a static cast CF-3 pump impeller and along a circumferential section of regions near the inside and outside diameter of centrifugally cast CF-3 and CF-8 pipes.

Similar variations in the ferrite content have also been observed in the ANL studies on CASS materials, obtained from actual reactor components. The measured ferrite content of vanes of a static-cast CF-3 pump impeller and along circumferential section of regions near the inside and outside diameter of centrifugally cast CF-3 and CF-8 pipes are higher near the outer surface than the inner surface. The values are about 20% higher for the CF-3 pipe (Heat P2) and 40% higher for the CF-8 pipe (Heat P1). In addition, the ferrite content of one of the pump impeller vane is about 40% higher than that of Vane 1. The ferrite contents estimated from the chemical composition by using Hull's equivalent factors are 17.7, 15.6, and 17.1% for the CF-8 pipe, CF-3 pipe, and CF-3 pump impeller, respectively. The estimated values are comparable to the measured average values of ferrite contents for the CF-3 pipe and pump impeller but lower than the measured values for the CF-8 pipe.

These observations indicate that if measured value of ferrite content is used for design calculations or analyses, several locations should be selected across the length and width of the component to ensure that it is representative of the entire component. The results also indicate that for centrifugally cast SS pipes, the extent of embrittlement is likely to increase from the inner surface towards the surface because of the increasing ferrite content.

The ferrite content in CASS structures depends on the chemical composition and the manufacturing process history of the material. Typically, it is (a) measured using metallographic examination or instruments that utilize the magnetic response of the casting or (b) estimated from the chemical composition of the casting. When the CMTR is available, the ferrite content is estimated from the chemical composition of the material, and measuring techniques are used when the CMTR is not available.

2.2.2.1 Measured Ferrite

Until 1973, the ferrite content in duplex structures such as CASS materials was determined by metallographic examination of the structure. A sample of the material was polished and etched to reveal the ferrite and austenite phases, and a grid was superimposed over the image of an optical microscope to determine, by point counting, the percentage of ferrite in the sample. The main drawback with this method is that the point-count estimates of ferrite can vary depending on the etching technique used to reveal the ferrite phase and on the number of grid points used in the measurements. Furthermore, as discussed, the ferrite content in most CASS components varies significantly in different regions of the component, and obtaining metallographic samples from various regions may not be practical.

Among the magnetic methods, the Magne-Gage and Feritescope are the most commonly used instruments for measuring the ferrite content in CASS materials. The Magne-Gage is a continuous-reading type of instrument that uses a spring to measure the attraction between a magnet and the material of unknown ferrite content, and the response is compared with that of a calibrated sample. Typically, the ferrite number (FN) is measured by using a Magne-Gage in accordance with standard American Welding Society (AWS) procedure A4.2-74.⁷⁴ The Feritescope operates on the magneto-induction principle, wherein the relative magnetic permeability of the specimen is measured. However, because the magnets or the probes of these instruments are small, the surface roughness or curvature of the sample is an important parameter that can change the magnetic linkage with the material being measured. In addition, phases other than ferrite and austenite may form in the material during service; these may alter the magnetic response of the material so that the indicated ferrite content is quite different from the content of a material with the same chemical composition that has undergone a different heat treatment.

2.2.2.2 Estimated Ferrite

Although a quantitative metallographic method gives the most accurate estimate of ferrite content, determining the percentage of ferrite from the chemical composition of the material is the most common method used to control ferrite during the solidification of the metal from a melt. The accuracy of these estimates, however, depends on the accuracy of the chemical analysis and on the degree of variability within the casting. In addition, these methods do not consider the effects of the casting process. The most commonly used methods for estimating ferrite are described below.

2.2.2.2.1 Hull's Equivalent Factor:

When a CMTR is available, the ferrite content is calculated from the chemical composition in terms of Hull's equivalent factors⁷¹ for Ni and Cr, given by

$$Cr_{eq} = Cr + 1.21(Mo) + 0.48(Si) - 4.99 \quad (3)$$

and

$$Ni_{eq} = (Ni) + 0.11(Mn) - 0.0086(Mn)^2 + 18.4(N) + 24.5(C) + 2.77, \quad (4)$$

where the concentrations of the various alloying and interstitial elements are given in wt.%. The concentration of N is often not available in a CMTR; if not known, it is assumed to be 0.04 wt.%. The ferrite content $\bar{\delta}_c$ is given by

$$\bar{\delta}_c = 100.3(Cr_{eq}/Ni_{eq})^2 - 170.72(Cr_{eq}/Ni_{eq}) + 74.22. \quad (5)$$

The measured ferrite content and values calculated from Hull's equivalent factor for the various CASS heats used in studies at ANL,¹² GF,¹ Electricité de France (EdF),²² National Power

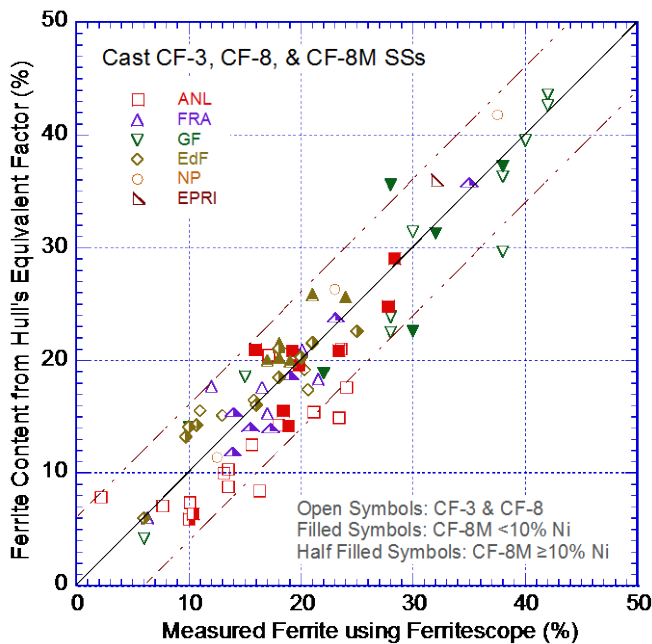


Figure 7.
Plots of measured ferrite content and values for various CASS materials calculated by using Hull's equivalent factor.

(NP),²¹ FRA,⁷ and the Electric Power Research Institute (EPRI)¹⁰ are shown in Fig. 7. For most heats, the difference between the estimated and measured values is $\pm 6\%$ ferrite. The results also indicate that the calculated ferrite content is generally lower than the measured values for CF-8M heats that contained $\geq 10\%$ Ni.

2.2.2.2.2 ASTM A800/800M Methodology:

In this methodology,⁷² the ferrite content of the casting is estimated from the central line of the of the Schoefer diagram⁷³ at the composition ratio of Cr equivalent, Cr_{eq} , to Ni equivalent, Ni_{eq} , determined from the formula:

$$Cr_{eq}/Ni_{eq} = (Cr + 1.5Si + 1.4Mo + Nb - 4.99)/(Ni + 30C + 0.5Mn + 26(N - 0.02) + 2.77) \quad (6)$$

The values of the composition ratio (Cr_{eq}/Ni_{eq}) for a given ferrite content (F), or vice versa, is then determined mathematically from the equation of the central line:

$$Cr_{eq}/Ni_{eq} = 0.9 + 3.38883 \times 10^{-2}F - 5.58175 \times 10^{-4}F^2 + 4.22861 \times 10^{-6}F^3 \quad (7)$$

The measured ferrite content and values calculated from the ASTM A800/A800M methodology for the same heats of CASS materials plotted in Fig. 7 are shown in Fig. 8. Since the Nb content is typically not reported for CASS CF-3, CF-8, and CF-8M materials, it is assumed to be zero and the ferrite content is calculated using Eqs. 6 and 7. Estimated values of ferrite if an Nb content of 0.2 wt.% is used would be about 7% higher for CASS materials with 5% ferrite and about 4% higher for materials with 30% ferrite. The results indicate that for ferrite contents more than 20%, the calculated ferrite content for several heats is lower than the measured values. Most of these heats with significantly lower calculated values contained 22.0–23.0 wt.% Cr and about 8.0–8.5 wt.% Ni. Ferrite contents estimated from the two methods, Hull's equivalent factor and ASTM A800/A800M method show excellent agreement for ferrite contents up to 20%. The ASTM A800/A800M method under predicts the ferrite content for CASS materials with more than 20% ferrite. Figure 9a shows the difference between the two methods.

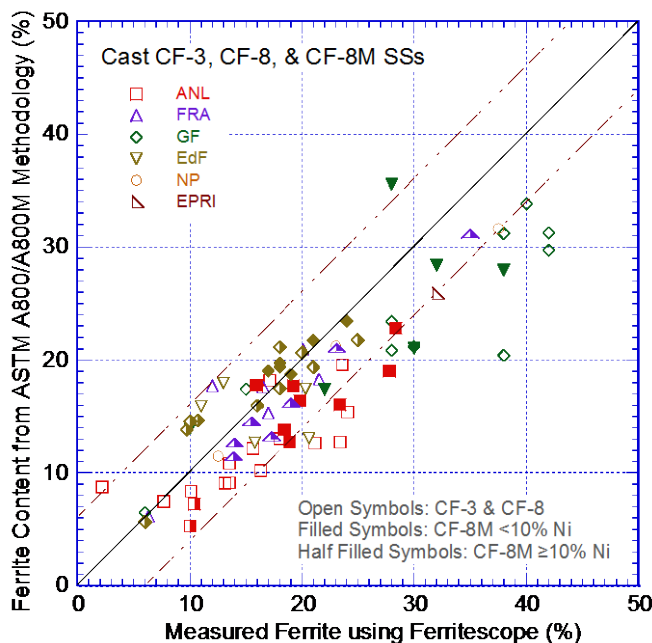


Figure 8.
Plots of measured ferrite content and values for various CASS materials calculated using the ASTM A800/A800M methodology.

2.2.2.2.3 Methodology Developed by EdF:

The expressions used by EdF to estimate ferrite content in a casting, are slightly different from those used in the ASTM A800/800M method. EdF has developed the following expression for estimating ferrite,

$$\text{Ferrite} = 21.8R^2 - 5.96R + 3.39, \quad (8)$$

where R is the ratio of Cr_{eq} and Ni_{eq} expressed as,

$$R = (Cr + Mo + 0.65Si - 17.6)/(Ni + 20C + 8.3N + 0.08Mn - 5.18). \quad (9)$$

A comparison of estimates of ferrite content based on the Hull's equivalent factor and EdF method is shown in Fig 9b. In general, the Hull's method predicts slightly higher ferrite contents. The two methods show good agreement for materials with up to 15% ferrite. The ferrite contents determined from the EdF method are compared with those from the ASTM A800/A800M method in Fig 10. The estimated values based of the EdF and A800/A800M methods show good agreement for ferrite contents up to 25%. The A800/A800M method under predicts for materials with ferrite content >25%.

2.3 Kinetics of Thermal Embrittlement

The degree of embrittlement, as documented in the NUREG/CR-4513, Rev. 1, is characterized in terms of the Charpy-impact energy of notched toughness specimens. The "best estimates" of the degree of embrittlement at reactor operating temperatures are obtained from Arrhenius extrapolations of laboratory data obtained at higher temperatures.¹ The aging time to reach a given degree of embrittlement at different temperatures is determined from:

$$t = 10^P \exp \left[\frac{Q}{R} \left\{ \frac{1}{T} - \frac{1}{673} \right\} \right], \quad (10)$$

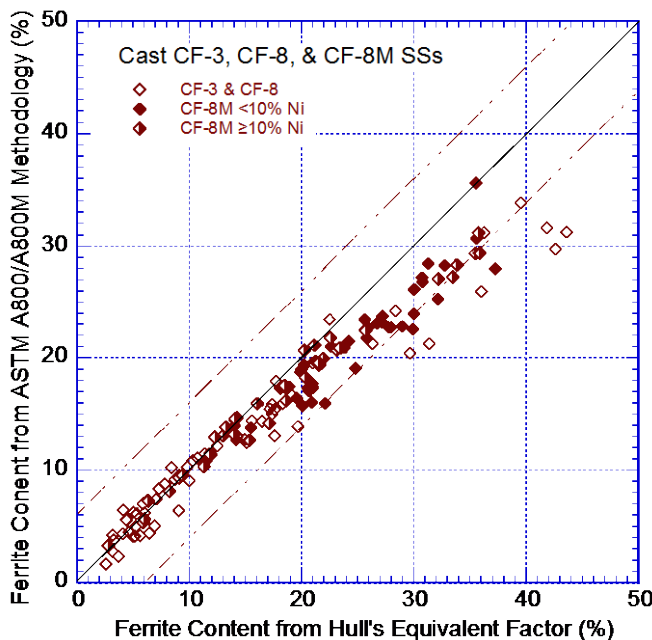


Figure 9a.
Plots of ferrite content calculated by using Hull's equivalent factor and those estimated from the ASTM A800/A800M methodology for various CASS materials.

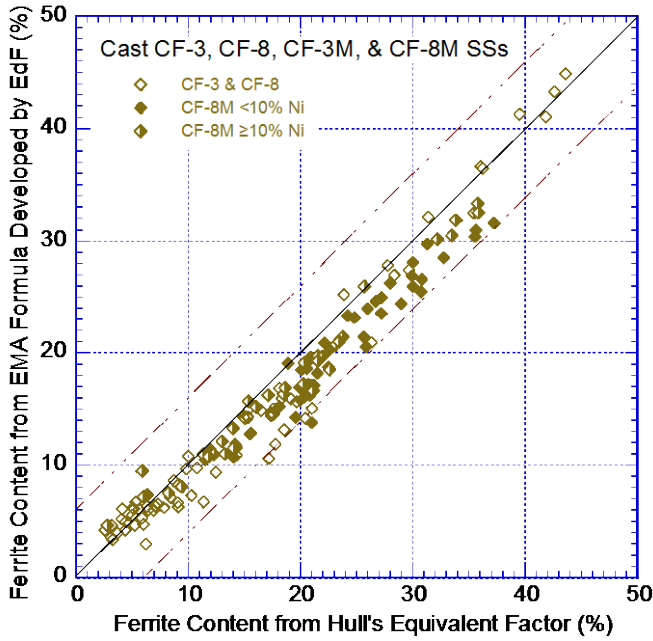


Figure 9b.
Plots of ferrite content for various CASS materials calculated by using Hull's equivalent factors and those determined from the EMA formula developed by EdF.

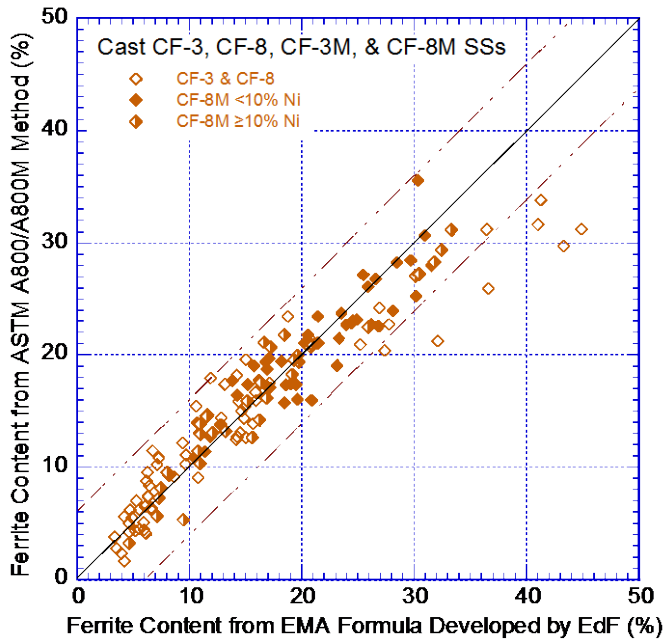


Figure 10.
Plots of ferrite content for various CASS materials estimated by using the ASTM A800/A800M methodology and those determined from the EMA formula developed by EdF.

where Q is the activation energy, R is the gas constant, T is the temperature, and P is an aging parameter that describes the combined effect of time and temperature on aging. It represents the degree of aging reached after 10^P h at 400°C (752°F). Thus, $P = 1$ for aging 10 h at 400°C . The aging parameter for any given aging condition is obtained by rewriting Eq. 10 so that,

$$P = \log_{10}(t) - \frac{1000Q}{19.143} \left(\frac{1}{T_s + 273} - \frac{1}{673} \right). \quad (11)$$

The activation energy for the process of embrittlement has been described by Slama et al.⁷ in terms of the chemical composition of the cast material. Thus,

$$Q(\text{kJ/mole}) = -182.6 + 19.9(\% \text{ Si}) + 11.08(\% \text{ Cr}) + 14.4(\% \text{ Mo}). \quad (12)$$

The activation energy calculated from Eq. 12 for the various CASS materials included in this study is in the range of 41–88 kJ/mole (9.8–21.0 kcal/mole) for CF-3 material, 43–91 kJ/mole (10.3–21.7 kcal/mole) for CF-8, 77–115 kJ/mole (18.4–27.5 kcal/mole) for CF-8M with <10% Ni, and 68–128 kJ/mole (16.3–30.6 kcal/mole) for CF-8M with ≥10% Ni. These values are generally lower than the values that were obtained from the mechanical property data (e.g., Charpy-impact) for most of the CASS materials, particularly for CF-3 and CF-8 materials. For example, the activation energies obtained experimentally from the studies at ANL, EdF/Framatome, and CEGB are in the range of 86–250 kJ/mole for CF-3, 63–253 kJ/mole for CF-8, 81–164 kJ/mole for CF-8M with <10% Ni, and 90–172 kJ/mole for CF-8M with ≥10% Ni. However, the calculated values for the CASS CF-3, CF-8, and CF-8M materials investigated in the GF study show good agreement with the experimental values of activation energies obtained from the Charpy-impact energy data for thermally aged materials.

Furthermore, the calculated values from Eq. 12 are significantly lower than the activation energy of spinodal decomposition in CASS materials. The spinodal decomposition and G-phase precipitation in low-temperature-aged CASS materials have been investigated by transmission electron microscopy (TEM), atom probe field ion microscopy (APFIM), small angle neutron scattering (SANS), and extraction replica techniques.^{60–67} The activation energy of the spinodal reaction in CF-3 SS was 250±30 kJ/mole (60±7 kcal/mole).⁶⁴ This value is comparable to that for Cr diffusion in Fe-Cr alloys. The lower values for the activation energy for thermal embrittlement of CASS materials are most likely due to other factors, such as the effect of the formation of carbides and nitrides at the phase boundaries or the effect of G-phase and/or γ_2 precipitation in ferrite, all of which can change the fracture mechanism of the aged material

For example, the precipitation of large carbides or nitrides at phase boundaries can initiate phase boundary separation by particle cracking. Consequently, a lower degree of spinodal decomposition (i.e., smaller amplitude of Cr fluctuation) is needed for a given change in mechanical properties. The material would show a reduction in impact strength faster than a material without phase boundary carbides would. However, the precipitation of carbides or nitrides occurs primarily at 400 or 450°C and is extremely slow at lower temperatures. Thus, the influence of phase boundary carbides would tend to increase the apparent activation energy of embrittlement measured from mechanical property data.

The other factor that can influence the overall activation energy for embrittlement is the precipitation of other second-phase particles in ferrite — in particular, the G phase (a multicomponent phase consisting of Ni, Si, Mo, Cr, and Fe and some Mn and C).^{62,66} The kinetics of G-phase precipitation depend on the chemical composition of the cast material.⁵ For some heats, the G phase is observed after times as short as 10,000 h at 400°C, while other heats require up to 70,000 h of aging at 400°C for G-phase formation. In general, precipitation of the G phase is faster in the Mo-containing CF-8M materials.^{5,60,62} The aging conditions for which the G phase has been detected by TEM or SANS techniques in various CASS materials are shown in Fig. 11. The kinetics for the decrease in the Charpy impact energy of the aged material are also plotted in the figure. The actual aging times for a given decrease in impact-energy varies significantly for the various heats (shown by the horizontal scatter bars in Fig. 11). Generally, the aging times for the CF-8M materials are lower than for the CF-3 or CF-8 materials.

The mechanism by which the G phase influences thermal embrittlement of CASS materials is not well understood. The precipitation of the G phase can influence the kinetics of embrittlement by either directly altering the kinetics of spinodal decomposition or by changing the deformation and fracture behavior of the ferrite matrix and thereby influencing the effectiveness of spinodal decomposition. The only experimental data on the kinetics of spinodal decomposition in CASS materials were obtained by modeling the amplitude of Cr fluctuations, measured by APFIM, in thermally aged CF-3 steel.¹⁸ The results yield an activation energy of 250 kJ/mole. No G phase was observed in the steel after 5,000 h at 400 or 350°C. As shown in Fig. 11, most heats require $\geq 10,000$ h at 400°C and $\geq 30,000$ h at 350°C before G-phase precipitates are detected.

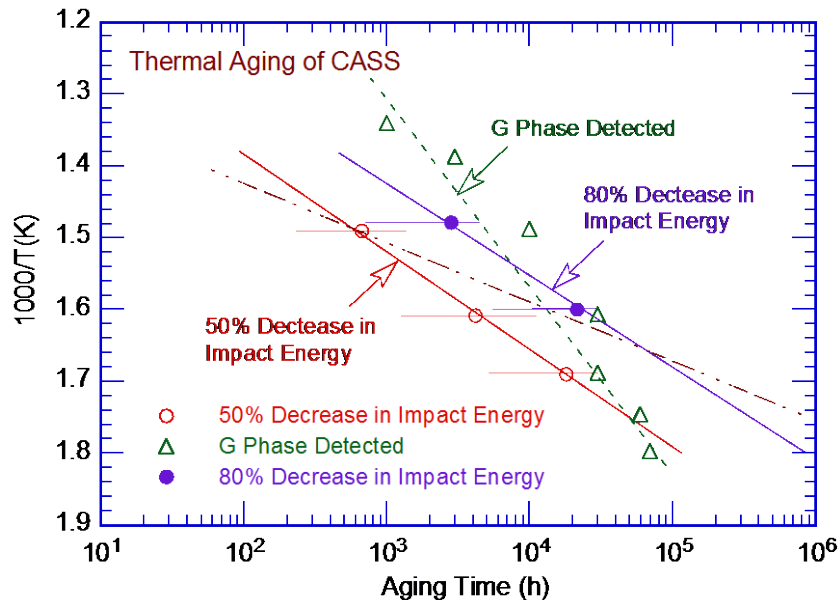


Figure 11. Arrhenius plots for the formation of the G phase and a reduction in impact energy.

The low values of activation energy obtained from mechanical property data (e.g., for the GF CASS materials) are most likely due to the effect of G-phase precipitation on the deformation behavior of the ferrite matrix. The concomitant precipitation of the G phase may alter the frequency (spacing) of Cr fluctuations produced by spinodal decomposition, which would be more effective in strain hardening. Thus, a lower degree of spinodal decomposition (i.e., lower amplitude of the Cr fluctuations) would be needed for a given change in mechanical properties. The G phase was observed in the GF heats of CASS materials, and the measured activation energies for thermal embrittlement obtained from the Charpy-impact data were between 63 and 106 kJ/mole.

The above methodology, however, assumes a unique aging behavior at 400°C (752°F), which is not observed for CASS materials produced at various foundries by using different manufacturing processes. The decrease in RT Charpy-impact energy during thermal aging at 400°C (752°F) of several heats of CASS materials^{1,7,10,12,13-15} is shown in Fig. 12. The results indicate that all materials reach “quasi-saturation” RT impact energy (i.e., a minimum value that would be achieved by the material after long-term aging, primarily due to spinodal decomposition of the ferrite). Although the decrease in the RT impact energy during aging at 400°C occurs primarily within 10,000 h, the impact energy for most CASS materials continues to decrease beyond 10,000 h,^{1,12-14} but at a much slower rate. Furthermore, thermal aging studies at EdF on numerous heats of CF-8M material have shown that the RT Charpy U-notch impact energy for

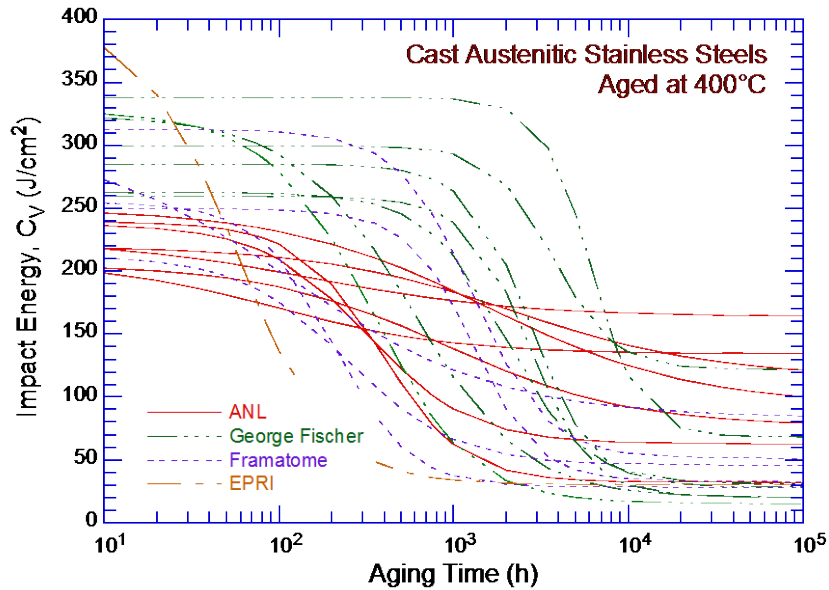


Figure 12. Decrease in Charpy-impact energy for various heats of CASS materials aged at 400°C.

materials aged for 10,000 h at 350°C is lower than for those aged at 400°C. However, after being aged further up to 30,000 h, the impact energy for materials aged at 350°C did not change significantly, whereas the impact energy for materials aged at 400°C decreased to a lower value than that reached by those aged at 350°C for 30,000 h.

Note that the proposed methodology for estimating the extent of thermal embrittlement of CASS materials is applicable to service times equivalent to 10,000 h at 400°C. This service time corresponds to $P = 4.0$. It represents ≥ 125 efpv at 290°C for CF-8/CF-3 materials and ≥ 30 efpv at 320°C for CF-8/CF-3 materials and ≥ 15 efpv for CF-8M materials used within primary pressure boundary components. For CF-8/CF-3 materials used in the core support structures and core internals, it represents ≥ 15 efpv at 350°C. The procedure for estimating the thermal embrittlement of CASS materials for longer service times will be established when additional long-term aging data on RT Charpy-impact energy and fracture toughness J-R curve are available for CF-8 and CF-8M materials. Limited data indicate that the concentration of (Ni+Si+Mo) in the material is an important parameter for further reduction in fracture properties of CASS components.

For a specific CASS material, the actual value of this quasi-saturation RT Charpy-impact energy is independent of aging temperature but depends strongly on the chemical composition of the material. It is lower for the Mo-bearing CF-8M materials than it is for the Mo-free CF-3 or CF-8 materials, and it decreases with an increase in the ferrite content and the concentration of C or N in the steel.

Figure 12 also indicates that for a given decrease in the RT Charpy-impact energy, the time for aging at 400°C varies by more than two orders of magnitude for the various heats. For example, the time required for the impact energy to start decreasing varies from about 50 h (EPRI heats) to more than 1000 h (GF heats). The time for the start of thermal aging effects varies from 50 to 500 h for the ANL and FRA heats. For some materials, the decrease in impact energy is very fast (i.e., low activation energy), and for others, it is slow (i.e., high activation energy). Typically, CASS materials that take longer for thermal embrittlement to start have low

activation energy, and materials that take short times for embrittlement to start have high activation energy. This behavior is consistent with the results of the parametric study of the manufacturing process parameters at EdF,²⁵ which showed that CASS materials that are solution-treated at a high temperature have a high ferrite content and their thermal embrittlement starts early during aging, but they are less susceptible to thermal embrittlement (e.g., activation energy for embrittlement is high). On the other hand, CASS materials that are solution-treated at a low temperature have low ferrite content and their thermal embrittlement starts late during aging, but they are very susceptible to thermal embrittlement (e.g., activation energy for embrittlement is low). Such differences may be attributed to compositional differences in the material due to differences in the casting process.

The results also indicate that for most CASS materials, the total time to reach saturation impact energy is approximately the same for all grades and heats of CASS materials. In other words, the time for thermal embrittlement to start plus the time for embrittlement to occur is about the same. CASS materials that start early take longer to embrittle, and materials that start late take a relatively shorter time to embrittle. Consequently, half the maximum change in RT Charpy-impact energy (i.e., parameter β) and the log of the time to achieve the β reduction in impact energy at 400°C (i.e., parameter θ) represent two important parameters for characterizing the kinetics of thermal embrittlement.¹⁶ The values of parameters β and θ for the various heats of CASS materials shown in Fig. 12 are listed in Table 2; parameter α is a shape factor.

Furthermore, microstructural examination of aged CASS materials suggests that materials that take longer for embrittlement to start at 400°C are associated with clusters of Ni-Si, Mo-Si, and Ni-Si-Mo in the ferrite matrix.^{5,60} These clusters are considered precursors of G-phase nucleation and precipitation. CASS materials with low activation energy (i.e., fast embrittlement) show G-phase precipitation after aging, but embrittlement at 400°C takes longer to start. CASS materials with high activation energy (i.e., slow embrittlement) do not contain the G phase but embrittlement at 400°C takes a relatively short time to start.^{5,60-62} The presence of Ni-Si-Mo clusters in the ferrite matrix of an unaged material may be considered a signature of materials that are potentially sensitive to thermal embrittlement (i.e., such materials show low activation energy for thermal embrittlement but take longer to embrittle at 400°C).

Since thermal embrittlement of CASS materials is caused primarily by spinodal decomposition of ferrite,^{5,11,12} the kinetics of thermal embrittlement are controlled by the amplitude and spacing of the Cr-rich regions in the ferrite. The low activation energies of thermal embrittlement are most likely caused by variations in the spacing of these regions. Atom probe field-ion microscopy studies indicate that the spacing between Cr fluctuations decreases with decreasing temperature.^{61,65} Therefore, production heat treatment and the casting process, both of which affect ferrite composition and microstructure of the material, would affect microstructural evolution during aging as well as the kinetics of embrittlement.

Based on these observations, in NUREG/CR-4513, Rev. 1, the change in RT Charpy-impact energy, C_V , as a function of time and temperature was expressed in terms of the RT saturation impact energy, C_{Vsat} , and the kinetics of embrittlement. The decrease in C_V with time was expressed as

$$\log_{10}C_V = \log_{10}C_{Vsat} + \beta\{1 - \tanh [(P - \theta)/\alpha]\}, \quad (13)$$

where the aging parameter P is determined from Eq. 11. The constants α and β are determined from the initial RT impact energy, C_{Vint} , and C_{Vsat} as follows:

Table 2. Chemical composition, ferrite content, and kinetics of thermal embrittlement for various heats of CASS materials.

Heat	Chemical Composition (wt.%)							Ferrite (%)		C_{Vsat} (J/cm ²)	Constants			Q (kJ/mole)
	Cr	Mo	Si	Ni	Mn	C	N	Calc.	Mea		β	θ	α	
<u>Argonne National Laboratory</u>														
52	19.49	0.35	0.92	9.40	0.57	0.009	0.052	10.3	13.5	161.8	–	–	–	–
51	20.13	0.32	0.86	9.06	0.63	0.010	0.058	14.3	18.0	115.9	0.139	3.53	1.15	204.7
47	19.81	0.59	1.06	10.63	0.60	0.018	0.028	8.4	16.3	163.7	0.069	2.29	1.20	195.7
P2	20.20	0.16	0.94	9.38	0.74	0.019	0.040	12.5	15.6	141.3	0.258	2.83	1.09	218.6
I	20.20	0.45	0.83	8.70	0.47	0.019	0.032	20.4	17.1	134.3	0.094	2.10	1.00	250.0
69	20.18	0.34	1.13	8.59	0.63	0.023	0.028	21.0	23.6	76.7	0.214	3.21	1.07	175.9
P1	20.49	0.04	1.12	8.10	0.59	0.036	0.057	17.6	24.1	53.7	0.305	2.57	0.75	252.7
61	20.65	0.32	1.01	8.86	0.65	0.054	0.080	10.0	13.1	93.3	0.214	3.48	1.20	197.8
59	20.33	0.32	1.08	9.34	0.60	0.062	0.045	8.8	13.5	89.1	0.197	3.14	1.20	249.4
68	20.64	0.31	1.07	8.08	0.64	0.063	0.062	14.9	23.4	47.1	0.301	2.88	0.68	161.1
60	21.05	0.31	0.95	8.34	0.67	0.064	0.058	15.4	21.1	44.8	0.291	2.89	0.88	210.9
56	19.65	0.34	1.05	9.28	0.57	0.066	0.030	7.3	10.1	117.6	–	–	–	–
74	19.11	2.51	0.73	9.03	0.54	0.064	0.048	15.5	18.4	63.1	0.269	3.44	0.70	95.0
75	20.86	2.58	0.67	9.12	0.53	0.065	0.052	24.8	27.8	32.1	0.436	2.82	0.51	139.0
66	19.45	2.39	0.49	9.28	0.60	0.047	0.029	19.6	19.8	87.9	0.208	3.16	1.57	163.9
64	20.76	2.46	0.63	9.40	0.60	0.038	0.038	29.0	28.4	41.1	0.338	2.81	0.60	147.3
65	20.78	2.57	0.48	9.63	0.50	0.049	0.064	20.9	23.4	59.7	0.260	2.99	0.59	153.8
P4	19.64	2.05	1.02	10.00	1.07	0.040	0.151	5.9	10.0	62.7	0.289	2.70	0.62	158.7
63	19.37	2.57	0.58	11.85	0.61	0.055	0.031	6.4	10.4	126.5	0.119	2.83	1.11	155.5
<u>Georg Fischer Co.</u>														
284	23.00	0.17	0.52	8.23	0.28	0.025	0.037	43.6	42.0	20.5	0.551	3.66	0.39	85.9
280	21.60	0.25	1.37	8.00	0.50	0.028	0.038	36.3	38.0	19.6	0.609	3.20	0.73	88.9
282	22.50	0.15	0.35	8.53	0.43	0.035	0.040	29.7	38.0	28.5	0.500	3.65	0.39	91.6
281	23.10	0.17	0.45	8.60	0.41	0.036	0.053	31.4	30.0	17.2	0.618	3.76	0.47	89.8
283	22.60	0.23	0.53	7.88	0.48	0.036	0.032	42.6	42.0	18.6	0.599	3.60	0.44	83.7
278	20.20	0.13	1.00	8.27	0.28	0.038	0.030	18.5	15.0	68.3	0.347	3.90	0.29	63.1
279	22.00	0.22	1.36	7.85	0.37	0.040	0.032	39.5	40.0	23.8	0.546	3.06	0.58	93.5
277	20.50	0.06	1.81	8.13	0.54	0.052	0.019	22.5	28.0	30.7	0.466	3.54	0.49	87.7
291	19.60	0.66	1.59	10.60	0.28	0.065	0.054	4.2	6.0	121.9	0.195	3.65	0.35	71.2
292	21.60	0.13	1.57	7.52	0.34	0.090	0.039	23.9	28.0	17.2	0.373	3.07	0.44	98.8
290	20.00	2.40	1.51	8.30	0.41	0.054	0.050	31.3	32.0	15.8	0.624	3.48	0.12	81.0
288	19.60	2.53	1.70	8.40	0.47	0.052	0.022	35.6	28.0	14.9	0.671	2.96	0.66	105.3
287	20.50	2.58	0.51	8.46	0.50	0.047	0.033	37.2	38.0	20.5	0.555	3.46	0.36	90.3
286	20.20	2.44	1.33	9.13	0.40	0.072	0.062	18.9	22.0	15.5	0.594	3.03	0.72	106.4
289	19.70	2.30	1.44	8.25	0.48	0.091	0.032	22.6	30.0	16.2	0.580	3.29	0.41	90.1
285	18.80	2.35	0.86	9.49	0.48	0.047	0.039	14.0	10.0	61.1	0.313	3.60	0.20	89.3
<u>Framatome</u>														
A	18.90	0.10	0.99	8.90	1.14	0.021	0.074	6.0	6.3	166.0	0.090	3.44	0.20	111.7
E	21.04	0.08	0.54	8.47	0.80	0.035	0.051	17.6	16.5	45.7	0.334	2.63	0.65	132.9
F	19.72	0.34	1.16	8.33	0.26	0.038	0.026	17.7	12.0	83.2	0.282	2.45	1.23	176.2
C	20.73	0.13	1.09	8.19	0.91	0.042	0.035	20.9	20.1	51.1	0.393	3.30	0.45	83.1
G	20.65	0.02	1.03	8.08	0.74	0.040	0.073	15.3	17.0	62.5	–	–	–	–
H	20.70	0.05	1.18	8.07	0.71	0.050	0.045	18.3	21.5	50.6	–	–	–	–
D	19.15	2.50	0.94	10.32	1.12	0.026	0.063	12.2	13.9	33.0	0.439	3.30	0.40	89.7
I	19.36	2.40	0.98	10.69	0.70	0.020	0.039	14.1	15.5	150.7	–	–	–	–
K	20.80	2.62	0.75	10.45	1.09	0.060	0.056	15.4	14.0	48.5	–	–	–	–
L	20.76	2.48	0.81	10.56	0.79	0.040	0.042	18.6	19.0	30.4	–	3.00	–	–
B	20.12	2.52	0.93	10.56	0.83	0.053	0.042	14.0	17.3	28.2	0.478	2.55	0.47	128.6
<u>Westinghouse</u>														
C148	20.95	2.63	0.53	9.48	1.02	0.061	0.056	22.1	14.0	53.1	–	2.80	–	–
<u>Electric Power Research Institute</u>														
EPRI	22.04	0.23	0.84	7.93	0.74	0.030	0.045	36.0	32.0	30.0	0.564	2.10	0.60	225.0

$$\alpha = -0.585 + 0.795 \log_{10} C_{V\text{sat}} \quad (14)$$

and

$$\beta = (\log_{10} C_{V\text{int}} - \log_{10} C_{V\text{sat}})/2. \quad (15)$$

The CMTR for a specific CASS component provides information on the chemical composition, tensile strength, and possibly the Charpy-impact energy of the material. If $C_{V\text{int}}$ is not known, a typical value of 200 J/cm² [or 160 J (118 ft-lb) for a standard Charpy V-notch specimen] may be used. The value of θ is not available for CASS components in the field, and can only be obtained from aging archival material for 5,000–10,000 h at 400°C (752°F). However, parametric studies show that the aging response at reactor temperatures is relatively insensitive to the values of θ .⁷⁵ However, the existing data indicate that θ varies with the material composition and ferrite content. Additional data on the kinetics of thermal embrittlement of CF-3, CF-3M, CF-8, and CF-8M materials containing a wide range of compositions and ferrite contents are needed to establish an expression correlating θ to the material composition. Based on the data listed in Table 2, a value of 2.9 for θ (i.e., mean of the experimental data) is used to estimate thermal embrittlement at 280–400°C (536–752°F). In the NUREG/CR-4513 methodology, the activation energy for thermal embrittlement is expressed in terms of both chemical composition and the constant θ .¹⁶ The activation energy Q (in kJ/mole) for CF-3 and CF-8 materials is given by

$$Q = 10 [74.52 - 7.20 \theta - 3.46 \text{ Si} - 1.78 \text{ Cr} + 148 \text{ N} - 61 \text{ C}], \quad (16)$$

and for CF-8M materials is given by

$$Q = 10 [74.52 - 7.20 \theta - 3.46 \text{ Si} - 1.78 \text{ Cr} - 4.35 \text{ Mn} + 23 \text{ N}]. \quad (17)$$

Equations 16 and 17 are slightly different from the expressions proposed by Slama et al. in 1983 (i.e. Eq. 12).⁷ These equations are applicable to compositions within ASTM Specification A351, with an upper limit of 1.2 wt.% for Mn content. Actual Mn content is used when CASS materials contain up to 1.2 wt.% Mn. For materials containing more than 1.2 wt.% Mn, 1.2 wt.% is assumed. Furthermore, the values of Q predicted from Eqs. 16 and 17 should be between a minimum of 65 kJ/mole (15.5 kcal/mole) and a maximum of 250 kJ/mole (59.8 kcal/mole) maximum; Q is assumed to be 65 kJ/mole if the predicted values are lower and 250 kJ/mole if the predicted values are higher. However, since several processes are responsible for thermal embrittlement of CASS materials, and each process has its own temperature dependence, the existing data indicates a change in activation energy of embrittlement with temperature.

The above expressions for estimating activation energy Q for thermal aging embrittlement of CASS materials agree qualitatively with the microstructural and mechanical property data. For example, an increase in the value of θ decreases the activation energy, as expected. The contributions of Si for all grades of CASS materials and of Mn for CF-8M materials are consistent with their effect on the formation of the G phase. These elements should promote precipitation of the G phase: hence, the coefficients for these elements should have a negative sign, because activation energy for thermal embrittlement is low for materials that show G-phase precipitation. An increase in C or N in the steel will promote carbide or nitride precipitation at high temperatures and thus increase the activation energy. The positive sign of the constant for the N content agrees with this behavior. The constant for the C content in steel, however, has a negative sign. It is likely that C also promotes the precipitation of the G phase, a multicomponent phase consisting of Ni, Si, Mo, Cr, and Fe and some Mn and C.^{62,67}

2.4 Extent of Thermal Embrittlement

All CASS materials reach the “saturation” RT impact energy (i.e., a minimum value achieved by the material primarily because of spinodal decomposition) after long-term aging. The actual value of the saturation RT impact energy for a specific CASS material is independent of the aging temperature (between 250-450°C) but depends strongly on the chemical composition of the steel. It is lower for the Mo-bearing CF-8M materials than for the Mo-free CF-3 or CF-8 materials, and it decreases with an increase in the ferrite content or the concentration of C or N in the steel.¹⁶ Typically, the extent of thermal embrittlement has been characterized by the RT “normalized” Charpy-impact energy (Charpy-impact energy per unit fracture area).

In the ANL studies,¹²⁻¹⁷ correlations have been developed for the extent of thermal embrittlement at quasi-saturation, C_{Vsat} (i.e., the minimum RT Charpy-impact energy that would be achieved for the material because of spinodal decomposition), in terms of the chemical composition of the material. The extent of thermal embrittlement as a function of the time and temperature of the reactor service is estimated from the extent of embrittlement at saturation and the correlations describing the kinetics of embrittlement, which are given in terms of the material chemical composition and the initial Charpy-impact energy, C_{Vint} , of the material in the unaged condition. If C_{Vint} is not known, a typical value of 200 J/cm² (118 ft-lb) is assumed. The fracture toughness J-R curve for the material is then obtained from the correlation between the fracture toughness parameters and the RT Charpy-impact energy used to characterize the extent of thermal embrittlement. A common lower-bound J-R curve for various grades of CASS materials of unknown chemical composition is defined for a given material specification, ferrite content, and temperature. Correlations are also developed for estimating changes in tensile strength and Ramberg/Osgood parameters for strain hardening.¹⁸ The methodology for estimating fracture properties of aged CASS materials has been updated in this report.

The extent of thermal embrittlement has been extended to operating times equivalent to 10,000 h at 400°C. The procedure for estimating thermal embrittlement for aging times beyond 10,000 h at 400°C will be established as and when RT Charpy-impact data are available for CF-8 and CF-8M materials aged for 10,000–40,000 h at 400°C. An aging time of 40,000 h at 400°C is equivalent to ≥60 efpY at 320°C for CF-8M and ≥120 efpY at 320°C for CF-8/CF-3 materials used in the primary pressure boundary components, and ≥45 efpY for CF-8/CF-3 materials used in reactor core support and core internals.

2.4.1 Charpy-Impact Energy

In the ANL studies,¹² different correlations are developed to estimate the saturation RT impact energy of the various grades of CASS materials. To ensure that the estimates are either accurate or conservative for all heats, the saturation RT impact energy for a specific material is determined by two slightly different expressions, both correlating the RT Charpy impact energy with a material parameter, ϕ , that depends on the material's ferrite content and its chemical composition. The lower value is used to estimate the mechanical properties of thermally aged CASS materials. The RT Charpy-impact energies at saturation (i.e., for CASS materials aged 10,000 h at 400°C), C_{Vsat} , observed experimentally at ANL,¹²⁻¹⁴ GF,¹ Westinghouse (WH),² TWI,⁶ FRA,⁷ EPRI¹⁰ CEGB,²¹ EdF,²² and MHI²⁸⁻³² are plotted as a function of the material parameter ϕ in Fig. 13. The data represents CF-3, CF-3M, CF-8, and CF-8M materials with 3 to 49% ferrite. The data for grades CF-3 and CF-8 are plotted together, and for grades CF-3M and CF-8M, materials containing <10% Ni are plotted separate from those containing ≥10% Ni.

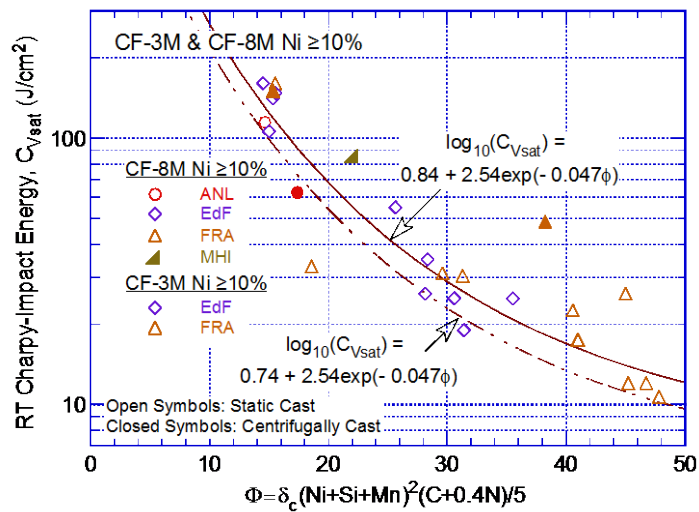
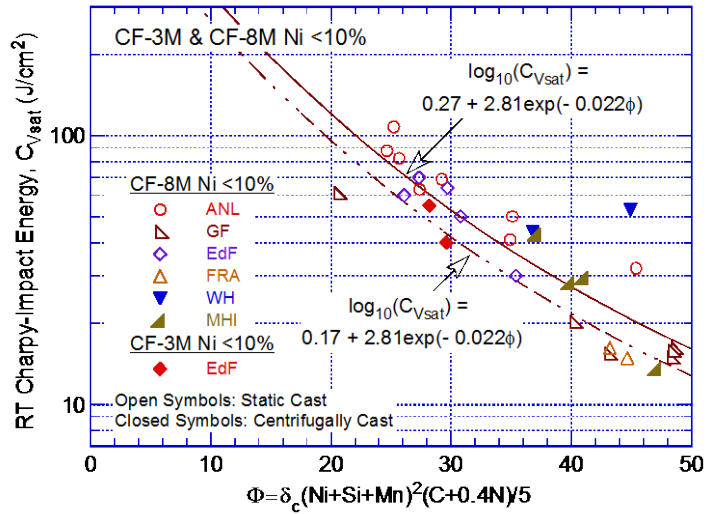
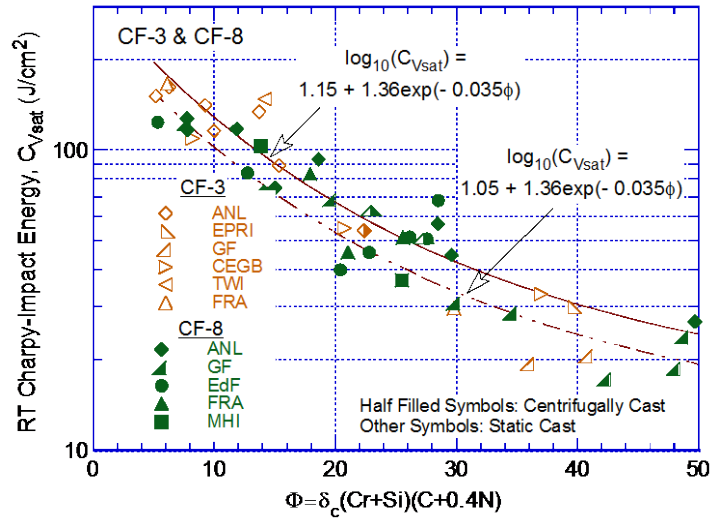


Figure 13. Correlation between RT Charpy-impact energy at saturation and the material parameter ϕ for CASS materials. δ_c is the calculated ferrite content.

A value of 10% Ni is used in this study to determine if primary γ (austenite) forms during solidification of the castings from the liquid. For CASS CF-8M compositions containing <10% Ni, the solidification sequence is as follows: Liq. \rightarrow Liq. + $\delta \rightarrow \delta$, with $\delta \rightarrow \gamma$ in the solid.⁷⁶ Austenite nucleates predominantly at ferrite grain boundaries and to a lesser extent at interdendritic locations within the ferrite. For CF-8M compositions containing $\geq 10\%$ Ni, the solidification sequence is likely to be as follows: Liq. \rightarrow Liq. + $\delta \rightarrow$ Liq. + $\delta + \gamma \rightarrow \delta + \gamma$, with $\delta \rightarrow \gamma$ continuing in the solid.⁷⁶ The austenite forms first in the liquid as a secondary phase enveloping the primary ferrite. Upon further cooling, it grows in the remaining liquid as well as into ferrite. The latter reaction continues below the solidus line. The actual microstructures of the casting depend on the Cr/Ni ratio for the specific composition. Because of significant differences in the composition and microstructure of the ferrite in CF-8M materials with <10 or $\geq 10\%$ Ni, separate expressions have been developed for these two materials.

The results indicate that for CF-3M and CF-8M materials, the original expressions correlating C_{Vsat} to the material parameter ϕ need to be revised to extend their applicability for materials containing more than 25% ferrite. The expressions for CF-3 and CF-8 materials do not require revision. For these grades, although experimental C_{Vsat} for a few heats with high values of ϕ is lower than the predicted value, the chemical composition of these heats was outside the ASTM specifications for CF-3 and CF-8 materials. The Cr content in these heats was significantly higher than the 21% maximum specified in the specifications, and for some materials, the Ni content was also lower than the 8% specified minimum.

For CF-3/CF-8 materials, the expressions in NUREG/CR-4513, Rev. 1, are retained. The best-fit expressions are used to avoid over conservatism in the estimation methodology. The saturation value of RT impact energy, C_{Vsat} , is the lower value determined from

$$\log_{10}C_{Vsat} = 1.15 + 1.36\exp(-0.035\Phi), \quad (18)$$

where the material parameter Φ is expressed as

$$\Phi = \delta_c(Cr + Si)(C + 0.4N), \quad (19)$$

and from

$$\log_{10}C_{Vsat} = 5.64 - 0.006\delta_c - 0.185Cr + 0.273Mo - 0.204Si + 0.044Ni - 2.12(C + 0.4N). \quad (20)$$

For CF-3M/CF-8M materials, the expressions between C_{Vsat} and ϕ have been revised. For materials with <10% Ni, the C_{Vsat} value is the lower value determined from

$$\log_{10}C_{Vsat} = 0.27 + 2.81\exp(-0.022\Phi), \quad (21)$$

where the material parameter Φ is expressed as

$$\Phi = \delta_c(Ni + Si + Mn)^2(C + 0.4N)/5, \quad (22)$$

and from

$$\log_{10}C_{Vsat} = 7.28 - 0.011\delta_c - 0.185Cr - 0.369Mo - 0.451Si - 0.007Ni - 4.71(C + 0.4N). \quad (23)$$

For materials with $\geq 10\%$ Ni, the saturation value of the RT impact energy C_{Vsat} is the lower value determined from

$$\log_{10}C_{Vsat} = 0.84 + 2.54\exp(-0.047\Phi), \quad (24)$$

where the material parameter Φ is expressed as

$$\Phi = \delta_c(\text{Ni} + \text{Si} + \text{Mn})^2(\text{C} + 0.4\text{N})/5, \quad (25)$$

and from

$$\log_{10}C_{Vsat} = 7.28 - 0.011 \delta_c - 0.185\text{Cr} - 0.369\text{Mo} - 0.451\text{Si} - 0.007\text{Ni} - 4.71(\text{C} + 0.4\text{N}). \quad (26)$$

If not known, the N content is assumed to be 0.04 wt.%. The correlations are optimized using mechanical property results on approximately 140 compositions of CASS materials that were aged up to 60,000 h at 290–350°C (554–662°F).

To provide a more realistic comparison, the data obtained for aging temperatures 400°C or higher are not used. Figure 14 shows the difference between the estimated C_{Vsat} values based on the original expressions in NUREG/CR-4513, Rev. 1, and the updated expression, for CF-8M and CF-3M materials. The original and updated curves are shown as solid and chain-dash lines, respectively. The chemical composition, ferrite content, and saturation RT Charpy-impact energy are given in Table 2.

The measured values of C_{Vsat} and the lower of the two values estimated from (a) the material parameter ϕ (Eqs. 18, 21, and 24) and (b) the material chemical composition and ferrite content δ_c (Eqs. 20, 23, and 26), are plotted in Fig. 15. The results indicate that the estimates based on Eqs. 18–26 are either accurate or conservative. However, the predicted C_{Vsat} for four heats

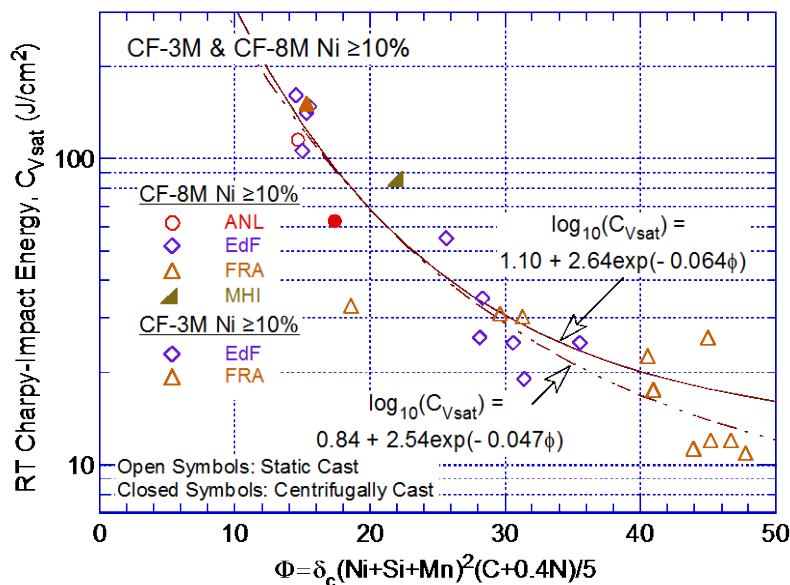


Figure 14. Comparison of the updated (chain-dash line) and original (solid line) correlation between the RT Charpy-impact energy at saturation and material parameter ϕ .

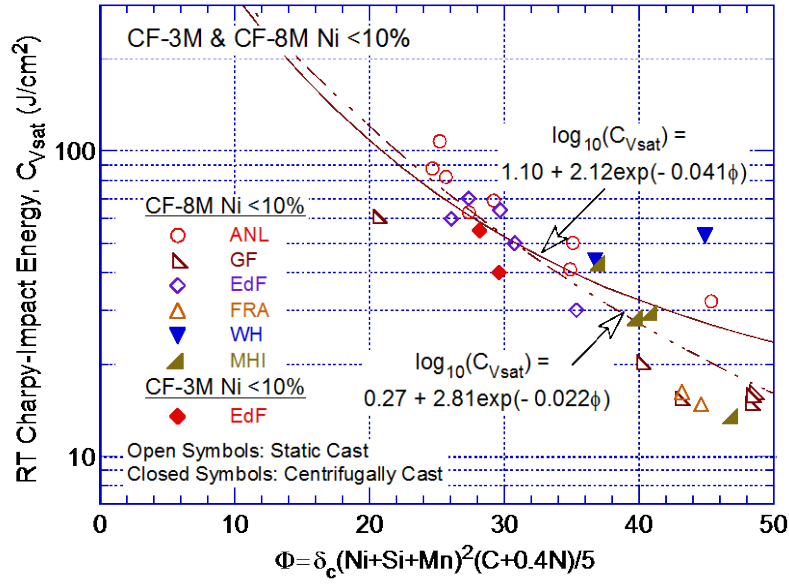


Figure 14. (Contd.)

(two CF-3 and two CF-8M materials) is significantly higher than the measured value. The reason for such a large difference is not clear. The expressions given by Eqs. 18–26 for estimating C_{Vsat} for a specific CASS material are correlated to the material's ferrite content and its chemical composition because a review of the thermal embrittlement data for aged CASS materials indicated that a correlation between the Charpy impact energy and ferrite content alone did not yield good results. The C_{Vsat} for CF-3, CF-8, and CF-8M materials shown in Fig. 13 is plotted as a function of the material ferrite content in Fig. 16; the results show a poor correlation.

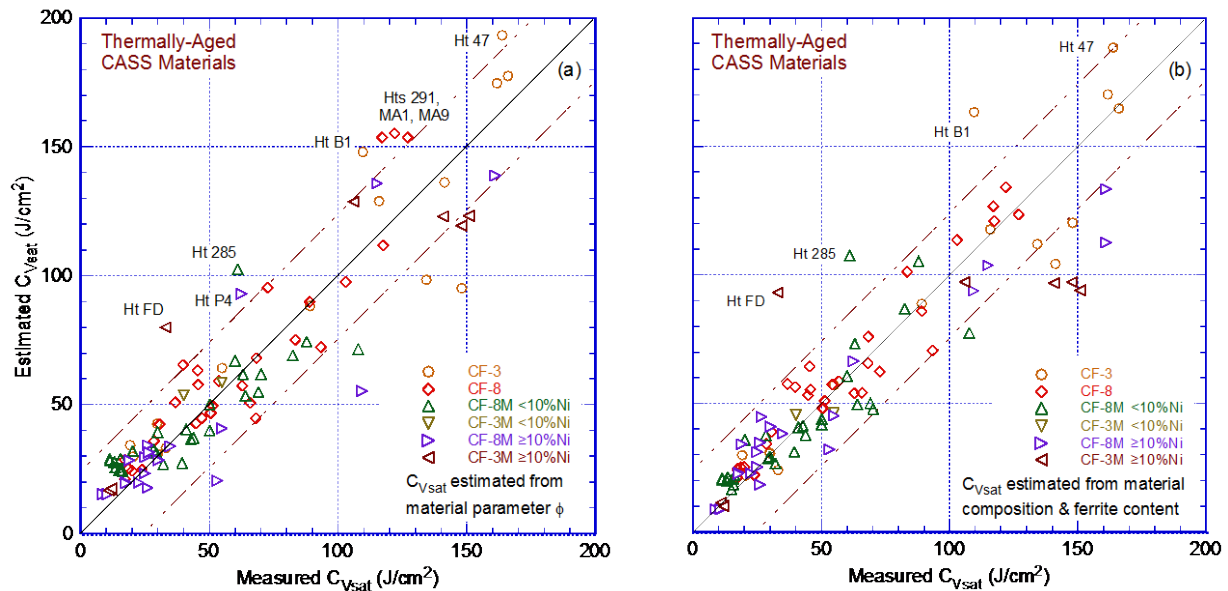


Figure 15. Measured values of saturation RT Charpy-impact energy for CF-3, CF-8, and CF-8M CASS materials and those estimated from (a) the material parameter ϕ , (b) the material composition and ferrite content, and (c) the lower of these two values.

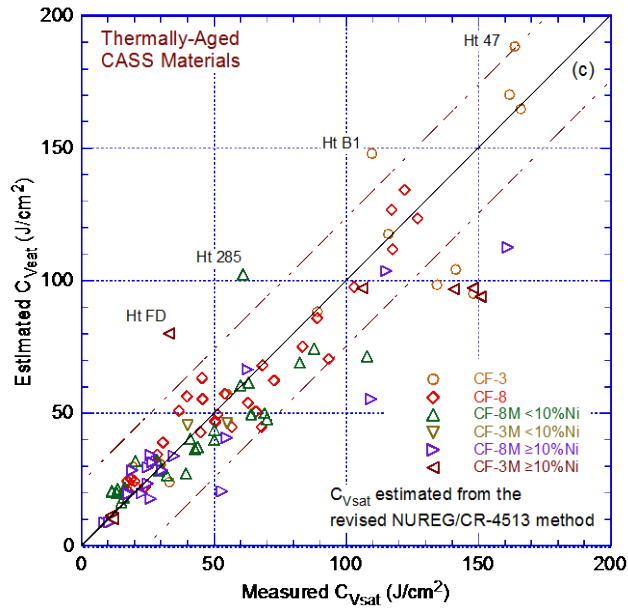


Figure 15. (Contd.)

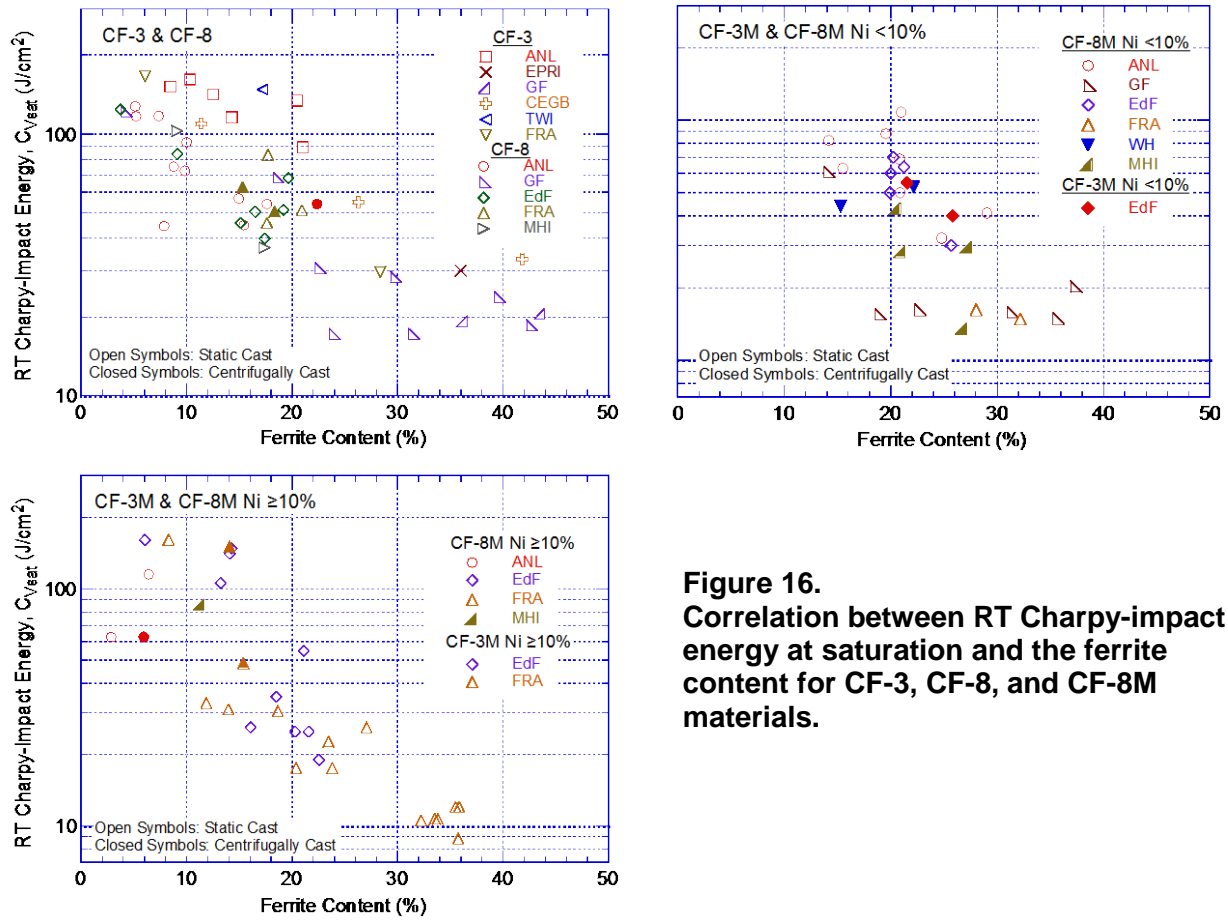


Figure 16. Correlation between RT Charpy-impact energy at saturation and the ferrite content for CF-3, CF-8, and CF-8M materials.

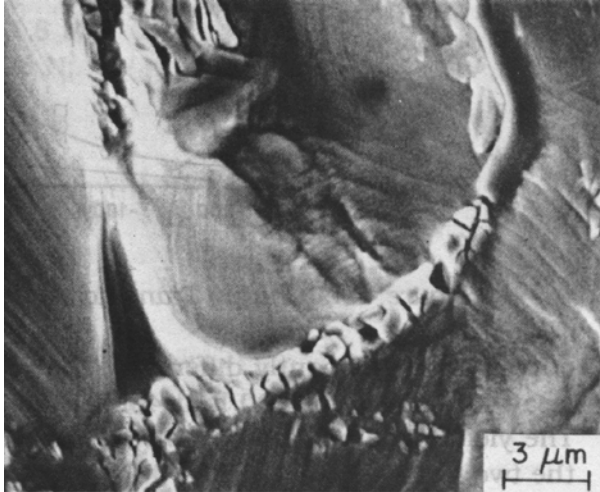


Figure 17.
Fracture surface of Charpy-
impact specimen of Heat 4331
aged for 700 h at 400°C and
tested at room temperature
(Ref. 12).

2.4.2 Effect of Trace Nb Content

Limited data indicate a significant reduction in the RT Charpy-impact energy of Heat 4331 of CF-8M material aged for only 700 h at 400°C. Unlike most CF-8M materials, which contain only trace amounts of Nb (e.g. <0.05 wt.%), Heat 4331 contained 0.2 wt.% Nb. The fracture surface of the Charpy-impact test specimen (Fig. 17) show that the phase boundaries are decorated with large Nb carbides (or carbo-nitrides) that can crack easily. These phase-boundary carbides alter the deformation and fracture behavior of the material, promoting initiation of cleavage by particle cracking. None of the other heats of CASS materials included in the ANL study contained more than trace amounts of Nb. The fracture surfaces of these heats of CASS materials exhibit, depending on the extent of embrittlement, a combination of dimpled ductile tearing, ductile shear failure, cleavage, and phase-boundary separation. For room-temperature tests, the amount of cleavage increased with the extent of embrittlement.

These differences in the fracture behavior of the Charpy-impact specimens are reflected in the ductile-to-brittle transition curves for thermally aged CASS materials. The effect of thermal aging on the transition curves for Heats 4331 (23.8% ferrite) and Heat 75 (24.8% ferrite) aged for different times at 400°C are shown in Fig. 18. The results show significant differences in the transition temperature for the two heats of CF-8M materials. The transition temperature at 81.25 J/cm² (i.e., 50 ft-lb) Charpy-impact energy for Heat 75 aged at 400°C for 2,570 h and 10,000 h is 65°C and 140°C, respectively; for Heat 4331 aged at 400°C for only 700 h, it is 220°C. Thus, the transition temperature is much higher for Heat 4331, even though it was aged for only 700 h. The results also indicate that although the Charpy-impact energy at 270–290°C is not significantly different for the three aging conditions, the RT Charpy-impact energy is much lower for Heat 4331 than for Heat 75 aged for longer times. For Heat 4331, the Charpy-impact energy at 290°C continues to decrease after aging at 400°C for more than 700 h.

These results indicate the potential effects of a trace amount of Nb content on the thermal embrittlement of CASS materials during service in LWRs. The ASTM Specifications A351 and A451 for the chemical composition of CF-3, CF-3M, CF-8, and CF-8M grades of CASS do not specify any maximum limit for the Nb content in the casting. Typically, the trace Nb content in these grades of CASS materials produced in the United States is very low (less than 0.05 wt.%). However, castings produced in Europe may contain higher levels of Nb. The source for higher Nb content is the use of Type 347 scrap metal to produce the casting. Consequently, the amount of Nb is often more than 0.05 wt.% if Type 347 scrap metal is used.

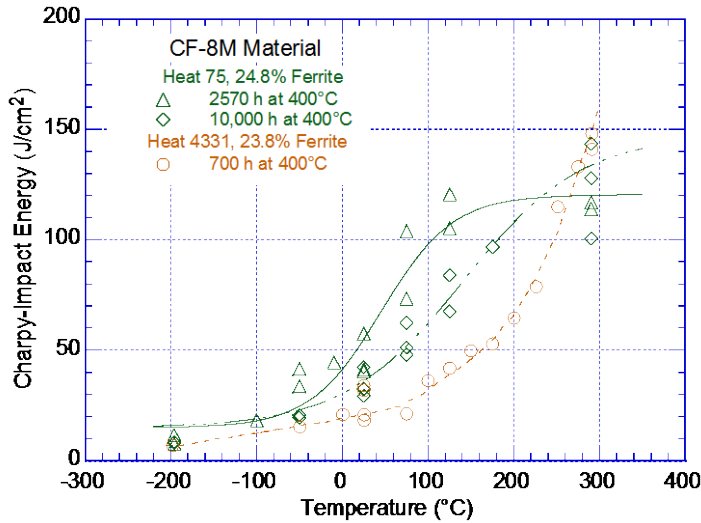


Figure 18. Ductile-to-brittle transition curves for Charpy-impact specimens of thermally aged Heats 4331 and 75 of CF-8M material (Ref. 12).

2.4.3 Fracture Toughness J-R Curve

The fracture toughness J-R curve for a specific CASS material can be estimated from its RT Charpy-impact energy. The J-R curve is expressed by the power-law relationship $J_d = C\Delta a^n$, where J_d is deformation J per ASTM Specifications E 813-85 and E 1152-87, Δa is a crack extension, and C and n are constants. The coefficient C, at RT (25°C) or reactor temperatures (290–320°C), and the RT Charpy-impact energy for aged and unaged CASS materials are plotted in Fig. 19a and b respectively, based on an updated fracture toughness database. Fracture toughness data from studies at ANL,^{12–15} FRA,^{7,8} EPRI,¹⁰ EdF,^{23,24,26} Mitsubishi Heavy Industries (MHI),^{28–32} The Welding Institute (TWI),⁶ and Materials Engineering Associates, Inc. (MEA),⁷⁷ are included in the figure. These plots provide a correlation between coefficient C of the Power-law J-R curve and RT Charpy-impact energy of the material. Thus, saturation values of C can be obtained from the saturation value of RT Charpy-impact energy.

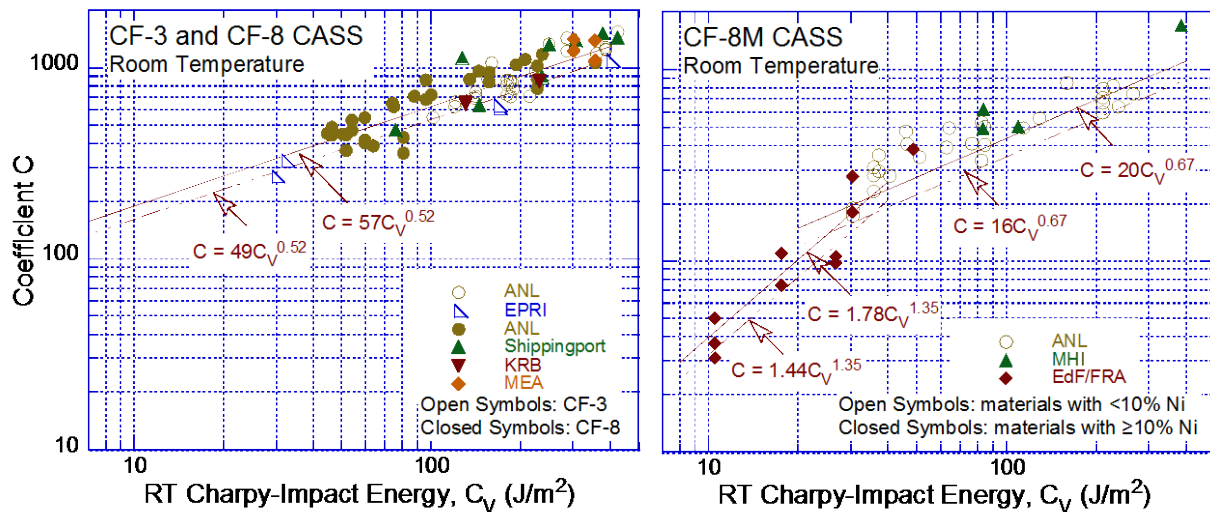


Figure 19a. Correlation between RT Charpy-impact energy and coefficient C at RT for CF-3, CF-8, CF-3M, and CF-8M CASS materials.

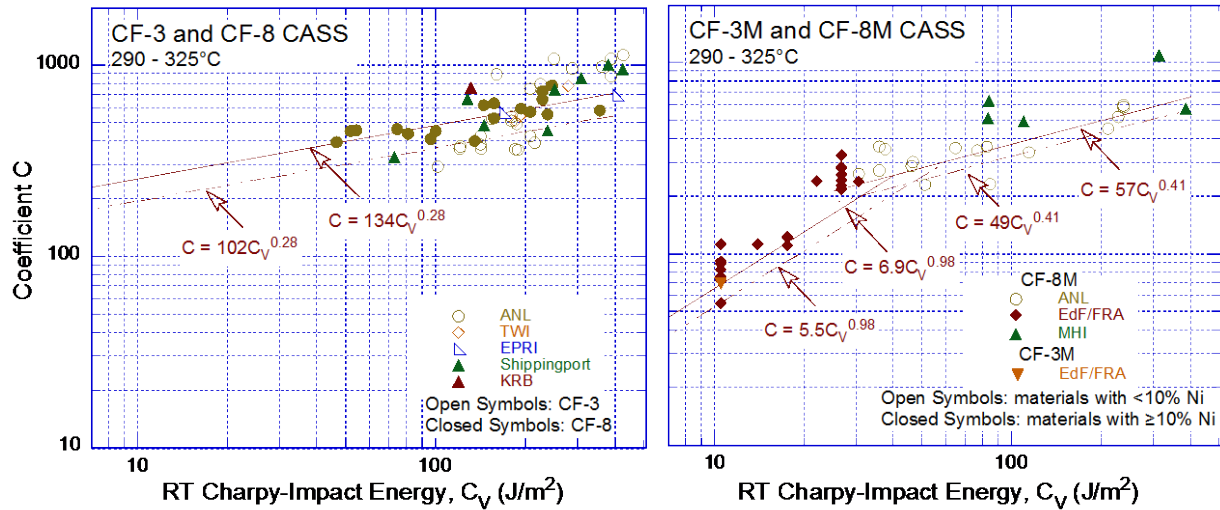


Figure 19b. Correlation between RT Charpy-impact energy and coefficient C at 290–320°C for CF-3, CF-8, CF-3M, and CF-8M CASS materials.

At both RT (25°C) and reactor temperatures (290–320°C), the coefficient C decreases with a decrease in the RT Charpy-impact energy. Separate correlations are obtained for CF-3 and CF-8 materials and for CF-8M materials; the latter show a larger decrease in the fracture toughness for a given impact energy. Furthermore, for CF-8M materials, the decrease in the values of coefficient C is much greater for RT Charpy-impact energy values that are less than about 35 J/cm² for fracture toughness tests at RT and 41–46 J/cm² for fracture toughness tests at reactor temperatures. However, all of the fracture toughness data for CF-8M materials with very low values of RT Charpy-impact energy are for materials containing ≥10% Ni. It is not clear whether CF-8M materials with <10% Ni also show a similar behavior.

As discussed later in this section, data on chemical compositions of CASS piping materials from a select sample of nuclear power plants (NPPs) in the United States indicate that at least 9% of the CF-8M materials currently used in operating NPPs contain more than 25% ferrite. For these materials, the methodology developed earlier in NUREG/CR-4513, Rev. 1, is not applicable for flaw tolerance evaluations. In this report, the methodology for estimating thermal embrittlement has been extended to cover CASS materials containing more than 25% ferrite. For CF-8M materials, a bilinear expression is developed between RT Charpy-impact energy and coefficient C of the power-law J-R curve.

To help ensure that the estimated J-R curve was conservative for all material and aging conditions, the correlations for estimating the J-R curves for static-cast materials were obtained by subtracting the value of the standard deviation for the fit to the data from the best-fit curve in Fig. 19; these curves are shown as chain dot curves. For centrifugally cast materials, the best-fit correlations were used; typically, the data scatter is considerably smaller for centrifugally cast materials than static cast materials. For CF-8M materials, the value of the RT Charpy-impact energy for the transition from one expression to the other varies between 35 and 46 J/cm² because of the differences in the standard deviation for the fit to the individual set of data.

For static-cast CASS materials, the coefficient C of the J-R curve at RT for CF-3 or CF-8 materials is expressed as

$$C = 49[C_V]^{0.52}; \quad (27)$$

for CF-8M materials with RT Charpy impact energy values ≥ 35 J/cm², it is expressed as

$$C = 16[C_V]^{0.67}; \quad (28)$$

and for CF-8M materials with RT Charpy impact energy values < 35 J/cm², it is expressed as

$$C = 1.44[C_V]^{1.35}. \quad (29)$$

For static-cast CASS materials, the coefficient C of the J-R curve at 290–320°C for CF-3 or CF-8 materials is expressed as

$$C = 102[C_V]^{0.28}; \quad (30)$$

for CF-8M materials with RT Charpy impact energy values of ≥ 46 J/cm², it is expressed as

$$C = 49[C_V]^{0.41}; \quad (31)$$

and for CF-8m materials with RT Charpy impact energy values < 46 J/cm², it is expressed as

$$C = 5.5[C_V]^{0.98}. \quad (32)$$

For centrifugally cast CASS materials, the coefficient C of the J-R curve at RT for CF-3 or CF-8 materials is expressed as

$$C = 57[C_V]^{0.52}; \quad (33)$$

for CF-8M materials with RT Charpy impact energy values ≥ 35 J/cm², it is expressed as

$$C = 20[C_V]^{0.67}; \quad (34)$$

and for CF-8M materials with RT Charpy impact energy values of < 35 J/cm², it is expressed as

$$C = 1.78[C_V]^{1.35}. \quad (35)$$

For centrifugally cast CASS materials, the coefficient C of the J-R curve at 290–320°C for CF-3 or CF-8 materials is expressed as

$$C = 134[C_V]^{0.28}; \quad (36)$$

for CF-8M materials with RT Charpy impact energy values ≥ 41 J/cm², it is expressed as

$$C = 57[C_V]^{0.41}; \quad (37)$$

and for CF-8M materials with RT Charpy impact energy values < 41 J/cm², it is expressed as

$$C = 6.9[C_V]^{0.98}. \quad (38)$$

The distribution of the value of the power-law J-R curve exponent, n, for various grades of thermally aged and unaged CASS materials is shown in Fig. 20. The available database consists of 129 fracture toughness J-R curve tests at RT and 141 tests at reactor temperatures

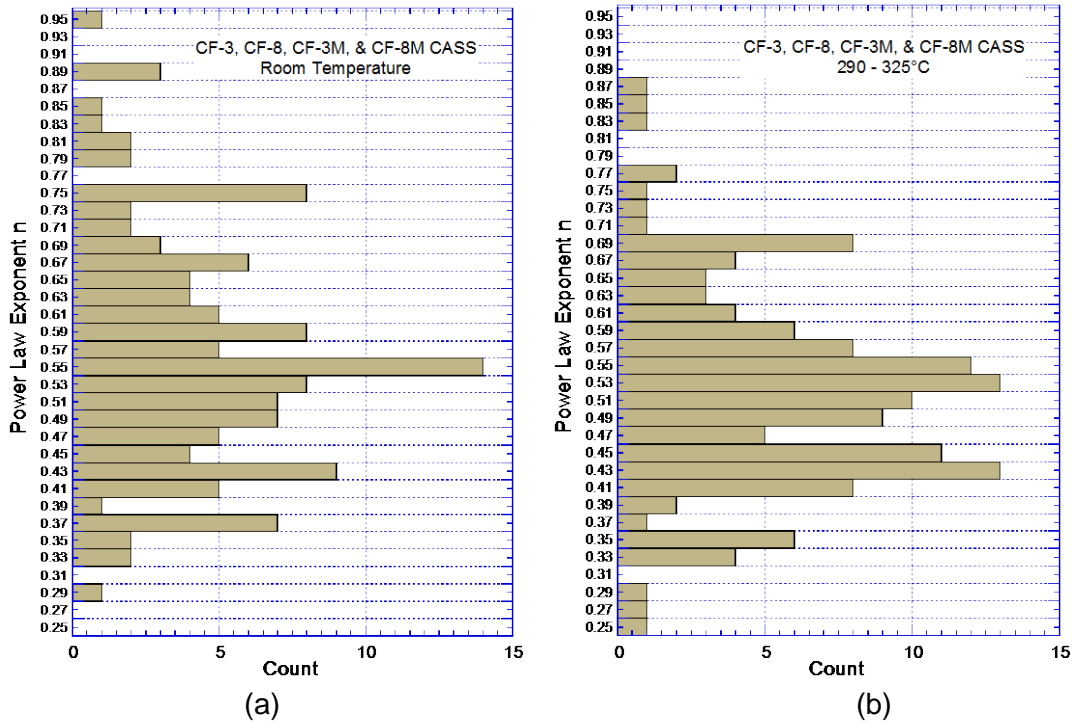


Figure 20. Distribution of the J-R curve exponent for various grades of thermally aged and unaged CASS materials at (a) room temperature and (b) 290–325°C.

of 290–325°C. In general, the exponent n is higher at RT than at reactor temperatures. The median value is 0.55 at RT and 0.50 at 290–325°C. The results show that only about 4% of the values at reactor temperature and less than 2% of them at RT are below a value of 0.33. However, an investigation of the thermal embrittlement of CASS materials at EdF indicated that exponent n of the power-law J-R curve can be as low as 0.2 for some heats of CF-8 and CF-8M materials, particularly at reactor temperatures.*

The exponent n of the power-law J-R curve has also been correlated with the RT Charpy-impact energy C_V . In NUREG/CF-4513, Rev. 1, to ensure that the estimated J-R curves were conservative, the correlations between exponent n and the corresponding RT Charpy-impact energy for the same material condition represented the lower-bound values of n . The updated data for the RT Charpy-impact energy and the corresponding value of fracture toughness J-R curve exponent n at RT and 290–325°C, for CF-3, CF-8, and CF-8M CASS materials, are plotted in Fig. 21. A review of the updated fracture toughness data indicates that some of the recent data are below the correlations in NUREG/CR-4513, Rev. 1,¹⁶ between exponent n and RT Charpy-impact energy. Consequently, the correlations¹⁶ for estimating the J-R curve exponent n have been revised; the updated correlations are slightly lower. The revised correlations representing the lower-bound values are shown in the Fig. 21.

For static-cast or centrifugally cast CASS materials, the exponent n at RT for CF-3 materials is

$$n = 0.16 + 0.13\log_{10}[C_V]; \quad (39)$$

* Per private communications with Dr. Sebastien Saillet, EdF, Research and Development, Department MMC, 77818 Moret sur Loing, France, in April 2015.

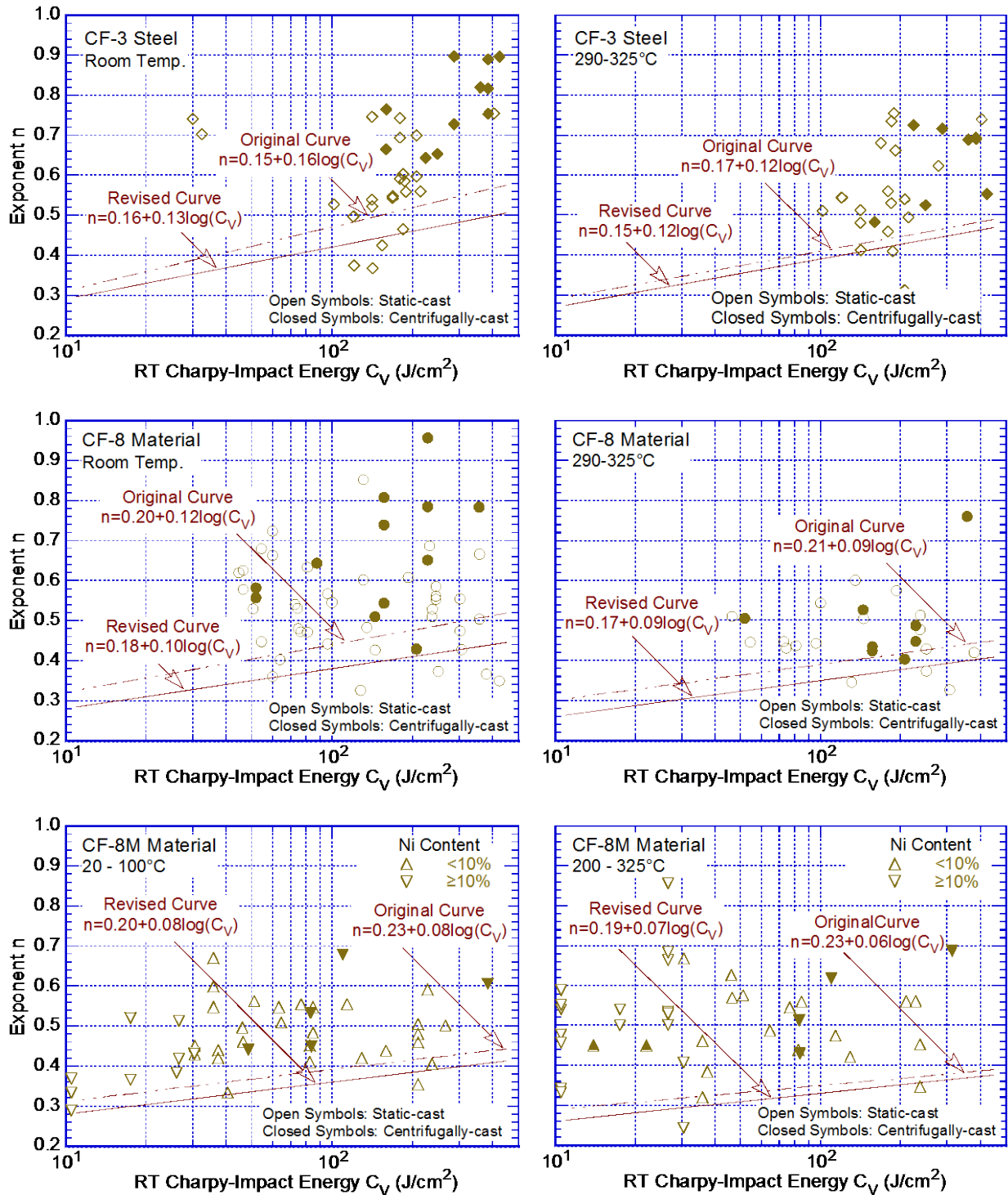


Figure 21. Correlation between the RT Charpy-impact energy and exponent n of the power-law J-R curve at RT and 290°C for CF-8M materials. The solid line bounds the existing data for exponent n as a function of RT Charpy-impact energy.

for CF-8 materials, it is

$$n = 0.18 + 0.10\log_{10}[C_V]; \quad (40)$$

and for CF-8M materials, it is

$$n = 0.20 + 0.08\log_{10}[C_V]. \quad (41)$$

For static-cast or centrifugally cast CASS materials, the exponent n at 290–320°C for CF-3 materials is

$$n = 0.15 + 0.12\log_{10}[C_V]; \quad (42)$$

for CF-8 materials, it is

$$n = 0.17 + 0.09 \log_{10}[C_V]; \quad (43)$$

and for CF-8M materials, it is

$$n = 0.19 + 0.07\log_{10}[C_V]. \quad (44)$$

Equations 27–44 may be used to determine the fracture toughness J-R curve of static- or centrifugally cast CF-3, CF-8, and CF-8M CASS materials from the RT Charpy-impact energy of the material. If the RT Charpy-impact energy is not known, then the saturation fracture toughness J-R curves for these CASS materials can be determined from their chemical composition available in the CMTRs using Eqs. 18–26 and Eqs. 27–44. The following observations can be drawn from this study of thermal embrittlement of CASS materials:⁴⁹

- (a) Among the grades considered, CF-8M materials have the smallest J_d value for a given crack extension. The value of J_d at a given crack extension for CF-8M materials is generally about half of that of the other grades.
- (b) CF-3, CF-3A, CF-8, and CF-8A materials show a similar extent of thermal aging. The value of J_d at a given crack extension for CF-8 and CF-8A materials is generally less than 10% lower than that for CF-3 and CF-3A materials.
- (c) Static-cast CASS materials are more susceptible to thermal aging than are the centrifugally cast materials. The value of J_d at a given crack extension for static-cast SS is generally about 20% lower than that for the centrifugally cast material with a similar ferrite content.
- (d) Although CF-8M materials show a similar extent of thermal aging on the fracture toughness J-R curve both at RT and at the reactor operating temperature, the value of J_d at a given crack extension for CF-3, CF-3A, CF-8, and CF-8A materials is generally about 20% lower at the reactor temperature than at RT.

These correlations are valid for static-cast and centrifugally cast CF-3, CF-3A, CF-8, CF-8A, and CF-8M materials defined by ASTM Specification A351. The criteria used in developing these correlations ensure that the estimated mechanical properties are adequately conservative for compositions of CASS materials within ASTM A351. The updated correlations are applicable to all compositions of CF-8M materials, including materials with ferrite contents above 25%. However, in the updated database, there were little or no fracture toughness J-R curve data for CF-3 and CF-8 materials with a C_{Vsat} of less than 30 J/cm² (17.7 ft-lb). Therefore, the correlations presented in this report may not be applicable to those compositions of CF-3

and CF-8 materials for which the estimated value of C_{Vsat} is less than 30 J/cm² (<17.7 ft-lb). Typically, such compositions would contain more than 30% ferrite. Furthermore, the correlations may not encompass all metallurgical factors that can arise from differences in production heat treatment or casting processes and may be overly conservative.

Note that these correlations account for the degradation of the mechanical properties of typical heats of CASS materials. They do not consider the initial fracture properties of the unaged material. Some CASS materials may have low initial fracture toughness, and the estimated J-R curves may be higher than the initial value. Therefore, some knowledge about the initial fracture toughness of the material is needed to justify the use of the estimated fracture toughness. The initial fracture toughness J-R curves may be estimated from the RT Charpy-impact energy of the unaged material.

Flaw tolerance methods are often used to develop ASME Code Section XI flaw acceptance standards or to justify alternatives to the ASME Code Section XI in-service inspection (ISI) requirements. Recently, EPRI Report 1019128 (December 2009),⁷⁸ presented a flaw tolerance approach based on elastic-plastic fracture mechanics considerations that could be used in combination with a demonstrated inspection method for managing the effects of the aging of CASS piping, particularly piping containing more than 20% ferrite content. The sources of the CASS data included (a) information obtained from a Westinghouse data search based on a random sampling of heats of CASS material from 15 plants (Table 3) and (b) data packages

Table 3. Primary circuit piping CASS material in Westinghouse plants (Ref. 78).

Plant Name	Size (MWe)	System Loops	Material Type
Beaver Valley 2	852	3	CF-8/CF-8A
Callaway 1	1157	4	CF-8/CF-8A
Catawba 1	1153	4	CF-8/CF-8A
Catawba 2	1153	4	CF-8/CF-8A
Comanche Peak 1	1150	4	CF-8/CF-8A
Farley 1	829	3	CF-8/CF-8A
Farley 2	829	3	CF-8/CF-8A
McGuire 1	1180	4	CF-8/CF-8A
McGuire 2	1180	4	CF-8/CF-8A
Millstone 3	1150	4	CF-8/CF-8A
North Anna 1	934	3	CF-8/CF-8A
North Anna 2	788	3	CF-8/CF-8A
South Texas 1	1250	4	CF-8/CF-8A
South Texas 2	1250	4	CF-8/CF-8A
Vogtle 1	1113	4	CF-8/CF-8A
Vogtle 2	1113	4	CF-8/CF-8A
Watts Bar 1	1177	4	CF-8/CF-8A
Watts Bar 2	1177	4	CF-8/CF-8A
Wolf Creek	1158	4	CF-8/CF-8A
Beaver Valley 1	852	3	CF-8M
Cook 1	1090	4	CF-8M
Cook 2	1054	4	CF-8M
Kewaunee	560	2	CF-8M
Prairie Island 2	530	2	CF-8M
Sequoyah 1	1140	4	CF-8M
Sequoyah 2	1140	4	CF-8M

from the Sandusky Foundry and Machine Co., NUREG/CR-5024, and Structural Integrity Associates. The CASS data were used to estimate the ferrite contents of a representative sample of CASS CF-3, CF-8, CF-8A, and CF-8M materials and to perform statistical analyses to study the distribution of the ferrite contents of these materials. When information for the Mo and N contents was not available, values of 0.5 and 0.04 (wt.%), respectively, were assumed.

The results yielded mean ferrite content and standard deviation values of 15.9% and 4.9% for CF-8 material (total of 333 data points) and 17.6% and 5.4% for CF-8M material (total of 147 data points). The total amounts of data for CF-3 were too small (fewer than 15 data points) to provide meaningful estimates. The distribution of the ferrite content for CF-8M materials (Fig. 22) indicated that nearly 9% of the heats of CF-8M material contained more than 25% ferrite. Therefore, the updated correlations presented in this report would be applicable to these heats of CF-8M material that are currently used in the U.S. PWRs. The expressions presented in Eqs. 27–38 are valid for CF-3, CF-8, and CF-8M materials with ferrite contents of up to 40%.

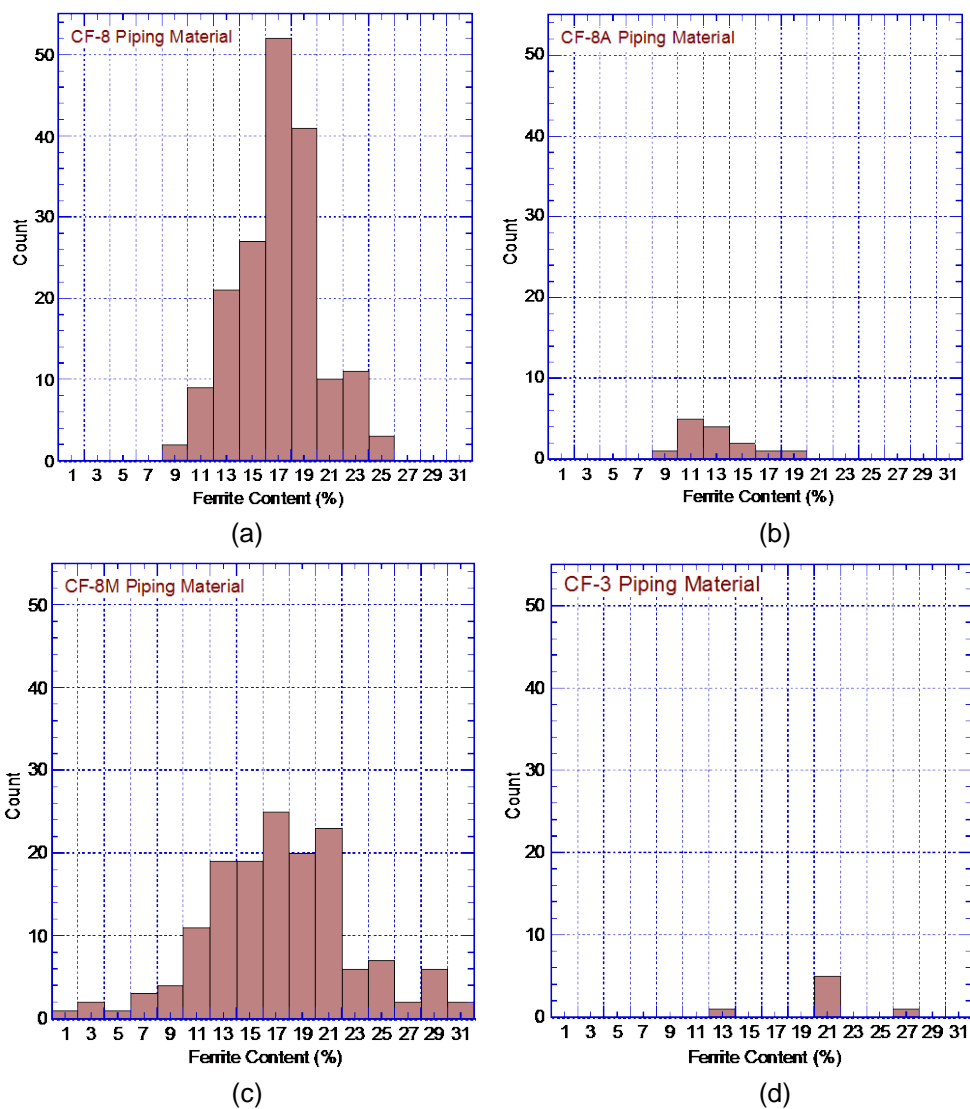


Figure 22. Distribution of ferrite content in CASS grades of (a) CF-8, (b) CF-8A, (c) CF-8M, and (d) CF-3 piping material in Westinghouse PWRs (Ref. 78).

2.4.3.1 Potential Effects of Reactor Coolant Environment

The potential effects of a simulated BWR primary coolant environment on the fracture toughness of sensitized Type 304 SS at 98 and 288°C were investigated by Nakajima et al. at displacement rates of 0.5, 0.01, and 0.001 mm/min.⁷⁹ The fracture toughness J-R curve tests at 98°C were conducted in air-saturated water, and the tests at 288°C were conducted in water containing 0.2 parts per million (ppm) or 8 ppm dissolved oxygen (DO). Three-point-bend specimens were used for the tests at 98°C and 1-T compact tension specimens at 288°C. The specimens were sensitized by being heat-treated at 650°C for 0.5, 1, 2, and 4 h; heat treatment for 2 h at 650°C was considered the standard sensitized condition. The experimental fracture toughness J-R curves at 98 and 288°C for several displacement rates in air and water environments are shown in Fig. 23. The results indicate no effect of displacement rate for the as-received Type 304 SS. However, for the sensitized material in water environment, the fracture toughness J decreased with a decreasing displacement rate and an increasing degree of sensitization. At 288°C, the effect of the water environment increased with an increasing DO in the environment. The fracture toughness J-R curves obtained at a 0.01 mm/min extension rate are representative of a typical fracture toughness J-R curve test. In the ANL studies on CASS materials, the J-R curve tests were conducted at an extension rate of about 0.02 mm/min.

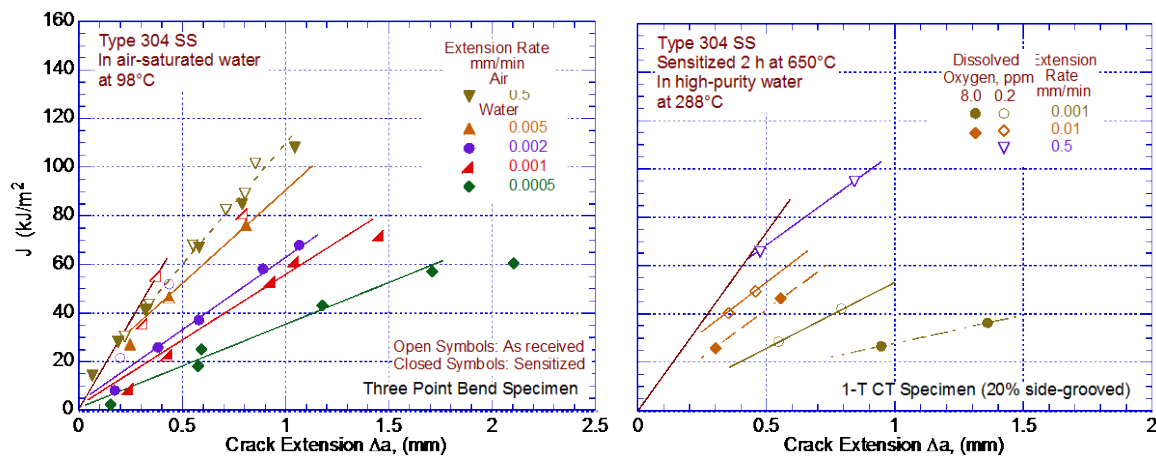


Figure 23. Fracture toughness J-R curves for sensitized Type 304 SS in simulated BWR coolant at 288°C and three different displacement rates (Ref. 79).

Potential effects of reactor coolant environment on fracture toughness have also been studied at ANL for neutron-irradiated wrought and cast austenitic SSs.⁴⁷ The results indicate that the effect of the environment may be insignificant for materials with poor fracture toughness (e.g., irradiated SSs or thermally aged CASS materials with J_{IC} values below 200 kJ/m²). However, a recent scoping study on low-temperature crack propagation (LTCP) for thermally aged CASS CF-8 material in PWR environments showed that the fracture toughness J-R curve is generally lower in PWR water than in air, and it is significantly lower in PWR shutdown water chemistry at 54°C than in air.⁸⁰ Fracture toughness J-R curve tests were conducted in air on 1-T CT specimens of CF-8 material (ANL Heat 68) that was thermally aged for about 138,000 h (about 15.8 years) at 350°C. The ferrite content calculated from Hull's equivalent factors was 15%; it was 23% when measured by a Feritescope. The specimens were either fatigue precracked in air at 54°C or were fatigue-plus-SCC precracked in PWR water at 315°C. The fracture toughness J-R curve data for these tests are shown in Fig. 24. Note that one of the specimens that was precracked in PWR water at 315°C was inadvertently tested at an elevated

temperature of 315°C in PWR primary water chemistry. The updated lower-bound J-R curve at RT for CF-8 material with 15–25% ferrite is also shown in the figure for comparison.

The results indicate that at 54°C, the J-R curve data in air are bounded, with an additional margin, by the updated lower-bound J-R curve. However, the J-R curve data for specimens precracked in air at 54°C and then tested in PWR shutdown water chemistry at 54°C are significantly below the lower-bound curve. The fractography of the test specimens show multiple fracture planes that are distinct from the primary plane established by the fatigue precrack. These results indicate an apparently large effect from the coolant environment on the fracture toughness; every material and test condition are identical for the two sets of duplicate tests, except one specimen is tested in air and the other in water. The specimens that are precracked in PWR water at 315°C and then tested in PWR water at 54°C or 315°C also show reduced fracture toughness relative to those tested in air, but the difference is less. The J-R curve data for the specimen that are cooled down from 315°C and tested at 54°C shutdown water chemistry are only marginally below the lower-bound J-R curve, and the data for the specimen that are precracked and tested at 315°C PWR primary water chemistry are slightly above the lower-bound curve.

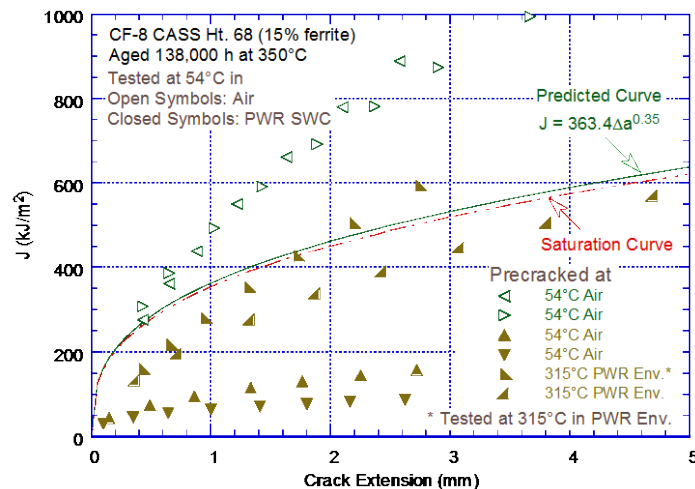


Figure 24. Fracture toughness J-R curve data for thermally aged Heat 68 of CF-8M plate at 54°C. The curve represents the lower bound curve at RT for static-cast CF-8 material (Ref. 80).

The large reduction in fracture toughness of the aged CASS CF-8 material is attributed to potential synergy between hydrogen embrittlement from LTCP and thermal embrittlement associated with decomposition of the ferrite at reactor temperatures.⁸⁰ The authors recommended that the multiple fracture paths during J-R curve testing should be examined to determine whether any microstructural features are associated with such behavior.

A similar low-fracture-toughness behavior has also been observed for Alloys 600 and 690 in hydrogenated water at 54°C and at low displacement rates (i.e., under quasi-static conditions).^{81,82} For Alloy 600, the J_{IC} value obtained at a displacement rate of 0.05 mm/h is 30% lower in hydrogenated water at 54–149°C than in air.⁸¹ For Alloy 690 tested in hydrogenated water at 54°C, the fracture toughness J_{IC} obtained at displacement rates of 0.005 to 15 mm/h is a factor of 16 lower than that observed at a displacement rate of 305 mm/h.⁸² The significant decrease in fracture toughness under a simulated PWR shutdown water chemistry has been attributed to hydrogen-induced intergranular cracking.

These results indicate that environment can further decrease the fracture toughness of materials relative to the fracture toughness obtained in air. For some heats of wrought and cast austenitic SSs and welds, some values of fracture toughness in coolant environments are likely to be below the lower-bound trend curve. In particular, the fracture toughness data for unirradiated, aged CF-8 material in a PWR SWC environment at 54°C are significantly lower because of the potential synergy between the hydrogen embrittlement and thermal embrittlement associated with the spinodal decomposition of the ferrite. However, it is not clear whether the large reduction in the fracture toughness of thermally aged CASS materials is unique and associated with PWR SWC conditions or it can occur under other low-temperature LWR environments. Therefore, the minimum acceptable fracture toughness J_{Ic} values for thermally aged CASS materials in LWR environments at temperatures less than 100°C are needed to establish the possible effects of LWR coolant environments on the thermal embrittlement of CASS materials.

2.4.3.2 Potential Effects of High Loading Rate

Typically, the fracture toughness of wrought SSs increases with increases in the loading rate. The limited data on the effect of the loading rate on the fracture toughness of CASS materials are somewhat inconsistent. Fracture toughness tests on a high-ferrite-content CF-3 material in the as-cast and aged conditions at three loading rates at RT and 300°C show no significant variation for the as-cast material with an increasing strain rate, either at RT or at 300°C.⁸³ However, for the RT tests on aged material, increasing the loading rate resulted in an increase in J_c but a decrease in the slope, dJ/da , of the J-R curve. The slowest loading rate was a quasi-static rate typical of J-integral testing. The second rate was approximately three orders of magnitude faster, and the highest rate was about one additional order of magnitude faster. Similarly, fracture toughness tests on CF-3M material (16% ferrite) aged for 1000 h at 500°C and tested at 0°C showed that increasing the loading rate reduced the crack initiation (J_{Ic}) as well as the slope of the J-R curve to about 18% of the values for quasi-static loading (Fig. 25).⁸⁴

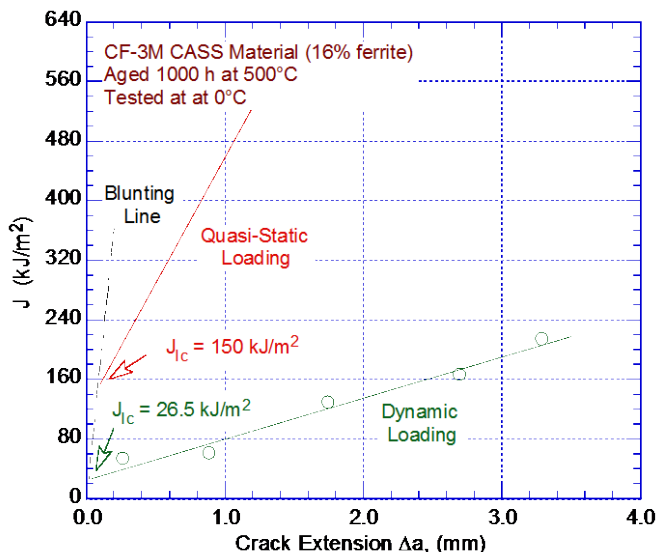


Figure 25. Fracture toughness J-R curves for thermally aged CF-3M at 0°C and quasi-static and dynamic loading rates (Ref. 84).

These limited data that indicate that an inverse loading rate affects the fracture toughness for thermally aged CASS materials need to be investigated further to determine the potential decrease in fracture toughness at loading rates that are associated with typical seismic activity.

2.5 Methodology for Estimating Thermal Embrittlement of CASS Materials

A flow diagram for estimating mechanical properties of CASS materials during reactor service is shown in Fig. 26. The estimation scheme is divided into three sections based on available material information. In Section A of the flow diagram, “predicted lower-bound” fracture toughness is defined for CF-3, CF-8, and CF-8M materials of unknown composition (i.e., when CMTR is not available). For materials with an unknown composition, when the ferrite content of the steel is known, a different lower-bound fracture toughness and impact energy are defined for materials containing <10%, >10–15%, >15–20%, >25–30%, or >30–40% ferrite. However, as discussed earlier in Section 2.2, it is important to make sure that the value of the ferrite content used in the estimation scheme is representative of the material.

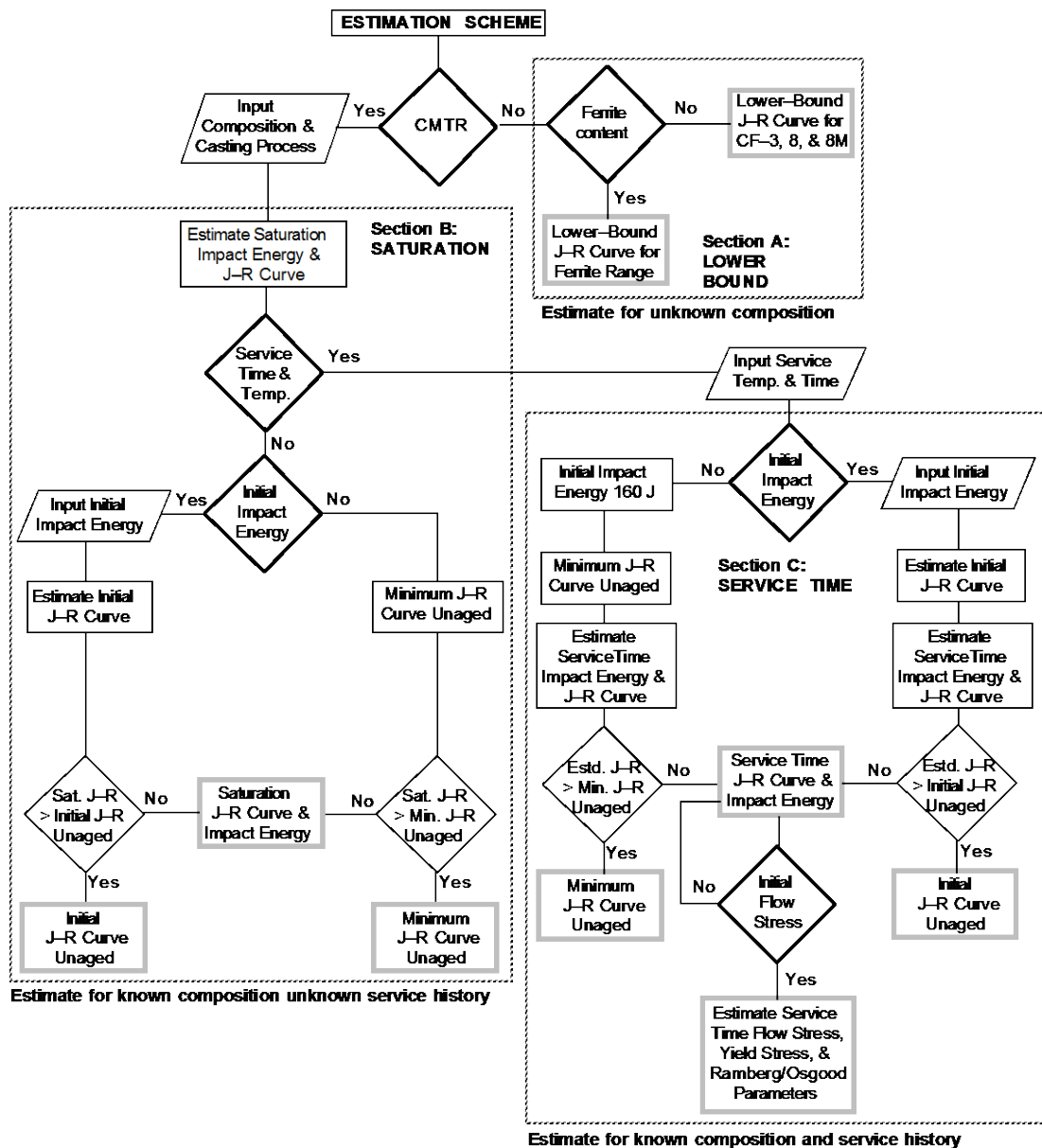


Figure 26. Flow diagram for estimating mechanical properties of thermally aged CASS materials in LWR systems.

Sections B and C of the flow diagram describe the methodology for estimating mechanical properties when a CMTR is available (i.e., the chemical composition of the CASS material is known). Section B describes the estimation of the “saturation” impact energy and fracture toughness J-R curve. The only information needed for these estimates is the chemical composition of the material, which is used to estimate the saturation J-R curve for the thermally aged material. However, the correlations presented in this report account for the degradation of mechanical properties due to thermal aging; they do not explicitly consider the initial fracture properties of the unaged material. Some heats of CASS materials may be inherently weak and have poor fracture properties in the unaged condition. For such materials, the estimated saturation fracture toughness based on the proposed methodology may be higher than the fracture toughness of the unaged material. Therefore, it is important to have some information about the fracture toughness of the unaged material. The material fracture toughness is generally not available in the CMTR. It can be estimated by using the expressions presented in Fig. 19 from the initial RT Charpy-impact energy of the unaged material, if known.

The available fracture toughness J-R curve data at 290–320°C (554–608°F) for unaged CASS materials are shown in Fig. 27a and the J-R curves for several heats of wrought Type 304 and 316 SSs^{19,77,85–88} are shown in Fig. 27b. The results indicate that the J-R curves for a few “weak” heats of static-cast CASS materials are lower than for wrought austenitic SSs. Therefore, the saturation fracture toughness properties that should be used for design analyses for thermally aged CASS materials depend on whether or not the estimated saturation fracture toughness is lower than the initial fracture toughness of the unaged materials. The initial fracture toughness of the material can be estimated from its RT Charpy-impact energy.

However, the fracture toughness of the CASS material is not available in CMTRs. Two different options are used to establish the saturation fracture toughness of the thermally aged material. In the first option, the initial RT Charpy-impact energy of the unaged material is known, and this value is used to estimate the initial fracture toughness of the material. CASS materials with poor fracture properties are relatively insensitive to thermal aging, and the fracture toughness of the material due to thermal aging during reactor service typically does not change significantly.

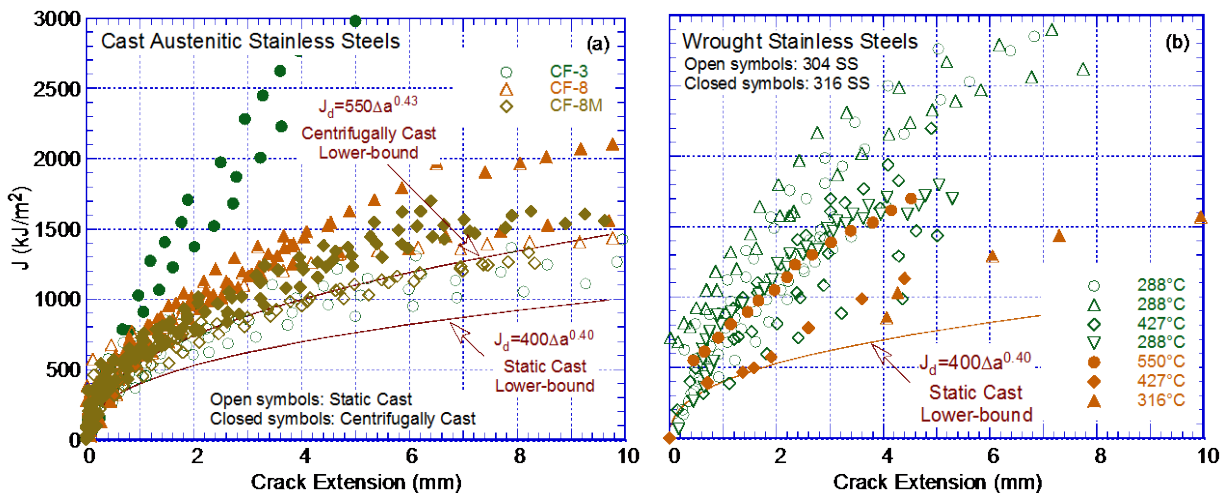


Figure 27. Predicted and measured fracture toughness J-R curves for unaged materials (a) CASS at 290–320°C and (b) wrought austenitic SSs at various temperatures (Refs. 19,77,85–88).

Therefore, if the estimated saturation fracture toughness of the aged material is higher than the fracture toughness of the unaged material, the latter is used as the worst-case toughness for that material.

In the second option, the initial RT Charpy-impact energy is not known; therefore, the minimum fracture toughness of all unaged heats and heat treatment conditions for CASS materials is used as an upper bound for the estimated fracture toughness. This minimum upper-bound fracture toughness of unaged CASS materials is used as the worst-case fracture toughness for the material if the estimated saturation fracture-toughness of thermally aged material is higher. Typically, the fracture toughness of unaged CASS materials is slightly higher at RT than it is at 290–320°C. However, for convenience, the minimum fracture toughness of unaged static-cast CASS materials at temperatures between RT and 320°C can be expressed as

$$J_d = 400[\Delta a]^{0.40}, \quad (45)$$

and that of centrifugally cast CASS materials can be expressed as

$$J_d = 550[\Delta a]^{0.43}. \quad (46)$$

Based on the recent data from Japan, the lower-bound J-R curve for unaged centrifugally cast material has been decreased relative to the original curve in NUREG/CR-4513, Rev. 1. The estimation of mechanical properties at any given time and temperature of service (i.e., service time properties) is described in Section C of the flow diagram. The initial impact energy of the unaged material is required for these estimates. If this is not known, the initial impact energy of 200 J/cm² (118 ft-lb) is assumed. However, similar to the procedure in Section B of the flow diagram, the initial fracture toughness of the unaged material or the minimum fracture toughness of unaged CASS materials is used as an upper bound for the estimates.

The methodology for estimating fracture toughness of thermally aged CASS materials presented in this report can be used to estimate the fracture toughness J-R curves at RT (25°C) or reactor temperatures (290–320°C). Fracture toughness J values at temperatures between 25 and 290°C can be obtained from a linear interpolation of the values at 25 and 290°C (77 and 608°F).

The initial tensile properties of the unaged material are needed for estimating the tensile strength and Ramberg/Osgood strain hardening parameters. If the initial flow stress of the CASS material is known, the J_{Ic} value and tearing modulus of the thermally aged material can then be determined from the estimated values of the J-R curve and flow stress of the aged material.

However, as mentioned earlier, the above methodology for estimating fracture toughness of CASS materials in reactor service is not applicable to CF-8M materials that have more than a trace amount of Nb. The chemical requirements for ASTM Specification A351 or A451 do not specify any upper limit for Nb. Typically, CF-8M steels contain only trace amounts of Nb. However, the Nb content could be high in castings produced by using Type 347 scrap metal. For example, in the ANL study, the measured RT Charpy-impact energy of a thermally aged heat of CF-8M steel containing about 23% ferrite and 0.2% Nb was significantly lower than that predicted from the above methodology. The fracture surface of the Charpy specimen showed that the phase boundaries were decorated with large Nb carbide particles that cracked easily. Therefore, for CF-8M materials with more than 15% ferrite, it would be advisable to determine the Nb content of the material and take appropriate actions if that content is 0.1% or higher.

The above methodology only accounts for the thermal embrittlement of CASS materials and is therefore applicable to materials outside the reactor core. It does not consider the effects of neutron embrittlement or the synergism between thermal and neutron embrittlement. For core internal components, which have a prolonged exposure both to elevated temperatures and to neutron radiation, the combined effects of thermal and neutron irradiation need to be evaluated. An acceptable approach for estimating the fracture toughness of CASS materials used in the reactor core is presented in Section 5 of this report.

3 ASSESSMENT OF THERMAL EMBRITTLEMENT

3.1 Estimation of Thermal Embrittlement of CASS Materials of Known Composition and Service Condition – Service Time Values

The RT Charpy-impact energy of a specific CASS material as a function of service time and temperature can be obtained from estimated C_{Vsat} (Eqs. 3–5 and 18–26) and the kinetics of embrittlement (Eqs. 11,13–17). A value of 2.9 for θ was assumed for all thermal aging conditions. The initial Charpy-impact energy, C_{Vint} , of the unaged steel is also needed for estimating the decrease in impact energy. If this is not known, a typical value of 200 J/cm² (118 ft-lb) is assumed. The RT Charpy-impact energy observed experimentally and that estimated from the chemical composition and initial impact energy of the CASS materials are presented in Figs. 19 and 20 of NUREG/CR-4513, Rev. 1. For convenience, these figures in NUREG/CR-4513 Rev. 1 are reproduced in Appendix B of this report.

The results indicated that in general, the estimates of RT Charpy-impact energy at aging temperatures of $\leq 330^{\circ}\text{C}$ ($\leq 626^{\circ}\text{F}$) were either accurate or conservative for all grades of CASS materials. A few heats showed poor agreement because either the estimated C_{Vsat} was higher than the experimental value (FRA Heat D and ANL Heat 47) or the estimated activation energy was high (FRA Heat C and GF Heat 278). Even at 350°C , because the θ values for most of the heats were either greater than or only slightly lower than 2.9, the estimated values of RT Charpy-impact energy showed good agreement with the experimental results. The EPRI heat and an EdF heat (experimental θ is 2.1 for both heats) alone show nonconservative estimates, at 350°C . Therefore, to ensure that the estimates are conservative, a θ value of 2.5 rather than 2.9 should be used at $330\text{--}360^{\circ}\text{C}$ ($626\text{--}680^{\circ}\text{F}$).

Once the RT Charpy-impact energy, C_V , is known, the service-time coefficient C and exponent n of the fracture toughness J-R curve are determined from Eqs. 27–38 and 39–44, respectively. The variation in the experimental values of coefficient C as a function of aging time and temperature is compared with that estimated from the methodology proposed in this report (i.e., material composition and the initial RT Charpy-impact energy) for at least one heat each of CF-3, CF-8, and CF-8M material in Figs. 28–31. As discussed earlier for the estimated values of RT Charpy-impact energy, the results indicate that at reactor operating temperatures (i.e., $280\text{--}350^{\circ}\text{C}$), the estimated change in the fracture toughness coefficient C with the aging time is either accurate or slightly conservative for all grades of CASS material.

The methodology and expressions for estimating the changes in (a) tensile flow and yield stresses and (b) the engineering stress-strain curve of CASS materials, as a function of time and temperature of service are described in NUREG/CR-6142.¹⁸ The tensile properties of aged CASS materials are determined from known material information (i.e., chemical composition and initial tensile strength of the steel). The fracture toughness J_{Ic} values for the service-aged CASS material can be determined from the estimated values of the fracture toughness J-R curve and flow stress.

The proposed methodology can be used to estimate the change in fracture toughness of CASS materials for known material composition and service conditions, particularly for service temperatures of $280\text{--}350^{\circ}\text{C}$ ($536\text{--}662^{\circ}\text{F}$). Examples of experimental and estimated fracture toughness J-R curves for several CF-3, CF-8, and CF-8M materials thermally aged for 30,000 h at 350°C or for 50,000 or 53,000 h at 320°C are shown in Figs. 32–38. Relative to the experimental results, the estimated J-R curves are either accurate or slightly conservative.

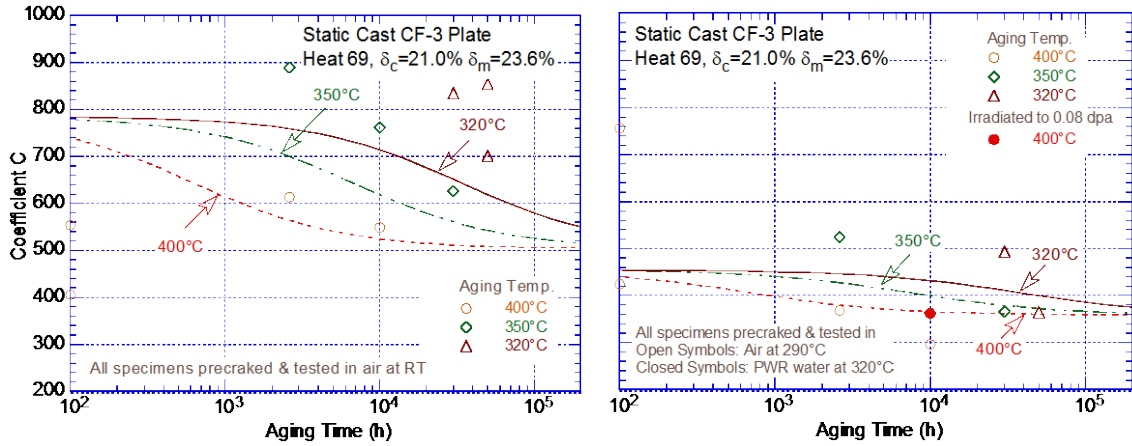


Figure 28. Estimated and experimental values of coefficient C of the J-R curve for static-cast CF-3 plate during thermal aging. Values at 100 h are for unaged material.

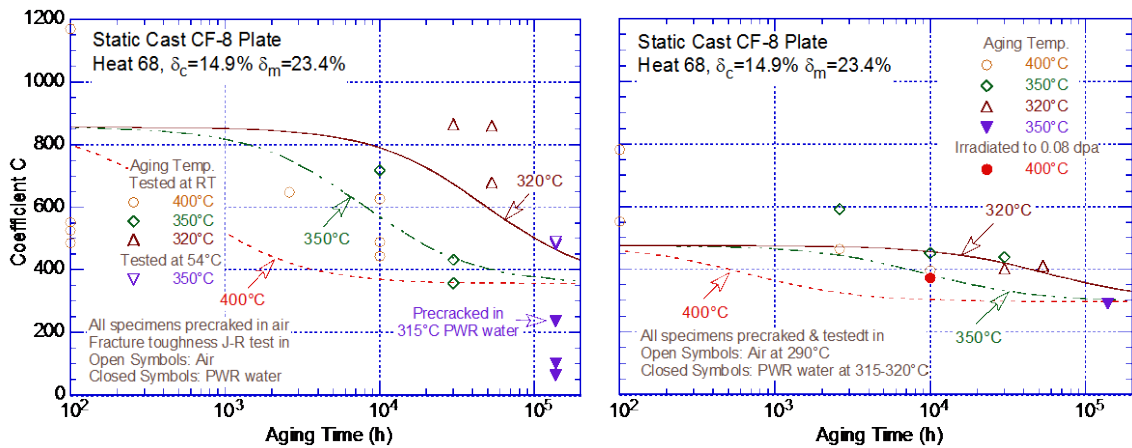


Figure 29. Estimated and experimental values of coefficient C of the J-R curve for static-cast CF-8 plate during thermal aging. Values at 100 h are for unaged material.

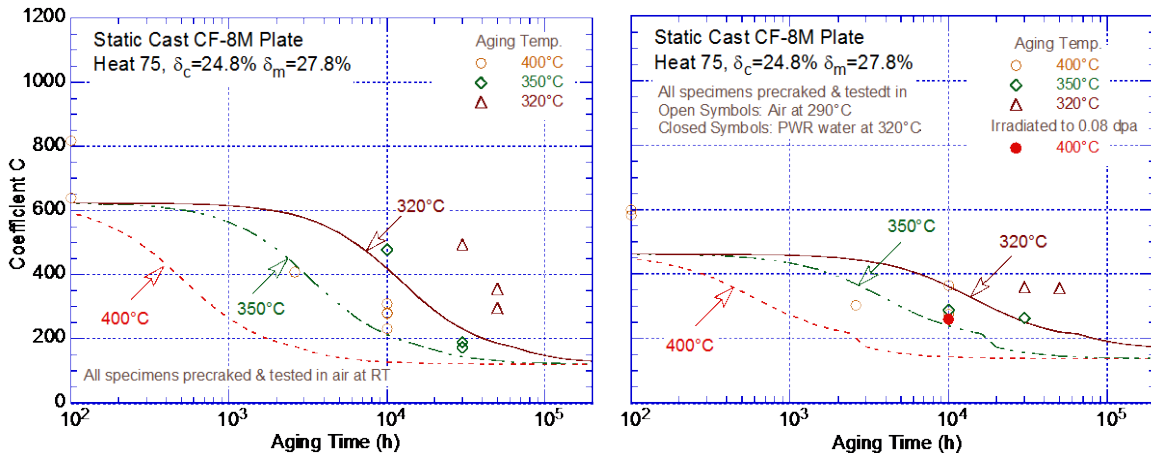


Figure 30. Estimated and experimental values of coefficient C of the J-R curve for static-cast CF-8M plate during thermal aging. Values at 100 h are for unaged material.

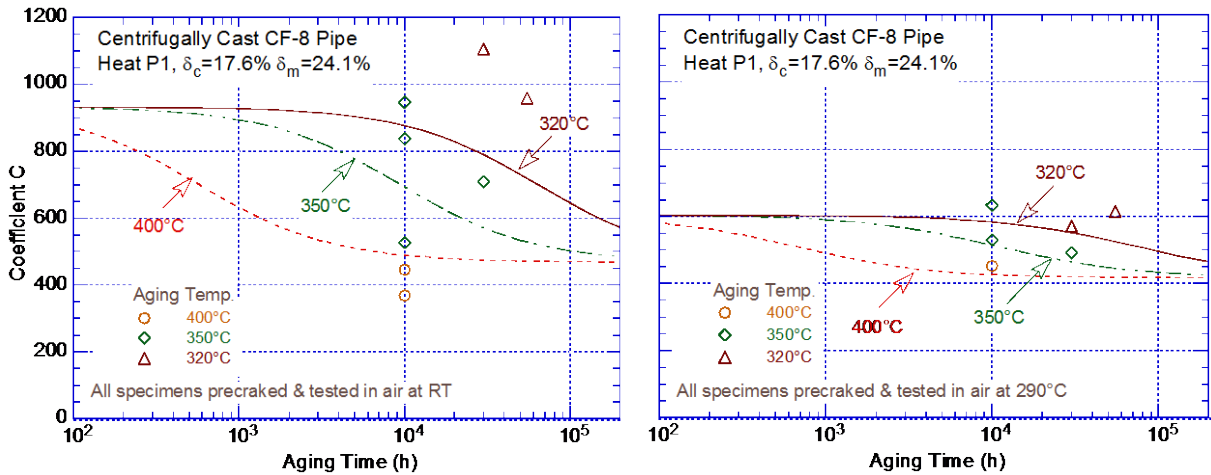


Figure 31. Estimated and experimental values of coefficient C of the J-R curve for centrifugally cast CF-8 pipe during thermal aging. Values at 100 h are for unaged material.

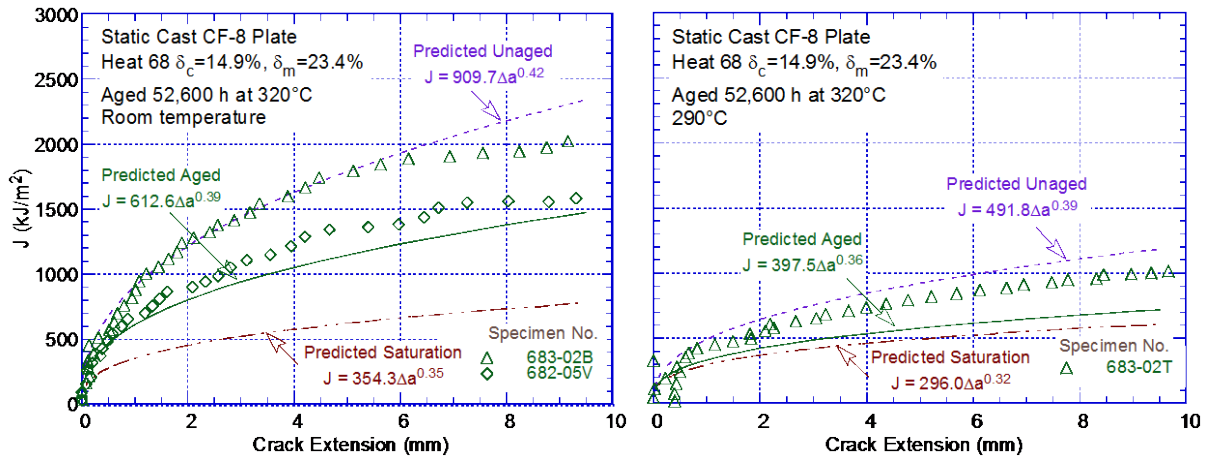


Figure 32. Experimental and estimated fracture toughness J-R curves at RT and 290°C for an ANL heat of a static cast CF-8 plate.

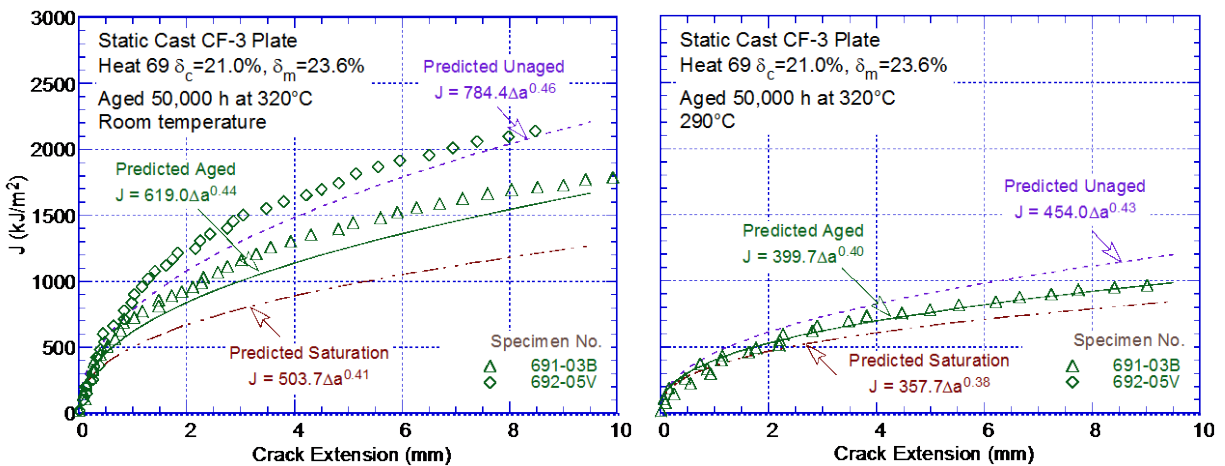


Figure 33. Experimental and estimated fracture toughness J-R curves at RT and 290°C for an ANL heat of a static cast CF-3 plate.

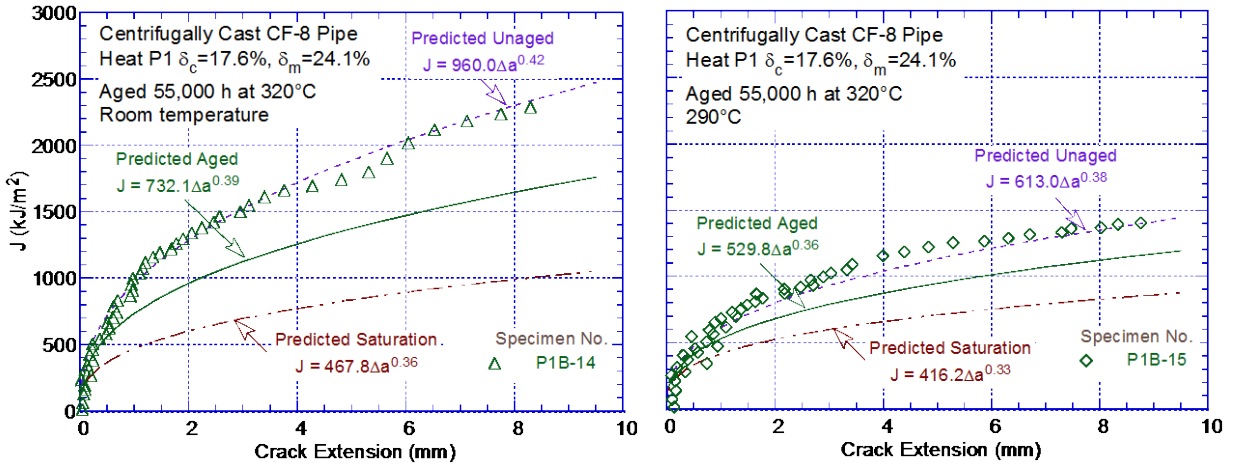


Figure 34. Experimental and estimated fracture toughness J-R curves at RT and 290°C for an ANL heat of a centrifugally cast CF-8 pipe.

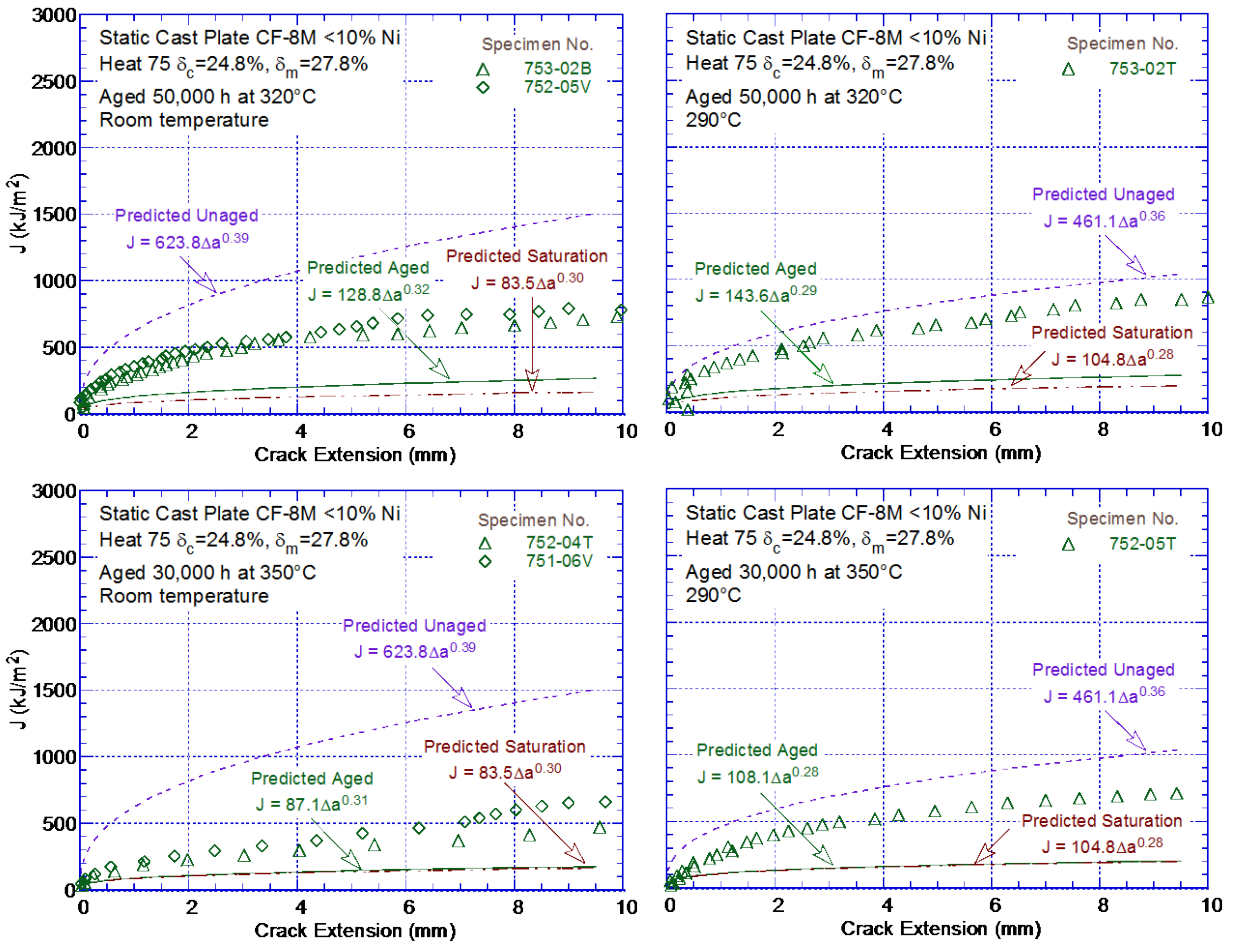


Figure 35. Experimental and estimated fracture toughness J-R curves at RT and 290°C for an ANL heat of a static cast CF-8M plate.

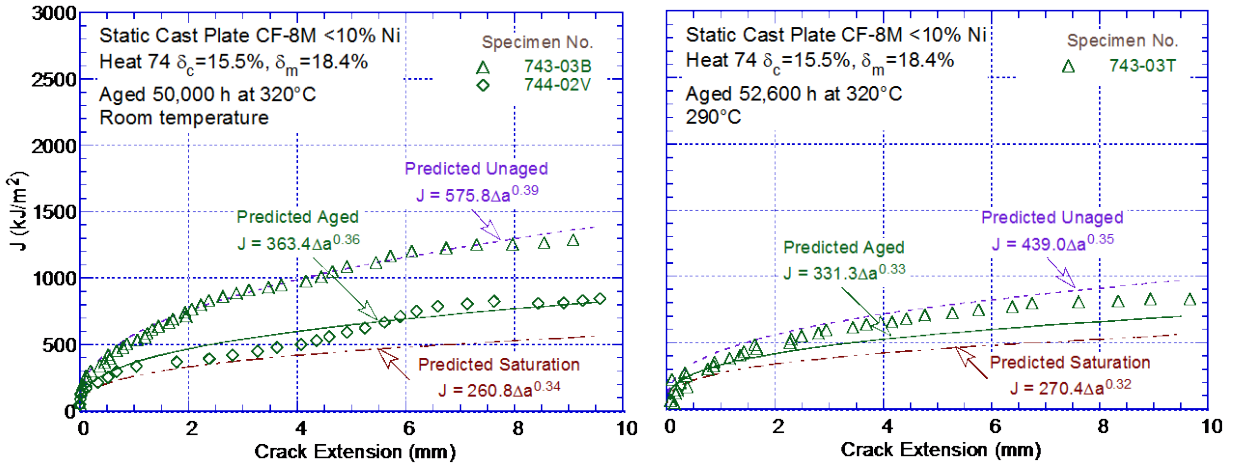


Figure 36. Experimental and estimated fracture toughness J-R curves at RT and 290°C for an ANL heat of a static cast CF-8M plate.

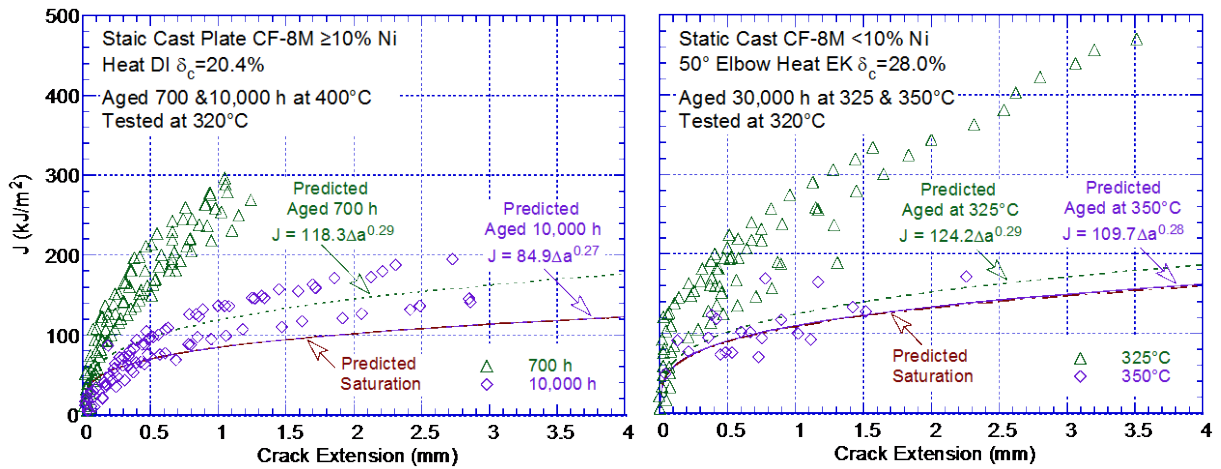


Figure 37. Experimental and estimated fracture toughness J-R curves at RT and 290°C for an EdF heats of a static cast CF-8M plate (Ht. DI) and a 50° elbow.

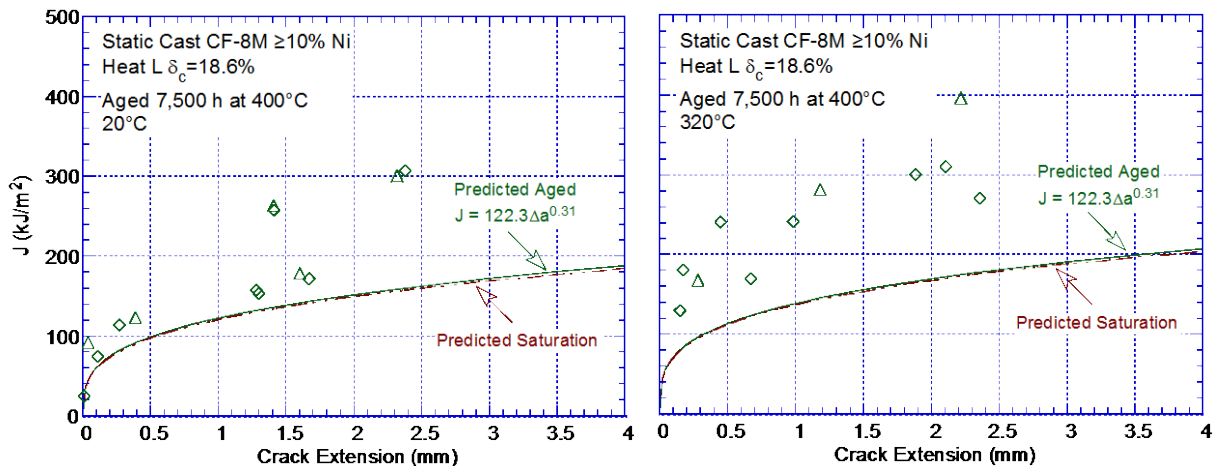


Figure 38. Experimental and estimated fracture toughness J-R curves at RT and 290°C for a MHI heat of a static cast CF-8M pipe.

3.2 Estimation of the Thermal Embrittlement of CASS Materials of Unknown Composition: Lower-Bound Values

The ANL methodology provides the expressions for estimating fracture toughness J-R curves of unaged and aged CASS materials as a function of the estimated RT Charpy-impact energy; which, in turn, is determined from the a material parameter that depends on the chemical composition and ferrite content of the material. However, for convenience, lower bound J-R curves are defined as a function of ferrite content in the CASS material. These curves bound at least 95% of the data. The fracture toughness J-R curve is defined by the power-law relationship $J_d = C\Delta a^n$, where J_d is deformation J per ASTM Specifications E 813-85 and E 1152-87, Δa is a crack extension, and C and n are constants. The coefficient C and exponent n for the lower-bound fracture toughness J-R curve are determined from the bounding value of C_{Vsat} for a range of ferrite contents in the CASS material.

First the bounding values of the saturation RT Charpy-impact energy, C_{Vsat} , for ferrite contents <10%, >10–15%, >15–20%, >20–25%, >25–30%, and >30–40% are established for each grade of CASS material from the plots of estimated C_{Vsat} and ferrite content, as shown in Fig. 39. The

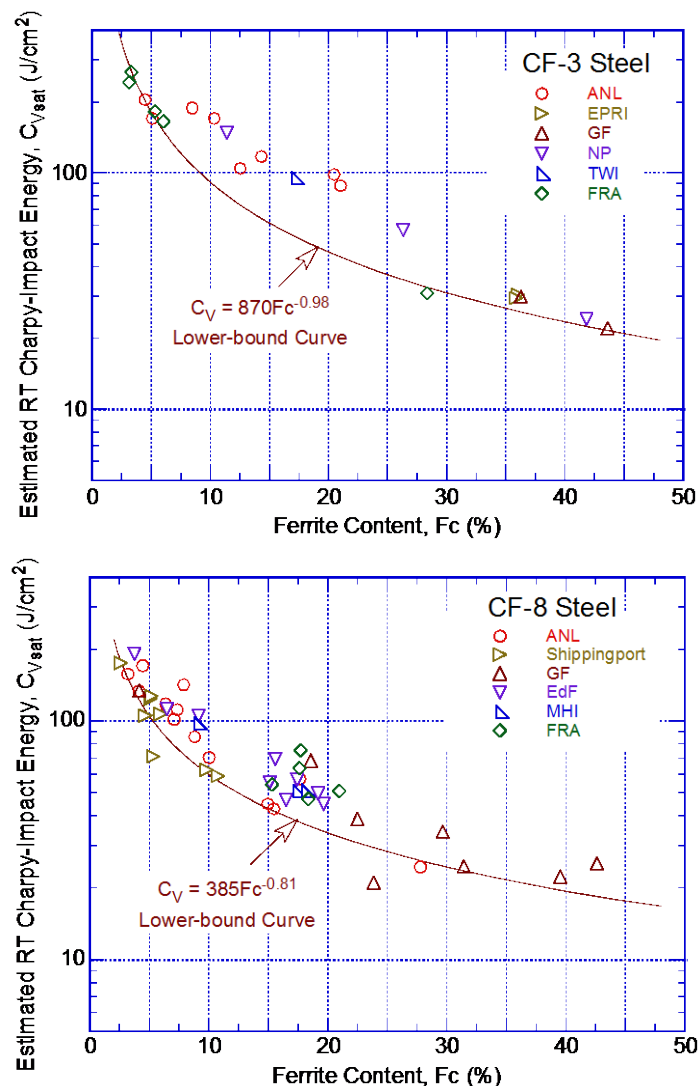


Figure 39. Correlation between saturation RT Charpy-impact energy and ferrite content.

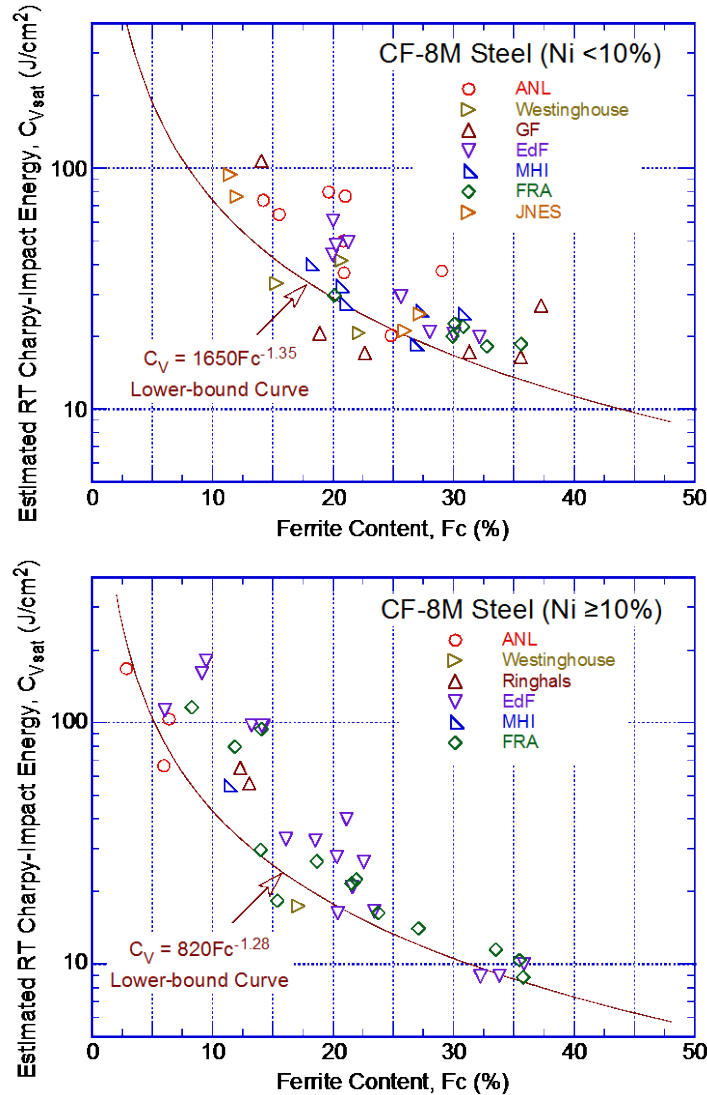


Figure 39. (Contd.)

RT C_{Vsat} for the different grades of CASS materials is the lower value determined from the sets of expressions given in Eqs. 18–26. Separate expressions are proposed for CF-8M materials containing <10% Ni and those containing $\geq 10\%$ Ni. The latter are most susceptible to thermal embrittlement than the other grades.

Note that the estimated and not measured value of RT Charpy-impact energy is used in this methodology because a value that is representative of a casting would require tests on several specimens taken from different portions of the casting. This may not be always possible. The estimated C_{Vsat} and the corresponding values of coefficient C and exponent n of the J-R curve at RT and 290–320°C (550–608°F) for CF-3, CF-8, and CF-8M with <10 and $\geq 10\%$ Ni and various ranges of ferrite content are listed in Table 4. The estimated lower-bound J-R curves at RT and at 290–320°C for some of the ferrite ranges, are shown in Figs. 40 and 41, respectively, for static-cast materials, and in Figs. 42 and 43, respectively, for centrifugally cast material. These plots are updated versions of Figs. 3 and 4 of NUREG/CR-4513, Rev. 1.¹⁶ The lower-bound fracture toughness J-R curves can be used for completely embrittled CASS materials of unknown composition.

Table 4. The lower-bound J-R curve at RT and 290–320°C for aged CASS materials.

Material Grade	Estimated C_{Vsat} (J/cm ²)	Static Cast Material				Centrifugally Cast Material			
		Room Temp.		290–320°C		Room Temp.		290–320°C	
		C	n	C	n	C	n	C	n
<i>Ferrite Content >30–40%</i>									
CF-3/CF-3A	27	270	0.35	256	0.32	314	0.35	336	0.32
CF-8/CF-8A	22	242	0.31	241	0.29	282	0.31	317	0.29
CF-8M (Ni <10%)	14	49	0.29	71	0.27	60	0.29	89	0.27
CF-8M (Ni ≥10%)	9	27	0.27	46	0.26	33	0.27	57	0.26
<i>Ferrite Content >25–30%</i>									
CF-3/CF-3A	31	292	0.35	267	0.33	340	0.35	351	0.33
CF-8/CF-8A	24	259	0.32	250	0.30	301	0.32	328	0.30
CF-8M (Ni <10%)	17	65	0.30	87	0.28	80	0.30	109	0.28
CF-8M (Ni ≥10%)	11	35	0.28	55	0.26	43	0.28	69	0.26
<i>Ferrite Content >20–25%</i>									
CF-3/CF-3A	37	321	0.36	281	0.34	373	0.36	369	0.34
CF-8/CF-8A	28	279	0.33	260	0.30	325	0.33	342	0.30
CF-8M (Ni <10%)	21	90	0.31	111	0.28	111	0.31	139	0.28
CF-8M (Ni ≥10%)	13	47	0.29	70	0.27	59	0.29	87	0.27
<i>Ferrite Content >15–20%</i>									
CF-3/CF-3A	46	360	0.38	298	0.35	418	0.38	392	0.35
CF-8/CF-8A	34	307	0.33	274	0.31	357	0.33	360	0.31
CF-8M (Ni <10%)	29	135	0.32	149	0.29	167	0.32	187	0.29
CF-8M (Ni ≥10%)	18	70	0.30	92	0.28	86	0.30	115	0.28
<i>Ferrite Content >10–15%</i>									
CF-3/CF-3A	61	416	0.39	323	0.36	484	0.39	424	0.36
CF-8/CF-8A	43	346	0.34	292	0.32	403	0.34	384	0.32
CF-8M (Ni <10%)	43	198	0.33	228	0.30	247	0.33	266	0.30
CF-8M (Ni ≥10%)	26	115	0.31	132	0.29	142	0.31	166	0.29
<i>Ferrite Content <10%</i>									
CF-3/CF-3A	91	512	0.41	361	0.39	595	0.41	474	0.39
CF-8/CF-8A	60	411	0.36	320	0.33	478	0.36	421	0.33
CF-8M (Ni <10%)	74	285	0.35	286	0.32	357	0.35	332	0.32
CF-8M (Ni ≥10%)	43	199	0.33	229	0.30	249	0.33	267	0.30

3.3 Screening Criteria for Susceptibility of CASS Materials to Thermal Embrittlement

An EPRI report on the thermal aging embrittlement of CASS components proposed using the J value at a crack extension of 2.5 mm (0.1 in.), $J_{2.5}$, to differentiate between nonsignificant and potentially significant reductions in the fracture toughness of thermally aged CASS materials.⁵⁰ Flaw tolerance evaluations were presented in Appendices A and B of the EPRI report to support the choice of a threshold value of $J_{2.5} = 255 \text{ kJ/m}^2$ (1456 in.-lb/in.²). The NRC staff found that the use of $J_{2.5} = 255 \text{ kJ/m}^2$ as a screening approach for the fracture toughness of CASS materials is acceptable.⁵¹ The screening criteria to determine the susceptibility of CASS components to thermal aging embrittlement are outlined in Table 1.⁵¹

The expressions presented in Fig. 39 and the methodology described in Section 2.4.3 for estimating the corresponding fracture toughness J-R curve for the RT Charpy-impact energy trend curves in Fig. 39 can be used to check the validity of the ferrite content criteria given in

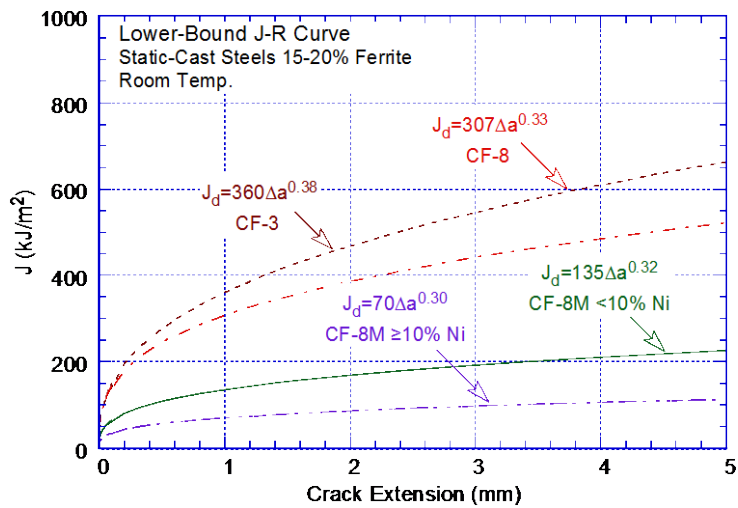
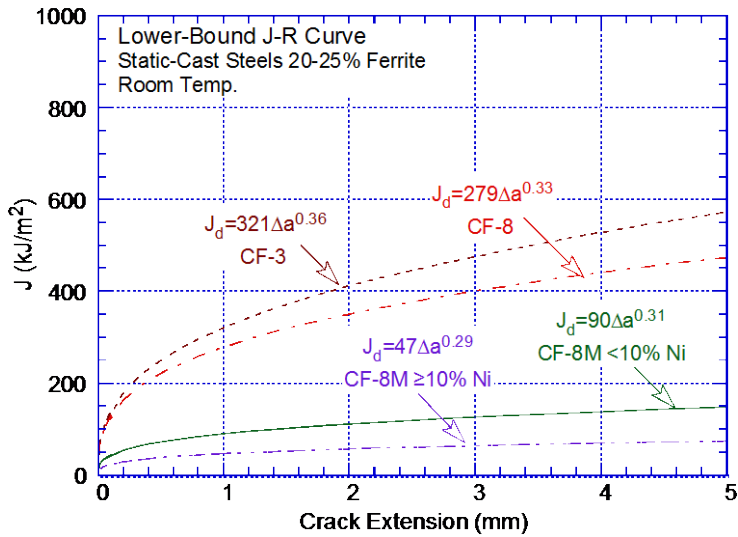
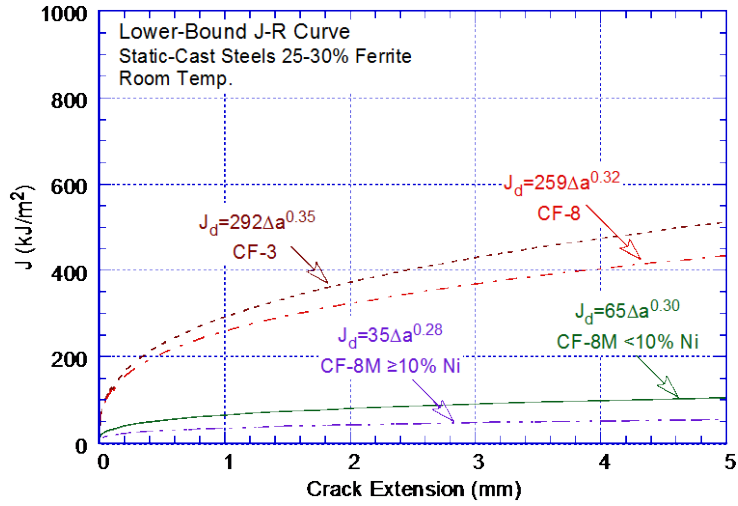


Figure 40. Estimated lower-bound J-R curves at RT for static-cast CASS materials with ferrite contents of >25–30%, >20–25%, and >15–20%.

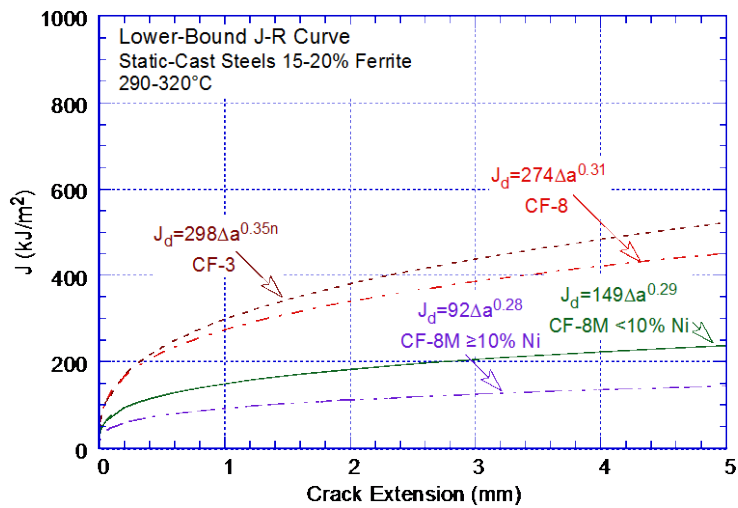
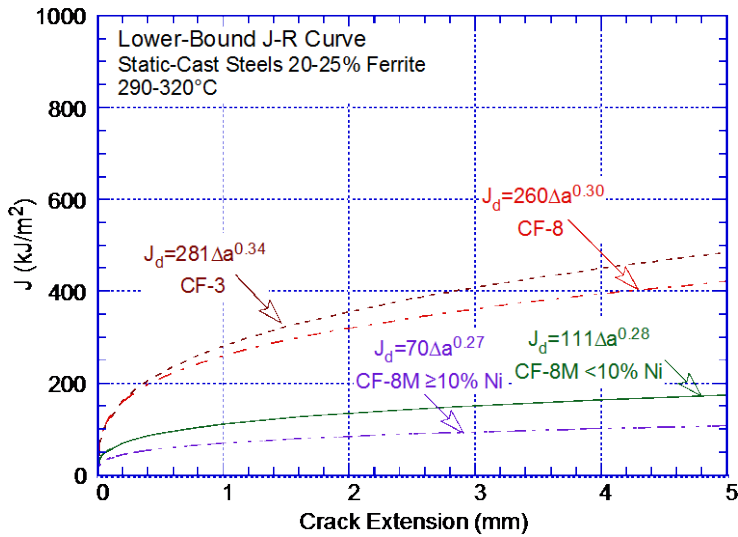
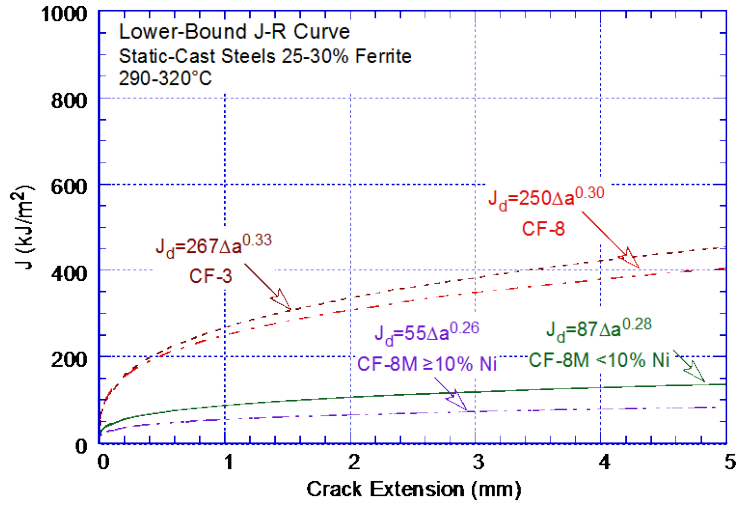


Figure 41. Estimated lower-bound J-R curves at 290–320°C for static-cast CASS materials with ferrite contents of >25–30%, >20–25%, and >15–20%.

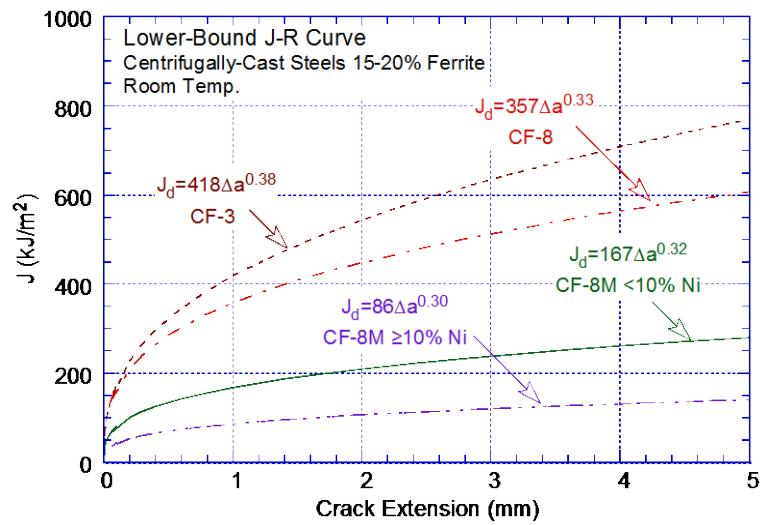
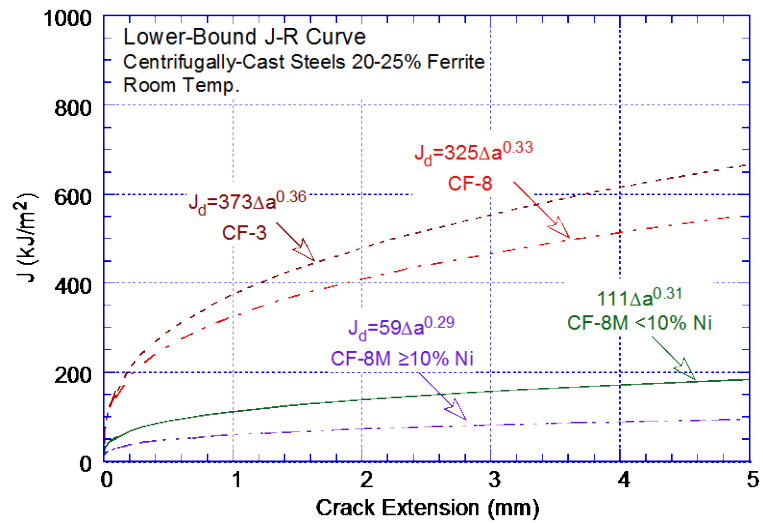
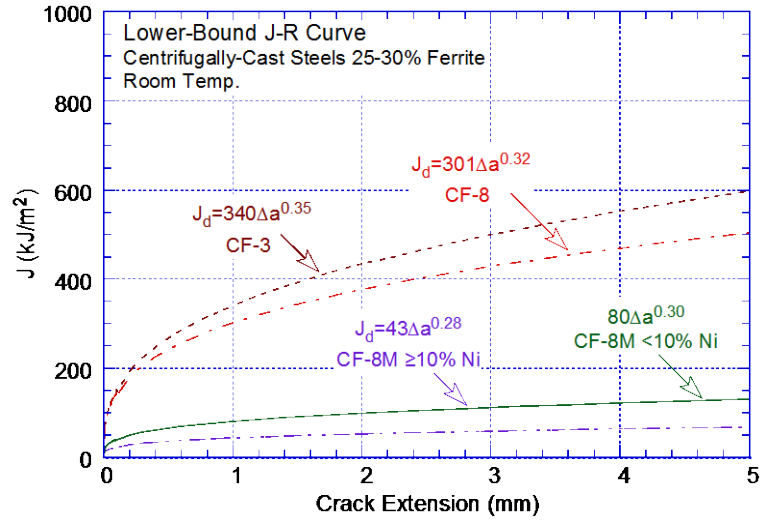


Figure 42. Estimated lower-bound J-R curves at RT for centrifugally cast CASS materials with ferrite contents of >25–30%, >20–25%, and >15–20%.

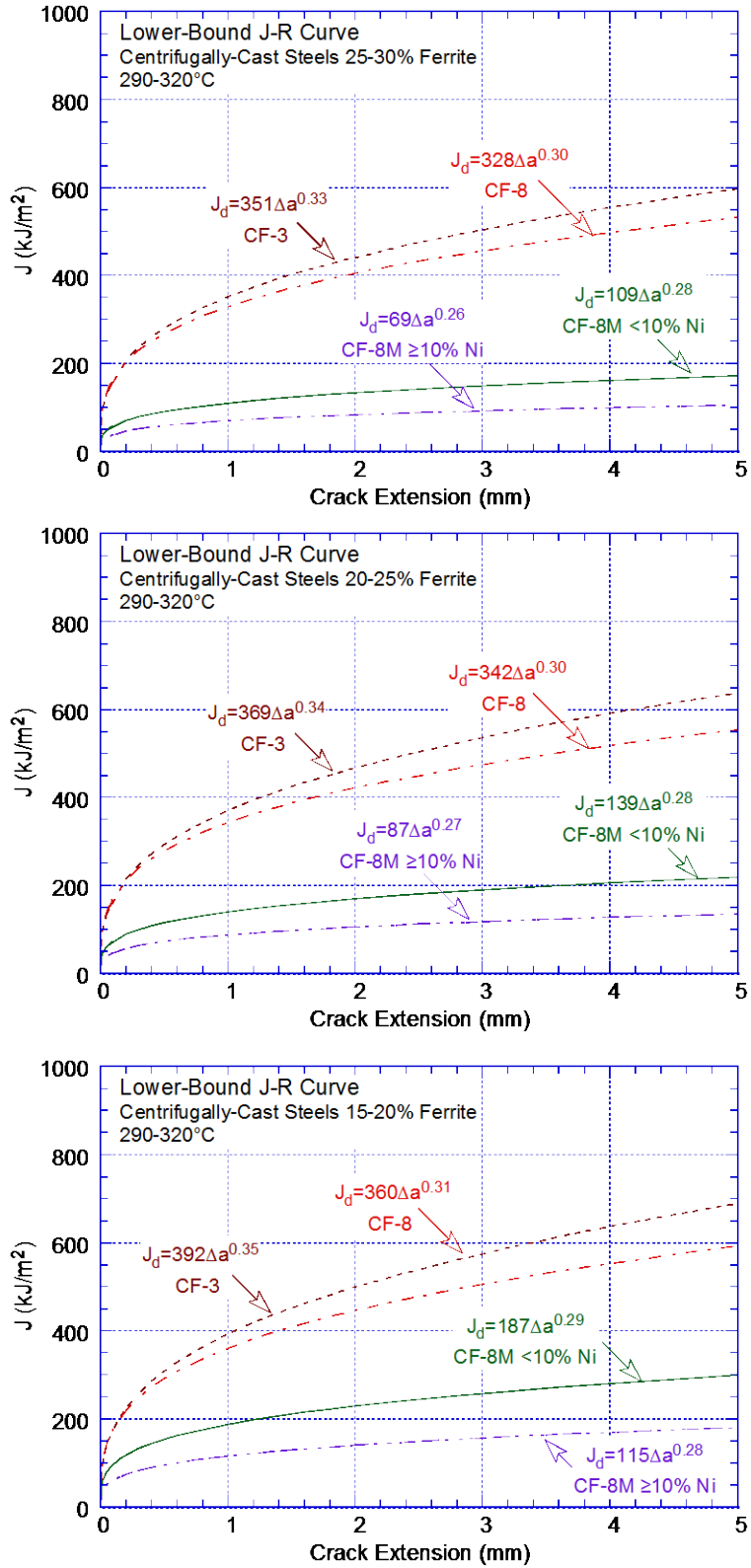


Figure 43. Estimated lower-bound J-R curves at 290–320°C for centrifugally cast CASS materials with ferrite contents of >25–30%, >20–25%, and >15–20%.

Table 1. The saturation $J_{2.5}$ corresponding to the RT Charpy-impact energy trend curves in Fig. 39 are shown in Figs. 44 and 45 for static-cast and centrifugally cast materials, respectively. In these figures, the updated screening criterion is represented by the ferrite content when the $J_{2.5}$ value decreases below the acceptable threshold value of 255 kJ/m².

The results indicate that for CF-3 and CF-8 materials, values of $J_{2.5}$ for both static-cast and centrifugally cast materials are significantly above the threshold value of 255 kJ/m². Therefore, the screening criterion that states that the reduction in fracture toughness due to thermal embrittlement of centrifugally cast CF-3 and CF-8 materials is "nonsignificant" is valid, and the criterion that the reduction in the fracture toughness of static-cast CF-3 and CF-8 materials is "significant" only for materials with more than 20% ferrite is a conservative criterion.

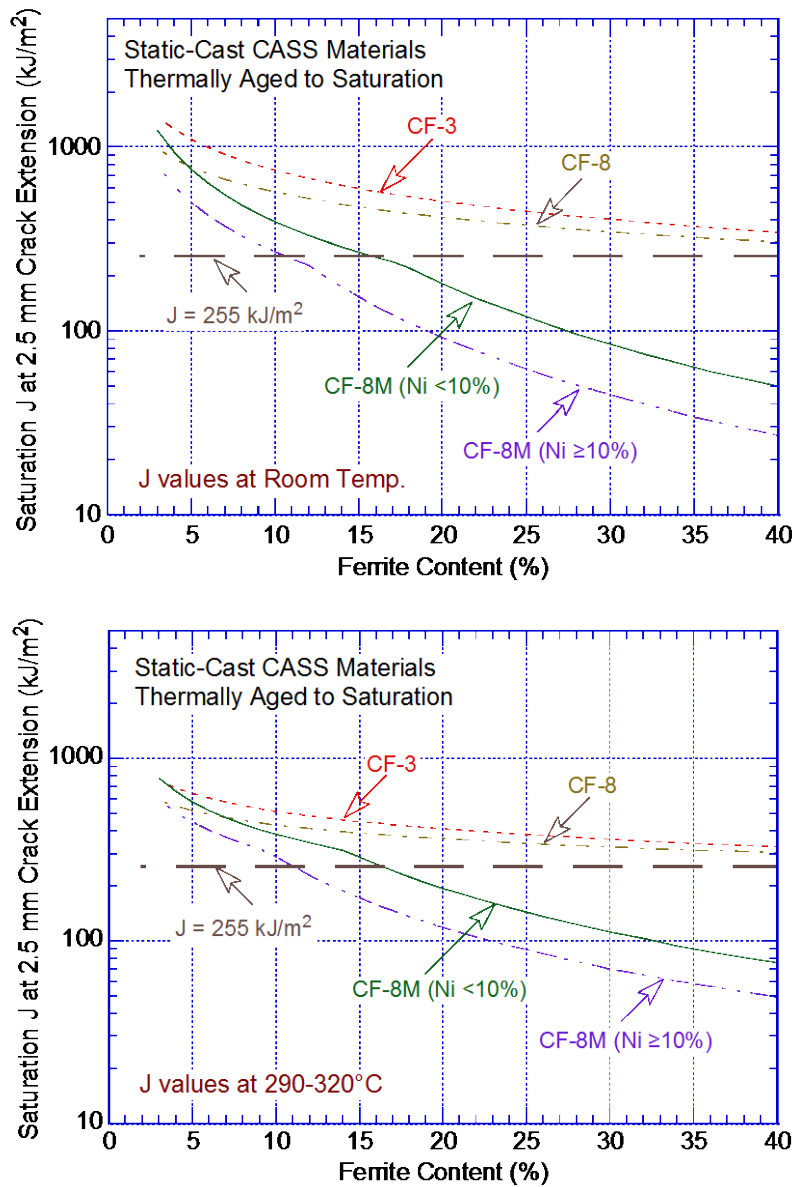


Figure 44. Saturation J at a 2.5 mm crack extension as a function of the ferrite content for static-cast CF-3, CF-8, and CF-8M CASS materials.

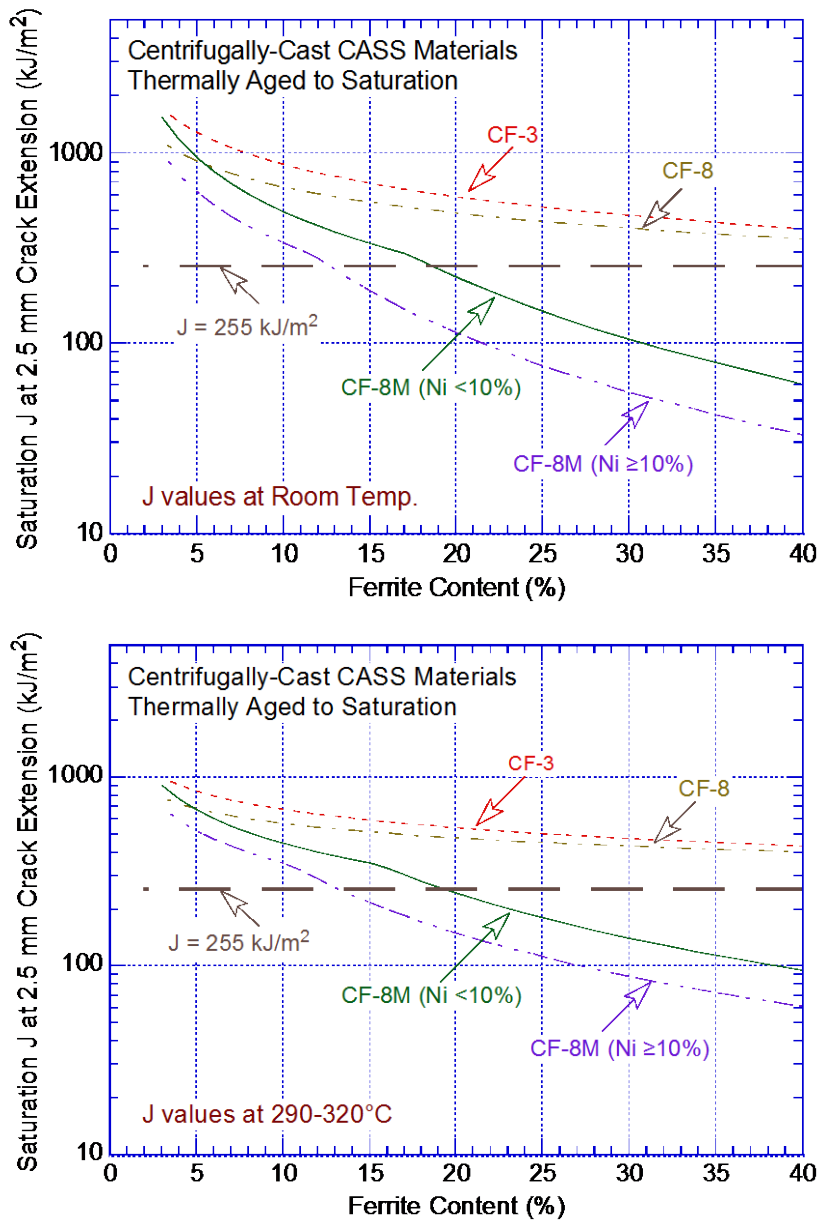


Figure 45. Saturation J at a 2.5 mm crack extension as a function of the ferrite content for centrifugally cast CF-3, CF-8, and CF-8M CASS materials.

The results for CF-8M steels with <10% Ni indicate that the $J_{2.5}$ values are above the 255 kJ/m² threshold value for static-cast materials with ferrite contents of <16% and for centrifugally cast materials with ferrite contents of <19%. Therefore, the existing criterion that the reduction in the fracture toughness of static-cast CF-8M materials containing <10% Ni is "significant" only for materials with more than 14% ferrite is also a conservative criterion. However, for centrifugally cast CF-8M materials containing <10% Ni, the threshold ferrite content above which the reduction in the fracture toughness of the material is considered "significant" should be decreased from 20% ferrite to 19% ferrite.

Similarly for CF-8M steels with ≥10% Ni, the $J_{2.5}$ values are above the 255 kJ/m² threshold value for ferrite contents of <11% for static-cast materials and <13% for centrifugally cast

materials. Therefore, for CF-8M materials containing $\geq 10\%$ Ni, the threshold ferrite content above which the reduction in the fracture toughness is considered "significant" should be decreased from 14% ferrite to 11% ferrite for static-cast materials and from 20% ferrite to 13% ferrite for centrifugally cast materials. The revised screening criteria for the thermal-aging susceptibility of CASS CF-3, CF-3M, CF-8, and CF-8M materials are given in Table 5. The screening criteria for the thermal-aging susceptibility of CASS materials that have been changed are as follows.

- (i) The criterion for static-cast and centrifugally cast CF-8M materials with $\geq 10\%$ Ni.
- (ii) The criterion for centrifugally cast CF-8M materials with $< 10\%$ Ni.

Table 5. Updated screening criteria for thermal-aging susceptibility of CASS CF-3, CF-8, and CF-8M materials.

Mo Content (wt.%)	Casting Method	Ferrite Content (%)	Susceptibility Determination
High (2.0–3.0) with $< 10\%$ Ni ($\geq 10\%$ Ni)	Static	≤ 14 (≤ 11)	Not susceptible
		> 14 (> 11)	Potentially susceptible
	Centrifugal	≤ 19 (≤ 13)	Not susceptible
		> 19 (> 13)	Potentially susceptible
Low (0.5 max.)	Static	≤ 20	Not susceptible
		> 20	Potentially susceptible
	Centrifugal	All	Not susceptible

3.4 Estimation of Tensile Flow Stress

This section is essentially the same as Section 3.4 of NUREG/CR-4513 Rev. 1. The tensile flow stress of aged CASS materials can be estimated from correlations between the ratio of the tensile flow stress of aged and unaged materials and a normalized aging parameter. Based on the analysis described in NUREG/CR-6142, the ratio of the tensile flow stress (R_f) of aged and unaged CASS materials ($\sigma_{faged}/\sigma_{funaged}$) is plotted as a function of a normalized aging parameter ($P - \theta + 2.9$) in Fig. 46. Flow stress is defined as the mean of the 0.2% yield strength and ultimate strength, and the aging parameter is normalized with respect to a θ value of 2.9. In NUREG/CR-4513, Rev. 1, the aging parameter P was determined from Eq. 11 and experimental values of activation energy. The correlations between R_f and the normalized aging parameter used for estimating flow stress were obtained by subtracting the value of the standard deviation for the fit to the data from the best-fit curve. At both RT and 290°C, the R_f increases with thermal aging; the increase in the flow stress of CF-3 steels is the smallest and the increase in the flow stress of CF-8M steels is the largest.

The tensile flow stress of aged CASS materials can be estimated from the initial tensile flow stress and the correlations given in Fig. 46. Note that the x-axis in these plots is reduced to P for a θ value of 2.9. At RT, the tensile-flow-strength ratio, $R_f = (\sigma_{faged}/\sigma_{funaged})$ for CF-3 steel is given by

$$R_f = 0.90 + 0.05P \quad (1.00 \leq R_f \leq 1.10); \quad (47)$$

for CF-8 steel, it is given by

$$R_f = 0.84 + 0.08P \quad (1.00 \leq R_f \leq 1.16); \quad (48)$$

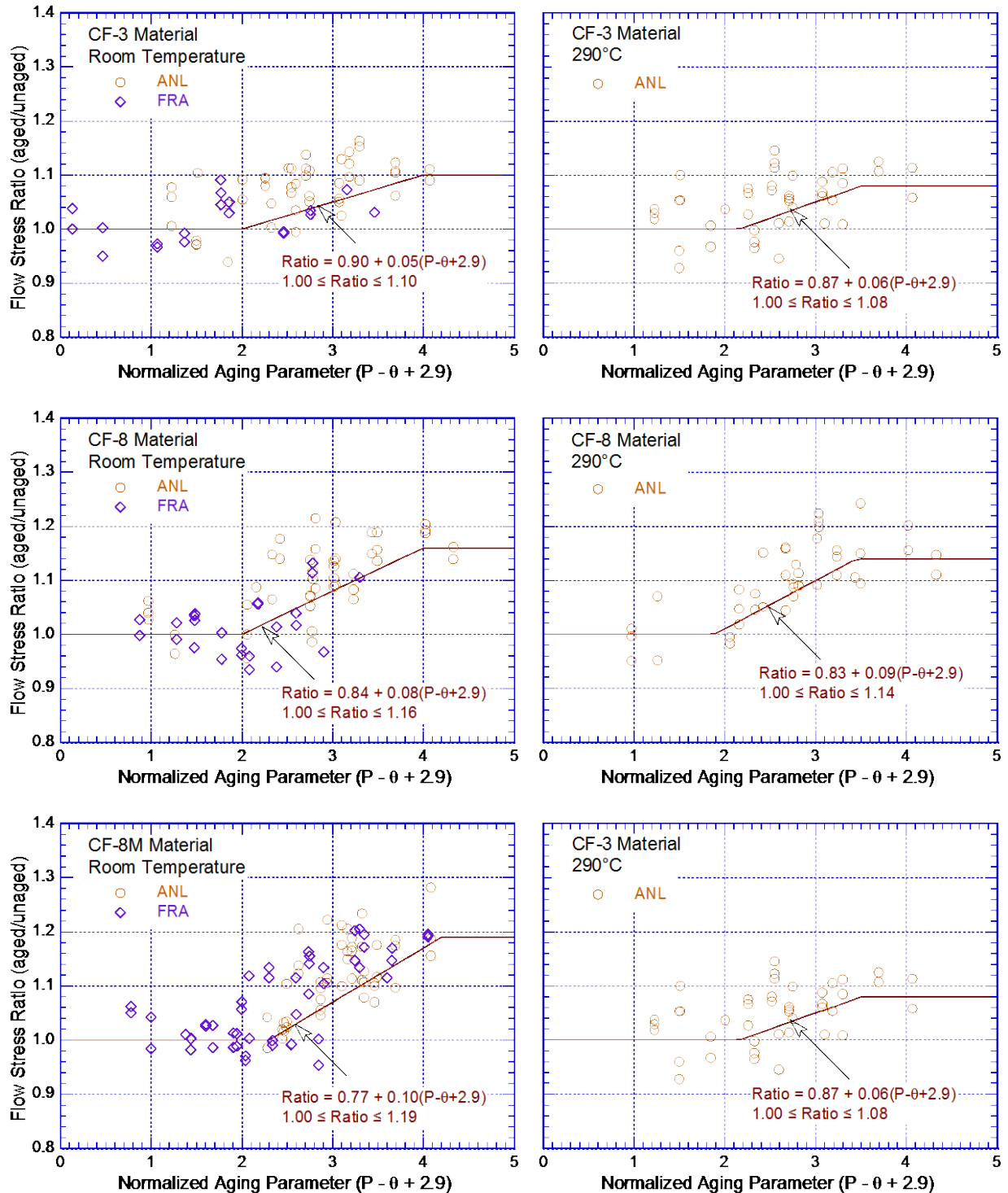


Figure 46. Flow stress ratio R_f of aged CF-3, CF-8, and CF-8M materials at RT and 290°C as a function of the normalized aging parameter. The solid lines represent correlations obtained by subtracting σ from the best-fit curve.

and for CF-8M steel, it is given by

$$R_f = 0.77 + 0.10P \quad (1.00 \leq R_f \leq 1.19). \quad (49)$$

At 290°C (554°F), the R_f for CF-3 steel is given by

$$R_f = 0.87 + 0.06P \quad (1.00 \leq R_f \leq 1.08); \quad (50)$$

and for CF-8 steel, it is given by

$$R_f = 0.83 + 0.09P \quad (1.00 \leq R_f \leq 1.14); \quad (51)$$

and for CF-8M steel, it is given by

$$R_f = 0.69 + 0.14P \quad (1.00 \leq R_f \leq 1.24). \quad (52)$$

The minimum and maximum values of the ratio R_f are given for each grade of steel and each temperature; a minimum or a maximum value is assumed, respectively, when the calculated ratio is smaller than the minimum ratio or greater than the maximum ratio.

Equations 50-52 are valid for service temperatures between 280 and 330°C (536 and 626°F) and ferrite contents of >7% for CF-8M steel and >10% for CF-3 and CF-8 steels. Thermal aging has little or no effect on the tensile strength of CASS materials with low ferrite content. The available database is inadequate for estimating the tensile properties at service temperatures of <280°C (<536°F). The estimated values of tensile flow stress at 290°C (554°F) and at RT for various heats of aged CASS materials are obtained by first determining the aging parameter from Eq. 11, and activation energy from Eqs. 14–17 (using a θ value of 2.9). The tensile flow stress is then estimated from Eqs. 47–52 and the initial flow stress of the material. The fracture toughness J_{Ic} values for aged CASS materials is then determined from the estimated J-R curve and flow stress. Only the chemical composition, the initial Charpy-impact energy, and the flow stress of the unaged material are used for the estimates. The estimated J_{Ic} values show good agreement with the experimental results; in most cases, the estimated J_{Ic} is lower but within 30% of the observed value.¹⁶

The data on the tensile properties of CASS materials indicate that the increase in yield strength due to thermal aging is much lower than the increase in ultimate strength. At RT, the tensile-yield-strength ratio $R_y = (\sigma_{yaged}/\sigma_{yunaged})$ for CF-3 steel is given by

$$R_y = 0.873 + 0.048P \quad (1.00 \leq R_y \leq 1.07); \quad (53)$$

for CF-8 steel, it is given by

$$R_y = 0.798 + 0.076P \quad (1.00 \leq R_y \leq 1.10); \quad (54)$$

and for CF-8M steel, it is given by

$$R_y = 0.708 + 0.092P \quad (1.00 \leq R_y \leq 1.10). \quad (55)$$

At 290°C (554°F), the tensile-yield-strength ratio $R_y = (\sigma_{faged}/\sigma_{funaged})$ for CF-3 steel is given by

$$R_y = 0.844 + 0.058P \quad (1.00 \leq R_y \leq 1.05); \quad (56)$$

for CF-8 steel, it is given by

$$R_y = 0.788 + 0.086P \quad (1.00 \leq R_y \leq 1.09); \quad (57)$$

and for CF-8M steel, it is given by

$$R_y = 0.635 + 0.129P \quad (1.00 \leq R_y \leq 1.14). \quad (58)$$

The minimum and maximum values of the tensile-yield-strength ratio R_y are given for each grade of steel and temperature. Equations 56–58 are valid for service temperatures between 280 and 330°C (536 and 626°F) and ferrite contents of >7% for CF-8M steel and >10% for CF-3 and CF-8 materials. Similar to the flow stress estimations, the aging parameter and activation energy are obtained from Eqs. 11 and 14–17 and by using θ value of 2.9. Tensile yield strength is then estimated from Eqs. 56–58 and the initial yield strength of the material. The results indicate that the estimated values are conservative for most material and aging conditions.

The engineering stress versus strain behavior of aged CASS materials can also be obtained from the estimated flow stress.¹⁸ The engineering stress-versus-strain curve is expressed by the Ramberg-Osgood equation

$$\frac{\varepsilon}{\varepsilon_0} = \frac{\sigma}{\sigma_0} + \alpha_1 \left(\frac{\sigma}{\sigma_0} \right)^{n_1}, \quad (59)$$

where σ and ε are engineering stress and strain, respectively; σ_0 is an arbitrary reference stress, often assumed to be equal to the flow or yield stress; the reference strain $\varepsilon_0 = \sigma_0/E$; α_1 and n_1 are Ramberg-Osgood parameters; and E is the elastic modulus. The Ramberg-Osgood equation can be rearranged to the form

$$\frac{E\varepsilon - \sigma}{\sigma_f} = \alpha_1 \left(\frac{\sigma}{\sigma_f} \right)^{n_1}, \quad (60)$$

which is more convenient for fitting stress-versus-strain data; α_1 can be determined at $\sigma/\sigma_f = 1$ and n_1 can be obtained from the slope of the log-log plot of Eq. 60. The parameter n_1 is different for the three grades of CASS materials but does not depend on the aging condition. The parameter α_1 decreases with aging and shows good correlation with the flow stress σ_f . For engineering stress-versus-strain curves up to 5% strain, the Ramberg-Osgood parameters at RT for CF-3 materials are given by

$$\alpha_1 = 143.9 - 0.267\sigma_f \quad (n_1 = 6.1); \quad (61)$$

for CF-8 steel, it is given by

$$\alpha_1 = 157.9 - 0.300\sigma_f \quad (n_1 = 6.4); \quad (62)$$

and for CF-8M steel, it is given by

$$\alpha_1 = 50.9 - 0.0724\sigma_f \quad (n_1 = 5.6). \quad (63)$$

At 290°C (554°F), the Ramberg-Osgood parameters for engineering stress-vs.-strain curves up to 5% strain, for CF-3 materials, are given by

$$\alpha_1 = 102.1 - 0.235\sigma_f \quad (n_1 = 6.2); \quad (64)$$

for CF-8 steel, it is given by

$$\alpha_1 = 153.3 - 0.373\sigma_f \quad (n_1 = 7.1); \quad (65)$$

and for CF-8M steel, it is given by

$$\alpha_1 = 145.9 - 0.314\sigma_f \quad (n_1 = 6.6). \quad (66)$$

Similar correlations have also been developed for stress-versus-strain curves up to 15% strain or up to the ultimate strength.¹⁸

4 USE OF METHODOLOGY IN ASME CODE, SECTION XI

This section is an addition to the report; it covers a topic that was not included in NUREG/CR-4513 Rev. 1. The estimated lower-bound fracture toughness J-R curves described in NUREG/CR-4513, Rev. 1 for thermally aged CASS materials were compared with the fracture toughness J-R curve used in the 1989 edition of the ASME Section XI, Subsection IWB-3640 “Evaluation Procedures and Acceptance Criteria for Austenitic Piping,” for evaluation of flux welds.⁴⁹ The comparison is shown in Fig. 47 for static-cast and centrifugally cast CASS materials. The results show that the lower-bound fracture toughness of thermally aged CASS material with up to 25% ferrite is similar to the fracture toughness J-R curve used in Subsection XI IWB-3640 to evaluate SAWs. The procedures in ASME Section XI Subsection IWB-3640 reduce the load bearing capacity of the SS component to account for the reduced fracture toughness of the SAWs, based on elastic-plastic fracture mechanics analyses.^{89,90} Because the lower-bound fracture toughness of thermally aged CASS steel is similar to the fracture toughness of SAWs used in the elastic-plastic fracture mechanics analyses of the 1989 edition of ASME Section XI IWB-3640, the procedures in IWB-3640 for SAWs are directly applicable to CASS materials.

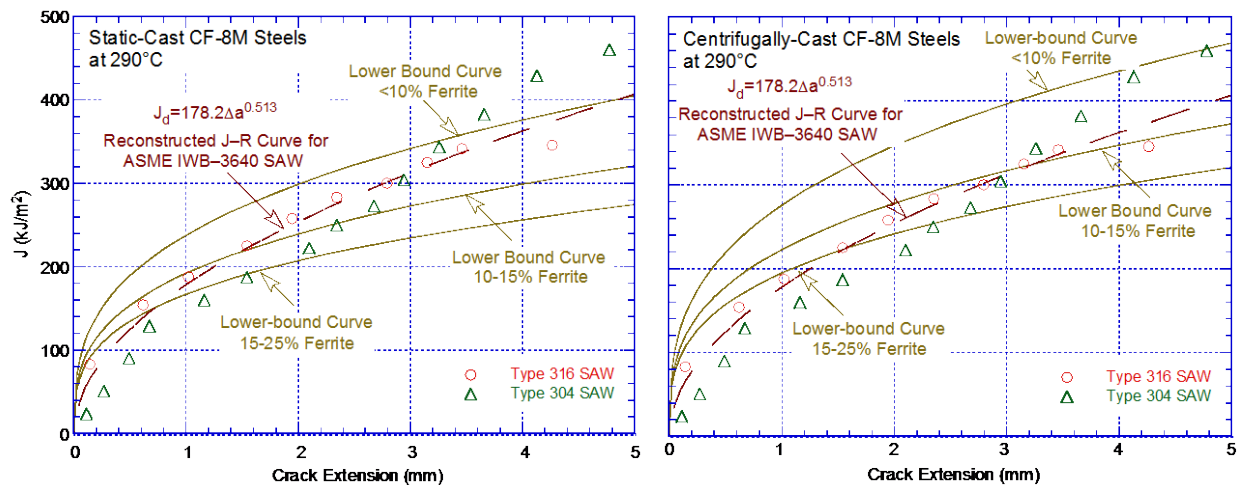


Figure 47. Comparison of the lower-bound J-R curve at 290°C for aged static-cast CF-8M material estimated by using the NUREG/CR-4513, Rev. 1, expressions, with the SAW data used to develop ASME Section XI, Subsection IWB-3640 evaluations.

Furthermore, since the flaw evaluation is based on the unaged material ultimate strength, this approach would be conservative. Experimental data indicate that the flow stress (i.e., half of the sum of the ultimate and yield strengths) is increased by about 10%, 14%, and 24% for CF-3 and CF-3A, CF-8 and CF-8A, and CF-8M materials, respectively.¹⁶ A higher ultimate stress would increase the load-bearing capability of a component. Therefore, the procedures developed in Subsection IWB-3640 for SAWs have been accepted for evaluating flaws in thermally aged CASS materials to address aging degradation concerns associated with license renewal applications.⁴⁹ The use of the IWB-3640 SAW procedures for evaluating flaws in thermally aged CASS components is considered conservative because, (a) the lower-bound fracture toughness of thermally aged CASS is similar to the fracture toughness used in IWB-3640 to evaluate SAW, (b) the actual fracture toughness of a thermally aged CASS component in a U.S. NPP would likely be higher than the ANL lower-bound fracture toughness, and (c) the thermally aged

components would be able to withstand more loads because of the increased ultimate strength resulting from thermal aging.

The ASME Section XI Subsection IWB-3641 "Evaluation Procedures Based on Flaw Size" states; Evaluation procedures based on flaw size may be used subject to the following:

- (a) The evaluation procedures and acceptance criteria are applicable to austenitic pipe NPS 4 or greater and portions of the adjoining pipe fittings within a distance of \sqrt{rt} of the weld centerline (where r is the nominal outside radius and t is the nominal thickness of the pipe).
- (b) The evaluation procedures and acceptance criteria are applicable to pipe and pipe fittings (and associated weld materials) which:
 1. are made of wrought stainless steel, Ni-Cr-Fe alloy, or cast stainless steel (with ferrite level less than 20% or 20FN;
 2. have a specified minimum yield strength less than 45 ksi; and
 3. have S_m values given in Table I-1.2 of Section III.
- (c) For cast stainless steel materials, adequate toughness for the pipe to reach limit load after aging shall be demonstrated.

The methodology and evaluation procedures are described in Subsections IWB-3641.1 and IWB-3641.2, respectively. A flaw growth analysis is performed on the detected flaw to determine the maximum growth during a specified evaluation period. The flaw evaluation is based on the analytical procedures described in Section XI Nonmandatory Appendix C to determine the critical flaw parameters. The maximum allowable flaw depth of a circumferential flaw under normal operating conditions is calculated from Table IWB-3641-1 for flaws in base metal and gas metal-arc weld (GMAW) and gas tungsten-arc weld (GTAW), and from Table IWB-3641-5 for flaws in SAW and shielded metal arc weld (SMAW). Similarly, the maximum allowable flaw depth of a circumferential flaw under emergency and faulted conditions is calculated from Table IWB-3641-2 and IWB-3641-6, respectively for base metal and GTAW/GMAW, and SAW/SMAW.

Thus, the use of the ASME Section XI, Subsection IWB-3640 (the 1989 edition), SAW procedures for evaluating flaws in thermally aged CASS components is considered to be a "screening" step to determine whether a further, detailed flaw evaluation that accounts for actual plant-specific material properties should be performed. The procedures in IWB-3640 for SAWs have been available since the winter 1985 Addenda for Section XI, and they have been applied successfully by utilities without resulting in unnecessary component repairs or replacements. However, note that the ANL methodology of NUREG/CR-4513, Rev. 1, is not applicable to CASS CF-8M materials containing >25% ferrite or to CF-8M materials containing more than trace amounts of Nb. Even then, the proposed flaw evaluation procedures, which are based on the lower-bound fracture toughness of thermally aged CASS materials, are expected to be sufficient in the vast majority of cases.

In this report, the plots in Fig. 47 have been updated to include a comparison of the new lower-bound fracture toughness J-R curve presented in Figs. 40 and 42 with the J-R curve of SAWs used to develop the ASME Section XI, Subsection IWB-3640 evaluations. The results for static-cast and centrifugally cast CF-8M materials containing <10% Ni or $\geq 10\%$ Ni, are shown in Figs. 48 and 49, respectively. These plots indicate that the use of the procedures in IWB-3640 for SAWs for evaluating flaws in aged CASS materials may not be adequate for CF-8M materials with $\geq 10\%$ Ni and containing >10% ferrite, particularly for static cast material.

Similarly, the IWB-3640 procedure for SAWs may not be adequate for CF-8M materials with <10% Ni and containing >15% ferrite static cast material and 20% ferrite for centrifugally cast materials. The lower-bound J-R curves listed in Table 4 and shown in Figs. 40–43 should be used for these materials.

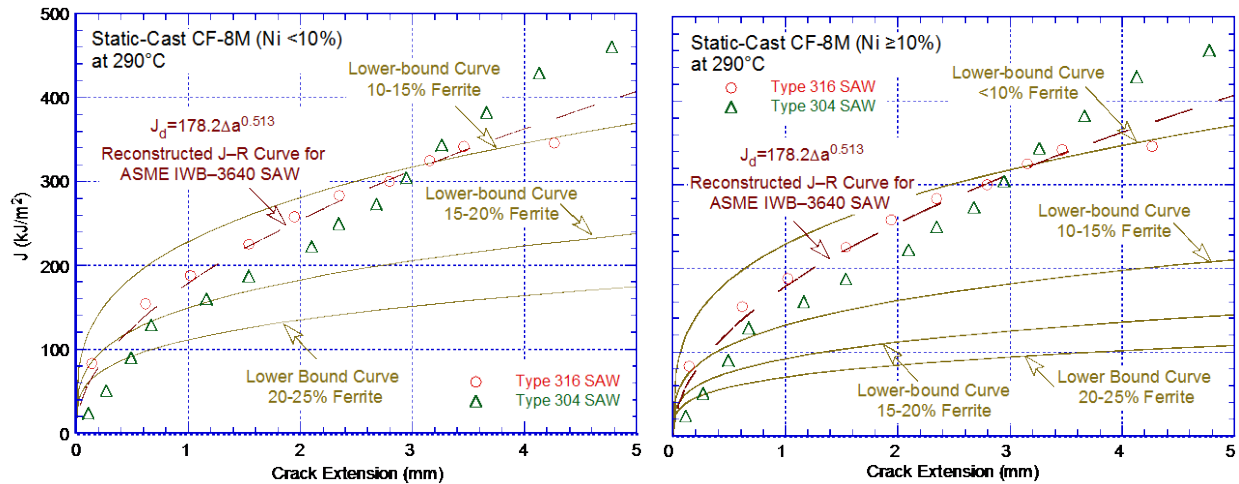


Figure 48. Comparison of the lower-bound J-R curve at 290°C for aged static-cast CF-8M material estimated by using the updated expressions, with the fracture toughness of SAW data used to develop ASME Section XI, Subsection IWB-3640 evaluations.

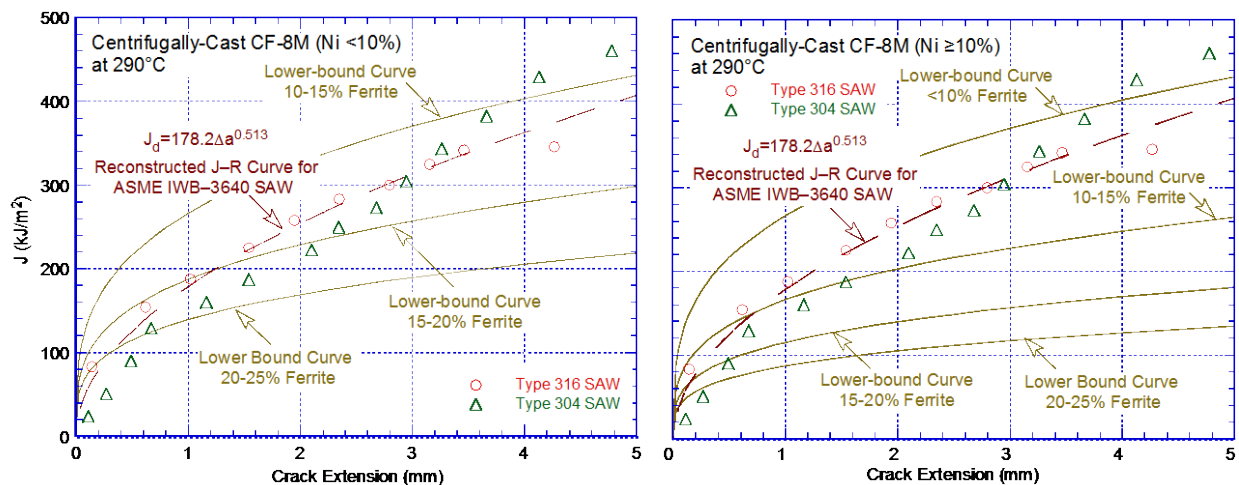


Figure 49. Comparison of the lower-bound J-R curve at 290°C for aged centrifugally cast CF-8M estimated by using the updated expressions, with the fracture toughness of SAW data used to develop ASME Section XI, Subsection IWB-3640 evaluations.

4.1 Current Editions of the ASME Code Section XI

As discussed above, the procedures developed in the 1989 edition of the ASME Code Subsection IWB-3640 for SAWs have been accepted for evaluating flaws in thermally aged CASS materials to address aging degradation concerns associated with license renewal

applications.⁴⁹ Although the revised lower-bound fracture toughness J-R curves shown in Figs. 48 and 49 indicate that the Subsection IWB-3640 flaw evaluation methodology may not be applicable to some heats of CF-8M materials, particularly those containing $\geq 10\%$ Ni, the IWB-3640 procedures are applicable for CF-3, CF-8, and some heats of CF-8M materials. However, in 1996, Tables IWB-3641-5 and 6 were deleted, Subsection IWB-3641.2 "Evaluation" item (c) was revised, and the maximum allowable flaw depth are now calculated using Tables IWB-3641-1 and 2 for normal operating conditions and emergency and faulted conditions respectively. In addition, Tables IWB-3641-1 and 2 were revised to include Z factors load multipliers that are used to modify stress ratio for performing flaw evaluations of austenitic welds fabricated by SMAW and SAW. The revised flaw evaluation methodology is applicable to cast stainless steels, with a minimum yield strength not greater than 310 MPa (45 ksi). However, the methodology does not address thermal aging effects for CASS materials.

Thus, in 1995 and later versions of the ASME Section XI Subsection IWB-3640 evaluation procedures and acceptance criteria for austenitic piping, determination of the allowable flaw depth based on Tables IWB-3641-5 and 6 has been replaced by the Z factor load multiplier approach to modify the stress ratio for SMAW and SAW flaw evaluations. However, the applicability of the SMAW/SAW flaw evaluations using the Z factor load multiplier approach to flaw evaluations of thermally aged CASS materials needs to be examined.

5 COMBINED EFFECTS OF THERMAL AND NEUTRON EMBRITTLEMENT

This section is an addition to the report; it covers topics that were not included in NUREG/CR-4513 Rev. 1. Reactor core internal components are subjected to prolonged periods of both elevated temperatures and neutron irradiation. The thermal aging and neutron irradiation embrittlement of CASS⁶⁻¹⁸ and wrought austenitic SSs³⁶⁻⁴⁷ have been investigated individually, but the possibility of a combined interaction between the thermal and neutron embrittlement of materials with a duplex structure is an issue associated with reactor core internal components that has been of concern. Recent data indicate that concurrent exposure to elevated temperatures and high neutron fluence levels could result in a combined effect, in which the service-degraded fracture toughness would be reduced from the levels predicted independently for either of the two mechanisms.^{91,92} Furthermore, for SSs with a duplex structure, neutron embrittlement of the ferrite phase occurs much faster than it does for the austenitic phase. The irradiation temperature is an important factor in establishing the extent of embrittlement of the ferrite.

As discussed earlier, the fracture toughness of unaged and unirradiated wrought SSs and CASS materials fall in Category III, with J_{IC} being above 150 kJ/m² (857 in.-lb/in.²). Fracturing of these materials occurs after a stable crack extension at stresses well above the yield strength. However, neutron irradiation can degrade the fracture toughness of these materials to the level of Category II materials (i.e., J_{IC} in the range of 30–150 kJ/m² [171–857 in.-lb/in.²]) or even Category I materials (i.e., $J_{IC} < 30$ kJ/m² [< 171 in.-lb/in.²]). Therefore, failure in neutron-irradiated materials may occur without general yielding, and either EPFM or LEFM is used for analyzing structural integrity and developing inspection guidelines for components fabricated from CASS materials. For wrought austenitic SSs and associated welds, the effect of neutron irradiation on the fracture toughness of these materials is estimated by defining a lower-bound curve expressed in terms of the fracture toughness parameters, such as the J_{IC} value or coefficient C of the J-R curve, as a function of the neutron dose (in dpa).^{39,42}

A list of CASS components in LWR core internals and their expected neutron dose during 60 years of service is presented in Table 6.^{44,93} Most of the components are fabricated from CF-8 material. The control rod guide tube (CRGT) spacer casting in Babcock & Wilcox (B&W) PWRs is fabricated from CF-3M. In General Electric (GE) BWRs, the CRGT base and low-pressure core injection (LPCI) coupling are fabricated from CF-3 or CF-8 materials. In the Combustion Engineering PWR, only the core support columns are fabricated from CF-8 material.

In an earlier study at ANL (NUREG/CR-7027),⁴⁷ a critical assessment of the neutron embrittlement of wrought austenitic SSs and CASS materials was performed to establish the effects of material parameters (e.g., composition, thermo-mechanical treatment, microstructure, microchemistry, yield strength, stacking fault energy) and environmental parameters (e.g., water chemistry, irradiation temperature, dose, dose rate) on neutron embrittlement.^{46,47} The results were used to (a) define a threshold fluence level above which irradiation effects on the fracture toughness of cast and wrought austenitic SSs are significant and (b) evaluate the potential for neutron embrittlement of these materials under LWR operating conditions. The results indicated that for the same irradiation conditions, the fracture toughness of thermally aged CASS material is lower than that of the heat-affected zone (HAZ) of SS base materials, which, in turn, is lower than that of solution-annealed SS base materials.

The combined effects of thermal aging and neutron irradiation embrittlement were also discussed.^{46,47} However, the fracture toughness data available at that time were inadequate to accurately evaluate the combined effects. The significant results from the earlier study (i.e., NUREG/CR-7027) and some recent studies on potential combined effects of thermal and neutron embrittlement are summarized below.

Table 6. LWR core internal components made of CASS materials and maximum neutron dose after 60 years of service (Refs. 44,93).

Component	Material	60-Year Dose (dpa)
<u>Babcock & Wilcox (B&W) PWR</u>		
Control rod guide tube (CRGT) spacer castings	CF-3M	Not available
Core support shield outlet nozzle	CF-8	Not available
Incore monitoring instrumentation guide tube spider	CF-8	Not available
<u>Combustion Engineering (CE) PWR</u>		
Core support columns	CF-8	0.15–1.50
Control element assembly (CEA) shrouds	CPF-8/CF-8	< 0.15
CEA shroud base	CF-8	0.15–1.05
Modified CEA shroud expansion shaft guides	CF-8	<0.15
<u>Westinghouse PWR</u>		
CRGT assembly lower flanges	CF-8	1.05–1.50
Mixing devices	CF-8	1.05–1.50
Upper head injection flow column base	CF-8	1.05–1.50
Upper support column base	CF-8	1.05–1.50
Bottom-mounted instrumentation columns cruciforms	CF-8	1.50–7.50
Lower internals assembly lower support casting	CF-8	<0.15
Lower internals assembly column bodies	CF-8	1.50–7.50
<u>General Electric (GE) BWR</u>		
Orificed fuel support (OFS)	CF-8	>0.45
CRGT base	CF-3/CF-8	<0.00015
Core spray sparger nozzle elbows	CF-8	<0.15
Jet pump transition piece	CF-8	>0.45
Jet pump restrainer bracket	CF-8	>0.45
Jet pump inlet mixer assembly	CF-8	>0.45
Jet pump inlet elbow	CF-8	>0.45
Jet pump inlet nozzle	CF-8	>0.45
Jet pump diffuser	CF-8	>0.45
Low-pressure core injection (LPCI) coupling	CF-3/CF-8	<0.75

5.1 Fracture Toughness of Irradiated Austenitic Stainless Steels

Until recently, most of the published experimental data on neutron embrittlement of austenitic SSs had been obtained on materials irradiated in high-flux fast reactors.⁹⁴⁻⁹⁹ In these studies, the embrittlement of the materials has been characterized in terms of tensile properties, Charpy-impact properties, and fracture toughness. The fracture toughness of structural materials is typically characterized by (a) the initiation toughness J_{Ic} and tearing modulus T for materials that fail after substantial plastic deformation (for EPFM analysis) and by (b) the critical stress

intensity factor K_{Ic} for materials that fail after little or no deformation (for LEFM analysis). In some studies, the power-law J-R curve parameters, coefficient C and exponent n, are also reported. The fracture toughness data have been obtained from compact tension (CT) or single-edge bend [SE(B)] specimens, and, in a few cases, from chevron notch short rod specimens. To reduce activity and facilitate handling, small specimens (e.g., \approx 8-mm-thick, $\frac{1}{4}$ -T CT) have been used in several studies. For these specimens, J values above 150 kJ/m^{1/2} and crack extensions beyond about 1.2 mm are above the validity limits based on ASTM Specification E 1820-06. However, a comparison of fracture toughness data obtained on 1-T CT and small-sized CT or SE(B) specimens show comparable J-versus- Δa values, even beyond the ASTM-defined validity limits.^{47,100} The small specimens yield equivalent J-R curve data at least for materials with J_{Ic} values up to about 300 kJ/m^{1/2} and maybe even higher.

Plots of J_{Ic} or K_{Ic} and K_{Jc} as a function of neutron dose are generally used for developing screening criteria for neutron embrittlement. In ASTM Specification E 1820-06, J_{Ic} is determined from the intersection of the best-fit power-law J-R curve with the 0.2-offset line parallel to the blunting line. The blunting line is defined as

$$J = m\sigma_f\Delta a, \quad (67)$$

where σ_f is the flow stress, Δa is the crack extension, and the constraint factor m is 2 or a value determined from the best fit of the experimental data. However, the analysis procedures, described in the ASTM specifications for J_{Ic} determination, are not applicable to austenitic SSs because of their extremely high toughness, ductility, and strain-hardening ability. The main difference concerns the expression for the crack-tip blunting line. For austenitic SSs, a value of 2 for m significantly over-predicts the crack extension due to crack blunting; therefore, it yields a non-conservative value of J_{Ic} .^{48,86} For austenitic SSs, a value of 4 for m better defines the blunting line. The constraint factor, M, which relates J to the crack tip opening displacement (CTOD) is given by the expression

$$J = M\sigma_y(CTOD). \quad (68)$$

The use of a higher value for M in Eq. 67 is consistent with the expected variation of M and σ_f with strain hardening. The factor M is 1 for materials with intermediate to high strengths and low strain hardening, and it is 2 for materials with low strengths and high strain hardening, such as austenitic SSs. For the latter, the yield strength is approximately two-thirds of the flow stress, and the crack extension associated with blunting is approximately one-third of CTOD.⁴⁸ Thus, for such materials, the crack tip blunting line is given by

$$J = M\sigma_y(CTOD) \approx 2(2\sigma_f/3)(3\Delta a) = 4\sigma_f\Delta a, \quad (69)$$

That is, Eq. 67 with M = 4. This relationship has been used to determine J_{Ic} in most investigations on neutron embrittlement.^{40,100} A value of 2 for M has also been used by some investigators.³⁹ The latter typically yields a higher value of J_{Ic} for Category III materials (i.e., with a $J_{Ic} > 150$ kJ/cm²). However, the difference in J_{Ic} values determined by using values of M of 2 or 4 is insignificant for Category II materials (i.e., with a J_{Ic} of < 100 kJ/cm²). Because, it is primarily the cases in which the fracture toughness of irradiated austenitic SSs has been reduced to Category II levels that are of interest for embrittlement evaluations, the effect of differences in the procedure to determine J_{Ic} is likely to be insignificant.

Another factor that may influence the reported values of J_{Ic} is the use of an effective yield stress instead of the measured yield stress. The K/size criteria were developed for materials that show

work hardening; therefore, they may not be applicable for materials irradiated to fluence levels where, on a local level, they do not strain harden. An effective yield stress, in which the irradiation-induced increase in yield strength is discounted by a factor of 2 for moderately irradiated materials¹⁰¹ and by a factor of 3 for highly irradiated materials,¹⁰² has been proposed to define K_{Ic} criteria for moderately to highly irradiated materials. Some studies have used such a yield stress to determine J_{Ic} .¹⁰⁰ Because J_{Ic} is a measure of fracture toughness at instability without a significant stable crack extension, the measured yield or flow stress of the irradiated materials seems more appropriate for J_{Ic} determinations. Nevertheless, the choice of measured or effective yield stress is likely to have an insignificant effect on the measured J_{Ic} of materials with poor fracture toughness.

5.1.1 Fracture Toughness J_{Ic}

The effects of neutron exposure (in dpa) on the fracture toughness of austenitic SSs at 25–427°C (77–842°F) have been investigated for SSs irradiated up to 90 dpa at 90–450°C (194–842°F) in fast reactors.^{41,48,103–112} The irradiation and test temperatures, respectively (with a few exceptions), were 325°C and 25°C for the data obtained by Kim et al.,⁴¹ 90–250°C and 25–250°C for the data obtained by Alexander et al.,¹⁰⁶ and 100–155°C and 125°C for the data obtained by Sindelar et al.¹⁰⁷ As discussed earlier in NRC topical reports NUREG/CR-6960¹⁰⁰ and NUREG/CR-7027,⁴⁷ the fast reactor data show substantial decrease in toughness at exposures of 1–10 dpa, and little or no further reduction in toughness beyond 10 dpa. The degradation in fracture properties appear to saturates at a J_{Ic} value of ~30 kJ/m² (171 in.-lb/in.²); that is, a K_{Jc} value of 75 MPa m^{1/2} (68.2 ksi in.^{1/2}).^{47,100} In addition, the failure mode changes from dimple fracture to channel fracture.

The fracture toughness J_{Ic} values for wrought and cast SSs irradiated in LWR,^{36-48,56,94-116} are shown in Fig. 50. The Westinghouse data for a heat of CASS CF-8 material irradiated to about 6–12 dpa are not included in the figure, because the irradiations were carried out in a fast reactor and the tests were conducted at RT. As discussed below, fracture toughness at reactor temperatures is expected to be lower. The fracture toughness data trend for LWR-irradiated materials is similar to the trend for the fast reactor data. Most of the fracture toughness J_{Ic} values for austenitic SSs irradiated in LWRs (288–316°C [550-601°F]) fall within the scatter band of the data obtained on materials irradiated in fast reactors, even though the LWR irradiations were at lower temperatures. However, the extent of embrittlement and the rate of decrease in fracture toughness vary among the various materials. Typically, for the same irradiation conditions, the fracture toughness of thermally aged CASS material is lower than the toughness of HAZ material, and that, in turn, is lower than the fracture toughness of solution-annealed SSs.

The Japan Power Electric Engineering and Inspection Corp. (JAPEIC) data for Type 304 SS irradiated to 3.0–5.3 dpa at LWR temperatures show very poor fracture toughness.³⁷ The J_{Ic} values are below the lower-bound curve for the fast reactor data. For the material irradiated to 4.5–5.3 dpa (shown as "+" in Fig. 50), 9 of 10 CT specimens showed no ductile crack extension, and the K_{Ic} values were 52.5–67.5 MPa m^{1/2} (47.7–61.4 ksi in^{1/2}).³⁷ In Fig. 50, the lowest fracture toughnesses with K_{Ic} or K_{Jc} values in the range of 36.8–40.3 MPa m^{1/2} (33.5–36.6 ksi in.^{1/2}) are for a Type 347 SS irradiated to 16.5 dpa in a PWR³⁷ and for a Type 304 SS irradiated to 7.4–8.4 dpa in a BWR.⁴⁵

The material's orientation also has a strong effect on fracture toughness. Fracture toughness J-R tests and microstructural and microchemistry characterization have been performed on Types 304 and 304L control-rod and top guide materials irradiated to 4.7–12.0 dpa in a BWR.

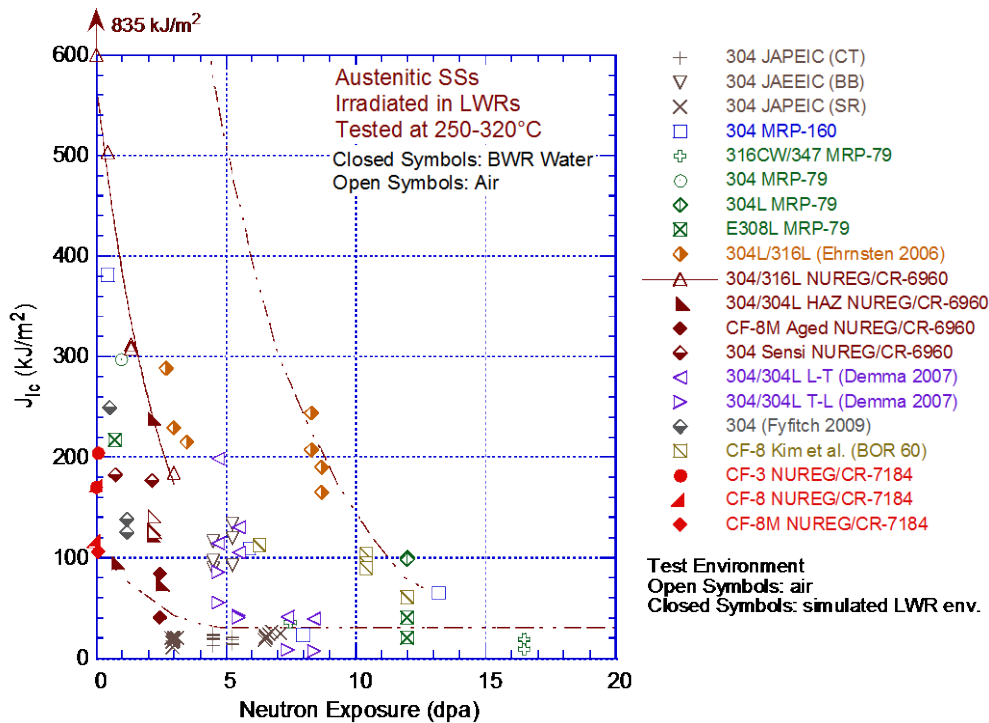


Figure 50. Change in fracture toughness J_{IC} as a function of neutron exposure for LWR irradiated austenitic SSs. Dashed lines represent the scatter band for the fast reactor data on SSs irradiated at 350–450°C (Refs. 36–40, 42–48, 56, 94, 100).

All materials consistently show lower fracture toughness in the T-L (transverse-longitudinal) orientation than in the L-T orientation (shown as isosceles triangles with their bases to the left or right, respectively, for T-L and L-T orientations).³⁹ The fracture toughness K_{IC} values are lower than the limiting value of 55 MPa m^{1/2} (50 ksi in.^{1/2}) that has been proposed by industry for flaw tolerance evaluations of irradiated austenitic SSs.^{38,39} The Type 304 control-rod material irradiated to 7.4–8.4 dpa, show poor fracture toughness (J_{IC} is 40 kJ/m² in L-T orientation and 7.5 kJ/m² in the T-L orientation). Microstructural characterization³⁹ show a fine distribution of the γ' phase with sizes in a range of 2–10 nm (average of 4.4 nm), and the density is 1–3 × 10²² m⁻³. The γ' phase is not observed in the Type 304 top guide material; it might influence the fracture toughness of these materials. The γ' phase has been observed at dose levels above 4 dpa in cold worked (CW) Type 316 SS irradiated under the PWR conditions.¹¹⁵

The lower fracture toughness along the T-L orientation has been attributed to the presence of stringers consisting of long, narrow particles oriented in the rolling direction. This microstructure results in a long, narrow quasi-cleavage structure parallel to the crack advance, thereby accelerating the crack advance.³⁹ The formation of the γ' phase due to changes in the microchemistry of the material caused by neutron irradiation appears to play an important role in the neutron embrittlement of austenitic SSs. The low J_{IC} of this material might be considered a special case of materials containing a high density of particles aligned in the rolling direction. Nonetheless, these results show that irradiated austenitic SSs, particularly those with material compositions that promote the formation of the γ' phase, can have very low fracture-toughness values. The contributions that additional precipitate phases, voids, and cavities can make to fracture toughness need to be further investigated.

5.1.2 Fracture Toughness J-R Curve

Fracture toughness J-R curve data have been obtained for Types 304, 304L, and 316L SSs, including weld HAZs, and CF-3, CF-8, and CF-8M CASS materials irradiated in LWRs up to about 14 dpa,^{37-47,100} and irradiated in fast reactors to much higher dose levels. The change in the fracture toughness J-R curve with the neutron dose for Type 304 SS irradiated under LWR conditions and tested at reactor operating temperatures is shown in Fig. 51. The decrease in fracture toughness is quite rapid up to about 6 dpa, and the toughness continues to decrease moderately at higher dose levels. The effects of various parameters (e.g., material type and heat treatment; test and irradiation temperatures; neutron energy spectrum, flux, dose) are discussed next.

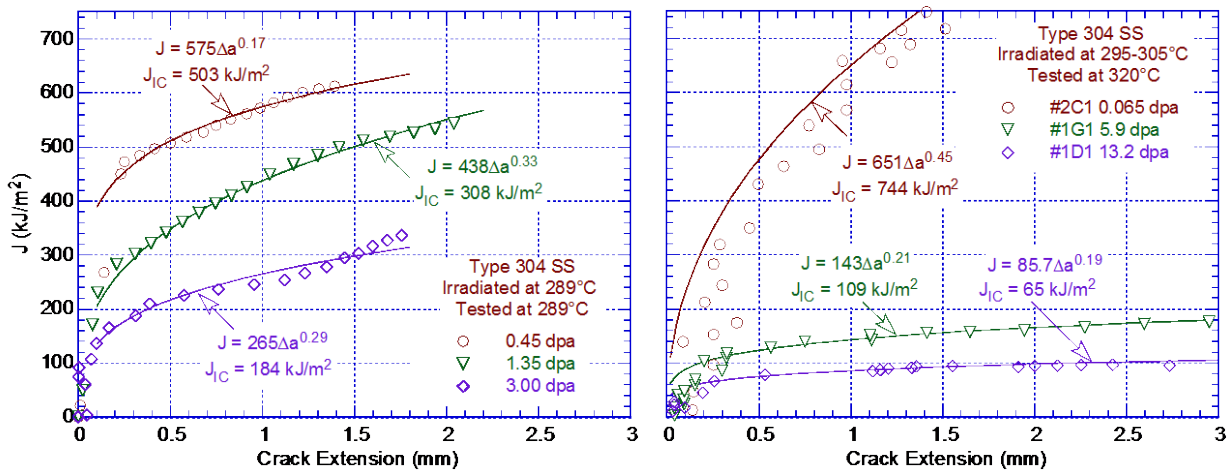


Figure 51. Fracture toughness J_{IC} as a function of neutron exposure for SSs (Refs. 45,100).

5.1.2.1 Irradiation Conditions

Fast reactor irradiations were at fluxes and temperatures higher than those typically observed in LWRs and had a different spectrum; the irradiation temperatures were 350–427°C (662–801°F). To accurately determine the effects of the neutron spectrum, flux, and temperature on the fracture properties of these materials, data on the same heat of material irradiated in a fast reactor and in an LWR to a comparable neutron dose are needed, but such data are not available. Although the general data trends appear to be similar for fast reactor irradiations and LWR irradiations, the tensile property data indicate that the tensile strength is higher and the ductility is lower for the BWR-irradiated materials than for the materials irradiated in fast reactors.^{47,100} However, the existing data are inadequate to determine the individual contributions of the irradiation temperature, flux, and energy spectrum to the degradation of fracture properties in irradiated austenitic SSs. Therefore, fast reactor data should be used only for establishing data trends and not for establishing the extent of embrittlement.

5.1.2.2 Material Type

Most of the J-R curve data on LWR-irradiated austenitic SSs have been obtained for Type 304 and 304L SSs. Data on Type 316, 316L, 316CW, and 347 SSs are very limited. Similarly, there have been only a few J-R curve tests on LWR-irradiated weld HAZ materials and CASS materials. Some differences in the fracture toughness data trends appear for the various grades of wrought austenitic SSs, but these differences may be artifacts of the limited data. For

example, the heat-to-heat variation for a particular grade may be comparable to the apparent differences between grades in the current data. A few select data from Fig 50 on wrought Types 304, 316, 304L, and 316L SS, Type 304/304L HAZ material, and sensitized Type 304 SS, are plotted in Fig. 52. Note that different symbol colors are used for the low-C (green) and high-C (orange) grades of SSs. The results indicate that the toughness of the high-C grades decreases faster than that of the low-C grades. There is little or no effect of sensitization treatment for high-C Type 304 SS. In addition, for the same irradiation conditions, the fracture toughness of the weld HAZ materials is lower than that of the solution-annealed materials. Example of fracture toughness J-R curves for irradiated, sensitized SS, SS weld HAZ material, and CASS CF-8M material, are shown in Fig. 53. However, these results are based on very limited data.

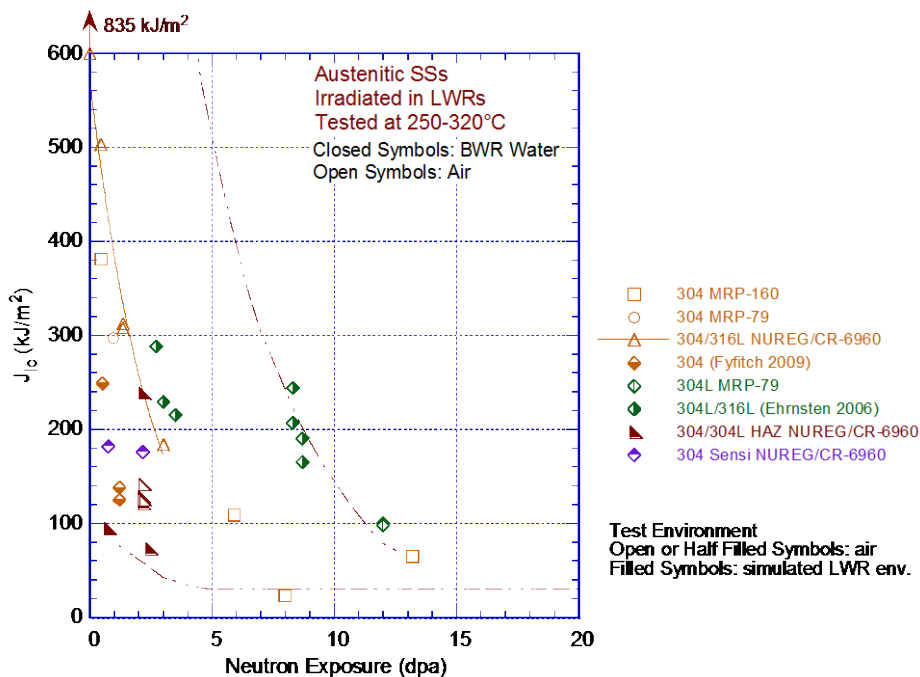


Figure 52. Change in fracture toughness J_{Ic} for a select data set as a function of neutron exposure for LWR irradiated austenitic SSs (Refs. 37–40,42,43,45–47,100).

The available data indicate that although the fracture toughness of unirradiated CW steels is lower than that of unirradiated solution-annealed steels, the decrease in the toughness of CW steels with neutron exposure is lower than and the J_{Ic} at saturation is higher than those values for irradiated solution-annealed steels.⁴⁷ However, the available data for CW steels are from fast reactor irradiations at relatively high temperatures of 400–427°C (752–800°F). The saturation J_{Ic} for CW SSs is likely to be lower for irradiations at LWR operating temperatures (i.e., 290–320°C [554–608°F]) and the differences may not be significant.

Unirradiated, thermally aged CASS materials have a lower fracture toughness than do wrought austenitic SSs, and their fracture toughness generally decreases more rapidly with neutron exposure than does that of solution-annealed materials. However, the existing data indicate that the saturation toughness for the CASS materials is not significantly different from that of solution-annealed SSs; the same bounding curve for J_{Ic} is applicable for both wrought austenitic SSs and CASS materials. Although CF-8 or CF-3 materials are used in the construction of

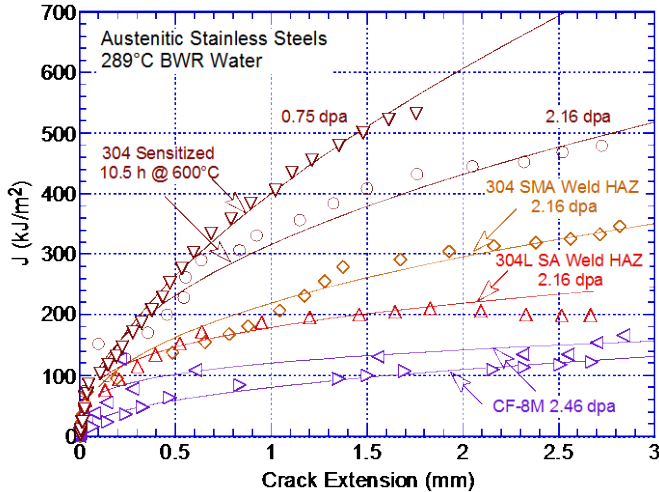


Figure 53. Fracture toughness J-R curves for sensitized Type 304 SS, weld HAZ materials of Type 304 and 304L SS, and CF-8M steel in high-purity water at 289°C (Ref. 47).

LWR core internals, in the ANL study, initially, the only data for LWR-irradiated CASS were data on CF-8M material. The reason was that significant amounts of experimental data from several heats of CF-3/CF-8 material are needed to accurately establish the lower-bound fracture toughness, whereas a few tests on CF-8M material can provide the worst-case value of fracture toughness for CF-3/CF-8 materials.

5.1.2.3 Test Temperature

The fracture toughness of unirradiated austenitic SSs is known to decrease as the test temperature is increased. The change in the J_{IC} of irradiated SSs as a function of test temperature is plotted in Fig. 54 for several grades of SSs and welds irradiated in LWRs and fast reactors. The results indicate that the fracture toughness of austenitic SS welds is lower than that of wrought SSs. For example, the J_{IC} values of a 308L weld irradiated to 0.7 dpa less than 200 kJ/m², and the value is slightly higher at 250°C than at RT. The results also indicate that for wrought SSs, the fracture toughness of materials irradiated to relatively low dose (<5 dpa) decreases with increasing test temperature in most cases. However, for steels

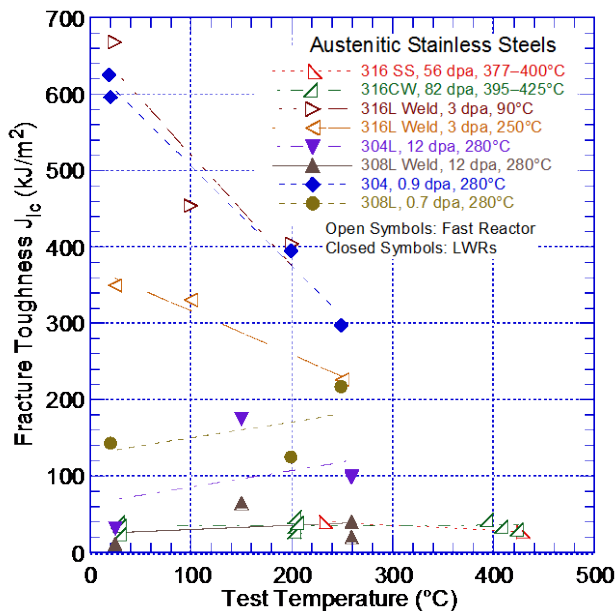


Figure 54. Fracture toughness J_{IC} of irradiated austenitic SSs and welds as a function of test temperature (Ref. 100).

irradiated to more than 12 dpa, the test temperature has little effect on fracture toughness. Note that at neutron dose of 12 dpa, the toughness value is already low, which makes it difficult to discern definitive trends. The data also indicate differences in the fracture morphology of highly irradiated materials. At temperatures above 230°C (446°F), the failure mode is predominantly channel fracture, characterized by a faceted fracture surface. It is associated with highly localized deformation along a narrow band of slip planes, in which the initial dislocation motion along the narrow band clears away the irradiation-induced defect structure, creating a defect-free channel that offers less resistance to subsequent dislocation motion. The localization of the deformation ultimately leads to channel failure.

5.1.2.4 Test Environment

Nearly all of the existing fracture toughness data have been obtained from tests in air and on specimens that were fatigue precracked at relatively low load ratios (typically 0.1–0.2) in RT air. However, in reactor core components, cracks are initiated primarily by SCC and have intergranular morphology, whereas the fatigue precracks in fracture toughness tests are always transgranular). In addition, the corrosion/oxidation reaction could influence fracture toughness. For example, hydrogen generated from the oxidation reaction could diffuse into the material and change the deformation behavior by changing the stacking-fault energy of the material. To investigate potential effects of the reactor coolant environment on the fracture toughness of austenitic SSs and CASS materials, J-R curve tests have been conducted on these materials in a BWR normal water chemistry (NWC) environment¹⁰⁰ and in low-DO, high-purity water or simulated PWR environments.⁹¹ The effect of the reactor coolant environment on the fracture toughness of CASS materials was discussed earlier in Section 2.4.3.1.

The results indicate that both NWC BWR and simulated low-DO PWR environment can decrease the fracture toughness of these materials. However, the effect may be insignificant for materials with poor fracture toughness (i.e., J_{IC} values of $<150 \text{ kJ/m}^2$),^{46,47,91,100} For example, the fracture toughness J-R curves for irradiated Type 304L SAW HAZ in air and water environments are essentially identical (Fig. 55). However, for a CF-8M material aged for more than 15 years at 350°C, the J-R curve data for specimens precracked in air at 54°C and then tested in an shutdown water chemistry PWR environment at 54°C are significantly lower than the data for those specimens tested in air (Fig. 24). The specimens precracked in PWR water

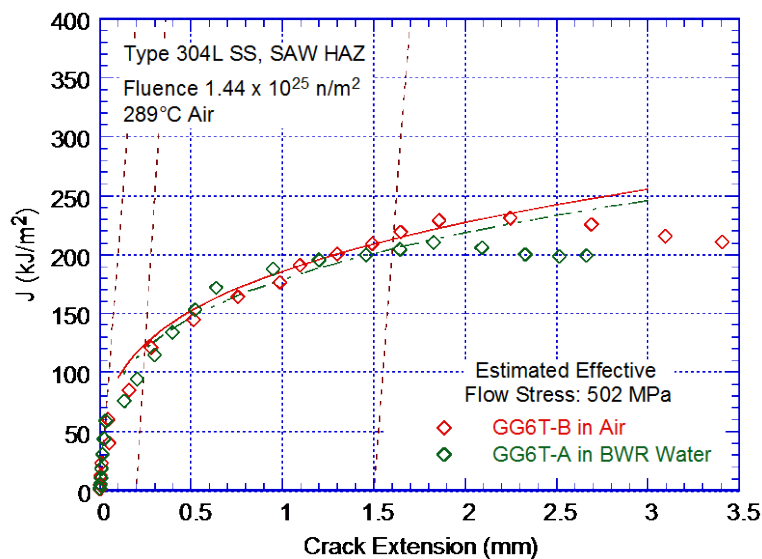


Figure 55.
Fracture toughness J-R curves for irradiated specimens of Type 304L SAW HAZ in air and NWC BWR environment (Ref. 47).

at 315°C and tested in PWR water also show reduced fracture toughness, but the effect is less.⁸⁰ The significant decrease in fracture toughness is attributed to the synergism between hydrogen embrittlement and thermal embrittlement. Similarly, J-R curve data for Type 316L gas tungsten arc (GTA) welds indicated that the reactor coolant environment could decrease the fracture toughness by up to 40% relative to that in air.¹¹⁷

The potential contribution of hydrogen-induced embrittlement has also been observed in the thermal embrittlement study at ANL. The J-R curves for the two tests on ¼-T CT specimens of thermally aged and irradiated CF-8M steel in NWC BWR water are shown in Fig. 56. Unfortunately, companion tests in air were not conducted on the irradiated material. However, the fracture toughness J-R curve obtained for 1-T CT specimens of unirradiated, thermally aged material are included in the figure. In the two tests in water, large load drops, accompanied by crack extensions of up to 0.5 mm in one specimen and 1.0 mm in the other, were observed at the onset of these crack extension. Such load drops are not typically observed during tests in air.¹⁶ Thus, although available fracture toughness data in reactor coolant environments are inclusive, the limited data suggest that there could be environmental effects on the fracture toughness of CASS material and austenitic SS welds, at least for materials with moderate or superior fracture toughness. Additional tests on irradiated CASS materials or SS welds in air and water environments are needed to determine the possible effects of LWR coolant environments on their fracture toughness.

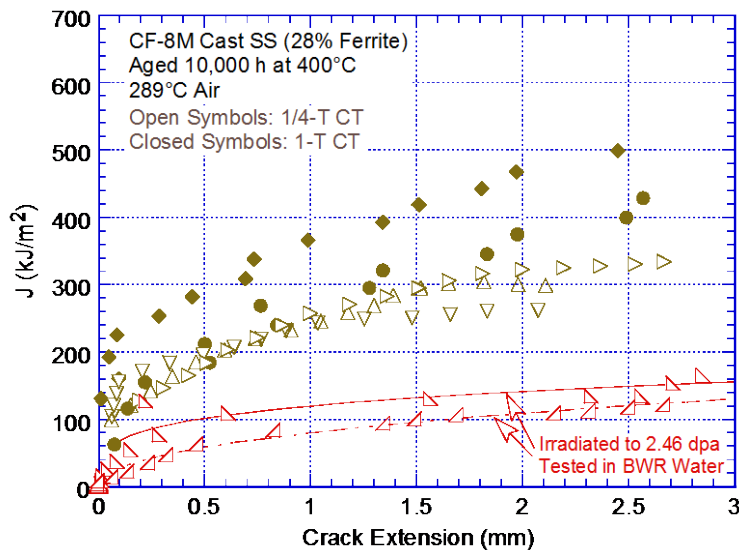


Figure 56.
Fracture toughness J-R
curves for thermally aged
and irradiated CF-8M steel
(Ref. 47).

5.1.2.5 Irradiation Temperature

The available data are not adequate to establish accurately the effects of the irradiation temperature on the fracture toughness of austenitic SSs. However, tensile data for austenitic SSs indicate that irradiation hardening is highest, and ductility loss is at its maximum at an irradiation temperature of ~300°C (~572°F).¹¹⁸ Thus, the J_{IC} values for all materials irradiated at temperatures above 350°C (662°F) (e.g., fast reactor irradiations), particularly for neutron exposures of more than 20 dpa, should be greater than the J_{IC} values for materials irradiated at temperatures of 290–320°C (554–608°F). As mentioned before, to accurately evaluate the potential effects of irradiation temperature on the fracture properties of austenitic SSs and CASS materials, fracture toughness data are needed for a specific heat of material irradiated in LWRs at temperatures of 280–370°C (536–798°F).

5.2 Lower-Bound Fracture Toughness Curve

In NUREG/CR-7027, the available fracture toughness data on wrought and cast austenitic SSs and associated welds irradiated in fast reactors or LWRs were reviewed and evaluated to define the lower-bound fracture toughness J_{Ic} value or coefficient C of the J-R curve as a function of neutron dose (in dpa).^{46,47} The lower-bound curves represent the change in fracture toughness parameters, such as the coefficient C of the power-law J-R curve and the corresponding J_{Ic} value, as a function of neutron dose. The trend curve considers the following:

- (a) The threshold neutron exposure for radiation embrittlement of austenitic SSs and a minimum fracture toughness for these materials irradiated to less than the threshold value,
- (b) The saturation neutron exposure and a saturation fracture toughness for materials irradiated to greater than this value, and
- (c) A description of the change in fracture toughness between the threshold and saturation neutron exposures.

The change in initiation toughness J_{Ic} of (a) wrought austenitic SSs and (b) CASS materials and weld metals as a function of neutron exposure (dpa) is shown in Fig. 57. The change in the lower-bound J_{Ic} value as a function of the neutron dose (dpa) is given by

$$J_{Ic} = 7.5 + 110 \exp[-0.35(\text{dpa})^{1.4}]. \quad (70)$$

Note that the JAPEIC data on Type 304 SS only is not bounded by the lower bound curve; the data were obtained on short rod specimens and not the standard fracture toughness CT specimens. The lower-bound curve is defined essentially by the austenitic SS weld data. The lower-bound curve represents the following:

- (i) Threshold dose of about 0.3 dpa for neutron embrittlement,
- (ii) Minimum fracture toughness J_{Ic} of ~ 116 kJ/m² for neutron doses below 0.1 dpa,
- (iii) Saturation threshold of about 5–7 dpa beyond which the fracture toughness of these materials appears to saturate,
- (iv) Saturation fracture toughness J_{Ic} of 7.5 kJ/m² (or K_{Ic} or K_{Jc} of 38 MPa m^{1/2}), and
- (v) Description of the change in toughness between 0.1 and 10 dpa.

The J_{Ic} value of ~ 116 kJ/m² for neutron doses below the threshold dose is appropriate for thermally aged and unaged CASS materials and SS flux welds. A value that is higher than 116 kJ/m² may be considered for the minimum fracture toughness J_{Ic} for wrought austenitic SSs irradiated below the threshold dose for neutron embrittlement. However, appropriate justification for using a higher value should be provided. The description of the change in fracture toughness below the threshold value would also change accordingly. The saturation J_{Ic} value of 7.5 kJ/m² does not change; it is the same for wrought and cast SSs and their welds. The K_{Jc} (MPa m^{1/2}) values determined from the lower-bound trend curve given by Eq. 70 are comparable to those predicted from the MRP lower-bound model proposed for PWRs⁴² at 0.3

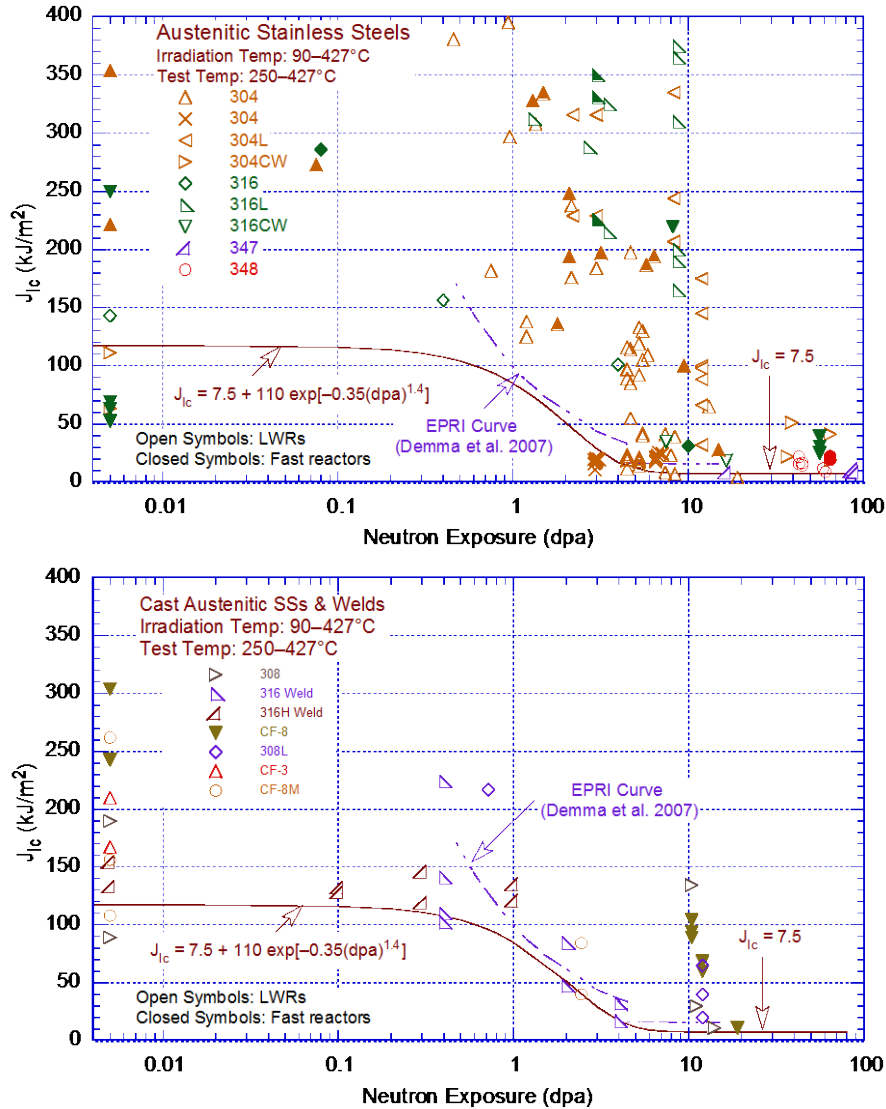


Figure 57. Change in initiation toughness J_{IC} of (a) wrought austenitic SSs and (b) CASS materials and weld metals as a function of neutron exposure. The data points plotted at 0.005 dpa are for unirradiated materials (Ref. 47).

and 7.0 dpa. The MRP model bounds all the fracture toughness data from fast reactors, BWRs, and PWRs and is given by the expression,

$$K_{Jc} = 180 - 142[1 - \exp(-dpa)]. \quad (71)$$

The existing fracture toughness J_{IC} data at 290–320°C for CASS materials irradiated under LWR conditions are plotted as a function of neutron dose in Fig. 58.^{37,41,42,80,95,98,100,109,117,119,120} Note that the fast-reactor irradiated data for a heat of CF-8 material (slashed square symbols) are included in the figure because they have been used for evaluating neutron embrittlement of CASS CF-8 materials in PWRs. Furthermore, the data were obtained at RT. Therefore, as shown in Fig. 54, the actual fracture toughness of moderate to high toughness materials is expected to be lower at reactor temperatures. The fracture toughness data obtained at ANL on neutron irradiated CASS materials in LWR environments and the data obtained earlier on these

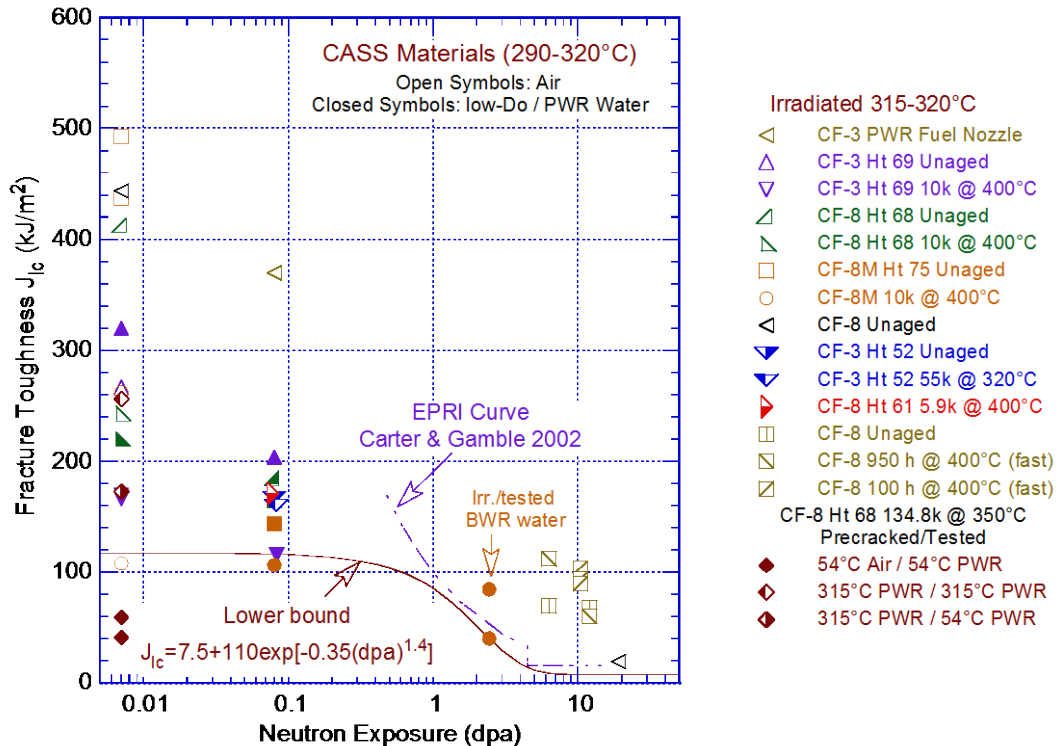


Figure 58. Plots of fracture toughness J_{IC} values as a function of neutron dose for (a) austenitic SS welds, (b) CASS materials, and (c) austenitic SS HAZ. Solid line represents the lower-bound J_{IC} values proposed in NUREG/CR-7027. The data points plotted at 0.007 dpa are for unirradiated materials.

materials in air are listed in Table 7. Note that the recent data obtained at ANL were for CASS materials irradiated to a neutron dose of 0.08 dpa. This irradiation level was selected to help understand the combined effects of thermal and neutron embrittlement on SSs with a duplex structure, consisting of both austenite and ferrite phases. It is well-established that at an irradiation dose of about 0.1 dpa, the neutron embrittlement of the ferrite phase is essentially complete, but the embrittlement of the austenite phase occurs at irradiation levels above a threshold value of 0.3 dpa. In addition, data on materials irradiated to less than 0.1 dpa are needed to accurately evaluate the possible effects of the synergism between thermal and neutron embrittlement of CASS materials and their welds.

Equations. 70 and 71 predict a saturation fracture toughness K_{IC} of 38 MPa m^{1/2}. For materials irradiated below the threshold dose for irradiation embrittlement, Eq. 70 predicts a minimum K_{IC} of about 151 MPa m^{1/2}, but the MRP (Eq. 71) expression predicts fracture toughness values that for some materials, such as SS weld HAZ, may be higher than the minimum toughness of the materials in the unirradiated condition. The existing data for BWR-irradiated austenitic SSs is not bounded by the disposition curve proposed by EPRI for BWRs. For example, at neutron doses of <0.7 dpa, the J_{IC} values based on the EPRI curve are higher than the minimum J_{IC} of some heats of wrought SSs and most thermally aged CASS with >15% ferrite.¹⁶ In addition, the saturation K_{IC} of 55 MPa m^{1/2} at 4.5 dpa for the EPRI curve is also higher than the value of 38 MPa m^{1/2} previously proposed by MRP for PWRs.⁴² The saturation K_{IC} for the EPRI curve was based on data for which the specimen orientation was unknown. As discussed above, recent data indicate that fracture toughness in the transverse orientation is nearly half of that in

Table 7 Fracture toughness J-R curve data on irradiated CASS CF-3, CF-8, and CF-8M materials in air and LWR environments.

Grade	Heat	Material Condition	Unirradiated Material in Air at 290°C			Unirradiated Material in Low-DO Water at 320°C			Irradiated Material ^a in Low-DO Water at 320°C		
			C	n	J _{Ic} (kJ/m ²)	C	n	J _{Ic} (kJ/m ²)	C	n	J _{Ic} (kJ/m ²)
CF-3	69 (21%)	Unaged	756	0.31	700	536	0.68	320	430	0.64	204
CF-3	69 (21%)	Unaged	425	0.54	266	–	–	–	–	–	–
CF-3	69 (21%)	Aged	296	0.51	167	353	0.66	170	362	0.85	116
CF-3	52 (14%)	Unaged	–	–	–	–	–	–	347	0.65	168
CF-3	52 (14%)	Aged	–	–	–	–	–	–	419	0.80	161
CF-8	68 (15%)	Unaged	783	0.27	753	-	-	>500	359	0.57	183
CF-8	68 (15%)	Aged	396	0.51	242	395	0.58	220	372	0.62	171
CF-8	61 (13%)	Aged	–	–	–	–	–	–	406	0.60	205
CF-8M	75 (25%)	Unaged	583	0.45	437	–	–	–	336	0.66	145
CF-8M	75 (25%)	Unaged	600	0.35	493	–	–	–	–	–	–
CF-8M	75 (25%)	Aged	274	0.46	156	–	–	–	259	0.64	106
CF-8M	75 (25%)	Aged	364	0.32	262	–	–	–	–	–	–
CF-8M	75 (25%)	Aged	–	–	–	–	–	–	120 ^b	0.24	84
CF-8M	75 (25%)	Aged	–	–	–	–	–	–	80 ^b	0.45	40

^a All specimens were irradiated to a neutron dose of 0.08 dpa at 315°C and tested in low-DO high-purity water or simulated PWR water at 320°C, except for the last two specimens (Heat 75), which were irradiated to 2.46 dpa at 297°C and tested at 289°C in high-purity water with 400 parts per billion (ppb) DO.

^b Tested at 289°C in high-purity water containing 400 ppb DO.

the longitudinal orientation.³⁹ Therefore, the bounding K_{Ic} values above 4.5 dpa are likely to be lower than 55 MPa m^{1/2}.

A fracture toughness J-R curve may be used to analyze material behavior for loading beyond J_{Ic}. The J-R curve is expressed in terms of the J integral and crack extension (Δa) by the power law $J = C(\Delta a)^n$. At dose levels below the threshold dose for saturation (i.e., at dose levels less than ~7 dpa), the effect of neutron irradiation on the fracture toughness of austenitic SSs can be represented by a decrease in the coefficient C of the power-law correlation for the J-R curve with neutron dose. The variation of the fracture toughness coefficient C as a function of neutron dose for the data shown in Fig. 58 is plotted in Fig. 59. One curve in the figure represents the disposition curve proposed by EPRI for BWRs,³⁸ and the other represents a trend curve proposed in NUREG/CR-7017 for coefficient C that bounds the existing data. For neutron dose less than 5 dpa, the existing fracture toughness data are bounded by the following expression for C:

$$C = 25 + 175 \exp[-0.35(\text{dpa})^{1.4}], \quad (72)$$

and an exponent n equal to 0.37 (i.e., median value of the experimental data). The exponent n of the power-law curve typically ranges from 0.35 to 0.70 for unirradiated materials and 0.16 to 0.65 for irradiated materials. Unlike the behavior seen for thermally aged cast austenitic SSs (in which exponent n typically decreases with a decrease in fracture toughness),¹⁶ no obvious trend of n with fluence is evident. Based on the material and irradiation conditions, a conservative value of 0.3 for exponent n may be used to evaluate the neutron embrittlement of these materials. Equation 72 yields a minimum C value of 192 kJ/m² (1094 in.-lb/in.²) for materials

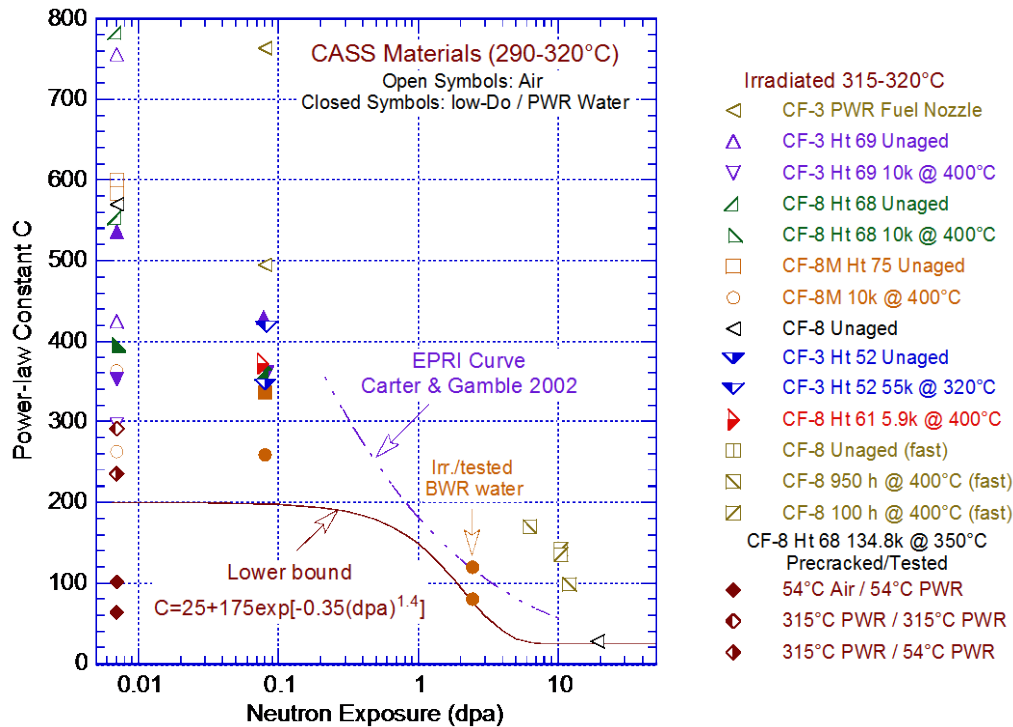


Figure 59. Coefficient C of the J-R curve as a function of neutron dose for CASS materials. Solid line represents the lower-bound C values proposed in NUREG/CR-7027. The data points plotted at 0.007 dpa are for unirradiated materials.

irradiated to less than 0.1 dpa and a minimum C value of $\sim 31 \text{ kJ/m}^2$ ($\sim 177 \text{ in.-lb/in.}^2$) for materials irradiated to 7 dpa.

For the data shown in Figs. 58 and 59, the J-integral values at a crack extension of 2.5 mm, $J_{2.5}$, are plotted as a function of neutron dose in Fig. 60. The solid curve in the figure represents the $J_{2.5}$ values that bound the existing experimental data. The curve was obtained by using the power-law J-R curve relationship, with coefficient C determined from Eq. 72 and the median value of 0.37 for exponent n. The lower-bound curve indicates that for CASS materials irradiated up to 0.5 dpa, the predicted $J_{2.5}$ values are above the screening value of 255 kJ/m^2 ($1456 \text{ in.-lb/in.}^2$).

Note that most of the J-R curve data for neutron irradiated SSs have been obtained on $\frac{1}{2}$ -T or $\frac{1}{4}$ -T CT specimens that were about 6-mm thick. Therefore, the validity of the fracture toughness data using the small CT specimens needs to be assessed. The fracture mechanics approach correlates the behavior of components with that of specimens by using the K parameter. It considers that if the two cracks have the same K, then they have the same strains and stresses in the region near the crack tip. The ASTM specifications for specimen K/size criteria are intended to ensure that the plastic zone is small enough and K is controlling the crack behavior. It has been often argued that since the K/size criterion was developed for materials that show work hardening and it may not be applicable for materials that are irradiated to fluence levels where, on a local level, they do not strain harden and exhibit strain softening. Recent investigations have evaluated the validity of the K/size criterion for irradiated materials by comparing the plastic strain distribution in a $\frac{1}{2}$ -T CT specimen estimated from finite element method calculations with experimentally observed plastic deformation area.^{121,122} The plastic

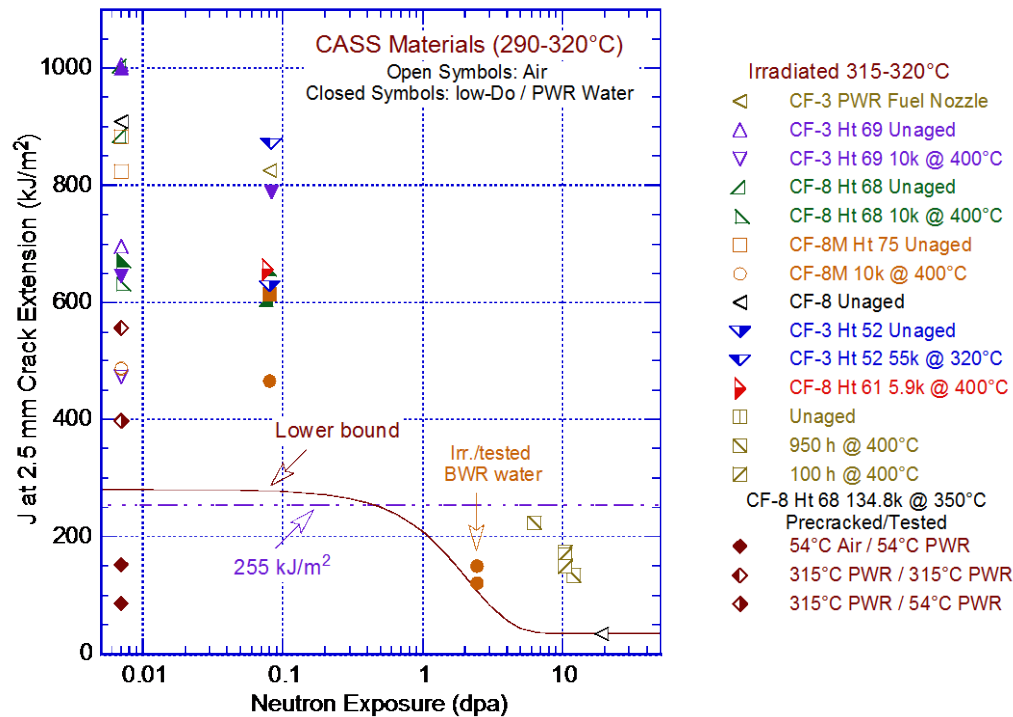


Figure 60. Fracture toughness $J_{2.5}$ values as a function of neutron dose for CASS materials. Solid line represents the lower-bound $J_{2.5}$ values proposed in NUREG/CR-7027. The data points plotted at 0.007 dpa are for unirradiated materials.

zone size was estimated to be 0.2–0.4 mm at $K = 30 \text{ MPa m}^{1/2}$.¹²¹ The results indicate that for an austenitic SS irradiated to $3 \times 10^{21} \text{ n/cm}^2$, the appropriate K range is at least $30 \text{ MPa m}^{1/2}$ for a (5.8-mm thick) CT specimen.

Figure 60 shows the results of two tests of CF-8M material thermally aged for 10,000 h at 400°C and then irradiated to well above the threshold dose for neutron embrittlement (shown as closed circles). The resulting $J_{2.5}$ values for these two tests are bounded by the proposed lower-bound J-R curve. As discussed above, since only CF-3/CF-8 and, in a few cases, CF-3M CASS materials are used for designs of all BWRs and PWRs, the data for CF-8M represent the worst-case values. Actual values for CF-3/CF-8 materials would be higher. However, there is little or no data on LWR-irradiated CF-3 and CF-8 materials to accurately establish the lower-bound J-R curves for these materials during service in LWRs. The only data for CF-8 material is for fast reactor irradiation. The existing data indicate that for the same neutron dose, the embrittlement of LWR irradiated materials is greater than that of materials irradiated in a fast reactor. In addition, the CF-8 data are on materials irradiated at 325°C; limited data indicate that the extent of embrittlement is greater under BWR service conditions than PWR service conditions.

5.3 Methodology for Incorporating Irradiation Effects on CASS Materials including the Combined Effects of Thermal and Neutron Embrittlement

5.3.1 Threshold Neutron Dose for Irradiation Effects

To account for the effects of thermal aging and neutron irradiation embrittlement on the fracture toughness of reactor core internal components, the NRC staff has proposed an aging

management program (AMP) for license renewal.¹²³ The program does not directly monitor for loss of fracture toughness that is induced by either thermal or neutron irradiation embrittlement. Instead, the impact of a loss of fracture toughness on component integrity is indirectly managed by using visual or volumetric examination techniques to monitor for cracking in the components. If cracking is detected in the components, a flaw tolerance evaluation is performed by using acceptable reduced fracture toughness properties.

The AMP for PWR vessel internals follows the guidance found in EPRI report MRP-227.¹²⁴ The AMP states that a loss of fracture toughness due to thermal and/or neutron embrittlement of CASS materials can occur as a result of exposure to neutron fluence of $>10^{19}$ n/cm² (E of >1 MeV) (i.e., 0.015 dpa) or if CASS material is more susceptible to thermal embrittlement. A fracture toughness value of 255 kJ/m² (1450 in.-lb/in.²) at a crack extension of 2.5 mm (0.1 in.) is used to differentiate between CASS materials that are not susceptible and those that might be susceptible to thermal embrittlement. The screening criteria to determine the susceptibility of CASS components to thermal aging embrittlement are outlined in Table 1.⁵¹ Based on the review and evaluation of the current fracture toughness data of thermally aged CASS materials, a proposed revision of the screening criteria is presented in Table. 5.

Regarding the neutron dose threshold above which the potential combined effects of thermal and neutron embrittlement are significant and need to be evaluated, the lower-bound curve shown in Fig. 60 indicates that for CASS materials irradiated up to 0.5 dpa, the predicted $J_{2.5}$ values are above the screening value of 255 kJ/m² (1456 in.-lb/in.²). If needed, the lower-bound fracture toughness curves described above can be used to perform a flaw tolerance evaluation. However, note that the fracture toughness of SS weld metals may be significantly lower than this threshold value (see Fig. 57).

5.3.2 Potential Effects of Thermal and Neutron Embrittlement

The embrittlement of the ferrite phase because of neutron irradiation occurs at lower dose levels than does embrittlement of the austenite phase. A shift in the nil-ductility transition (NDT) temperature of up to 150°C (302°F) has been observed in pressure vessel steels irradiated to 0.07–0.15 dpa.¹²⁵ Thus, embrittlement of ferrite is expected to occur at 0.05–0.50 dpa, whereas any significant neutron embrittlement of the austenite phase occurs only at above ~0.4 dpa (Fig. 58-60). In recent studies at ANL, fracture toughness tests have been conducted in LWR environments on unaged and aged heats of CF-3, CF-8, and CF-8M materials that were either in an unirradiated condition or irradiated to a neutron dose of 0.08 dpa at 315°C in the Halden reactor. The results are shown in Fig. 61. The ferrite contents of the CF-3, CF-8, and CF-8M materials, determined from Hull's equivalent factors were, 21.0%, 14.9%, and 24.8%, respectively. The results indicate that only the J_{IC} values are slightly lower for the aged and irradiated materials than those that were only aged or irradiated. The values of coefficient C and $J_{2.5}$ show no effect from combined thermal and neutron embrittlement.

Similarly, the fracture toughness data for two other heats of thermally aged and irradiated CF-8 material (Heats 52 and 61, containing 14% and 13% ferrite, respectively) yield $J_{2.5}$ values that are significantly above 255 kJ/m². Therefore, the existing data indicate little or no combined effect from thermal and neutron irradiation. Furthermore, the fracture toughness ($J_{2.5}$) values of aged CASS CF-3 and CF-8 materials irradiated to a neutron dose of less than 0.5 dpa are above the screening value of 255 kJ/m² (1456 in.-lb/in.²) proposed by EPRI.⁹³

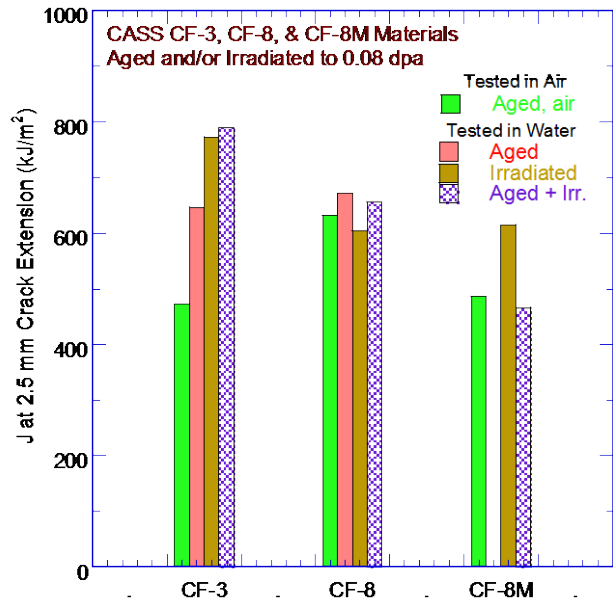
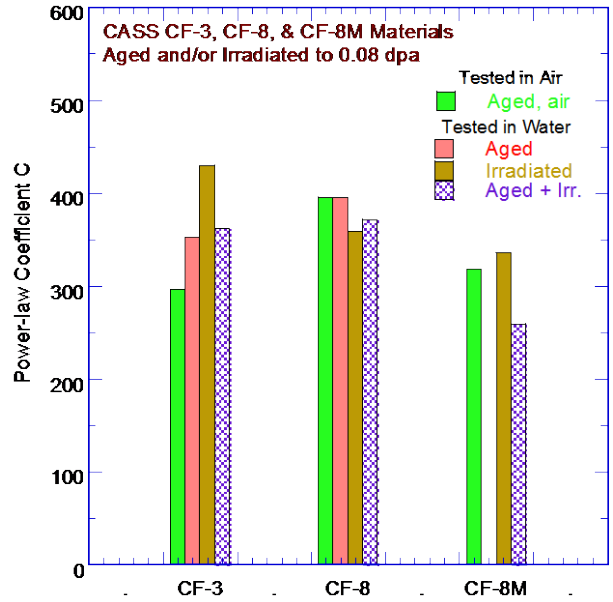
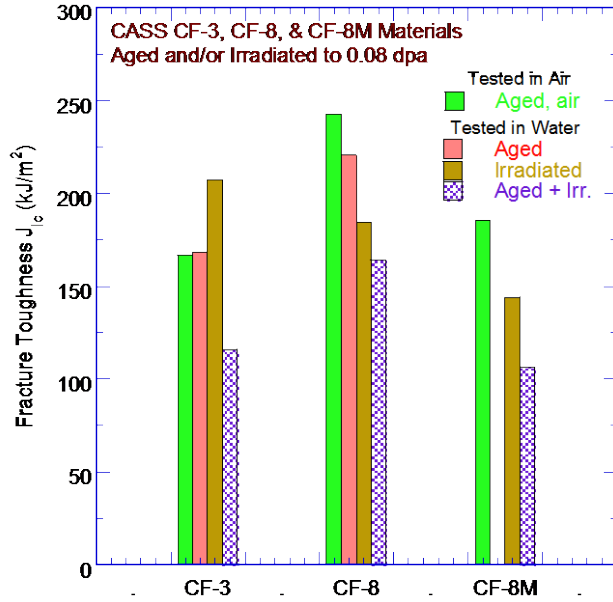


Figure 61. Comparison of the fracture toughness J_{IC} , coefficient, and $J_{2.5}$ value obtained in air and LWR environment at 290–320°C of CF-3, CF-8, and CF-8M materials in the unaged and aged as well as unirradiated and irradiated conditions.

6 SUMMARY

The procedure and correlations presented earlier in NUREG/CR-4513, Rev. 1, for predicting the Charpy-impact energy and fracture toughness J-R curve of aged CASS CF-3, CF-3M, CF-8, and CF-8M materials from known material information have been updated by using a much larger database. The applicability of the methodology has been extended to materials with ferrite contents of up to 40%. In addition, for CASS materials used in the reactor core support structure and core internal components, recommendations are provided for evaluating the combined effects of thermal and neutron embrittlement.

As in NUREG/CR-4513 Rev. 1, the fracture toughness and tensile properties of a specific CASS material are estimated from the extent and kinetics of thermal embrittlement. Thermal embrittlement of CASS materials is characterized in terms of RT Charpy-impact energy. Thus, the extent of thermal embrittlement represents the change in Charpy-impact energy. The extent of thermal embrittlement at "saturation" (i.e., the minimum impact energy that can be achieved for the material after long-term aging) is determined from the chemical composition of the steel and its ferrite content. The Charpy-impact energy as a function of the time and temperature of the reactor service is estimated from the kinetics of thermal embrittlement, which are expressed by the activation energy for the degradation of Charpy-impact energy due to thermal aging. The activation energy is also determined from the chemical composition of the material and ferrite content. The initial impact energy of the unaged steel is required for these estimates. The fracture toughness J-R curve for the material (expressed by coefficient C and exponent n) is then obtained from correlations between the RT Charpy-impact energy and fracture toughness parameters. A common lower-bound J-R curve for CASS materials with an unknown chemical composition is also defined for a given grade of material, range of ferrite contents (e.g., <10%, >10–15%, >15–20%, >20–25%, >25–30%, and >30–40%), and temperature. The method for estimating the mechanical properties of CASS materials during reactor service is described.

For CASS materials used in the reactor core support structures and core internal components, the available data are inadequate to definitively establish the effects of thermal and neutron embrittlement of various CASS materials as a function of service time and temperature. The combined effects of thermal and neutron embrittlement are estimated from the lower-bound fracture toughness curves expressed as a function of neutron dose. The fracture toughness is defined in terms of the coefficient C, exponent n, and J_{Ic} of the fracture toughness J-R curve. However, the existing data are inadequate to definitively determine the combined effects of thermal and neutron embrittlement of CASS materials. Experimental data on aged material irradiated in LWRs to neutron doses <0.01 dpa are needed to better define such effects.

The tensile yield and flow stresses and the Ramberg/Osgood parameters for tensile strain hardening are estimated from the flow stress of the unaged material and the kinetics of embrittlement. The fracture toughness J_{Ic} values for aged CASS materials are then determined from the estimated J-R curve and flow stress. Only the chemical composition, initial Charpy-impact energy, and flow stress of the unaged material are needed for the estimates.

The significant differences between NUREG/CR-4513 Rev. 1 and this report are as follows:

- (i) *Embrittlement-Charpy-impact Energy*: Eqs. 18–26 correspond to Eqs. 3.2.4–3.2.12 of Rev. 1; Eqs. 21 and 24 are updated versions of Eqs. 3.2.7 and 3.2.10, all others are the same. For CF-8M materials, the correlation between the RT Charpy-impact energy and material parameter ϕ was revised; the effect is significant for CF-8M materials with Ni content of $\geq 10\%$.

- (ii) *Embrittlement-Fracture Toughness J-R Curve*: Eqs. 27–44 correspond to Eqs. 3.2.13–3.2.26 of Rev. 1. Eqs. 29 and 35 are new and Eqs. 39–44 are updated versions of 3.2.15, 16, 19, 22,23, and 26.

For CF-8M materials, the correlations between the RT Charpy-impact energy and coefficient C of the J-R curve at RT and at 290–320°C have been extended to include CASS materials with a ferrite content of up to 40%. The new correlations are applicable to materials with relatively poor RT Charpy-impact energies (i.e., <35–45 J/m²). In addition, the correlations between the RT Charpy-impact energy and exponent n of the J-R curve at RT and at 290–320°C have been revised. Estimates of n made from using the updated expressions are slightly lower, particularly for CF-8 materials.

- (iii) *Minimum Fracture Toughness of Unaged CASS Materials*: Eq. 45 is the same as Eq. 3.2.27 of Rev. 1 and Eq. 46 is an updated version of Eq. 3.2.28. The minimum fracture toughness J-R curve for centrifugally cast CASS materials, was revised; the coefficient C of the J-R curve was decreased from 650 to 550.
- (iv) New lower-bound curves are presented for correlating the saturation RT Charpy-impact energy and the ferrite content for CF-3, CF-3M, CF-8, and CF-8M materials. These correlations are used to define the lower-bound J-R curves for CASS materials containing ferrite in a specific range (e.g., <10%, >10–15%, >15–20%, >20–25%, >25–30%, and >30–40%).
- (v) Recommendations are provided for estimating the lower-bound fracture toughness curves for CASS materials used in the reactor core support structures and core internal components.

These updated expressions for estimating fracture toughness of CASS materials during reactor service have the following impact on the criteria proposed by NRC (Table 1) for determining the susceptibility of various categories of CASS components to thermal aging embrittlement. Based on the casting process and whether the materials contains low Mo (0.5 wt.% max.) or high Mo (2.0–3.0 wt.%), the proposed criteria specify the ferrite content above which the material would be susceptible to thermal embrittlement. The updated criteria are presented in Table 5.

- The criteria for low-Mo CF-3 and CF-8 materials have not changed. All centrifugally cast materials and static cast materials containing ≤20% ferrite are not susceptible to thermal embrittlement. Only static cast materials containing >20% ferrite are potentially susceptible.
- The criteria for CF-8M materials depend on whether the material contains ≥10 wt.% Ni.
 - The criterion for static cast CF-8M materials containing <10% Ni has not changed. Static cast materials with ≤14% ferrite are not susceptible and with >14% ferrite are potentially susceptible.
 - The criterion for centrifugally cast CF-8M materials containing <10% Ni has been revised. The threshold value of ferrite content has been decreased from 20% to 19% ferrite. Centrifugally cast materials with ≤19% ferrite are not susceptible and with >19% ferrite are potentially susceptible to thermal embrittlement.
 - The criterion for static cast CF-8M materials containing ≥10% Ni has been revised. The threshold value of ferrite content has been decreased from 14% to 11% ferrite. Static cast materials with ≤11% ferrite are not susceptible and with >11% ferrite are potentially susceptible to thermal embrittlement.

- The criterion for centrifugally cast CF-8M materials containing $\geq 10\%$ Ni has been revised. The threshold value of ferrite content has been decreased from 20% to 13% ferrite. Centrifugally cast materials with $\leq 13\%$ ferrite are not susceptible and with $> 13\%$ ferrite are potentially susceptible to thermal embrittlement.

The methodology presented in this report is only applicable to service times that are equivalent to 10,000 h at 400°C. This corresponds to

- ≥ 125 efpy at 290°C for CF-8/CF-3 materials, and
- ≥ 30 efpy at 320°C for CF-8/CF-3 and ≥ 15 efpy for CF-8M materials used within primary pressure boundary components, and
- ≥ 15 efpy at 350°C for CF-8/CF-3 materials used in the reactor core internals.

Additional long-term aging data are needed to estimate fracture properties for longer service times. Furthermore, this methodology may not be applicable for CF-8M materials with more than a trace amount of Nb, particularly for materials containing $> 15\%$ ferrite. The methodology also does not consider the potential effect of reactor coolant environment on fracture toughness. Limited data indicate significant effect of environment, particularly at low temperatures (e.g., shutdown water chemistry at 54°C). In addition, the existing fracture toughness data on LWR-irradiated CF-8/CF-3 materials is inadequate to accurately establish the lower-bound J-R curves for these materials as a function of neutron dose.

7 REFERENCES

1. Trautwein, A., and W. Gysel, "Influence of Long Time Aging of CF-8 and CF-8M Cast Steel at Temperatures between 300 and 500°C on the Impact Toughness and the Structure Properties," in *Spectrum, Technische Mitteilungen aus dem+GF+Konzern*, No. 5, May 1981; also in *Stainless Steel Castings*, V.G. Behal and A.S. Melilli, eds., STP 756, pp. 165–189, 1982.
2. Landerman, E.I., and W.H. Bamford, "Fracture Toughness and Fatigue Characteristics of Centrifugally Cast Type 316 Stainless Steel Pipe after Simulated Thermal Service Conditions," in *Ductility and Toughness Considerations in Elevated-Temperature Service*, MPC 8, pp. 99–127, ASME, New York, NY, 1978.
3. Solomon, H.D., and T.M. Devine, "Influence of Microstructure on the Mechanical Properties and Localized Corrosion of a Duplex Stainless Steel," in *Micon 78: Optimization of Processing, Properties, and Service Performance through Microstructural Control*, STP 672, p. 430, H. Abrams, G.N. Maniar, D.A. Nail, and H.D. Solomon, eds., ASTM, Philadelphia, PA, 1979.
4. Solomon, H.D., and T.M. Devine, Jr., "Duplex Stainless Steels — A Tale of Two Phases," in *Duplex Stainless Steels*, R.A. Lula, ed., pp. 693–756, ASM, Materials Park, OH, 1983.
5. Chung, H.M., and O.K. Chopra, "Kinetics and Mechanism of Thermal Aging Embrittlement of Duplex Stainless Steels," *Environmental Degradation of Materials in Nuclear Power Systems — Water Reactors*, pp. 359–370, G.J. Theus and J.R. Weeks, eds., Metallurgical Society, Warrendale, PA, 1988.
6. Hale, G.E., and S.J. Garwood, "The Effect of Aging on the Fracture Behaviour of Cast Stainless Steel and Weldments," *Mater. Sci. Technol.* 6, 230–235, 1990.
7. Slama, G., P. Petrequin, and T. Mager, "Effect of Aging on Mechanical Properties of Austenitic Stainless Steel Castings and Welds," presented at SMIRT Post-Conference Seminar 6, *Assuring Structural Integrity of Steel Reactor Pressure Boundary Components*, Monterey, CA, Aug. 29–30, 1983.
8. Meyzaud, Y., P. Ould, P. Balladon, M. Bethmont, and P. Soulat, "Tearing Resistance of Aged Cast Austenitic Stainless Steel," *Int. Conf. on Thermal Reactor Safety (NUCSAFE 88)*, Avignon, France, pp. 397–408, 3 October 1988.
9. Bethmont, M., Y. Mezaud, and P. Soulat, "Properties of Cast Austenitic Materials for Light Water Reactors," *Int. J. Pres. Ves. & Piping* 66, 221–229, 1996.
10. McConnell, P., and J.W. Sheckherd, "Fracture Toughness Characterization of Thermally Embrittled Cast Duplex Stainless Steel, Report NP-5439, Electric Power Research Institute, Palo Alto, CA, September 1987.
11. Chopra, O.K., and H.M. Chung, "Effect of Low-Temperature Aging on the Mechanical Properties of Cast Stainless Steels," in *Properties of Stainless Steels in Elevated Temperature Service*, M. Prager, ed., MPC-Vol. 26 / PVP-Vol. 132, pp. 79–105, ASME, New York, NY, 1988.

12. Chopra, O.K., and A. Sather, Initial Assessment of the Mechanisms and Significance of Low-Temperature Embrittlement of Cast Stainless Steels in LWR Systems, NUREG/CR-5385, ANL-89/17, August 1990.
13. Chopra, O.K., A. Sather, and L.Y. Bush, "Long Term Embrittlement of Cast Stainless Steels in LWR Systems: Semiannual Report, April-September 1989," NUREG/CR-4744, Vol. 4, No. 2, ANL-90/49, June 1991.
14. Chopra, O.K., "Long-Term Embrittlement of Cast Duplex Stainless Steels in LWR Systems, Semiannual Report Oct. 1990 – March 1991, NUREG/CR-4744, Vol. 6, No. 1, ANL-91/22, August 1992.
15. Chopra, O.K., "Long-Term Embrittlement of Cast Duplex Stainless Steels in LWR Systems, Semiannual Report Oct. 1991 – March 1992, NUREG/CR-4744, Vol. 7, No. 1, ANL-92/42, May 1993.
16. Chopra, O.K., "Estimation of Fracture Toughness of Cast Stainless Steels during Thermal Aging in LWR Systems," NUREG/CR-4513, Rev. 1, ANL-93/22, August 1994.
17. Chopra, O.K. and W.J. Shack, "Mechanical Properties of Thermally Aged Cast Stainless Steels from Shippingport Reactor Components," NUREG/CR-6275, ANL-94/37, April 1995.
18. Michaud, W.F., P.T. Toben, W.K. Soppet, and O.K. Chopra, "Tensile-Property Characterization of Thermally Aged Cast Stainless Steels," NUREG/CR-6142, ANL-93/35, February 1994.
19. Mills, W.J., "Heat-to-Heat Variations in the Fracture Toughness of Austenitic Stainless Steels," *Eng. Fract. Mech.*, 30 (4), 469–492, 1988.
20. Mills, W.J., "Fracture Toughness of Aged Stainless Steel Primary Piping and Reactor Vessel Materials," *J. Pressure Vessel Technol. (Trans ASME)* 109, 440–448, 1987.
21. Pumphrey, P.H., and K.N. Akhurst, "Aging Kinetics of CF3 Cast Stainless Steel in Temperature Range 300-400°C," *Mater. Sci. Technol.* 6, 211–219, 1990.
22. Bonnet, S., J. Bourgoin, J. Champredonde, D. Guttman, and M. Guttman, "Relationship between Evolution of Mechanical Properties of Various Cast Duplex Stainless Steels and Metallurgical and Aging Parameters: An Outline of Current EDF Programmes," *Mater. Sci. Technol.* 6, 221–229, 1990.
23. Jayet-Gendrot, S., P. Ould, and P. Balladon, "Effect of Fabrication and Test Parameters on the Fracture Toughness of Aged Cast Duplex Stainless Steels," *Fonteveraud III*, Vol. 1, pp. 90–97, French Nuclear Energy Society, 1994.
24. Jayet-Gendrot, S., P. Ould, and T. Meylogan, "Fracture Toughness Assessment of In-Service Aged Primary Circuit Elbows Using Mini-CT Specimens Taken from Outer Skin," *Nucl. Eng. and Design* 184, 3–11, 1998.

25. Massoud, Jean-Paul, C. Boveyron, P. Ould, G. Bezdikian, and H. Churier-Bosseneq, "Effect of the Manufacturing Porcess on the Thermal Aging of PWR Duplex Stainless Steel Components," *ASME 6th Intl. Conf. on Nucl. Eng. (ICONE-6)*, American Society of Mechanical Engineers, New York, NY, paper ICINE-6085, 1998.
26. Le Delliou, P., G. Bezdikian, P. Ould, and N. Safa, "Full-Scale Test on an Aged Cast Duplex Stainless Steel Lateral Connection: Results and Analysis," PVP2006-IVPVT-11-94005, in *Proc. of 2006 ASME Pressure Vessel and Piping Conf.*, July 23–27, 2006, Vancouver, BC, Canada, 2006.
27. Faidy, C., "Flaw Evaluation in Elbows Through French RSEM Code," PVP2010-25085, in *Proc. of ASME 2010 Pressure Vessel and Piping Division/K-PVP Conf.*, Bellevue, WA, July 18–22, 2010.
28. Tanaka, T., S. Kawaguchi, N. Sakamoto, and K. Koyama, "Thermal Aging of Cast Duplex Stainless Steels," *Joint ASME/JSME Pressure Vessels and Piping Conference – Structural Integrity of Pressure Vessels, Piping, and Components*, Honolulu, HI, July 23–27, pp. 141–146, 1995.
29. Suzuki, I., M. Koyama, S. Kawaguchi, H. Mimaki, M. Akiyama, T. Okuba, Y. Mishima, and T.R. Mager, "Long Term Thermal Aging of Cast Duplex Stainless Steels," *Intl. Conf. on Nucl. Eng. (ICONE-4)*, American Society of Mechanical Engineers, New York, NY, pp. 253–257, 1996.
30. Hojo, K., I. Muroya, S. Kawaguchi, K. Koyama, and K. Sakai, "Application of the Two-Criteria Approach to the Austenitic Cast Stainless Steel Pipe," *The 5th Intl. Conf. on Nucl. Eng. (ICONE-5)*, ICONE5-2379, May 26–30, American Society of Mechanical Engineers, New York, NY, 1997.
31. Kawaguchi, S., T. Nagasaki, and K. Koyama, "Prediction Method of Tensile Properties and Fraqtur Toughness of Thermally Aged Cast Duplex Stainless Steel Piping," PVP2005-71528, in *Proc. of ASME PVP-2005 ASME Pressure Vessel and Piping Division Conf.*, July 17–21, 2005.
32. JNES (Japan Nuclear Energy Safety Organization), "Investigation Report on the Integrity of Thermally-Embrittled Cast Stainless Steel Pipe," JNES-SS-0602, Nuclear Energy System Safety Division, April 2006.
33. Bruemmer, S.M., et al., "Critical Issue Reviews for the Understanding and Evaluation of Irradiation-Assisted Stress Corrosion Cracking," EPRI TR-107159, Electric Power Research Institute, Palo Alto, CA, 1996.
34. Bruemmer, S.M., E.P. Simonen, P.M. Scott, P.L. Andresen, G.S. Was, and J.L. Nelson, "Radiation-Induced Material Changes and Susceptibility to Intergranular Failure of Light-Water-Reactor Core Internals," *J. Nucl. Mater.* 274, 299–314, 1999.
35. Edwards, D., E. Simonen, and S. Bruemmer, "Radiation-Induced Segregation Behavior in Austenitic Stainless Steels: Fast Reactor versus Light Water Reactor Irradiations," Paper No. P0139, in *Proc. 13th Intl. Conf. on Environmental Degradation of Materials in Nuclear Power Systems – Water Reactors*, T.R. Allen, P.J. King, and L. Nelson, eds., Canadian Nuclear Society, Toronto, Canada, 2007.

36. Herrera, M.L., et al., "Evaluation of the Effects of Irradiation on the Fracture Toughness of BWR Internal Components," *Proc. ASME/JSME 4th Intl. Conf. on Nucl. Eng. (ICONE-4)*, Vol. 5, pp. 245–251, A.S. Rao, R.M. Duffey, and D. Elias, eds., American Society of Mechanical Engineers, New York, NY, 1996.
37. Xu, H., and S. Fyfitch, "Materials Reliability Program: A Review of Radiation Embrittlement for Stainless Steels (MRP-79)," Rev. 1, EPRI Report 1008204, Electric Power Research Institute, Palo Alto, CA, September 2004.
38. Carter, R.G., and R.M. Gamble, "Assessment of the Fracture Toughness of Irradiated Stainless Steel for BWR Core Shrouds," presented at *Fontevraud 5 Intl. Symp., Contribution of Materials Investigation to the Resolution of Problems Encountered in Pressurized Water Reactors*, Avignon, France, pp. 381–392, September 25, 2002.
39. Demma, A., R. Carter, A. Jenssen, T. Torimaru, and R. Gamble, "Fracture Toughness of Highly Irradiated Stainless Steels in Boiling Water Reactors," Paper No. 114, in *Proc. 13th Intl. Conf. on Environmental Degradation of Materials in Nuclear Power Systems – Water Reactors*, T.R. Allen, P.J. King, and L. Nelson, eds., Canadian Nuclear Society, Toronto, Ontario, Canada, 2007.
40. Ehnsten, U., K. Wallin, P. Karjalainen-Roikonen, S. van Dyck, and P. Ould, "Fracture Toughness of Stainless Steels Irradiated to ≈ 9 dpa in Commercial BWRs," in *Proc. 6th Intl. Symp. on Contribution of Materials Investigations to Improve the Safety and Performance of LWRs*, Vol. 1, Fontevraud 6, pp. 661–670, French Nuclear Energy Society, SFEN, Fontevraud Royal Abbey, France, September 18–22, 2006.
41. Kim C., R. Lott, S. Byrne, M. Burke, and G. Gerzen, "Embrittlement of Cast Austenitic Stainless Steel Reactor Internals Components," in *Proc. 6th Intl. Symp. on Contribution of Materials Investigations to Improve the Safety and Performance of LWRs*, Vol. 1, Fontevraud 6, French Nuclear Energy Society, SFEN, Fontevraud Royal Abbey, France, pp. 671–682, September 18–22, 2006.
42. Fyfitch, S., H. Xu, A. Demma, R. Carter, R. Gamble, and P. Scott, "Fracture Toughness of Irradiated Stainless Steel in Nuclear Power Systems," in *Proc. 14th Intl. Conf. on Environmental Degradation of Materials in Nuclear Power Systems – Water Reactors*, American Nuclear Society, Lagrange Park, IL, pp. 1307–1313, 2009.
43. Fyfitch, S., H. Xu, K. Moore, and R. Gurdal, "Materials Reliability Program: PWR Internals Material Aging Degradation Mechanism Screening and Threshold Values (MRP-175)," Report 1012081, Electric Power Research Institute, Palo Alto, CA, December 2005.
44. Mehta, H.S., B.D. Frew, R.M. Horn, F. Hua, S. Ranganath, and R.G. Carter, "Thermal Aging and Neutron Embrittlement Evaluation of Cast Austenitic Stainless Steels," PVP2010-25974, in *Proc. of PVP2010 2010 ASME Pressure Vessel and Piping Conf.*, July 18–22, 2010, Bellevue, WA, 2010.
45. Electric Power Research Institute, Materials Reliability Program, "Fracture Toughness Testing of Decommissioned PWR Core Internals Material Samples (MRP-160)," Report 1012079, Electric Power Research Institute, Palo Alto, CA, September 2005.
46. Chopra, O.K., and A.S. Rao, "A Review of Irradiation Effects on LWR Core Internal Materials - Neutron Embrittlement," *J. Nucl. Mater.* 412, 195–208, 2011.

47. Chopra, O.K., "Degradation of LWR Core Internal Materials Due to Neutron Irradiation," NUREG/CR-7027, December 2010.
48. Mills, W.J., "Fracture Toughness of Type 304 and 316 Stainless Steels and Their Welds," *Intl. Mater. Rev.* 42 (2), 45–82, 1997.
49. Lee, S., P.T. Kuo, K. Wichman, and O. Chopra, "Flaw Evaluation of Thermally Aged Cast Stainless Steel in Light-Water Reactor Applications," *Int. J. Pres. Ves. and Piping*, pp. 37–44, 1997.
50. Nickell, R.E., and M.A. Rinckel, "Evaluation of Thermal Aging Embrittlement for Cast Austenitic Stainless Steels Components in LWR Reactor Coolant Systems," EPRI TR-106092, Electric Power Research Institute, Palo Alto, CA, 1997.
51. Grimes, C.I. (U.S. Nuclear Regulatory Commission, License Renewal and Standardization Branch), "License Renewal Issue No. 98-0030, Thermal Aging Embrittlement of Cast Stainless Steel Components," letter to D.J. Walters (Nuclear Energy Institute), May 19, 2000.
52. Griesbach, T.J., V. Marthandam, H.H. Quia, and P. O'Regan, "Plant Support Engineering: Flaw Tolerance Evaluation of Thermally Aged Cast Austenitic Stainless Steel Piping," Report 1016236, Electric Power Research Institute, Palo Alto, CA, December 20, 2007.
53. Harris, D., H. Qian, D. Dedhia, N. Cofie, and T. Griesbach, "Nondestructive Evaluation: Probabilistic Reliability Model for Thermally Aged Cast Austenitic Stainless Steel Piping," Report 1024966, Electric Power Research Institute, Palo Alto, CA, December 2012.
54. Griesbach, T., N. Cofie, D. Hasrris, and D. Dedhia, "Materials Reliability Program: Technical Basis for ASME Section XI Code Case on Flaw Tolerance of Cast Austenitic Stainless Steel (CASS) Piping (MRP-362)," Report 3002000672, Electric Power Research Institute, Palo Alto, CA, October 2013.
55. Fyfitch, S., H. Xu, T. Worsham, R. Lott, and J. McKinley, "Materials Reliability Program: Thermal Aging and Neutron Embrittlement Assessment of Cast Austenitic Stainless Steels and Stainless Steel Welds in PWR Internals (MRP-276)," Report 1020959, Electric Power Research Institute, Palo Alto, CA, May 2010.
56. Frew, B., R. Horn, F. Hua, H. Mehta, and S. Ranganath, BWRVIP-234: BWR Vessel and Internals Project, Thermal Aging and Neutron Embrittlement Evaluation of Cast Austenitic Stainless Steels for BWR Internals, Report 1019060, Electric Power Research Institute, Palo Alto, CA, December 2009.
57. Heger, J.J., "885°F Embrittlement of the Ferritic Chromium-Iron Alloys," *Met. Progress*, 60 (2), p. 55, 1951.
58. Grobner, P.J. "The 885°F (475°C) Embrittlement of Ferritic Stainless Steels," *Metall. Trans.* 4 (1), pp. 251–260, 1973.
59. Nichol, T.J., A. Datta, and G. Aggen, "Embrittlement of Ferritic Stainless Steels," *Metall. Trans.* 11A, 573, 1980.

60. Chung, H.M., and T.R. Leax, "Embrittlement of Laboratory- and Reactor-Aged CF3, CF8, and CF8M Duplex Stainless Steels," *Mater. Sci. Technol.*, 6, 249–262, 1990.
61. Auger, P., F. Danoix, A. Menand, S. Bonnet, J. Bourgoïn, and M. Guttman, "Atom Probe and Transmission Electron Microscopy Study of Aging of Cast Duplex Stainless Steels," *Mater. Sci. Technol.*, 6, 301–313, 1990.
62. Vrinat, M., P. Cozar, and Y. Meyzaud, "Precipitated Phases in the Ferrite of Aged Cast Duplex Stainless Steels," *Scripta Metall.*, 20, 1101–1106, 1986.
63. Joly, P., R. Cozar, and A. Pineau, "Effect of Crystallographic Orientation of Austenite on the Formation of Cleavage Cracks in Ferrite in an Aged Duplex Stainless Steel," *Scripta Metall.*, 24, 2235–2240, 1990.
64. Sassen, J.M., M.G. Hetherington, T.J. Godfrey, and G.D.W. Smith, "Kinetics of Spinodal Reaction in the Ferrite Phase of a Duplex Stainless Steel," in *Properties of Stainless Steels in Elevated Temperature Service*, M. Prager, ed., MPC Vol. 26, PVP Vol. 132, pp. 65–78, M. Prager, ed., ASME, New York, NY, 1988.
65. Brown, J.E., A. Cerezo, T.J. Godfrey, M.G. Hetherington, and G.D.W. Smith, "Quantitative Atom Probe Analysis of Spinodal Reaction in Ferrite Phase of Duplex Stainless Steel," *Mater. Sci. Technol.*, 6, 293–300, 1990.
66. Bentley, J., M.K. Miller, S.S. Brenner, and J.A. Spitznagel, "Identification of G-phase in Aged Cast CF-8 Type Stainless Steel," in *Proc. 43rd Electron Microscopy Society of America*, pp. 328–329, G. W. Bailey, ed., San Francisco Press, 1985.
67. Miller, M.K., and J. Bentley, "Characterization of Fine-Scale Microstructures in Aged Primary Coolant Pipe Steels," in *Environmental Degradation of Materials in Nuclear Power Systems-Water Reactors*, G. J. Theus and J. R. Weeks, eds., pp. 341–349, The Metallurgical Society, Warrendale, PA, 1988.
68. Kawaguchi, S., N. Sakamoto, G. Takano, F. Matsuda, Y. Kikuchi, and L. Mraz, "Microstructural Changes and Fracture Behavior of CF8M Duplex Stainless Steel after Long-Term Aging," *Nucl. Eng. and Design* 174, 273-285, 1997.
69. Jansson, C., "Degradation of Cast Stainless Steel Elbows after 15 Years in Service," presented at *Fontevraud II Intl. Symp.*, Royal Abbey of Fontevraud, France, September 10–14, 1990.
70. Schaeffler, A.L., "Selection of Austenitic Electrodes for Welding Dissimilar Metals," *Welding Journal*, Vol. 26, No. 10, pp. 601–620, 1947.
71. Hull, F.C., "Delta Ferrite and Martensite Formation in Stainless Steels," *Welding Journal*, Vol. 52 (5), pp. 193s–203s, Research Supplement, May 1973.
72. ASTM A 800/A 800M, "Standard Practice for Steel Casting, Austenitic Alloy, Estimating Ferrite Content Thereof," American Society of Testing and Materials, West Conshohocken, PA, 2001.

73. Schoefer, E. A., "A diagram for estimation of Ferrite Content in Stainless Steel Castings," in Appendix to Mossbauer-Effect Examination of Ferrite in Stainless Steel Welds and Castings, by L. J. Schwartzgruber et al., *Welding Journal*, Vol. 53 (1), pp. 10s–12s, Research Supplement, 1974.
74. AWS A4.2-74, Standard Procedures for Calibrating Magnetic Instruments to Measure Delta Ferrite Content of Austenitic Stainless Steel Weld Metal," American Welding Society, Miami, FL, 1974.
75. Chopra, O.K., "Estimation of Fracture Toughness of Cast Stainless Steels during Thermal Aging in LWR Systems," NUREG/CR-4513, Rev. 0, ANL-90/42, June 1991.
76. Leone, G.L., and H.W. Kerr, "Ferrite to Austenite Transformation in Stainless Steels," *Welding Research Supplement*, pp13-s to 21-s, American Welding Society and Welding Research Council, January 1982.
77. Hiser, A. L., "Fracture Toughness Characterization of Nuclear Piping Steels," NUREG/CR-5118, MEA-2325, Materials Engineering Associates, Inc., November 1989.
78. Griesbach, T.J., V. Marthandam, and H. Qian, "Nondestructive Evaluation: Flaw Tolerance Evaluation of Thermally Aged Cast Austenitic Stainless Steel Piping," EPRI 1019128, Electric Power Research Institute, Palo Alto, CA, December 2009.
79. Nakajima, N., S. Shima, H. Nakajima, and T. Kondo, "The Fracture Toughness of Sensitized 304 Stainless Steel in Simulated Reactor Water," *Nucl. Eng. Des.*, 93, 95–106, 1986.
80. Morra, M., "Program on Technology Innovation: Scoping Study of Low Temperature Crack Propagation for 182 Weld Metal in BWR Environments and for Cast Austenitic Stainless Steel in PWR Environments (Revision 1)," EPRI 1020957, Electric Power Research Institute, Palo Alto, CA, May 2010.
81. Mills, W.J., and C.M. Brown, "Fracture Toughness of Alloy 600 and an EN82H Weld in Air and Water," *Metall. and Mater. Trans. A*, 32 (5), 1161–1174, 2001.
82. Brown, C.M. and W.J. Mills, "Fracture Toughness of Alloy 690 and EN52 Welds in Air and Water," *Metall. and Mater. Trans. A*, 33A (6), 1725–1735, 2002.
83. McConnell, P., W. Sheckherd, and D.M. Morris, "Properties of Thermally Embrittled Cast Duplex Stainless Steel." *J. Mater. Eng.*, 11 (3), 227–236. 1989.
84. Anzai, H., J. Kuniya, and I. Masaoka, "Effect of 475°C Embrittlement on Fracture Resistance of Cast Duplex Stainless Steel," *Trans. Iron Steel Inst. Japan*, 28, 400–405, 1988.
85. Vassilaros, M.G., R.A. Hays, and J.P. Gudas, "Investigation of the Ductile Fracture Properties of Type 304 Stainless Steel Plate, Welds, and 4-inch Pipe," in *Proc. 12th Water Reactor Safety Research Information Meeting*, NUREG/CP-0058, Vol. 4, pp. 176–189, U.S. Nuclear Regulatory Commission, Washington, DC, 1985.

86. Balladon, P., J. Heritier, and P. Rabbe, "Influence of Microstructure on the Ductile Rupture Mechanisms of a 316L Steel at Room and Elevated Temperatures," *Fracture Mechanics: 14th Symp., Vol. II: Testing and Applications*, ASTM STP 791, pp. 496–516, American Society for Testing and Materials, Philadelphia, PA, 1983.
87. Wilkowski, G.M., et al., "Degraded Pipe Program – Phase II, Semiannual Report," NUREG/CR-4082, Vols. 2, June 1985.
88. Bamford, W. H., and A.J. Bush, "Fracture Behavior of Stainless Steels," *Elastic-Plastic Fracture*, STP-668, ASTM, Philadelphia, PA, pp. 553–577, 1979.
89. EPRI Section XI Task Group for Piping Flaw Evaluation, *Evaluation of Flaws in Austenitic Piping*, EPRI NP-4690-SR, Nuclear Power Division, Electric Power Research Institute, Palo Alto, CA, July 1986.
90. Section XI Task Group for Piping Flaw Evaluation, ASME Code, "Evaluation of Flaws in Austenitic Steel Piping." *J. Press. Vessel Technol.* 108 (3), 352–366, 1986.
91. Chen, Y., B. Alexandreanu, and K. Natesan, "Crack Growth Rate and Fracture Toughness Tests on Irradiated Cast Stainless Steels," NUREG/CR-7184, ANL-12/56, June 2015.
92. Chen, Y., B. Alexandreanu, and K. Natesan, "Technical Letter Report on the Cracking of Irradiated Cast Stainless Steels with Low Ferrite Content," ANL-14/16, Argonne National Laboratory, Argonne, IL, November 2014.
93. Meyer, T., C. Boggess, S. Byrne, R. Schwirian, F. Gift, and R. Gold, "Materials Reliability Program: Screening, Categorization, and Ranking of Reactor Internals Components for Westinghouse and Combustion Engineering PWR Design (MRP-191)," EPRI Report 1013234, Electric Power Research Institute, Palo Alto, CA, November 2006.
94. Dufresne, J., B. Henry, and H. Larsson, "Fracture Toughness of Irradiated AISI 304 and 316L Stainless Steels," *Effects of Radiation on Structural Materials*, ASTM STP 683, pp. 511–528, J. A. Sprague and D. Kramer, eds., American Society for Testing and Materials, Philadelphia, PA, 1979.
95. Picker, C., A.L. Stott, and H. Cocks, "Effects of Low-Dose Fast Neutron Irradiation on the Fracture Toughness of Type 316 Stainless Steel and Weld Metal," in *Proc. Specialists Meeting on Mechanical Properties of Fast Reactor Structural Materials*, Paper IWGFR 49/440-4, Chester, UK, 1983.
96. Huang, F.H., "The Fracture Characterization of Highly Irradiated Type 316 Stainless Steel," *Int. J. Fracture* 25, 181–193, 1984.
97. Bernard, J., and G. Verzeletti, "Elasto-Plastic Fracture Mechanics Characterization of Type 316H Irradiated Stainless Steel up to 1 dpa," *Effects of Radiation on Materials: 12th Intl. Symp.*, ASTM STP 870, pp. 619-641, F.A. Garner and J.S. Perrin, eds., American Society for Testing and Materials, Philadelphia, PA, 1985.
98. Michel, D.J., and R.A. Gray, "Effects of Irradiation on the Fracture Toughness of FBR Structural Materials," *J. Nucl. Mater.* 148, 194–203, 1987.

99. Mills, W.J., L.A. James, and L.D. Blackburn, "Results of Fracture Mechanics Tests on PNC SU 304 Plate," Westinghouse Hanford Report HEDL-7544, Hanford Engineering Development Laboratory, Richland, WA, 1985.
100. Chopra, O.K., and W.J. Shack, "Crack Growth Rates and Fracture Toughness of Irradiated Austenitic Stainless Steels in BWR Environments," NUREG/CR-6960, ANL-06/58, March 2008.
101. Andresen, P.L., F.P. Ford, S.M. Murphy, and J.M. Perks, "State of Knowledge of Radiation Effects on Environmental Cracking in Light Water Reactor Core Materials," in *Proc. 4th Intl. Symp. on Environmental Degradation of Materials in Nuclear Power Systems – Water Reactors*, pp. 1.83–1.121 NACE, Houston, TX, , 1990.
102. Jenssen, A., K. Gott, P. Efsing, and P.O. Andersson, "Crack Growth Behavior of Irradiated Type 304L Stainless Steel in Simulated BWR Environment," in *Proc. 11th Intl. Symp. on Environmental Degradation of Materials in Nuclear Power Systems – Water Reactor*, pp. 1015–1024, 2003.
103. O'Donnell, I.J., H. Huthmann, and A.A. Tavassoli, "The Fracture Toughness Behaviour of Austenitic Steels and Weld Metal Including the Effects of Thermal Aging and Irradiation," *Intl. J. Pressure Vessels and Piping* 65 (3), 209–220, 1996.
104. Van Osch, E.V., M.G. Horsten, and M.I. De Vries, "Fracture Toughness of PWR Internals," *ECN Contribution to CEC Contract on PWR Internals-Part 2 (ETNU/CT/94/0136-F)*, ECN-I-97-010 (71747/NUC/EvO/mh/006274), Netherlands Energy Research Foundation ECN, Petten, the Netherlands, 1997.
105. De Vries, M.I., "Fatigue Crack Growth and Fracture Toughness Properties of Low Fluence Neutron-Irradiated Type 316 and Type 304 Stainless Steels," in *Influence of Radiation on Mechanical Properties: 13th Symposium (Part II)*, ASTM STP 956, pp. 174–190, F.A. Garner et al., eds., American Society of Testing and Materials, Philadelphia, PA, 1987.
106. Alexander, D.J., J.E. Pawel, L.M. Grossbeck, A. F. Rowcliffe, and K. Shiba, "Fracture Toughness of Irradiated Candidate Materials for ITER First Wall/Blanket Structures," in *Effect of Radiation on Materials: 17th Intl. Symp.*, ASTM STP 1270, pp. 945–970, American Society of Testing and Materials, Philadelphia, PA, 1996.
107. Sindelar, R.L., G.R. Caskey, Jr., J.K. Thomas, J.R. Hawthorne, A.L. Hiser, R.A. Lott, J.A. Begley, and R.P. Shogan, "Mechanical Properties of 1950s Vintage Type 304 Stainless Steel Weldment Components after Low Temperature Neutron Irradiation," in *16th Intl. Symp. on Effects of Radiation on Materials*, ASTM STP 1175, pp. 714–746, American Society of Testing and Materials, Philadelphia, PA, 1993.
108. Sindelar, R.L., P. Lam, A.J. Duncan, B.J. Wiersma, K.H. Subramanian, and J.B. Edler, "Development and Application of Materials Properties for Flaw Stability Analysis in Extreme Environment Service," PVP2007-26660, in *Proc. of PVP2007 ASME Pressure Vessel and Piping Conf.*, July 22–26, 2007, San Antonio, TX, 2007.
109. Haggag, F.M., W.R. Corwin, and R.K. Nanstad, "Effects of Irradiation on the Fracture Properties of Stainless Steel Weld Overlay Cladding," *Nucl. Eng. and Design* 124, 129–141, 1990.

110. Hamilton, M.L., F.H. Huang, W. J.S. Yang, and F.A. Garner, "Mechanical Properties and Fracture Behavior of 20% Cold-Worked 316 Stainless Steel Irradiated to Very High Neutron Exposures," in *Influence of Radiation in Material, Properties: 13th Intl. Symp. (Part II)*, ASTM STP 956, pp. 245–270, American Society of Testing and Materials, Philadelphia, PA, 1987.
111. Little, E.A., "Dynamic J-Integral Toughness and Fractographic Studies of Fast Reactor Irradiated Type 321 Stainless Steel," in *Effects of Radiation on Material, Properties: 12th Intl. Symp.*, ASTM STP 870, pp. 563–579, American Society of Testing and Materials, Philadelphia, PA, 1985.
112. Haggag, F.J., W.L. Server, W.G. Reuter, and J.M. Beeston, "Effects of Irradiation Fluence and Creep on Fracture Toughness of Type 347/348 Stainless Steels," ASTM STP 870, pp. 548–562, American Society of Testing and Materials, Philadelphia, PA, 1985.
113. Mills, W.J., "Fracture Toughness of Irradiated Stainless Steels Alloys," *Nucl. Technol.* 82 (3), 290–303, 1988.
114. Ould, P., P. Balladon, and Y. Meyzaud, *Bull. Cercle Etud. Metaux* 15, 31.1–31.12, 1988.
115. Fukuya, K., K. Fuji, H. Nishioka, and Y. Kitsunai, "Evolution of Microstructure and Microchemistry in Cold-worked 316 Stainless Steel under PWR Irradiations," *J. Nucl. Sci. and Technol.* 43 (2), 159–173. 2006.
116. Hale, G.E., and S.J. Garwood, "Effect of Aging on Fracture Behaviour of Cast Stainless Steel and Weldments," *Mater. Sci. Technol.*, 6, 230-236, 1990.
117. Lucas, T.R., R.G. Ballinger, H. Hanninen, and T. Saukkonen, "Effect of Thermal Aging on SCC, Material Properties and Fracture Toughness of Stainless Steel Weld Metals," in the *15th Intl. Conf. on Environmental Degradation of Materials in Nuclear Power Systems – Water Reactors*, pp. 883–900, J.T. Busby, G. Ilevbare, and P.L. Andresen, eds., The Minerals, Metals & Materials Society, Warrendale, PA, 2011.
118. Lucas, G.E., "The evolution of Mechanical Property Change in Irradiated Austenitic Stainless Steels," *J. Nucl. Mater.* 206, 287–305, 1993.
119. Chen, Y., O.K. Chopra, E.E. Gruber, and W.J. Shack, "Irradiated Assisted Stress Corrosion Cracking of Austenitic Stainless Steels in BWR Environments," NUREG/CR-7018, ANL-09/17, June 2010.
120. Gavenda, D.J., W.F. Michaud, T.M. Galvin, W.F. Burke, and O.K. Chopra, "Effects of Thermal Aging on Fracture Toughness and Charpy-Impact Strength of Stainless Steel Pipe Welds," NUREG/CR-6428, ANL-95/47, 1996.
121. Nakamura, T., M. Koshiishi, T. Torimaru, Y. Kitsunai, K. Takakura, K. Nagata, M. Ando, Y. Ishiyama, and A. Jenssen, "Correlation between IASCC Growth Behavior and Plastic Zone Size of Crack Tip in 3.5 dpa Neutron Irradiated Type 304L SS CT Specimen," Proc. 13th Intl. Conf. on Environmental Degradation of Materials in Nuclear Power Systems - Water Reactors, T. R. Allen, P. J. King, and L. Nelson, eds., Paper No. P0030, Canadian Nuclear Society, Toronto, Canada, 2007.

122. Sumiya, R., S. Tanaka, K. Nakata, K. Takakura, M. Ando, T. Torimaru, and Y. Kitsunai, "K Validity Criterion of Neutron Irradiated Type 316L Stainless Steel CT Specimen for SCC Growth Test," Proc. 13th Intl. Conf. on Environmental Degradation of Materials in Nuclear Power Systems - Water Reactors, T. R. Allen, P. J. King, and L. Nelson, eds., Paper No. P0072, Canadian Nuclear Society, Toronto, Canada, 2007.
123. NRC, Generic Aging Lessons Learned (GALL) Report, NUREG-1801, Rev. 2, Washington, D.C., Dec. 2010.
124. MRP-227-A, Materials Reliability Program: Pressurized Water Reactor Internals Inspection and Evaluation Guidelines, EPRI Report 1022863, Electric Power Research Institute, Palo Alto, CA, Dec. 23, 2011.
125. Eason, E. D., J. E. Wright, and G. R. Odette, "Improved Embrittlement Correlations for Reactor Pressure Vessels," NUREG/CR-6551 (MSC 970501), Nov. 1998.

APPENDIX A: MATERIAL INFORMATION

The various grades of CASS materials and their product form, heat designation, chemical composition, and mechanical properties such as Charpy-impact energy, tensile properties, and fracture toughness J-R curves of materials in the as-cast condition or after thermal aging in the laboratory at temperatures between 290 and 400°C up to 60,000 h are presented in the following tables.

Table A1. The chemical composition, product form, and ferrite content of the various CASS materials included in the present study.

Heat ID	Process	Product	Chemical Composition (wt.%) [*]											Ferrite (%)		Source	Ref.		
			C	Mn	Si	P	S	Ni	Cr	Mo	N	Calc.	Meas.						
Grade CF-3																			
47	Static	Keel block	0.018	0.60	1.06	0.007	0.006	10.63	19.81	0.59	0.028	8.4	16.3		ANL	A1-6,20			
48	Static	Keel block	0.01	0.60	1.08	0.009	0.006	10.46	19.55	0.30	0.072	5.1	-		ANL	A1-6,20			
49	Static	Keel block	0.01	0.60	0.95	0.010	0.007	10.69	19.41	0.32	0.065	4.4	-		ANL	A1-6,20			
50	Static	Keel block	0.34	0.60	1.10	0.016	0.007	9.14	17.89	0.33	0.079	6.2	-		ANL	A1-6,20			
51	Static	Keel block	0.010	0.63	0.86	0.014	0.005	9.06	20.13	0.32	0.058	14.3	18.0		ANL	A1-6,20			
52	Static	Keel block	0.009	0.57	0.92	0.012	0.005	9.40	19.49	0.35	0.052	10.3	13.5		ANL	A1-6,20			
P3	Centrifugal	Pipe 0.58 m OD	0.021	1.06	0.88	0.017	0.014	8.45	18.89	0.01	0.168	-	-		ANL	A1-6,20			
P2	Centrifugal	Pipe 0.93 m OD 73-mm wall	0.019	0.74	0.94	0.019	0.006	9.38	20.20	0.16	0.040	12.5	15.6		ANL	A1-6,20			
I	Static	Pump impeller	0.019	0.47	0.83	0.030	0.011	8.70	20.20	0.45	0.032	20.4	17.1		ANL	A1-6,20			
69	Static	Slab/Plate	0.023	0.63	1.13	0.015	0.005	8.59	20.18	0.34	0.028	21.0	23.6		ANL	A1-6,20			
EPRI	Static	-	0.030	0.74	0.84	-	-	(7.93)	22.04	0.23	0.045	36.0	32.0		EPRI	A13			
284	Static	-	0.025	0.28	0.52	-	-	8.23	23.00	0.17	0.037	43.6	42.0		GF	A17			
280	Static	-	0.028	0.50	1.37	0.015	0.006	8.00	21.60	0.25	0.038	36.3	38.0		GF	A17			
B1	Static	-	0.025	0.40	0.68	-	-	9.06	19.49	0.23	0.027	11.4	12.5		CEGB	A8			
B2	Static	-	0.025	0.40	0.68	-	-	8.69	21.38	0.23	0.027	26.3	23.0		CEGB	A8			
B3	Static	-	0.026	0.40	0.72	-	-	8.42	22.78	0.23	0.029	41.8	37.5		CEGB	A8			
TWI	Static	Plate	0.030	0.42	0.69	0.025	0.001	8.50	19.90	0.28	0.025	17.2	19.0		TWI	A24			
FA	Static	-	0.021	1.14	0.99	0.037	-	8.90	18.90	0.10	0.074	6.0	6.3		Framatome	A15			
F3329	Static	-	0.030	0.82	1.43	-	-	8.20	21.40	0.03	0.040	28.4	-		Framatome	A14			
Grade CF-3M with ≥10% Ni																			
C5	Static	-	0.020	0.70	0.99	-	-	10.60	19.30	2.38	0.040	14.1	10.0		EdF	A9			
FD	Static	-	0.026	1.12	0.94	-	-	10.32	19.15	2.44	0.063	11.8	13.9		-	A15			
F1	Centrifugal	-	0.020	0.70	0.98	-	-	10.69	19.36	2.40	0.039	14.1	15.5		-	A15			

Table A1. (Contd.)

Heat	Chemical Composition (wt.%) [*]													Ferrite (%)		Source	Ref.
	ID	Process	Product	C	Mn	Si	P	S	Ni	Cr	Mo	N	Calc.	Meas.			
C	Static	Elbow C	0.026	1.03	1.25	-	-	10.24	21.90	2.68	0.040	35.5	-	EdF/Framatome	A11		
EL	Static	90°elbow EL	0.030	1.06	1.15	-	-	10.30	21.85	2.72	0.039	33.5	-	EdF/Framatome	A10		
Sc	Static	Sc2/3 elbow	0.024	1.09	1.21	-	-	10.45	22.10	2.70	0.037	35.9	-	EdF/Framatome	A11		
Grade CF-8																	
53	Static	Keel block	0.065	0.64	1.16	0.012	0.009	9.23	19.53	0.39	0.049	6.4	-	ANL	A1-6,20		
54	Static	Keel block	0.063	0.55	1.03	0.011	0.005	9.17	19.31	0.35	0.084	4.1	-	ANL	A1-6,20		
56	Static	Keel block	0.066	0.57	1.05	0.007	0.007	9.28	19.65	0.34	0.030	7.3	10.1	ANL	A1-6,20		
57	Static	Keel block	0.056	0.62	1.08	0.009	0.004	9.27	18.68	0.34	0.047	4.4	-	ANL	A1-6,20		
58	Static	Keel block	0.056	0.62	1.12	0.010	0.005	10.89	19.53	0.33	0.040	3.2	-	ANL	A1-6,20		
59	Static	Keel block	0.062	0.60	1.08	0.008	0.007	9.34	20.33	0.32	0.045	8.8	13.5	ANL	A1-6,20		
60	Static	Keel block	0.064	0.67	0.95	0.008	0.006	8.34	21.05	0.31	0.058	15.4	21.1	ANL	A1-6,20		
61	Static	Keel block	0.054	0.65	1.01	0.007	0.007	8.86	20.65	0.32	0.080	10.0	13.1	ANL	A1-6,20		
68	Static	Slab/Plate	0.063	0.64	1.07	0.021	0.014	8.08	20.64	0.31	0.062	14.9	23.4	ANL	A1-6,20		
73	Static	Slab/Plate	0.070	0.72	1.09	0.028	0.016	8.54	19.43	0.25	0.053	7.1	7.7	ANL	A1-6,20		
C1	Static	Pump Casing	0.039	1.20	1.18	0.033	0.008	9.37	19.00	0.65	0.040	7.9	2.2	ANL	A1-6,20		
P1	Centrifugal	Pipe 0.89 m OD 73-mm wall	0.036	0.59	1.12	0.026	0.013	8.10	20.49	0.04	0.057	17.6	24.1	ANL	A1-6,20		
CC4	Static	-	0.056	1.11	1.42	-	-	9.64	20.10	0.01	0.067	5.3	6.0	Shippingport	A7		
CA4	Static	Cold Check valve	0.056	1.10	1.45	0.018	0.009	8.84	20.26	0.01	0.041	10.8	10.9	Shippingport	A7		
CA7	Static	Cold Check valve	0.058	1.09	1.43	0.018	0.009	8.72	20.22	0.01	0.041	-	-	Shippingport	A7		
CB7	Static	Cold Check valve	0.052	1.07	1.36	0.018	0.011	8.85	19.12	0.02	0.053	5.9	3.2	Shippingport	A7		
VR	Static	Spare Pump Volute	0.046	0.50	1.14	0.027	0.017	9.56	20.79	0.04	0.049	9.8	16.2	Shippingport	A7		
MB2	Static	Hot Shutoff valve	0.042	0.72	0.51	0.043	0.017	10.77	19.74	0.19	0.073	2.6	1.9	Shippingport	A7		
MA9	Static	Hot Shutoff valve	0.052	0.72	0.24	0.041	0.011	10.54	20.78	0.24	0.051	5.1	10.0	Shippingport	A7		
MA1	Static	Hot Shutoff valve	0.052	0.72	0.22	0.039	0.013	10.50	20.74	0.24	0.049	5.2	9.5	Shippingport	A7		
PV	Static	Pump Volute	0.108	1.11	0.89	0.032	0.008	9.30	19.83	0.38	0.027	4.7	13.0	Shippingport	A7		
KRB	Static	Pump Cover	0.062	0.31	1.17	-	-	8.03	22.00	0.17	0.038	27.8	-	KRB Reactor	A1-6,20		
277	Static	-	0.052	0.54	1.81	-	-	8.13	20.50	0.06	0.019	22.5	28.0	GF	A17		
278	Static	-	0.038	0.28	1.00	0.008	0.019	8.27	20.20	0.13	0.030	18.6	15.0	GF	A17		
279	Static	-	0.040	0.37	1.36	-	-	(7.85)	22.00	0.22	0.032	39.5	40.0	GF	A17		
281	Static	-	0.036	0.41	0.45	-	-	8.60	23.10	0.17	0.053	31.4	30.0	GF	A17		
282	Static	-	0.035	0.43	0.35	-	-	8.53	22.50	0.15	0.040	29.7	38.0	GF	A17		
283	Static	-	0.036	0.48	0.53	-	-	(7.88)	22.60	0.23	0.032	42.6	42.0	GF	A17		

Table A1. (Contd.)

Heat ID	Process	Product	Chemical Composition (wt.%) [*]											Ferrite (%)		Source	Ref.	
			C	Mn	Si	P	S	Ni	Cr	Mo	N	Calc.	Meas.					
291	Static	-	0.065	0.28	1.59	-	-	-	10.60	19.60	0.66	0.054	4.2	6.0	GF	A17		
292	Static	-	0.090	0.34	1.57	0.018	0.016	(7.52)	21.60	0.13	0.039	23.9	28.0	GF	A17			
C'5	Centrifugal	-	0.034	0.62	1.04	-	-	9.00	20.70	0.17	0.040	15.57	11.0	EdF	A9			
FE	Static	-	0.035	0.80	0.54	0.022	0.012	8.47	21.04	0.08	0.051	17.59	16.5	Framatome	A15			
FF	Static	-	0.038	0.26	1.16	0.020	0.010	8.33	19.72	0.34	0.026	17.71	12.0	Framatome	A15			
FC	Static	-	0.042	0.91	1.09	0.027	14.000	8.19	20.73	0.13	0.035	20.93	20.1	Framatome	A15			
FG	Centrifugal	-	0.040	0.74	1.03	0.024	0.016	8.08	20.65	0.02	0.073	15.30	17.0	Framatome	A15			
FH	Centrifugal	-	0.050	0.71	1.18	0.032	0.017	8.07	20.70	0.05	0.045	18.34	21.5	Framatome	A15			
A-F	Static	Pipe	0.059	0.70	1.07	-	-	8.21	19.19	0.13	0.039	9.11	-	Kansai/MHI	A19			
A-G	Static	Pipe	0.051	0.56	1.20	-	-	8.08	20.41	0.12	0.042	17.40	-	Kansai/MHI	A19			
B-G	Static	Elbow	0.040	0.66	1.51	-	-	8.51	20.69	0.25	0.053	18.13	-	JPEIC/MHI	A21,22			
Grade CF-8M with <10% Ni																		
758	Static	Elbow	0.040	0.84	0.69	0.018	-	9.66	19.23	3.12	0.040	20.8	19.2	ANL	A1-6,20			
205	Centrifugal	Pipe	0.040	0.93	0.63	0.019	-	(8.80)	(17.88)	3.37	0.040	21.0	15.9	ANL	A1-6,20			
70	Static	Slab/Plate	0.066	0.55	0.72	0.021	0.016	9.01	19.17	2.30	0.049	14.2	18.9	ANL	A1-6,20			
74	Static	Slab/Plate	0.064	0.54	0.73	0.022	0.016	9.03	19.11	2.51	0.048	15.5	18.4	ANL	A1-6,20			
75	Static	Slab/Plate	0.065	0.53	0.67	0.022	0.012	9.12	20.86	2.58	0.052	24.8	27.8	ANL	A1-6,20			
64	Static	Keel block	0.038	0.60	0.63	0.006	0.005	9.40	20.76	2.46	0.038	29.0	28.4	ANL	A1-6,20			
65	Static	Keel block	0.049	0.50	0.48	0.012	0.007	9.63	20.78	2.57	0.064	20.9	23.4	ANL	A1-6,20			
66	Static	Keel block	0.047	0.60	0.49	0.012	0.007	9.28	19.45	2.39	0.029	19.6	19.8	ANL	A1-6,20			
285	Static	-	0.047	0.48	0.86	-	-	9.49	18.80	2.35	0.039	14.0	10.0	GF	A17			
286	Static	-	0.072	0.40	1.33	0.044	0.015	9.13	20.20	2.44	0.062	18.9	22.0	GF	A17			
287	Static	-	0.047	0.50	0.51	-	-	(8.46)	20.50	2.58	0.033	37.2	38.0	GF	A17			
288	Static	-	0.052	0.47	1.70	-	-	(8.40)	19.60	2.53	0.022	35.6	28.0	GF	A17			
289	Static	-	0.091	0.48	1.44	-	-	(8.25)	19.70	2.30	0.032	22.6	30.0	GF	A17			
290	Static	-	0.054	0.41	1.51	-	-	(8.30)	20.00	2.40	0.050	31.3	32.0	GF	A17			
EK	Static	50°elbow	0.035	0.89	1.08	-	-	9.70	21.10	2.51	0.054	28.0	-	-	A10			
EK	Static	Ex. elbow	0.034	0.88	1.05	-	-	9.55	21.15	2.51	0.054	30.0	-	Framatome	A10			
EC	Static	Sc1 elbow	0.033	0.86	1.01	-	-	9.40	21.20	2.51	0.054	32.2	-	-	A11			
C2375	Centrifugal	Pipe	0.050	0.86	0.74	-	-	9.46	19.93	2.55	0.040	20.7	21.0	Westinghouse	A25,26			
C1488	Centrifugal	Pipe	0.061	1.02	0.53	-	-	9.48	20.95	2.63	0.056	22.1	14.0	Westinghouse	A25,26			
B-E	Static	-	0.070	0.44	1.12	-	-	9.20	19.80	2.10	0.027	18.1	-	JPEIC/MHI	A21,22			
B-F	Static	-	0.050	0.54	1.11	-	-	9.10	20.50	2.30	0.021	30.8	-	JPEIC/MHI	A21,22			

Table A1. (Contd.)

Heat ID	Process	Product	Chemical Composition (wt.%) [*]											Ferrite (%)		Source	Ref.	
			C	Mn	Si	P	S	Ni	Cr	Mo	N	Calc.	Meas.					
B-E	Static	-	0.070	0.44	1.12	-	-	9.20	19.80	2.10	0.027	18.1	-	JPEIC/MHI	A21,22			
B-F	Static	-	0.050	0.54	1.11	-	-	9.10	20.50	2.30	0.021	30.8	-	JPEIC/MHI	A21,22			
B-B	Centrifugal	Pipe	0.053	0.80	0.95	-	-	9.52	20.52	2.20	0.045	20.6	-	JPEIC/MHI	A21,22			
A-B	Centrifugal	Pipe	0.053	0.80	0.95	-	-	9.52	20.52	2.20	0.045	20.6	-	Kansai/MHI	A19			
A-C	Centrifugal	Pipe	0.044	0.62	1.16	-	-	9.10	20.60	2.24	0.049	27.2	-	Kansai/MHI	A19			
A-D	Centrifugal	Pipe	0.059	0.76	0.96	-	-	9.28	20.61	2.15	0.049	21.0	-	Kansai/MHI	A19			
A-E	Centrifugal	Pipe	0.050	0.84	1.30	-	-	9.32	20.75	2.30	0.042	26.8	-	Kansai/MHI	A19			
L-Hi	-	Large Pipe	0.046	0.88	1.26	0.024	0.007	9.26	20.47	2.22	0.032	27.2	-	JNES 2006	A18			
L-Lo	-	Large Pipe	0.050	0.82	0.90	0.025	0.005	9.96	19.58	2.23	0.058	12.0	-	JNES 2006	A18			
M-Hi	-	Med. Pipe	0.046	0.78	1.30	0.024	0.007	9.57	20.88	2.28	0.043	26.0	-	JNES 2006	A18			
M-Lo	-	Med. Pipe	0.050	0.84	0.79	0.025	0.005	9.86	19.29	2.29	0.056	11.5	-	JNES 2006	A18			
Grade CF-8M with ≥10% Ni																		
P4	Centrifugal	Pipe 0.58 m OD 32-mm wall	0.040	1.07	1.02	0.019	0.016	10.00	19.64	2.05	0.151	5.9	10.0	ANL	A1-6,20			
62	Static	Keel block	0.063	0.72	0.56	0.007	0.005	12.39	18.29	2.57	0.030	2.8	-	ANL	A1-6,20			
63	Static	Keel block	0.055	0.61	0.58	0.007	0.006	11.85	19.37	2.57	0.031	6.4	10.4	ANL	A1-6,20			
Rhot	Static	Hot-leg elbow	0.037	0.77	1.03	0.022	0.008	10.60	20.00	2.09	0.044	13.0	10.3	Ringhals	A23			
Rcrs	Static	Cold-leg elbow	0.039	0.82	1.11	0.020	0.012	10.50	19.60	2.08	0.037	12.3	9.7	Ringhals	A23			
Y1422	Static	45° connection	0.040	0.80	0.90	-	-	10.48	21.94	2.49	0.040	27.1	-	EdF/Framatome	A12			
Y4331	Static	-	0.045	0.76	1.16	-	-	10.10	20.70	2.59	0.038	-	-	Framatome	A14			
Y3296	Static	-	0.035	0.67	1.21	-	-	10.20	22.20	2.65	0.040	35.8	35.0	Framatome	A14			
FK	Centrifugal	-	0.060	1.09	0.75	0.016	0.016	10.45	20.80	2.62	0.056	15.4	14.0	Framatome	A15			
FL	Static	-	0.040	0.79	0.81	0.021	0.016	10.56	20.76	2.48	0.042	18.6	19.0	Framatome	A15			
FB	Static	-	0.053	0.83	0.93	0.024	0.013	10.56	20.12	2.52	0.042	14.0	17.3	Framatome	A15			
A	Static	Plate A	0.036	0.69	1.21	-	-	10.30	22.20	2.66	0.043	33.8	-	EdF/Framatome	A11			
B	Static	Plate B	0.045	0.76	1.16	-	-	10.07	20.70	2.59	0.038	23.4	-	EdF/Framatome	A11			
CC	Static	Plate CC	0.038	0.71	1.20	-	-	10.43	22.11	2.75	0.042	32.2	-	EdF/Framatome	A10			
DI	Static	Plate DI	0.050	0.80	1.17	-	-	10.20	20.70	2.58	0.045	20.4	-	EdF/Framatome	A10			
B-A	Centrifugal	Pipe	0.050	0.90	1.51	-	-	10.30	21.30	3.10	0.060	25.7	-	JPEIC/MHI	A21,22			
B-C	Centrifugal	Pipe	0.048	0.84	0.64	-	-	10.46	20.01	2.16	0.051	11.3	-	JPEIC/MHI	A21,22			
A-A	Centrifugal	Pipe	0.048	0.84	0.64	-	-	10.46	20.01	2.16	0.051	11.3	-	Kansai/MHI	A19			

* Values higher than those specified in ASTM A531 Grades CF-3, CF-3M, CF-8, and CF-8M are underlined, and lower values are within parentheses.

APPENDIX B: J-R CURVE CHARACTERIZATION

The J-R curve tests were performed according to ASTM Specifications E 813-85 (Standard Test Method for J_{Ic} , a Measure of Fracture Toughness) and E 1152-87 (Standard Test Method for Determining J-R Curve). Compact-tension (CT) specimens, 25.4 mm (1 in.) thick with 10% side grooves, were used for the tests. The CT specimen design is similar to the specimen of ASTM Specification E 399, the notch region is modified in accordance with E 813 and E 5112 to permit measurement of load-line displacement by axial extensometer. The extensometer was mounted on razor blades that were screwed onto the specimen along the load-line.

Prior to testing, the specimens were fatigue-precracked at room temperature and at load levels within the linear elastic range. The final ratio of the initial crack length to width (a/W) after precracking was about 0.55. The final 1-mm (0.04-in.) crack extension was carried out at a load range of 13 kN (2.92 kip) to 1.3 kN (0.292 kip), K_{max} was $<25 \text{ MPa}\cdot\text{m}^{1/2}$ ($22.6 \text{ ksi}\cdot\text{in.}^{1/2}$). After precracking, all specimens were side-grooved by 20% of the total specimen thickness (i.e., 10% per side), to ensure uniform crack growth during testing.

The J-R curve tests were performed on an Instron testing machine with 90 kN (20 kip) maximum load capacity. The load and load-line displacement data were digitized with digital voltmeters and stored on a disk for post test analysis and correction of the test data. The single-specimen compliance procedure was used to estimate the crack extension. Rotation and modulus corrections were applied to the compliance data. Both deformation theory and modified forms of the J integral were evaluated for each test.

After each test, the specimen was heated to 350°C to heat-tint the exposed fracture surface. The specimen was then fractured at liquid nitrogen temperature. The initial (i.e., fatigue precrack) and final (test) crack lengths were measured optically for both halves of the fractured specimen. The crack lengths were determined by the 9/8 averaging technique (i.e., the two near-surface measurements were averaged and the resultant value averaged with the remaining seven measurements).

The fracture toughness J_{Ic} values were determined in accordance with ASTM Specifications E 813-81 and E 813-85. For the former, J_{Ic} is defined as the intersection of the blunting line given by $J = 2\sigma_f \Delta a$, and the linear fit of the J-vs.- Δa test data between the 0.15-mm and 1.5-mm exclusion lines. The flow stress, σ_f , is the average of the 0.2% yield strength and the ultimate strength. The ASTM Specification E 813-85 procedure defines J_{Ic} as the intersection of the 0.2-mm offset line with the power-law fit (of the form $J = C\Delta a^n$) of the test data between the exclusion lines. J-R curve tests on CASS materials indicate that a slope of four times the flow stress ($4\sigma_f$) for the blunting line expresses the J-vs.- Δa data better than the slope of $2\sigma_f$ that is defined in E 813-81 or E 813-85. The fracture toughness J_{Ic} values were determined with the $4\sigma_f$ slope for the blunting line and the 0.2-mm offset line.

The tearing modulus was also evaluated for each test. The tearing modulus is given by $T = E(dJ/da)/\sigma_f^2$, where E is the Young's modulus and σ_f is the flow stress. The ASTM E 813-81 value of tearing modulus is determined from the slope dJ/da of the linear fit to the J-vs.- Δa data. For the power law curve fits, an average value of dJ/da was calculated^{A27} to obtain average tearing modulus. The fracture toughness results obtained at Argonne on several experimental and commercial heats of CASS materials aged up to 58,000 h at 290, 320, 350, 400, and 450°C, (554, 608, 662, 752, and 842°F) and for the service-aged materials from the KBR pump

cover plate and the decommissioned Shippingport reactor valve bodies and pump volute and impeller,^{A1-A7} are given in Table B1. Fracture toughness data from studies at EPRI,^{A13} EdF,^{A9-12} Framatome,^{A14,15} several institutions in Japan,^{A18,19,21,22} Westinghouse,^{A25,26} and TWI,^{A24} are also included. The actual fracture toughness J-R curve data (J vs. Δa) for various grades and heats of unaged and aged CASS materials are given in Table B2. Note that for a few test specimens, the modified-J values are listed instead of deformation-J. These J-R curves are identified as J_m vs. Δa in Table B2, and the rest as J_d vs. Δa . For these tests, the J_{Ic} , coefficient C, and exponent n, corresponding to the deformation-J and modified-J values are listed in Table B3. The tensile test data for thermally aged CASS materials from the Argonne study are presented in NUREG/CR-6142.^{A6}

Data Analysis Procedure

The compliance method was used to determine the crack length during the tests. The Hudak-Saxena calibration equation^{A28} was used to relate the specimen load-line elastic compliance C_i on an unloading/loading sequence with the crack length a_i . The compliance, i.e., slope ($\Delta\delta/\Delta P$) of the load-line displacement-vs.-load record obtained during the unloading/loading sequence, is given by

$$U_{LL} = \frac{1}{(B_e E_e C_i) + 1}, \quad (B-1)$$

and

$$a_i/W = 1.000196 - 4.06319(U_{LL}) + 11.242(U_{LL})^2 - 106.043(U_{LL})^3 + 464.335(U_{LL})^4 - 650.677(U_{LL})^5 \quad (B-2)$$

where E_e is the effective elastic modulus, B_e is the effective specimen thickness expressed as $B - (B - B_N)^2/B$, and W is specimen width.

Both rotation and modulus corrections are applied to the compliance data. The modulus correction^{A28} is used to account for the uncertainties in testing, i.e., in the values of initial crack length determined by compliance and measured optically. The effective modulus E_M is determined from

$$E_e = \frac{1}{C_o B_e} \left(\frac{W + a_o}{W - a_o} \right)^{1/2} f \left(\frac{a_o}{W} \right), \quad (B-3)$$

and

$$f \left(\frac{a_o}{W} \right) = 2.163 + 12.219 \left(\frac{a_o}{W} \right) - 20.065 \left(\frac{a_o}{W} \right)^2 - 0.9925 \left(\frac{a_o}{W} \right)^3 + 20.609 \left(\frac{a_o}{W} \right)^4 - 9.9314 \left(\frac{a_o}{W} \right)^5, \quad (B-4)$$

where C_o is initial compliance, B_e is effective specimen thickness, and a_o is the initial physical crack size measured optically.

To account for crack-opening displacement in CT specimens, the crack size should be corrected for rotation.^{A29} The corrected compliance is calculated from

$$\theta = \text{Sin}^{-1} \left[\left(\frac{d_m}{2} + D \right) / (D^2 + R^2)^{1/2} \right] - \tan^{-1} \left(\frac{D}{R} \right), \quad (\text{B-5})$$

and

$$C_c = C_m / \left[\left(\frac{H^*}{R} \text{Sin}\theta - \text{Cos}\theta \right) \left(\frac{D}{R} \text{Sin}\theta - \text{Cos}\theta \right) \right], \quad (\text{B-6})$$

where C_c and C_m are the corrected and measured elastic compliance at the load line, H^* is the initial half span of load points, R is the radius of rotation of the crack centerline $[(W + a)/2]$, a is the updated crack length, D is one-half of the initial distance between the displacement points (i.e., half gage length), d_m is the total measured load-line displacement, and θ is the angle of rotation of a rigid-body element about the unbroken midsection line.

The J value is calculated at any point on the load-vs.-load-line displacement record by means of the relationship

$$J = J_{el} + J_{pl}, \quad (\text{B-7})$$

where J_{el} is the elastic component of J and J_{pl} is the plastic component of J . For a CT specimen, at a point corresponding to the coordinates P_i and δ_i on the specimen load-vs.-load-line displacement record, a_i is $(a_o + \Delta a_i)$, and the deformation J is given by

$$J_{d(i)} = \frac{(K_i)^2 (1 - \nu^2)}{E_e} + J_{pl(i)}, \quad (\text{B-8})$$

where, from ASTM method E 399,

$$K_{(i)} = \left[\frac{P_i}{(BB_N W_e)^{1/2}} \right] f \left(\frac{a_i}{W} \right), \quad (\text{B-9})$$

with

$$f \left(\frac{a_i}{W} \right) = \left[2 + \left(\frac{a_i}{W} \right) \right] \left[0.886 + 4.64 \left(\frac{a_i}{W} \right) - 13.32 \left(\frac{a_i}{W} \right)^2 + 14.72 \left(\frac{a_i}{W} \right)^3 - 5.6 \left(\frac{a_i}{W} \right)^4 \right] / \left[1 - \left(\frac{a_i}{W} \right) \right], \quad (\text{B-10})$$

and

$$J_{pl(i)} = \left[J_{pl(i-1)} + \left(\frac{\eta_i}{b_i} \right) \frac{A_{pl(i)} - A_{pl(i-1)}}{B_N} \right] \left[1 - \left(\frac{\gamma_i}{b_i} \right) (a_i - a_{i-1}) \right], \quad (B-11)$$

where ν is Poisson's ratio, b is the uncracked ligament, A_{pl} is the plastic component of the area under the load-vs.-load-line displacement record, and η is a factor that accounts for the tensile component of the load as given by

$$\eta_i = 2 + 0.522b_i/W, \quad (B-12)$$

and γ a factor that accounts for limited crack growth as given by

$$\gamma_i = 1 + 0.76b_i/W, \quad (B-13)$$

The modified J values (i.e., J_M) are calculated from the relationship (Ref. A30)

$$J_{M(i)} = J_{d(i)} + \Delta J_i, \quad (B-14)$$

where

$$\Delta J_i = \Delta J_{i-1} + \left(\frac{\gamma_i}{b_i} \right) J_{pl(i)} (a_i - a_{i-1}), \quad (B-15)$$

According to ASTM Specification E 1152-87, the J_D -R curves are valid only for crack growth up to 10% of the initial uncracked ligament. In addition, they show a dependence on specimen size. The J_M -R curves have been demonstrated to be independent of specimen size and yield valid results for larger crack growth.

Data Qualification

The various validity criteria specified in ASTM Specification E 813-85 for J_{Ic} and in ASTM Specification E 1152-87 for the J-R curve were used to qualify the results from each test. The various criteria include maximum values of crack extension and J-integral; limits for initial uncracked ligament, effective elastic modulus, optically measured physical crack length, and spacing of J- Δa data points. The ω criterion^{A31} was also used to ensure that a region of J dominance exists.

For the present investigation, most of the unaged or short-term-aged specimens yielded invalid J_{Ic} values because of the relatively high toughness of the material. The reasons for the discrepancies are data point spacing, shape of the final crack front, or size of the uncracked ligament. In general, the size of the uncracked ligament or the specimen thickness was inadequate for the unaged or short-term-aged specimens because of the relatively high toughness of the material. The J_{max} limit for the J-vs.- Δa data was ignored in most tests to obtain a good power-law fit of the test data.

The shape of the crack front was also very irregular for most CASS materials. This may be attributed to the coarse grain structure of the casting and differences in ferrite morphology.

CASS materials with large columnar grains, in particular, showed significant variation in crack length along the width of a specimen. Furthermore, the crack front always had a leading crack near the edges of the specimen. The near-surface measurements of the final physical crack length were often $>\pm 1.02$ mm, the maximum value allowed for data qualification.

The fracture surfaces often showed uncracked ridges or ligaments along the direction of crack extension. The uncracked ligaments add significant error to the estimation of crack length by compliance. Therefore, the difference between the crack extension predicted from elastic compliance and the average measured physical crack extension is more than the maximum value allowed by ASTM E 1152.

All tests showed significant load relaxation during the unloading/reloading cycle for estimating crack length by elastic compliance. All unloadings were 25% of the load. The load at the end of the unloading/reloading cycle is always lower than it was at the start of the unloading cycle. The difference is appreciable for the room-temperature test. Therefore, the initial 20-30% of the unloading curve were ignored in estimating crack length.

Table B1. The fracture toughness J-R curves, tensile properties and Charpy-impact energy of unaged and aged CASS Materials.

Heat ID	Specimen ID	Process	Calc. Ferrite (%)	Aging Temp (°C)	Aging Time (h)	Test Temp (°C)	Coeff. C	Exponent n	Jic (kJ/m ²)	Yield Stress (MPa)	Ultimate Stress (MPa)	Flow Stress (MPa)	Elongation (%)	Red. in Area (%)	Charpy Impact Energy (J/cm ²)	RT Charpy Impact Energy (J/c m ²)	Source	Ref.
CF-3																		
	I	I1S-03	S	20.4	-	25	718.5	0.694	475.9	251.1	571.6	411.3	76.3	76.6	179.7	179.7	ANL	A20
	I	I1S-01	S	20.4	-	25	861.5	0.591	623.9	251.1	571.6	411.3	76.3	76.6	179.7	179.7	ANL	A20
	I	I2S-01	S	20.4	-	25	811.6	0.743	478.2	251.1	571.6	411.3	76.3	76.6	179.7	179.7	ANL	A20
	I	I1S-07	S	20.4	320	30000	707.5	0.560	453.5	262.9	583.4	423.1	49.7	63.5	214.4	214.4	ANL	A2
	I	I1S-06	S	20.4	350	10000	741.1	0.522	497.8	299.8	634.0	466.9	66.3	69.3	141.2	141.2	ANL	A20
	I	I1S-04	S	20.4	350	10000	705.8	0.539	455.9	299.8	634.0	466.9	66.3	69.3	141.2	141.2	ANL	A20
	I	I2S-03	S	20.4	350	10000	684.2	0.747	330.2	299.8	634.0	466.9	66.3	69.3	141.2	141.2	ANL	A20
	I	I1S-02	S	20.4	-	-	512.6	0.459	386.1	168.8	399.6	284.2	36.2	63.2	140.7	179.7	ANL	A20
	I	I2S-02	S	20.4	-	-	536.9	0.561	376.7	168.8	399.6	284.2	36.2	63.2	140.7	179.7	ANL	A20
	I	I1S-08	S	20.4	320	30000	394.2	0.494	251.8	171.1	447.9	309.5	25.1	59.7	194.1	214.4	ANL	A3
	I	I1S-05	S	20.4	350	10000	385.5	0.480	249.9	186.8	420.6	303.7	36.6	49.1	130.1	141.2	ANL	A20
	I	I2S-04	S	20.4	350	10000	425.0	0.512	274.5	186.8	420.6	303.7	36.6	49.1	130.1	141.2	ANL	A20
	P2	P2B-03	C	12.5	-	-	1250.6	0.817	1271.7	219.4	569.9	394.7	78.7	73.8	385.8	385.8	ANL	A20
	P2	P2B-01	C	12.5	-	-	1250.6	0.890	1300.1	219.4	569.9	394.7	78.7	73.8	385.8	385.8	ANL	A20
	P2	P2T-01	C	12.5	-	-	1241.6	0.754	1365.3	219.4	569.9	394.7	78.7	73.8	385.8	385.8	ANL	A20
	P2	P2T-19	C	12.5	290	58000	1542.2	0.897	2272.4	263.6	583.8	423.7	58.3	79.3	424.5	424.5	ANL	A4
	P2	P2B-16	C	12.5	320	55000	1327.2	0.654	1284.5	249.7	605.2	427.5	49.4	78.3	248.7	248.7	ANL	A4
	P2	P2T-06	C	12.5	350	3000	1178.3	0.820	935.4	-	-	-	-	-	360.4	360.4	ANL	A20
	P2	P2T-08	C	12.5	350	10000	1221.9	0.897	913.3	255.6	601.5	428.6	75.1	84.2	286.7	286.7	ANL	A20
P2	P2T-10	C	12.5	350	10000	1426.5	0.728	1468.0	255.6	601.5	428.6	75.1	84.2	286.7	286.7	ANL	A20	
P2	P2B-11	C	12.5	350	30000	960.6	0.643	688.4	240.1	620.3	430.2	67.7	73.2	224.3	224.3	ANL	A2	
P2	P2B-06	C	12.5	400	10000	1053.6	0.765	747.1	-	-	-	-	-	209.2	209.2	ANL	A20	
P2	P2T-04	C	12.5	400	10000	1059.3	0.666	820.2	234.9	610.0	422.4	-	73.4	159.5	159.5	ANL	A20	
P2	P2B-02	C	12.5	-	-	1080.9	0.691	1483.5	-	-	-	-	-	176.7	176.7	ANL	A20	
P2	P2T-02	C	12.5	-	-	873.7	0.694	892.3	149.4	396.0	272.7	43.5	65.9	300.5	385.8	ANL	A20	
P2	P2T-20	C	12.5	290	58000	1128.0	0.554	1,314.8	149.4	396.0	272.7	43.5	65.9	300.5	385.8	ANL	A4	
P2	P2B-17	C	12.5	320	55000	1076.4	0.525	1,192.3	170.9	416.7	293.8	35.5	72.3	-	424.5	424.5	ANL	A4
P2	P2T-07	C	12.5	350	3000	980.8	0.689	1060.3	170.0	417.4	293.7	31.4	65.2	-	248.7	248.7	ANL	A20
P2	P2T-09	C	12.5	350	10000	964.9	0.717	1033.8	-	-	-	-	-	347.5	360.4	ANL	A20	
P2	P2B-12	C	12.5	350	30000	796.5	0.726	650.7	156.1	414.3	285.2	44.1	70.1	321.6	286.7	ANL	A3	
P2	P2T-05	C	12.5	400	10000	893.1	0.484	874.6	152.8	431.3	292.1	36.1	59.8	344.5	224.3	ANL	A20	
69	692-08B	S	21.0	-	-	405.4	0.597	204.4	276.1	594.8	435.5	55.6	51.7	207.1	207.1	ANL	A20	
69	692-08T	S	21.0	-	-	552.0	0.700	267.0	276.1	594.8	435.5	55.6	51.7	207.1	207.1	ANL	A20	

Table B1. (Contd.)

Heat ID	Specimen ID	Process	Calc. Ferrite (%)	Aging Temp (°C)	Aging Time (h)	Test Temp (°C)	Coeff. C	Exponent n	Jic (kJ/m ²)	Yield Stress (MPa)	Ultimate Stress (MPa)	Flow Stress (MPa)	Elongation (%)	Red. in Area (%)	Charpy Impact Energy (J/cm ²)	RT Charpy Impact Energy (J/cm ²)	Source	Ref.
69	691-06T	S	21.0	320	30000	25	834.2	0.586	567.2	277.2	570.7	424.0	31.5	57.6	187.0	187.0	ANL	A2
69	691-03B	S	21.0	320	50000	25	701.0	0.466	486.0	249.7	605.2	427.5	49.4	78.3	184.4	184.4	ANL	A4
69	692-05V	S	21.0	320	50000	25	854.0	0.603	557.9	249.7	605.2	427.5	49.4	78.3	184.4	184.4	ANL	A4
69	691-04B	S	21.0	350	2570	25	888.8	0.425	702.9	294.0	640.8	467.4	65.1	74.3	154.1	154.1	ANL	A4
69	691-01T	S	21.0	350	10000	25	770.8	0.559	514.0	263.7	631.2	447.4	53.5	74.7	188.6	188.6	ANL	A2
69	691-04T	S	21.0	350	30000	25	626.2	0.497	406.7	262.8	663.4	463.1	51.6	71.7	120.1	120.1	ANL	A2
69	691-03B	S	21.0	400	2570	25	64.2	0.368	454.9	277.3	661.0	469.1	48.4	66.5	141.6	141.6	ANL	A20
69	696-01T	S	21.0	400	10000	25	548.3	0.527	323.1	275.9	681.4	478.7	53.5	67.7	101.5	101.5	ANL	A2
69	691-05B	S	21.0	450	2570	25	661.4	0.375	495.1	267.2	678.3	472.7	46.6	72.3	121.1	121.1	ANL	A20
69	693-07T	S	21.0	-	-	290	756.3	0.312	700.1	183.9	419.0	301.4	34.8	61.6	257.7	207.1	ANL	A20
69	693-01V	S	21.0	-	-	290	424.8	0.540	266.3	183.9	419.0	301.4	34.8	61.6	257.7	207.1	ANL	A1,A2
69	691-07T	S	21.0	320	30000	290	492.9	0.410	376.5	170.7	420.0	295.4	23.6	59.1	213.0	187.0	ANL	A3
69	691-03T	S	21.0	320	50000	290	364.9	0.530	210.8	-	-	339.8	-	-	176.0	184.4	ANL	A4
69	691-06T	S	21.0	350	2570	290	523.7	0.259	450.9	173.1	451.3	312.2	32.3	53.8	261.2	154.1	ANL	A20
69	691-02T	S	21.0	350	10000	290	362.6	0.756	158.4	168.1	421.5	294.8	26.5	60.8	169.3	188.6	ANL	A3
69	691-03T	S	21.0	350	30000	290	365.5	0.545	210.3	191.9	454.7	323.3	29.4	51.4	159.8	120.1	ANL	A3
69	691-05T	S	21.0	400	2570	290	368.5	0.412	255.0	163.9	444.8	304.4	33.2	33.2	140.6	141.6	ANL	A20
69	697-01T	S	21.0	400	10000	290	296.4	0.510	166.8	185.1	488.1	336.6	24.8	48.2	135.0	101.5	ANL	A3
69	691-03T	S	21.0	450	2570	290	376.0	0.305	261.9	176.7	478.4	327.6	28.0	48.0	123.8	121.1	ANL	A20
TWI	-	S	17.2	-	-	300	777.0	0.624	504.0	255.5	585.3	420.4	48.5	-	-	278.3	TWI	A24
TWI	-	S	17.2	400	1000	300	508.9	0.736	274.5	244.0	591.0	295.5	50.0	-	-	191.3	TWI	A24
TWI	-	S	17.2	400	10000	300	543.4	0.663	297.3	244.3	594.7	297.3	49.3	-	-	184.8	TWI	A24
CF-3M ≥10%Ni																		
EL		S	33.5	400	3000	320	69.8	0.407	37.7	258.0	670.0	464.0	-	-	-	10.5	EdF	A10
CF-8																		
68	683-05B	S	14.9	-	-	25	552.8	0.586	324.4	276.8	523.6	400.2	40.9	51.3	245.4	245.4	ANL	A20
68	683-05T	S	14.9	-	-	25	485.5	0.554	282.3	276.8	523.6	400.2	40.9	51.3	245.4	245.4	ANL	A20
68	683-03V	S	14.9	-	-	25	526.0	0.562	311.8	276.8	523.6	400.2	40.9	51.3	245.4	245.4	ANL	A20
68	683-06T	S	14.9	Ann.	-	25	1170.2	0.529	1,097.4	276.8	523.6	400.2	40.9	51.3	237.4	237.4	ANL	A2
68	682-06T	S	14.9	320	30000	25	864.1	0.484	647.3	320.0	602.6	461.3	49.8	74.1	135.1	135.1	ANL	A2
68	683-02B	S	14.9	320	52600	25	860.1	0.568	596.3	308.3	609.2	458.8	49.6	71.2	96.0	96.0	ANL	A4
68	682-05V	S	14.9	320	52600	25	679.5	0.442	492.3	308.3	609.2	458.8	49.6	71.2	96.0	96.0	ANL	A4
68	681-04B	S	14.9	350	2570	25	1037.7	0.608	798.0	288.2	600.5	444.3	63.1	74.4	192.9	192.9	ANL	A20

Table B1. (Contd.)

Heat ID	Specimen ID	Process	Calc. Ferrite (%)	Aging Temp (°C)	Aging Time (h)	Test Temp (°C)	Coeff. C	Exponent n	Jic (kJ/m ²)	Yield Stress (MPa)	Ultimate Stress (MPa)	Flow Stress (MPa)	Elongation (%)	Red. in Area (%)	Charpy Impact Energy (J/cm ²)	RT Charpy Impact Energy (J/cm ²)	Source	Ref.
68	682-02T	S	14.9	350	10000	25	719.1	0.546	475.2	287.2	603.9	445.5	53.1	76.8	100.0	100.0	ANL	A2
68	682-04T	S	14.9	350	30000	25	430.4	0.634	205.1	289.2	640.0	464.6	48.0	69.8	80.6	80.6	ANL	A2
68	681-06V	S	14.9	350	30000	25	357.5	0.472	206.0	289.2	640.0	464.6	48.0	69.8	80.6	80.6	ANL	A2
68	681-03B	S	14.9	400	2570	25	648.6	0.531	408.4	292.0	643.7	467.8	75.0	64.3	74.1	74.1	ANL	A20
68	681-01T	S	14.9	400	10000	25	487.6	0.578	360.5	306.2	643.3	474.8	39.1	57.2	46.4	46.4	ANL	A2
68	681-03V	S	14.9	400	10000	25	443.4	0.626	214.0	306.2	643.3	474.8	39.1	57.2	46.4	46.4	ANL	A2
68	682-08B	S	14.9	400	10000*	25	627.4	0.481	412.7	306.2	643.3	474.8	39.1	57.2	74.7	74.7	ANL	A4
68	681-04T	S	14.9	450	2570	25	467.7	0.448	294.7	300.4	643.0	471.7	41.5	53.7	54.2	54.2	ANL	A20
68	681-05B	S	14.9	450	2570	25	532.9	0.680	252.6	300.4	643.0	471.7	41.5	53.7	54.2	54.2	ANL	A20
68	C340	S	14.9	350	138000	54	480.2	0.653	-	-	-	-	-	-	-	-	GE	A16
68	C341	S	14.9	350	138000	54	487.9	0.547	-	-	-	-	-	-	-	-	GE	A16
68	683-07T	S	14.9	-	-	290	783.0	0.271	753.1	159.6	404.8	282.2	33.6	60.6	287.1	245.4	ANL	A20
68	683-06B	S	14.9	Ann.	-	290	553.1	0.513	413.0	159.6	404.8	282.2	33.6	60.6	220.5	237.4	ANL	A3
68	682-07T	S	14.9	320	30000	290	401.9	0.601	225.3	172.3	447.6	309.9	37.3	56.6	221.2	135.1	ANL	A3
68	683-02T	S	14.9	320	52600	290	410.8	0.443	274.0	203.3	479.9	341.6	37.6	52.4	202.4	96.0	ANL	A4
68	681-06T	S	14.9	350	2570	290	592.8	0.575	406.3	185.1	452.4	318.8	41.7	57.8	147.5	192.9	ANL	A20
68	682-03T	S	14.9	350	10000	290	451.5	0.544	281.6	166.6	473.8	320.2	28.8	50.9	207.6	100.0	ANL	A3
68	682-05T	S	14.9	350	30000	290	438.6	0.437	303.8	192.2	464.0	328.1	28.8	49.7	187.7	80.6	ANL	A3
68	681-05T	S	14.9	400	2570	290	464.9	0.431	335.4	163.1	463.1	313.1	32.1	47.1	139.6	74.1	ANL	A20
68	681-02T	S	14.9	400	10000	290	396.2	0.510	242.5	185.3	480.0	332.7	31.1	42.4	144.0	46.4	ANL	A3
68	681-03T	S	14.9	450	2570	290	454.9	0.446	312.2	180.7	495.3	338.0	35.5	39.7	124.8	54.2	ANL	A20
C1	C1B-03	S	7.9	-	-	25	549.0	0.664	306.3	-	-	356.2	-	-	59.7	59.7	ANL	A20
C1	C1B-01	S	7.9	-	-	25	404.6	0.361	291.9	-	-	356.2	-	-	59.7	59.7	ANL	A20
C1	C1B-02	S	7.9	-	-	25	416.5	0.724	185.3	-	-	356.2	-	-	59.7	59.7	ANL	A20
C1	C1B-18	S	7.9	320	30000	25	447.5	0.530	270.9	-	-	360.0	-	-	50.5	50.5	ANL	A4
C1	C1B-08	S	7.9	350	10000	25	390.3	0.402	265.9	-	-	360.0	-	-	63.8	63.8	ANL	A4
C1	C1B-11	S	7.9	350	30000	25	451.3	0.620	241.9	-	-	365.0	-	-	44.6	44.6	ANL	A4
C1	C1B-04	S	7.9	-	-	290	-	-	-	-	-	241.1	-	-	-	-	ANL	A20
C1	C1B-05	S	7.9	-	-	290	362.4	0.527	236.4	-	-	241.4	-	-	-	-	ANL	A20
C1	C1B-19	S	7.9	320	30000	290	323.1	0.591	184.8	-	-	245.0	-	-	-	-	ANL	A4
C1	C1B-09	S	7.9	350	10000	290	357.8	0.619	205.9	-	-	245.0	-	-	-	-	ANL	A4
C1	C1B-12	S	7.9	350	30000	290	373.8	0.420	273.0	-	-	250.0	-	-	-	-	ANL	A4
P1	P1B-03	C	17.6	-	-	25	866.5	0.652	9,592.2	246.4	583.5	414.9	57.8	67.9	228.3	228.3	ANL	A20
P1	P1B-01	C	17.6	-	-	25	776.1	0.785	413.3	246.4	583.5	414.9	57.8	67.9	228.3	228.3	ANL	A20

Table B1. (Contd.)

Heat ID	Specimen ID	Process	Calc. Ferrite (%)	Aging Temp (°C)	Aging Time (h)	Test Temp (°C)	Coef. C	Exponent n	Jic (kJ/m ²)	Yield Stress (MPa)	Ultimate Stress (MPa)	Flow Stress (MPa)	Elongation (%)	Red. in Area (%)	Charpy Impact Energy (J/cm ²)	RT Charpy Impact Energy (J/cm ²)	Source	Ref.
P1	P1T-01	C	17.6	-	-	25	1017.4	0.958	560.3	246.4	583.5	414.9	57.8	67.9	228.3	228.3	ANL	A20
P1	P1T-17	C	17.6	290	58000	25	1058.9	0.784	784.2	264.8	549.0	406.9	65.8	65.1	356.4	356.4	ANL	A4
P1	P1B-11	C	17.6	320	30000	25	1105.6	0.429	1,002.3	279.1	596.0	437.5	52.8	76.2	207.3	207.3	ANL	A2
P1	P1B-14	C	17.6	320	55000	25	967.9	0.510	723.6	293.3	667.6	480.4	61.1	56.7	144.7	144.7	ANL	A4
P1	P1T-08	C	17.6	350	10000	25	526.3	0.808	209.1	275.5	622.6	449.0	77.2	72.6	156.4	156.4	ANL	A20
P1	P1B-06	C	17.6	350	10000	25	945.8	0.544	707.3	275.5	622.6	449.0	77.2	72.6	156.4	156.4	ANL	A20
P1	P1T-06	C	17.6	350	10000	25	837.6	0.740	468.0	275.5	622.6	449.0	77.2	72.6	156.4	156.4	ANL	A20
P1	P1B-09	C	17.6	350	30000	25	708.2	0.644	409.0	271.7	629.6	450.7	53.2	62.4	87.7	87.7	ANL	A2
P1	P1B-05	C	17.6	400	10000	25	445.0	0.582	338.7	285.7	668.9	477.3	57.7	56.1	51.7	51.7	ANL	A20
P1	P1T-04	C	17.6	400	10000	25	368.0	0.558	186.8	285.7	668.9	477.3	57.7	56.1	51.7	51.7	ANL	A20
P1	P1B-02	C	17.6	-	-	290	664.1	0.448	554.7	155.1	428.4	291.7	36.1	48.6	255.8	228.3	ANL	A20
P1	P1T-02	C	17.6	-	-	290	733.8	0.488	630.9	155.1	428.4	291.7	36.1	48.6	255.8	228.3	ANL	A20
P1	P1T-18	C	17.6	290	58000	290	579.3	0.760	332.6	173.2	417.0	295.1	37.2	53.4	-	356.4	ANL	A4
P1	P1B-12	C	17.6	320	30000	290	571.2	0.403	456.3	175.2	436.9	306.1	27.1	52.4	-	207.3	ANL	A3
P1	P1B-15	C	17.6	320	55000	290	615.4	0.527	451.9	194.3	448.4	321.4	35.3	57.5	-	144.7	ANL	A4
P1	P1B-07	C	17.6	350	10000	290	529.9	0.424	400.7	178.2	454.4	316.3	42.9	60.7	244.7	156.4	ANL	A20
P1	P1T-07	C	17.6	350	10000	290	633.3	0.435	542.1	178.2	454.4	316.3	42.9	60.7	244.7	156.4	ANL	A20
P1	P1B-10	C	17.6	350	30000	290	491.5	0.595	294.0	192.9	470.2	331.6	25.1	48.2	-	-	ANL	A3
P1	P1T-05	C	17.6	400	10000	290	451.7	0.505	293.7	165.1	493.9	329.5	35.6	50.3	133.5	51.7	ANL	A20
CA4	CA4-01T	S	10.8	264	113900	25	631.8	0.427	476.3	227.5	526.7	377.1	60.6	69.4	145.3	145.3	ANL	A7
CA4	CA4-02T	S	10.8	400	10000	25	469.9	0.473	301.9	-	-	-	-	-	76.1	76.1	ANL	A7
CA4	CA4-01B	S	10.8	Ann.	-	290	475.9	0.698	291.7	-	-	-	-	-	225.3	-	ANL	A7
CA4	CA4-02B	S	10.8	264	113900	290	484.0	0.504	361.2	141.8	381.7	261.7	37.6	49.1	179.0	145.3	ANL	A7
VR	VRI-01	S	9.8	-	-	25	884.1	0.510	699.6	273.0	537.0	405.0	54.1	67.3	237.1	237.1	ANL	A7
VR	VRO-02	S	9.8	400	10000	25	248.9	0.541	122.6	274.3	626.8	450.5	33.2	50.7	72.5	72.5	ANL	A7
VR	VRO-01	S	9.8	-	-	290	457.6	0.477	332.4	159.0	374.0	266.5	32.5	48.0	226.7	237.1	ANL	A7
VR	VRI-02	S	9.8	400	10000	290	331.6	0.448	213.8	184.7	425.5	305.1	22.4	33.1	105.7	72.5	ANL	A7
MA9	MA9-01I	S	5.1	<281	113900	25	1504.1	0.367	1,677.1	229.3	490.4	359.8	66.1	78.2	379.4	379.4	ANL	A7
MA9	MA9-02O	S	5.1	400	10000	25	1117.9	0.326	1,093.5	236.4	508.0	372.2	32.6	65.9	127.6	127.6	ANL	A7
MA9	MA9-01O	S	5.1	<281	113900	290	1010.6	0.420	1,120.6	159.9	359.5	259.7	31.1	43.9	240.9	379.4	ANL	A7
MA9	MA9-02I	S	5.1	400	10000	290	668.0	0.277	629.2	144.1	375.2	259.6	36.2	49.2	186.7	127.6	ANL	A7
MA1	MA1-01T	S	5.2	264	113900	25	1306.4	0.374	1,407.0	230.6	468.8	349.7	30.1	62.2	250.4	250.4	ANL	A7
MA1	MA1-01B	S	5.2	264	113900	290	745.7	0.429	739.1	132.1	319.9	226.0	24.7	41.7	201.5	250.4	ANL	A7

Table B1. (Contd.)

Heat ID	Specimen ID	Process	Calc. Ferrite (%)	Aging Temp (°C)	Aging Time (h)	Test Temp (°C)	Coeff. C	Exponent n	Jic (kJ/m ²)	Yield Stress (MPa)	Ultimate Stress (MPa)	Flow Stress (MPa)	Elongation (%)	Red. in Area (%)	Charpy Impact Energy (J/cm ²)	RT Charpy Impact Energy (J/cm ²)	Source	Ref.	
PV	PVC-01	S	4.7	Ann.	-	25	1422.8	0.350	1,545.7	-	-	-	-	-	423.8	423.8	ANL	A7	
PV	PVI-02	S	4.7	264	113900	25	1386.5	0.428	1,508.8	230.1	510.5	370.3	58.1	81.7	306.9	306.9	ANL	A7	
PV	PVO-01	S	4.7	400	10000	25	603.0	0.450	424.6	-	-	-	-	-	-	-	ANL	A7	
PV	PVI-01	S	4.7	Ann.	-	290	951.0	0.277	978.6	-	-	-	-	-	309.1	423.8	ANL	A7	
PV	PVC-02	S	4.7	264	113900	290	855.7	0.327	857.6	157.4	374.3	265.9	38.5	56.4	257.6	306.	ANL	A7	
PV	PVO-02	S	4.7	400	10000	290	517.4	0.465	388.4	-	-	-	-	-	-	-	ANL	A7	
KRB	KRB-06R	S	27.8	284	68000	25	639.4	0.853	263.4	295.5	559.9	427.7	44.1	65.6	131.1	131.1	ANL	A2	
KRB	KRB-01C	S	27.8	284	68000	25	657.1	0.602	396.2	295.5	559.9	427.7	44.1	65.6	131.1	131.1	ANL	A1	
KRB	KRB-04C	S	27.8	Ann.	-	25	843.9	0.687	531.6	298.1	557.9	428.0	48.3	68.1	232.0	232.0	ANL	A1,A2	
KRB	KRB-05R	S	27.8	284	68000	290	764.3	0.346	681.1	200.6	457.5	329.0	34.1	54.5	321.2	131.1	ANL	A1,A2	
MEA	-	-	-	-	-	25	1085.3	0.667	882.5	-	-	413.0	-	-	-	357.5	MEA	A2	
MEA	-	-	-	-	-	25	1383.8	0.504	1,427.1	-	-	413.0	-	-	-	357.5	MEA	A2	
MEA	-	-	-	-	-	25	1401.7	0.475	1,356.8	-	-	461.7	-	-	-	301.9	MEA	A2	
MEA	-	-	-	-	-	25	1220.8	0.555	1,057.1	-	-	461.7	-	-	-	301.9	MEA	A2	
CF-8M <10%Ni																			
758	758-02C	S	20.8	400	18000	25	209.0	0.591	91.2	-	-	501.0	-	-	69.6	69.6	ANL	A2	
758	758-03C	S	20.8	400	18000	25	239.1	0.607	103.4	-	-	501.0	-	-	69.6	69.6	ANL	A2	
758	758-01C	S	20.8	400	18000	290	268.8	4.000	167.2	-	-	397.1	-	-	118.1	-	ANL	A1,A2	
205	205-25C	C	21.0	400	18000	25	493.9	0.555	275.8	-	-	451.7	-	-	113.8	113.8	ANL	A2	
205	207-10C	C	21.0	-	-	290	637.0	0.526	473.9	-	-	320.5	-	-	271.6	-	ANL	A1,A2	
205	207-09C	C	21.0	-	-	290	718.8	0.405	615.1	-	-	320.5	-	-	271.6	-	ANL	A1,A2	
205	205-24C	C	21.0	400	18000	290	340.0	0.475	207.2	-	-	338.9	-	-	116.3	113.8	ANL	A1,A2	
74	743-05B	S	15.5	-	-	25	795.4	0.481	610.3	273.3	536.9	405.1	63.0	66.9	210.1	210.1	ANL	A20	
74	743-05T	S	15.5	-	-	25	710.6	0.355	577.1	273.3	536.9	405.1	63.0	66.9	210.1	210.1	ANL	A20	
74	743-03V	S	15.5	-	-	25	599.0	0.460	418.5	273.3	536.9	405.1	63.0	66.9	210.1	210.1	ANL	-	
74	745-03V	S	15.5	-	-	25	667.9	0.505	464.2	273.3	536.9	405.1	63.0	66.9	210.1	210.1	ANL	A4	
74	747-03V	S	15.5	-	-	25	628.2	0.531	403.0	273.3	536.9	405.1	63.0	66.9	210.1	210.1	ANL	A2	
74	743-03B	S	15.5	320	50000	25	532.2	0.452	344.8	304.3	645.9	475.1	45.9	61.4	82.4	82.4	ANL	A4	
74	744-02V	S	15.5	320	50000	25	335.9	0.410	207.8	304.3	645.9	475.1	45.9	61.4	82.4	82.4	ANL	A4	
74	741-06T	S	15.5	350	2570	25	852.6	0.439	692.1	265.0	556.0	410.5	60.7	70.1	159.1	159.1	ANL	A20	
74	742-05T	S	15.5	350	30000	25	391.6	0.548	208.6	266.1	628.5	447.3	44.2	58.5	63.0	63.0	ANL	A2	

Table B1. (Contd.)

Heat ID	Specimen ID	Process	Calc. Ferrite (%)	Aging Temp (°C)	Aging Time (h)	Test Temp (°C)	Coeff. C	Exponent n	Jic (kJ/m ²)	Yield Stress (MPa)	Ultimate Stress (MPa)	Flow Stress (MPa)	Elongation (%)	Red. in Area (%)	Charpy Impact Energy (J/cm ²)	RT Charpy Impact Energy (J/cm ²)	Source	Ref.
74	741-03B	S	15.5	400	2570	25	556.5	0.420	389.0	268.2	591.0	429.6	42.9	56.7	128.9	128.9	ANL	A20
74	741-01T	S	15.5	400	10000	25	409.0	0.555	218.7	265.6	619.5	442.5	45.2	70.4	76.5	76.5	ANL	A2
74	741-03T	S	15.5	450	2570	25	404.0	0.483	238.8	258.3	618.6	438.5	51.2	56.7	84.6	84.6	ANL	A20
74	741-05B	S	15.5	450	2570	25	502.9	0.548	289.4	258.3	618.6	438.5	51.2	56.7	84.6	84.6	ANL	A20
74	743-07T	S	15.5	-	-	290	452.9	0.562	285.1	168.2	427.6	297.9	30.4	58.7	181.9	210.1	ANL	A4
74	743-03T	S	15.5	320	52600	290	363.0	0.439	233.2	218.0	488.5	353.3	29.2	42.8	147.4	82.4	ANL	A4
74	741-05T	S	15.5	400	2570	290	138.2	0.421	309.3	166.2	485.1	325.7	28.5	57.1	135.2	128.9	ANL	A4
74	741-02T	S	15.5	400	10000	290	348.9	0.546	195.3	178.4	500.6	339.5	32.3	48.8	142.9	76.5	ANL	A3
74	741-04T	S	15.5	450	3000	290	232.9	0.561	100.7	171.2	493.0	332.1	22.1	40.7	94.4	84.6	ANL	A3
75	752-08T	S	24.8	-	Unaged	25	639.4	0.405	463.2	322.0	600.1	461.1	43.7	71.4	236.9	236.9	ANL	A1,A2
75	753-05T	S	24.8	-	Ann.	25	817.6	0.591	537.4	322.0	600.1	461.1	43.7	71.4	228.3	228.3	ANL	A2
75	751-07T	S	24.8	290	30000	25	749.3	0.501	515.2	316.0	619.5	467.8	44.6	71.7	266.0	266.0	ANL	A2
75	752-06T	S	24.8	320	30000	25	493.4	0.509	281.2	358.7	713.5	536.1	41.8	55.7	64.3	64.3	ANL	A2
75	753-02B	S	24.8	320	50000	25	295.3	0.440	167.7	365.2	726.3	545.7	29.3	40.9	37.3	37.3	ANL	A4
75	752-05V	S	24.8	320	50000	25	355.8	0.420	214.0	365.2	726.3	545.7	29.3	40.9	37.3	37.3	ANL	A4
75	752-02T	S	24.8	350	10000	25	478.0	0.496	274.2	346.4	732.8	539.6	41.9	55.9	46.0	46.0	ANL	A2
75	752-04T	S	24.8	350	30000	25	189.4	0.429	104.3	320.4	741.9	531.1	29.4	36.0	30.5	30.5	ANL	A2
75	751-06V	S	24.8	350	30000	25	172.2	0.451	90.9	320.4	741.9	531.1	29.4	36.0	30.5	30.5	ANL	A2
75	751-03B	S	24.8	400	2570	25	407.3	0.461	238.4	339.9	717.6	528.7	36.0	64.2	46.3	46.3	ANL	A2
75	751-01B	S	24.8	400	10000	25	281.2	0.599	123.8	367.7	747.4	557.6	32.3	45.6	35.8	35.8	ANL	A2
75	751-01T	S	24.8	400	10000	25	231.4	0.670	88.9	367.7	747.4	557.6	32.3	45.6	35.8	35.8	ANL	A2
75	751-03V	S	24.8	400	10000	25	309.2	0.548	149.6	367.7	747.4	557.6	32.3	45.6	35.8	35.8	ANL	A2
75	753-06B	S	24.8	400	10000*	25	277.8	0.334	181.5	367.7	747.4	557.6	32.3	45.6	40.5	40.5	ANL	A4
75	751-04T	S	24.8	450	2570	25	348.1	0.563	170.4	313.2	733.8	523.5	28.6	40.0	51.1	51.1	ANL	A2
75	752-08B	S	24.8	-	Unage	290	583.3	0.453	436.8	194.2	472.8	333.5	28.3	54.1	164.8	236.9	ANL	A1,A2
75	752-03V	S	24.8	-	Unage	290	600.0	0.347	493.4	194.2	472.8	333.5	28.3	54.1	164.8	236.9	ANL	A1,A2
75	753-05B	S	24.8	-	Ann.	290	518.5	0.562	329.8	194.2	472.8	333.5	28.3	54.1	201.5	228.3	ANL	A3
75	752-07T	S	24.8	320	30000	290	358.0	0.488	210.0	237.7	562.3	400.0	25.2	46.2	160.0	64.3	ANL	A3
75	753-02T	S	24.8	320	50000	290	354.5	0.385	234.4	254.2	575.8	415.0	24.1	43.5	124.7	37.3	ANL	A4
75	752-03T	S	24.8	350	10000	290	288.2	0.627	129.5	214.9	604.9	409.9	28.6	40.1	151.5	46.0	ANL	A3

Table B1. (Contd.)

Heat ID	Specimen ID	Process	Calc. Ferrite (%)	Aging Temp (°C)	Aging Time (h)	Test Temp (°C)	Coeff. C	Exponent n	Jic (kJ/m ²)	Yield Stress (MPa)	Ultimate Stress (MPa)	Flow Stress (MPa)	Elongation (%)	Red. in Area (%)	Charpy Impact Energy (J/cm ²)	RT Charpy Impact Energy (J/cm ²)	Source	Ref.	
75	752-05T	S	24.8	350	30000	290	262.6	0.669	108.4	233.5	604.8	419.2	24.5	31.4	111.9	30.5	ANL	A3	
75	751-05T	S	24.8	400	2570	290	301.9	0.571	150.2	203.2	591.1	397.2	26.4	41.0	115.5	46.3	ANL	A3	
75	751-02T	S	24.8	400	10000	290	274.2	0.462	156.1	207.5	612.8	410.1	24.5	36.9	135.8	35.8	ANL	A3	
75	751-02V	S	24.8	400	10000	290	363.6	0.320	262.0	207.5	612.8	410.1	24.5	36.9	135.8	35.8	ANL	A3	
75	751-03T	S	24.8	450	2570	290	230.1	0.577	107.1	208.2	602.2	405.2	24.9	28.9	82.0	51.1	ANL	A3	
EK	-	S	28.0	350	30000	320	112.3	0.450	-	-	-	-	-	-	-	13.9	EdF	A10	
EK	-	S	28.0	325	30000	320	241.7	0.450	-	-	-	-	-	-	-	22.0	EdF	A10	
L-Hi	-	C	23.7	-	-	325	574.2	0.592	356.0	220.5	501.5	361.0	30.0	-	-	-	JNES	A18	
L-Hi	-	C	23.7	450	13300	325	166.1	0.432	92.0	218.0	592.5	405.3	13.5	-	54.6	-	JNES	A18	
L-Lo	-	C	11.4	-	-	325	522.7	0.803	276.6	147.0	400.5	273.7	38.9	-	-	-	JNES	A18	
L-Lo	-	C	11.4	450	13300	325	329.0	0.578	173.7	161.5	500.5	331.0	24.5	-	143.4	-	JNES	A18	
M-Hi	-	C	22.7	-	-	325	487.4	0.577	300.0	201.0	448.5	324.8	35.0	-	-	-	JNES	A18	
M-Hi	-	C	22.7	450	13300	325	182.0	0.444	100.0	209.5	606.5	408.0	15.8	-	79.6	-	JNES	A18	
CF-8M ≥10%Ni																			
Y1422	-	S	27.1	400	980	100	67.4	0.384	38.0	250.0	528.0	389.0	-	-	26.0	26.0	EdF/FRA	12	
Y4331	-	S	23.2	400	700	320	217.7	0.665	-	-	-	-	-	-	-	26.6	FRA	A14	
Y4331	-	S	23.2	400	700	320	228.6	0.528	-	-	-	-	-	-	-	26.6	FRA	A14	
Y4331	-	S	23.2	400	700	320	260.7	0.501	-	-	-	-	-	-	-	26.6	FRA	A14	
Y4331	-	S	23.2	400	700	320	283.6	0.857	-	-	-	-	-	-	-	26.6	FRA	A14	
Y4331	-	S	23.2	400	700	320	281.9	0.536	-	-	-	-	-	-	-	26.6	FRA	A14	
Y4331	-	S	23.2	400	700	320	328.6	0.684	-	-	-	-	-	-	-	26.6	FRA	A14	
Y4331	-	S	23.2	400	700	20	105.1	0.513	48.7	324.0	739.0	531.5	20.0	-	26.6	26.6	FRA	A14	
Y4331	-	S	23.2	400	700	100	97.6	0.418	-	-	-	-	-	-	-	26.6	FRA	A14	
Y4331	-	S	23.2	400	10000	20	74.1	0.366	42.7	333.0	672.0	502.5	11.0	-	17.5	17.5	FRA	A14	
Y4331	-	S	23.2	400	10000	100	109.4	0.520	-	-	-	-	-	-	-	17.5	FRA	A14	
Y4331	-	S	23.2	400	10000	320	123.3	0.541	56.4	225.0	565.0	395.0	-	-	-	17.5	FRA	A14	
Y3296	-	S	35.8	400	1000	320	91.3	0.478	44.6	276.0	679.0	477.5	-	-	-	10.5	FRA	A14	
Y3296	-	S	35.8	400	1000	320	112.4	0.342	68.6	276.0	679.0	477.5	-	-	-	10.5	FRA	A14	
Y3296	-	S	35.8	400	1000	320	88.6	0.541	39.1	276.0	679.0	477.5	-	-	-	10.5	FRA	A14	
Y3296	-	S	35.8	400	1000	320	82.7	0.333	50.4	276.0	679.0	477.5	-	-	-	10.5	FRA	A14	
Y3296	-	S	35.8	400	1000	320	72.5	0.457	36.2	276.0	679.0	477.5	-	-	-	10.5	FRA	A14	

Table B1. (Contd.)

Heat ID	Specimen ID	Process	Calc. Ferrite (%)	Aging Temp (°C)	Aging Time (h)	Test Temp (°C)	Coeff. C	Exponent n	Jic (kJ/m ²)	Yield Stress (MPa)	Ultimate Stress (MPa)	Flow Stress (MPa)	Elongation (%)	Red. in Area (%)	Charpy Impact Energy (J/cm ²)	RT Charpy Impact Energy (J/cm ²)	Source	Ref.
Y3296	-	S	35.8	400	1000	320	55.4	0.553	23.5	276.0	679.0	477.5	-	-	-	10.5	FRA	A14
Y3296	-	S	35.8	400	1000	20	50.2	0.334	30.0	381.0	649.0	515.0	3.6	-	10.5	10.5	FRA	A14
Y3296	-	S	35.8	400	1000	20	30.9	0.369	17.3	381.0	649.0	515.0	-	-	10.5	10.5	FRA	A14
Y3296	-	S	35.8	400	1000	100	37.0	0.290	-	-	-	-	-	-	-	10.5	FRA	A14
FK	-	C	15.4	-	-	25	742.6	0.635	481.9	400.6	-	200.3	-	-	-	-	FRA	A15
FK	-	C	15.4	427	3000	25	383.2	0.441	304.0	510.8	-	255.4	-	-	48.5	48.5	FRA	A15
FL	-	S	18.6	400	7500	25	179.8	0.431	108.0	539.8	-	269.9	-	-	30.4	30.4	FRA	A15
FL	-	S	18.6	400	7500	200	276.8	0.407	156.7	473.0	-	236.5	-	-	-	30.4	FRA	A15
FL	-	S	18.6	400	7500	320	240.2	0.244	159.5	427.5	-	213.8	-	-	-	30.4	FRA	A15
CC	-	S	32.2	400	1000	320	76.1	0.589	30.9	276.0	679.0	477.5	-	-	-	10.5	EdF	A10
DI	-	S	20.4	400	10000	320	110.8	0.500	53.6	225.0	565.0	395.0	-	-	-	17.5	EdF	A10
DI	-	S	20.4	400	700	320	243.3	0.530	-	-	-	-	-	-	-	26.6	EdF	A10
A-A	-	C	11.3	-	-	25	1698.0	0.606	2,311.0	249.9	539.9	394.9	-	-	384.7	384.7	Kansai/MHI	A19
A-A	-	C	11.3	400	30	25	-	-	-	250.0	540.5	395.2	-	-	312.1	312.1	Kansai/MHI	A19
A-A	-	C	11.3	400	3000	25	-	-	-	257.4	595.4	426.4	-	-	127.4	127.4	Kansai/MHI	A19
A-A	-	C	11.3	400	10000	25	507.8	0.679	242.7	250.3	634.3	442.3	-	-	109.4	109.4	Kansai/MHI	A19
A-A	-	C	11.3	400	20000	25	496.7	0.533	287.5	276.7	630.7	453.7	-	-	83.0	83.0	Kansai/MHI	A19
A-A	-	C	11.3	400	40000	25	625.0	0.450	427.3	281.5	649.5	465.5	-	-	83.5	83.5	Kansai/MHI	A19
A-A	-	C	11.3	-	-	325	573.7	0.873	270.4	165.9	441.9	303.9	-	-	363.5	384.7	Kansai/MHI	A19
A-A	-	C	11.3	400	30	325	1097.8	0.688	1,248.9	160.0	460.7	310.3	-	-	395.6	312.1	Kansai/MHI	A19
A-A	-	C	11.3	400	3000	325	-	-	-	155.4	479.4	317.4	-	-	261.1	127.4	Kansai/MHI	A19
A-A	-	C	11.3	400	10000	325	493.7	0.619	291.4	150.3	492.3	321.3	-	-	166.5	109.4	Kansai/MHI	A19
A-A	-	C	11.3	400	20000	325	514.1	0.513	345.3	158.7	504.7	331.7	-	-	158.6	83.0	Kansai/MHI	A19
A-A	-	C	11.3	400	40000	325	632.1	0.430	498.0	163.5	501.5	332.5	-	-	159.1	83.5	Kansai/MHI	A19
B-C	-	C	11.3	-	-	25	1725.7	0.663	-	-	-	-	-	-	-	-	JPEIC/MHI	A21,22
B-C	-	C	11.3	400	2211	25	797.6	0.744	-	-	-	-	-	-	-	-	JPEIC/MHI	A21,22
B-C	-	C	11.3	400	28028	25	450.2	0.485	-	-	-	-	-	-	-	-	JPEIC/MHI	A21,22
B-C	-	C	11.3	-	-	316	1228.3	0.826	-	145.9	414.6	280.2	-	-	317.4	-	JPEIC/MHI	A21,22
B-C	-	C	11.3	400	2211	316	720.4	0.490	601.2	162.9	448.9	305.9	-	-	257.8	-	JPEIC/MHI	A21,22
B-C	-	C	11.3	400	28028	316	509.9	0.510	349.2	144.9	487.7	316.3	-	-	146.3	-	JPEIC/MHI	A21,22

Table B2. (Contd.)

Δa (mm)	J_m (kJ/m ²)	J_d (kJ/m ²)	Δa (mm)	J_m (kJ/m ²)																					
P2T-06	25°C	P2B-07	25°C	P2T-08	25°C	P2T-10	25°C	P2B-11	25°C	P2B-06	400°C	P2T-04	400°C	P2T-02	290°C	P2B-02	290°C								
350°C	3000 h	350°C	3000 h	350°C	10000 h	350°C	10000 h	350°C	30000 h	400°C	400°C	400°C	400°C	-	-	-	-								
0.154	96.5	0.200	193.2	0.133	105.8	0.097	176.5	0.000	44.2	0.163	232.2	0.095	107.7	0.209	184.0										
0.446	676.7	0.362	377.6	0.242	450.1	0.460	485.3	0.033	124.4	0.292	406.3	0.238	240.3	0.471	693.4	0.169									
0.654	922.6	0.485	527.0	0.253	679.7	0.642	679.7	0.088	145.5	0.360	539.0	0.333	381.3	0.634	657.7	0.347									
0.992	1,291.5	0.793	895.9	0.616	1,032.7	0.653	909.0	0.113	156.1	0.448	663.4	0.421	472.4	0.827	806.6	0.626									
1.277	1,642.9	0.962	1,018.8	0.834	1,270.9	0.835	997.2	0.186	179.7	0.659	812.4	0.599	455.4	1.067	973.0	0.873									
1.570	1,959.1	0.977	1,141.9	1.004	1,535.7	0.871	1,129.6	0.117	218.9	0.741	629.5	0.789	612.7	1.353	1,148.0	1.198									
1.978	2,363.1	1.162	1,247.2	1.137	1,500.3	1.004	1,288.5	0.311	242.9	0.925	786.8	0.993	795.0	1.601	1,331.9	1.453									
2.193	2,573.8	1.185	1,511.1	1.330	2,003.5	1.040	1,403.2	0.354	304.0	1.251	1,095.1	1.211	968.9	1.996	1,497.8	1.755									
2.548	2,793.1	1.332	1,484.4	1.621	2,197.5	1.258	1,659.1	0.172	357.0	1.551	1,283.7	1.442	1,151.0	2.368	1,681.3	1.871									
2.956	3,056.2	1.431	1,660.2	2.373	2,700.3	1.404	1,800.3	0.391	438.2	1.728	1,482.6	1.762	1,357.9	2.716	1,873.7	2.134									
2.987	3,161.7	1.632	1,818.2	2.505	3,071.1	1.621	2,232.8	0.312	499.9	2.082	1,681.1	2.048	1,523.4	2.801	2,075.8	2.475									
3.134	3,223.0	1.670	1,967.7	2.578	3,230.0	1.924	2,471.0	0.486	525.7	2.173	1,808.3	2.219	1,744.2	3.235	2,267.9	2.575									
3.226	3,328.4	1.770	2,152.3	2.760	3,256.3	2.094	2,470.9	0.503	554.5	2.743	1,987.4	2.651	1,931.7	3.622	2,530.5	2.923									
3.311	3,425.0	1.847	2,319.4	2.929	3,424.0	2.288	2,682.7	0.547	583.5	2.912	2,135.9	3.077	2,127.8			3.248									
3.395	3,433.7	1.977	2,503.9	3.269	3,591.5	2.591	2,894.4	0.484	615.8	3.049	2,205.4	3.408	2,268.5			3.597									
		2.154	2,661.9	3.572	3,829.7	2.675	3,229.9	0.440	648.9	3.303	2,307.5	3.696	2,409.3			3.922									
		2.046	2,838.2	4.081	4,094.2	2.942	3,114.9	0.631	677.4	3.478	2,418.4	3.935	2,554.6			4.441									
		2.177	3,022.7	4.652	4,358.7	3.331	3,335.4	0.575	707.8	3.825	2,574.0	4.577	2,763.1			4.976									
		2.269	3,031.3	5.307	4,640.8	3.597	3,564.8	0.501	743.5	4.017	2,695.9	5.049	2,950.2			5.533									
		2.238	3,198.6	5.937	4,922.9	4.191	3,873.4	0.616	778.3	4.380	2,862.6	5.823	3,223.0			6.060									
		2.423	3,383.0	6.386	5,196.4	4.470	4,164.6	0.653	803.4	4.915	3,088.3	6.541	3,504.2			6.494									
		2.438	3,567.8	7.102	5,478.4	5.076	4,437.9	0.671	857.2	5.580	3,292.0	7.711	3,994.9												
		2.676	3,743.3	7.988	5,813.3	5.950	4,799.3	0.877	947.9	6.038	3,501.4	8.542	4,365.0												
		2.792	3,769.4	8.521	6,095.5	6.799	5,160.7	1.040	980.2	6.587	3,765.5	9.503	4,779.0												
		2.815	3,927.8	8.606	6,157.3	7.600	5,486.9	1.149	1009.8	7.638	4,030.6	10.683	5,192.4												
		2.984	4,121.0			8.559	5,830.6	1.087	1052.9	8.498	4,241.0	11.674	5,508.7												
		3.231	4,314.1			9.433	6,041.9	1.235	1122.9	9.270	4,566.8	11.834	5,552.6												
		3.354	4,322.6			9.615	6,112.4	1.387	1242.0	9.867	4,848.9														
		3.601	4,506.9					1.420	1282.1	10.858	5,103.2														
		3.747	4,709.0					1.737	1303.2	11.237	5,314.9														
		4.086	4,910.7					1.760	1341.8	11.353	5,367.8														
		4.209	5,121.6					1.906	1375.5																
		4.279	5,112.7					1.726	1433.3																
		4.664	5,358.3					1.952	1499.6																
		5.173	5,638.8					2.305	1518.2																
		5.311	5,937.7					2.111	1625.1																
		5.835	6,174.2					2.575	1709.1																
		6.089	6,499.2																						

Table B2. (Contd.)

Δa (mm)	J_d (kJ/m ²)	Δa (mm)	J_d (kJ/m ²)	Δa (mm)	J_m (kJ/m ²)	Δa (mm)	J_m (kJ/m ²)	Δa (mm)	J_d (kJ/m ²)	Δa (mm)	J_m (kJ/m ²)	Δa (mm)	J_d (kJ/m ²)	Δa (mm)	J_m (kJ/m ²)	Δa (mm)	J_d (kJ/m ²)								
P2T-20	290°C	P2B-17	290°C	P2T-07	290°C	P2T-09	290°C	P2B-12	290°C	P2T-05	290°C	P2B-08B	290°C	P2T-08T	25°C	P2B-06T	25°C							25°C	
290°C	58000 h	320°C	55000 h	350°C	3000 h	350°C	10000 h	350°C	30000 h	400°C	10000 h	-	-	-	320°C	320°C	30000 h							30000 h	
0.010	36.7	0.000	39.4	0.097	79.6	0.087	79.7	0.020	24.0	0.299	320.9	0.063	0.122	40.1	0.009	41.2								41.2	
0.000	62.4	0.000	97.6	0.127	186.1	0.251	139.2	0.059	62.9	0.340	381.8	0.110	0.226	95.5	0.012	75.6								75.6	
0.000	118.8	0.000	128.4	0.264	325.5	0.289	325.5	0.047	119.0	0.421	486.9	0.125	0.334	261.2	0.146	116.1								116.1	
0.142	147.4	0.035	160.4	0.244	372.2	0.317	518.5	0.122	151.3	0.482	553.3	0.200	0.441	309.8	0.181	145.7								145.7	
0.000	180.4	0.000	194.5	0.381	431.6	0.471	711.2	0.085	186.7	0.571	630.8	0.322	0.587	358.3	0.198	204.7								204.7	
0.201	210.0	0.153	229.5	0.566	564.1	0.732	803.7	0.198	221.7	0.788	735.8	0.381	0.616	405.6	0.066	268.6								268.6	
0.015	244.5	0.051	272.4	0.449	544.6	0.800	916.7	0.302	257.9	0.842	796.7	0.441	0.634	456.4	0.251	336.7								336.7	
0.000	280.2	0.175	315.6	0.712	716.7	1.052	969.3	0.412	293.5	0.972	890.7	0.524	0.756	506.7	0.278	401.4								401.4	
0.177	312.7	0.179	360.6	0.810	809.6	1.109	1,049.0	0.278	335.2	1.074	951.5	0.524	0.974	556.4	0.361	465.2								465.2	
0.067	350.1	0.243	406.2	0.859	896.0	1.099	1,155.6	0.565	370.6	1.094	995.8	0.783	1.069	610.2	0.442	527.2								527.2	
0.399	381.5	0.190	455.5	1.083	988.3	1.186	1,261.8	0.502	412.2	1.302	995.4	0.890	1.277	660.1	0.624	569.0								569.0	
0.055	425.4	0.291	502.3	1.190	1,247.8	1.302	1,254.9	0.647	451.8	1.480	1,104.0	1.062	1.592	738.2	0.618	619.3								619.3	
0.201	500.8	0.194	555.1	1.326	1,220.5	1.592	1,387.3	0.595	495.7	1.711	1,250.1	1.354	2.006	815.8	0.654	657.8								657.8	
0.435	535.6	0.612	594.0	1.473	1,346.5	1.843	1,586.3	0.578	540.8	2.155	1,404.7	1.660	2.258	897.0	0.706	689.7								689.7	
0.412	576.5	0.455	649.0	1.609	1,472.5	2.133	1,791.9	0.599	586.2	2.567	1,550.4	1.700	2.546	976.4	0.735	741.7								741.7	
0.512	615.4	0.527	700.9	1.463	1,446.5	2.462	1,984.1	0.806	625.0	3.021	1,699.4	1.916	3.066	1,085.1	0.895	768.2								768.2	
0.411	661.5	0.492	756.0	1.824	1,624.9	2.838	2,262.8	0.826	669.2	3.625	1,908.4	2.376	3.582	1,186.7	0.937	809.1								809.1	
0.240	711.0	0.889	794.6	2.087	1,777.0	3.535	2,520.6	0.997	709.7	4.203	2,098.4	2.612	3.508	1,202.5	1.054	847.1								847.1	
0.601	741.5	0.668	857.6	2.243	1,902.9	4.116	2,785.3	0.914	760.4	5.281	2,348.9	3.057	4.244	1,327.4	1.316	922.0								922.0	
0.568	785.3	0.842	907.7	2.437	1,915.3	4.997	3,056.0	1.034	804.0	5.910	2,604.4	3.903	4.362	1,311.5	1.520	998.1								998.1	
0.656	826.7	0.834	965.0	2.593	2,054.6	5.577	3,327.4	1.091	857.7	5.956	2,614.3	4.551	4.950	1,432.6	1.342	1094.9								1094.9	
0.568	876.5	1.039	1011.7	2.690	2,060.8	6.458	3,571.4	1.062	917.4	6.967	2,829.6	5.316	5.804	1,576.9	1.666	1122.6								1122.6	
0.826	910.2	1.037	1070.2	2.992	2,239.4	7.019	3,849.5	1.146	981.3	7.699	3,065.8	6.081	6.599	1,717.5	1.783	1157.6								1157.6	
0.671	964.1	1.170	1122.0	3.333	2,457.8	7.978	4,080.0	1.361	1053.5	7.818	3,079.0	6.184	7.393	1,850.1	2.009	1232.1								1232.1	
0.677	1011.9	1.193	1179.9	3.694	2,669.5	8.394	4,258.6	1.657	1137.4	8.618	3,252.5	6.978	8.188	2,018.1	2.395	1389.3								1389.3	
0.882	1047.8	1.149	1244.2	4.200	2,907.1	8.539	4,298.2	1.682	1239.0	8.767	3,285.8	7.670	9.013	2,194.0	2.783	1530.1								1530.1	
0.704	1105.4	1.211	1301.8	4.764	3,124.5	8.656	4,324.5	2.012	1320.5	9.568	3,486.5	8.582	9.999	2,350.0	3.155	1677.2								1677.2	
1.058	1134.2	1.519	1339.2	5.387	3,308.2			2.242	1408.7	10.369	3,673.5	9.744	10.955	2,494.2	3.554	1754.7								1754.7	
0.912	1189.4	1.571	1395.2	5.864	3,526.0			2.609	1484.0	11.066	3,854.2	11.170	12.191	2,669.5	3.878	1855.2								1855.2	
1.255	1216.8	1.708	1446.5	6.331	3,717.2			2.613	1590.2	11.244	3,887.5	12.346	13.353	2,813.4	4.370	1934.3								1934.3	
1.064	1278.1	1.825	1499.5	6.429	3,743.4			3.074	1654.3	11.808	4,007.5	13.655	2,148.6	4.937	2016.5									2016.5	
1.258	1365.6	2.041	1613.3	7.100	3,900.2			3.377	1729.2	11.926	4,027.5													4,027.5	
1.407	1456.6	2.445	1737.2	7.168	3,919.9			3.575	1815.9															1815.9	
1.633	1487.3	2.786	1790.6	7.771	4,077.1			3.924	1902.1															1902.1	
1.738	1529.2	3.024	1943.3	7.878	4,096.6			4.375	1969.4															1969.4	
1.818	1574.6	3.390	1989.4	8.219	4,235.0			4.835	2047.3															2047.3	
1.894	1570.1	3.721	2036.2	8.325	4,227.9																				
				8.394	4,280.9																				

Table B2. (Contd.)

Δa (mm)	J_d (kJ/m ²)	Δa (mm)	J_m (kJ/m ²)	Δa (mm)	J_d (kJ/m ²)	Δa (mm)	J_d (kJ/m ²)	Δa (mm)	J_d (kJ/m ²)	Δa (mm)	J_m (kJ/m ²)								
681-02T	290°C	681-03T	290°C	C1B-03	25°C	C1B-01	25°C	C1B-02	23°C	C1B-18	25°C	C1B-08	25°C	C1B-11	25°C	C1B-04	290°C		
400°C	10000 h	450°C	2570 h	-	-	-	-	-	-	320°C	30000 h	350°C	10000 h	350°C	-	-	30000 h	350°C	
0.000	29.2	0.031	22.3	0.115	31.2	0.069	44.4	0.053	32.9	0.000	19.5	0.000	51.8	0.000	0.126	76.3	18.6	0.000	18.6
0.086	70.8	0.093	51.2	0.130	90.4	0.064	95.3	0.149	75.6	0.000	53.8	0.037	88.9	0.000	0.098	133.6	52.1	0.000	52.1
0.015	118.6	0.018	174.1	0.191	141.3	0.148	123.2	0.160	110.1	0.025	92.2	0.113	128.6	0.110	0.221	160.8	89.1	0.110	89.1
0.000	144.9	0.107	227.5	0.228	185.7	0.129	151.2	0.206	126.5	0.259	132.5	0.090	168.8	0.110	0.350	194.8	128.2	0.110	128.2
0.171	170.8	0.255	267.4	0.293	223.4	0.213	207.0	0.325	179.1	0.263	174.9	0.214	210.4	0.119	0.408	219.3	210.4	0.119	169.8
0.243	195.8	0.286	305.3	0.231	246.4	0.312	246.4	0.405	197.2	0.320	219.0	0.334	252.5	0.279	0.369	233.0	252.5	0.279	211.7
0.347	222.6	0.555	342.8	0.297	257.9	0.443	284.2	0.443	231.7	0.365	264.7	0.518	295.0	0.372	0.484	250.7	295.0	0.372	254.2
0.502	248.4	0.726	427.4	0.442	299.0	0.438	326.9	0.493	271.1	0.436	310.6	0.666	337.1	0.496	0.510	287.4	337.1	0.496	297.4
0.629	275.0	0.765	387.1	0.488	343.4	0.726	369.7	0.600	289.2	0.570	356.6	0.946	377.5	0.696	0.809	322.8	377.5	0.696	340.3
0.620	303.0	0.874	471.8	0.587	387.7	0.972	405.8	0.700	330.2	0.813	400.9	1.180	418.0	0.835	0.762	371.9	418.0	0.835	383.7
0.463	335.5	1.185	509.2	0.663	453.5	1.160	453.5	0.753	349.9	1.017	445.7	1.455	456.7	0.919	0.915	355.5	445.7	0.919	429.5
0.788	360.5	1.384	555.7	0.830	517.7	1.521	497.8	0.768	369.7	1.202	482.4	1.806	493.5	1.170	0.961	386.8	493.5	1.170	472.4
0.866	388.1	1.481	598.0	1.023	588.9	1.785	538.9	0.880	389.4	1.282	521.4	2.125	528.0	1.214	1.282	435.8	528.0	1.214	518.7
1.093	412.4	1.781	599.7	1.254	662.7	2.162	580.0	0.964	412.4	1.524	556.9	2.486	561.5	1.281	1.550	480.7	556.9	1.281	566.2
1.231	437.6	2.170	663.8	1.461	755.8	2.826	642.4	1.006	430.4	1.814	589.3	2.718	606.5	1.681	1.898	531.0	606.5	1.681	603.1
1.539	489.7	2.539	730.7	1.913	855.9	3.384	688.4	1.087	451.8	1.842	629.1	2.995	650.0	1.714	2.273	578.9	629.1	1.714	649.1
1.850	542.0	2.874	810.6	2.017	847.6	1.527	492.8	1.125	474.8	2.230	658.0	3.331	698.1	1.954	2.618	630.3	698.1	1.954	691.1
2.006	575.3	4.003	882.5	2.396	940.6	1.787	541.2	1.224	496.2	2.431	699.5	3.666	744.2	2.228	2.913	675.2	744.2	2.228	729.1
2.371	597.7	4.091	886.4	2.678	1,042.9	2.158	581.0	1.359	515.9	2.688	739.0	4.027	788.6	2.442	3.307	741.9	788.6	2.442	768.6
2.681	622.5	4.864	967.6	2.718	1,033.4	2.826	640.0	1.394	534.8	3.073	771.8	4.486	825.8	3.095	3.993	808.4	825.8	3.095	786.5
2.890	651.5	5.301	1,025.7	3.188	1,152.0	3.383	686.6	1.562	555.3	3.551	798.1	4.963	860.6	3.536	4.445	870.2	860.6	3.536	808.6
3.286	679.4	5.885	1,103.2	3.730	1,276.4	4.101	731.8	1.587	579.7	3.843	829.5	6.004	878.4	3.827	5.052	951.4	878.4	3.827	837.8
3.672	713.0	7.197	1,207.3	4.471	1,425.1	4.324	774.6	1.677	609.5	4.212	866.9	6.863	885.3	4.206	5.589	1,029.3	885.3	4.206	878.5
4.151	747.7	8.757	1,322.9	5.189	1,562.1	5.089	826.0	1.783	649.7	4.603	901.3	7.226	922.0	4.611	6.139	1,170.5	922.0	4.611	915.4
4.602	781.2	10.055	1,442.7	6.162	1,699.0	5.775	885.9	2.035	686.6	4.948	944.4	7.408	990.0	5.075	6.295	1,126.8	990.0	5.075	961.6
4.990	830.3	11.397	1,574.1	7.008	1,823.1	6.317	924.4	2.178	733.6	5.519	970.1	7.880	1,036.3	5.258	6.718	1,207.9	1,036.3	5.258	1,024.8
5.491	870.9	12.695	1,701.6	7.773	1,947.2	6.477	928.7	2.463	775.0	6.117	988.2	8.302	1,079.4	5.706	7.368	1,292.4	1,079.4	5.706	1,086.6
5.841	916.8			8.635	2,122.7	6.955	984.3	2.641	817.0	6.647	1,006.8	8.738	1,117.4	6.101	8.187	1,409.3	1,006.8	6.101	1,146.6
6.551	935.9			9.433	2,251.1	7.466	1,027.1	3.193	917.6	7.139	1,041.0	9.308	1,138.4	6.451	9.161	1,536.0	1,041.0	6.451	1,207.2
7.106	957.1			9.640	2,276.7	8.072	1,095.6	3.826	1,017.4	7.928	1,047.0	10.192	1,114.0	6.831	10.220	1,620.6	1,047.0	6.831	1,263.9
7.639	979.2			10.533	2,388.0	8.869	1,168.3	4.485	1,117.0	8.543	1,056.5			7.401	10.347	1,630.3		7.401	1,303.0
8.300	986.0			11.491	2,537.8	9.858	1,258.2	5.012	1,219.7	9.032	1,076.0			7.920	11.167	1,727.8		7.920	1,323.9
8.664	1012.0			11.634	2,559.2	10.639	1,339.5	5.985	1,356.6	9.530	1,091.5			8.674	13.18.5	1,844.8		8.674	1,318.5
9.171	1027.9			13.468	2,636.2	10.735	1,339.5	6.878	1,493.7	10.036	1,101.8			9.084	13.172	1,948.8		9.084	1,346.5
9.657	1034.3			13.595	2,653.4	12.043	1,433.7	7.788	1,656.2					9.543	13.68.7	1,961.8		9.543	1,368.7
10.098	1045.4					12.824	1,532.1	9.367	1,835.9					10.030				10.030	1,382.7
10.551	1051.5					12.968	1,540.7	9.830	1,930.1					10.512				10.512	1,392.3
								10.755	2,092.7										

Table B2. (Contd.)

Δa (mm)	J_m (kJ/m ²)	Δa (mm)	J_d (kJ/m ²)	Δa (mm)	J_d (kJ/m ²)	Δa (mm)	J_m (kJ/m ²)	Δa (mm)	J_d (kJ/m ²)	Δa (mm)	J_m (kJ/m ²)	Δa (mm)	J_d (kJ/m ²)	Δa (mm)	J_d (kJ/m ²)	Δa (mm)	J_d (kJ/m ²)							
C1B-05	290°C	C1B-19	290°C	C1B-09	290°C	C1B-12	290°C	P1B-03	25°C	P1B-01	25°C	P1T-01	25°C	P1T-17	25°C	P1B-11	25°C	25°C	25°C	25°C	25°C	25°C	25°C	25°C
-	-	320°C	10000 h	350°C	10000 h	350°C	30000 h	-	-	-	-	-	-	290°C	320°C	30000 h	30000 h	30000 h						
0.042	19.1	0.128	35.0	0.035	35.0	0.000	21.4	0.107	78.5	0.512	464.8	0.275	353.8	0.036	0.000	32	32	32	32	0.000	32	0.000	32	40.4
0.053	50.4	0.283	58.6	0.011	58.6	0.165	43.9	0.260	229.1	0.642	497.3	0.343	471.8	0.040	0.000	86	86	86	86	0.000	86	0.000	86	111.8
0.088	27.2	0.217	82.8	0.282	82.8	0.052	68.5	0.405	307.5	0.909	719.9	0.870	864.4	0.139	0.025	147	147	147	147	0.035	147	0.025	147	137.1
0.111	42.2	0.191	109.2	0.234	109.2	0.320	94.1	0.557	536.9	1.146	903.1	1.008	1,021.6	0.095	0.035	196	196	196	196	0.035	196	0.035	196	165.2
0.068	83.1	0.182	136.3	0.328	136.3	0.031	122.5	0.726	635.0	1.268	955.3	0.984	1,166.1	0.072	0.000	247	247	247	247	0.000	247	0.000	247	259.5
0.140	128.1	0.466	165.8	0.254	165.8	0.158	150.5	0.656	746.7	1.337	1,007.6	1.160	1,310.1	0.144	0.018	299	299	299	299	0.018	299	0.018	299	295.2
0.213	160.8	0.284	194.7	0.319	194.7	0.108	180.1	1.001	844.4	1.406	1,079.7	1.266	1,493.6	0.298	0.000	350	350	350	350	0.000	350	0.000	350	316.3
0.327	216.6	0.692	220.4	0.590	220.4	0.038	216.1	1.031	916.5	1.528	1,125.3	1.511	1,676.8	0.274	0.002	405	405	405	405	0.002	405	0.002	405	384.0
0.312	243.9	0.455	239.1	0.603	252.4	0.253	249.6	1.237	1,060.4	1.674	1,177.5	1.663	1,879.9	0.406	0.158	459	459	459	459	0.158	459	0.158	459	432.4
0.461	256.1	0.824	268.1	0.848	281.1	0.431	283.6	1.597	1,230.2	1.781	1,242.9	1.908	2,082.8	0.315	0.214	518	518	518	518	0.214	518	0.214	518	500.5
0.552	288.8	0.881	299.9	0.771	314.6	0.722	316.4	2.082	1,469.3	1.903	1,308.2	2.053	2,082.5	0.422	0.248	576	576	576	576	0.248	576	0.248	576	566.3
0.621	287.4	0.995	332.5	0.753	348.5	0.871	351.8	2.531	1,592.7	2.311	1,501.8	2.374	2,259.3	0.564	0.259	631	631	631	631	0.259	631	0.259	631	636.4
0.747	335.1	1.212	363.0	0.957	378.3	1.029	387.6	2.877	1,739.3	2.627	1,651.8	2.634	2,462.2	0.616	0.287	688	688	688	688	0.287	688	0.287	688	723.6
0.976	375.9	1.222	397.8	0.951	412.0	1.240	422.2	3.183	1,832.2	3.079	1,832.4	3.094	2,737.3	0.584	0.488	750	750	750	750	0.488	750	0.488	750	825.3
1.320	435.8	1.663	423.8	1.460	434.4	1.753	438.1	3.545	1,956.9	3.543	2,015.1	3.546	3,026.7	0.649	0.495	811	811	811	811	0.495	811	0.495	811	881.4
1.645	497.0	1.663	458.4	1.708	460.7	1.600	480.6	3.764	2,086.1	4.146	2,211.9	4.081	3,289.5	0.784	0.611	869	869	869	869	0.611	869	0.611	869	927.4
1.921	563.3	2.085	483.1	2.154	482.3	2.178	506.3	4.156	2,207.5	4.855	2,397.4	4.774	3,557.5	0.912	0.756	924	924	924	924	0.756	924	0.756	924	994.6
2.420	646.6	2.079	518.3	2.257	512.3	2.188	545.1	4.495	2,364.0	5.586	2,595.0	5.361	3,911.6	0.952	0.842	986	986	986	986	0.842	986	0.842	986	1021.7
2.777	730.7	2.462	543.8	2.688	545.2	2.643	572.1	4.789	2,518.5	6.463	2,816.5	6.011	4,234.7	0.906	0.943	1054	1054	1054	1054	0.943	1054	0.943	1054	1048.0
3.432	829.3	2.556	576.3	2.836	585.5	2.840	611.4	5.307	2,708.8	7.319	3,036.9	6.643	4,576.5	1.007	1.104	1126	1126	1126	1126	1.104	1126	1.104	1126	1076.3
3.950	926.7	2.731	607.3	3.160	620.3	3.243	644.0	5.785	2,884.9	8.100	3,285.8	7.287	4,909.5	1.200	0.874	1192	1192	1192	1192	0.874	1192	0.874	1192	1126.0
4.783	1,025.9	3.185	632.2	3.443	655.1	3.538	678.4	6.243	3,128.0	8.413	3,356.1	7.931	5,250.1	1.261	1.063	1265	1265	1265	1265	1.063	1265	1.063	1265	1203.4
5.475	1,120.1	3.433	663.7	4.057	686.2	4.099	712.3	7.016	3,369.6	8.602	5,574.6	8.602	5,574.6	1.215	1.369	1348	1348	1348	1348	1.369	1348	1.369	1348	1229.7
5.616	1,120.1	3.851	688.4	4.422	724.9	4.365	757.4	7.818	3,597.8	9.731	5,839.0	9.731	5,839.0	1.424	1.436	1413	1413	1413	1413	1.436	1413	1.436	1413	1279.1
6.138	1,211.1	4.050	720.6	4.998	752.0	4.845	791.8	8.304	3,798.2	8.304	3,798.2	8.304	3,798.2	1.647	1.575	1474	1474	1474	1474	1.575	1474	1.575	1474	1326.6
7.099	1,337.8	4.658	739.3	5.329	789.2	5.119	834.1	9.014	3,965.2	9.014	3,965.2	9.014	3,965.2	1.656	1.545	1553	1553	1553	1553	1.545	1553	1.545	1553	1384.6
8.087	1,474.2	4.705	783.2	5.819	816.2	5.830	860.8	9.555	4,167.7	9.555	4,167.7	9.555	4,167.7	1.621	1.823	1640	1640	1640	1640	1.823	1640	1.823	1640	1432.9
8.228	1,487.2	5.170	819.0	6.261	842.9	6.372	892.5	10.229	4,370.1	10.229	4,370.1	10.229	4,370.1	1.738	2.030	1711	1711	1711	1711	2.030	1711	2.030	1711	1482.6
9.570	1,607.5	5.626	850.8	6.675	870.5	6.889	922.6	10.229	4,370.1	10.229	4,370.1	10.229	4,370.1	1.980	2.396	1769	1769	1769	1769	2.396	1769	2.396	1769	1588.9
10.728	1,721.2	6.135	875.8	7.011	901.4	7.411	949.6	10.229	4,370.1	10.229	4,370.1	10.229	4,370.1	2.008	2.767	1859	1859	1859	1859	2.767	1859	2.767	1859	1616.9
10.884	1,737.5	6.523	905.3	7.343	931.4	7.841	980.0	10.229	4,370.1	10.229	4,370.1	10.229	4,370.1	2.397	3.058	2029	2029	2029	2029	3.058	2029	3.058	2029	1720.5
12.000	1,841.5	7.119	917.6	7.677	959.5	8.220	1,000.8	10.229	4,370.1	10.229	4,370.1	10.229	4,370.1	2.517	3.361	2158	2158	2158	2158	3.361	2158	3.361	2158	1824.0
12.861	1,958.5	7.689	927.1	8.178	971.8	8.623	1,029.0	10.229	4,370.1	10.229	4,370.1	10.229	4,370.1	2.923	3.625	2250	2250	2250	2250	3.625	2250	3.625	2250	1930.5
12.917	1,965.0	8.355	924.0	8.648	982.9	9.194	1,048.1	10.229	4,370.1	10.229	4,370.1	10.229	4,370.1	3.295	3.964	2360	2360	2360	2360	3.964	2360	3.964	2360	2080.9
		8.649	948.7	8.932	1,007.7	9.623	1,075.4	10.229	4,370.1	10.229	4,370.1	10.229	4,370.1	3.574	4.374	2507	2507	2507	2507	4.374	2507	4.374	2507	2110.9
		9.578	963.5	9.375	1,018.6	9.375	1,018.6	10.229	4,370.1	10.229	4,370.1	10.229	4,370.1	3.998	4.865	2679	2679	2679	2679	4.865	2679	4.865	2679	2128.1
		10.114	960.7	9.689	1,035.2	9.689	1,035.2	10.229	4,370.1	10.229	4,370.1	10.229	4,370.1	4.450	5.313	2836	2836	2836	2836	5.313	2836	5.313	2836	2145.9
															5.863									2233.7

Table B2. (Contd.)

Δa (mm)	J_d (kJ/m ²)	Δa (mm)	J_m (kJ/m ²)	Δa (mm)	J_d (kJ/m ²)	Δa (mm)	J_m (kJ/m ²)	Δa (mm)	J_d (kJ/m ²)	Δa (mm)	J_m (kJ/m ²)	Δa (mm)	J_d (kJ/m ²)	Δa (mm)	J_m (kJ/m ²)	Δa (mm)	J_d (kJ/m ²)											
743-03V	25°C	745-03V	25°C	747-03V	25°C	743-03B	25°C	744-02V	320°C	741-06T	25°C	742-05T	25°C	741-03B	400°C	741-01T	25°C	741-03B	400°C	741-01T	25°C	741-03B	400°C	741-01T	25°C	741-03B	400°C	
-	-	-	-	-	-	320°C	50000 h	320°C	50000 h	350°C	50000 h	350°C	30000 h	400°C	400°C	400°C	30000 h	400°C	400°C	400°C	30000 h	400°C	400°C	400°C	30000 h	400°C	400°C	
0.037	28.8	0.000	28.83	0.037	28.83	0.000	58.7	0.000	18.4	0.073	190.9	0.000	38.0	0.006	0.000	0.000	38.0	0.006	0.000	0.000	60.8	0.050	13.6	0.000	33.4	0.000	0.000	
0.106	76.4	0.000	76.39	0.106	76.39	0.000	121.9	0.004	50.6	0.043	240.9	0.000	60.8	0.050	20.4	0.173	60.8	0.050	20.4	0.173	52.2	0.077	52.2	0.173	52.2	0.077	52.2	
0.111	129.4	0.081	129.39	0.111	129.39	0.001	156.2	0.006	86.3	0.082	286.4	0.141	97.4	0.077	52.2	0.173	97.4	0.077	52.2	0.173	52.2	0.077	52.2	0.173	52.2	0.077	52.2	
0.074	175.0	0.064	174.98	0.074	174.98	0.049	191.1	0.008	126.9	0.215	347.7	0.172	124.5	0.056	108.9	0.155	124.5	0.056	108.9	0.155	124.5	0.056	108.9	0.155	124.5	0.056	108.9	
0.144	194.8	0.134	191.7	0.069	222.83	0.120	264.1	0.113	169.3	0.209	411.4	0.197	168.8	0.118	156.6	0.410	168.8	0.118	156.6	0.410	168.8	0.118	156.6	0.410	168.8	0.118	156.6	
0.069	222.8	0.274	230.3	0.215	275.67	0.196	301.6	0.329	211.6	0.274	472.7	0.317	215.1	0.174	204.2	0.591	215.1	0.174	204.2	0.591	215.1	0.174	204.2	0.591	215.1	0.174	204.2	
0.215	275.7	0.160	320.1	0.199	332.28	0.365	337.8	0.518	253.5	0.339	515.9	0.544	261.6	0.176	265.5	0.809	261.6	0.176	265.5	0.809	261.6	0.176	265.5	0.809	261.6	0.176	265.5	
0.246	303.6	0.340	367.3	0.369	397.1	0.457	364.8	0.679	296.8	0.401	568.2	0.625	308.4	0.256	322.2	0.883	308.4	0.256	322.2	0.883	308.4	0.256	322.2	0.883	308.4	0.256	322.2	
0.395	363.4	0.372	403.7	0.544	427.77	0.552	392.4	1.047	336.4	0.502	627.3	0.865	369.8	0.414	383.5	1.167	369.8	0.414	383.5	1.167	369.8	0.414	383.5	1.167	369.8	0.414	383.5	
0.369	397.1	0.512	444.6	0.699	493.31	0.676	450.4	1.787	366.4	0.582	688.6	1.134	400.7	0.544	444.8	1.422	400.7	0.544	444.8	1.422	400.7	0.544	444.8	1.422	400.7	0.544	444.8	
0.544	427.8	0.562	485.9	0.831	559.31	0.797	476.8	2.378	392.6	0.641	747.7	1.202	448.5	0.716	499.2	1.837	448.5	0.716	499.2	1.837	448.5	0.716	499.2	1.837	448.5	0.716	499.2	
0.699	493.3	0.639	518.6	0.897	592.15	0.866	504.9	2.809	419.4	0.804	804.5	1.518	494.5	0.993	562.8	2.216	494.5	0.993	562.8	2.216	494.5	0.993	562.8	2.216	494.5	0.993	562.8	
0.710	527.3	0.701	586.6	1.003	624.32	1.061	530.8	3.272	447.1	0.931	861.4	1.773	537.8	1.129	621.8	2.545	537.8	1.129	621.8	2.545	537.8	1.129	621.8	2.545	537.8	1.129	621.8	
0.831	559.3	0.831	625.3	1.172	652.89	1.195	556.6	3.630	475.9	1.086	927.3	1.912	584.6	1.474	683.1	2.869	584.6	1.474	683.1	2.869	584.6	1.474	683.1	2.869	584.6	1.474	683.1	
0.897	592.2	0.931	664.4	1.417	707.22	1.236	584.9	4.075	500.3	1.282	988.6	2.329	624.5	1.773	750.0	3.308	624.5	1.773	750.0	3.308	624.5	1.773	750.0	3.308	624.5	1.773	750.0	
1.003	624.3	1.124	709.5	1.543	735.61	1.442	639.4	4.353	528.6	1.418	1,047.7	2.709	658.4	2.056	805.1	3.705	658.4	2.056	805.1	3.705	658.4	2.056	805.1	3.705	658.4	2.056	805.1	
1.172	652.9	1.247	756.1	1.739	767.63	1.639	662.4	4.594	558.0	1.617	1,143.3	3.166	698.4	2.540	898.1	4.164	698.4	2.540	898.1	4.164	698.4	2.540	898.1	4.164	698.4	2.540	898.1	
1.417	707.2	1.442	799.4	1.881	795.14	1.711	688.9	4.915	591.1	1.898	1,237.5	3.815	729.8	3.140	981.6	4.629	729.8	3.140	981.6	4.629	729.8	3.140	981.6	4.629	729.8	3.140	981.6	
1.739	767.6	1.625	842.6	2.170	818.01	1.958	710.6	5.252	622.5	2.247	1,324.7	4.313	776.0	3.821	1066.7	5.039	776.0	3.821	1066.7	5.039	776.0	3.821	1066.7	5.039	776.0	3.821	1066.7	
1.881	795.1	1.881	890.2	2.424	869.61	1.932	739.5	5.614	666.1	2.969	1,436.7	4.972	838.0	4.664	1,174.5	5.805	838.0	4.664	1,174.5	5.805	838.0	4.664	1,174.5	5.805	838.0	4.664	1,174.5	
2.170	818.0	2.179	933.4	2.607	893.7	2.059	766.0	5.893	711.6	3.777	1,559.8	5.482	893.9	5.404	1,293.6	6.240	893.9	5.404	1,293.6	6.240	893.9	5.404	1,293.6	6.240	893.9	5.404	1,293.6	
2.424	869.6	2.541	970.2	2.789	916.55	2.369	832.6	6.201	753.3	4.181	1,673.0	6.182	956.6	6.070	1,401.4	7.072	956.6	6.070	1,401.4	7.072	956.6	6.070	1,401.4	7.072	956.6	6.070	1,401.4	
2.607	893.7	3.033	1004.4	3.051	951.01	2.632	862.4	6.583	788.5	4.719	1,768.8	6.999	996.0	7.091	1,514.9	7.793	996.0	7.091	1,514.9	7.793	996.0	7.091	1,514.9	7.793	996.0	7.091	1,514.9	
3.051	951.0	3.452	1038.7	3.283	985.26	2.877	886.7	7.123	808.0	5.138	1,899.1	7.820	1040.1	8.186	1,628.4	8.586	1040.1	8.186	1,628.4	8.586	1040.1	8.186	1,628.4	8.586	1040.1	8.186	1,628.4	
3.283	985.3	4.045	1078.4	3.819	1045.8	3.113	911.9	7.625	824.1	5.661	2,017.7	8.475	1088.1	9.015	1,741.8	9.463	1088.1	9.015	1,741.8	9.463	1088.1	9.015	1,741.8	9.463	1088.1	9.015	1,741.8	
3.606	1013.3	4.610	1107.0	4.074	1091.5	3.465	930.7	8.436	810.4	6.229	2,193.3	9.251	1113.6	10.155	1,855.3	10.264	1113.6	10.155	1,855.3	10.264	1113.6	10.155	1,855.3	10.264	1113.6	10.155	1,855.3	
4.074	1091.5	5.070	1142.3	4.389	1132.2	3.710	950.1	8.905	815.1	7.110	2,339.8	9.912	1140.6	11.146	1,968.8	10.930	1140.6	11.146	1,968.8	10.930	1140.6	11.146	1,968.8	10.930	1140.6	11.146	1,968.8	
4.389	1132.2	5.554	1175.5	4.684	1171.1	4.163	978.7	9.256	830.5	7.723	2,486.8	10.607	1155.1	12.330	2,105.0	11.714	1155.1	12.330	2,105.0	11.714	1155.1	12.330	2,105.0	11.714	1155.1	12.330	2,105.0	
4.684	1171.2	6.009	1204.6	5.018	1204.3	4.914	1087.8	9.573	848.1	8.947	2,666.8	11.413	1144.6				1144.6											
5.018	1204.4	6.495	1228.3	5.364	1234.2	5.720	1163.7	9.993	848.1	9.993	2,835.7																	
5.364	1234.2	7.089	1251.0	5.885	1259.3	6.108	1202.3	10.814	848.1	10.814	2,988.0																	
5.885	1259.3	7.775	1253.5	6.215	1298.1	6.740	1228.0	11.904	848.1	11.904	3,174.0																	
6.215	1298.2	8.357	1269.7	6.613	1328.6	7.308	1250.5	12.533	848.1	12.533	3,372.2																	
6.613	1328.7	8.860	1270.7	6.893	1367.3	7.969	1256.6		848.1																			
6.893	1367.4	9.366	1276.9	7.240	1398.2	8.542	1266.1		848.1																			
7.240	1398.3	9.894	1275.0	7.562	1426.9	9.084	1289.6		848.1																			
7.562	1426.9	10.425	1267.6			9.687	1303.1		848.1																			

Table B2. (Contd.)

Δa (mm)	J_m (kJ/m ²)	Δa (mm)	J_m (kJ/m ²)	Δa (mm)	J_d (kJ/m ²)																				
741-03T	25°C	741-05B	25°C	743-08T	290°C	74x-xxx	290°C	741-05T	290°C	741-02T	290°C	741-04T	290°C	752-08T	290°C	753-05T	25°C								
450°C	2570 h	450°C	2570 h	-	50000 h	320°C	50000 h	400°C	400°C	400°C	2570 h	450°C	3000 h	-	Annealed	-									
0.073	50.1	0.026	25.0	0.044	28.8	0.037	28.8	0.000	0.000	0.000	36.7	0.117	11.0	0	0.000	0.000	14.94							31.9	
0.043	143.3	0.110	4.7	0.252	216.9	0.106	76.4	0.050	0.050	0.030	84.6	0.174	29.9	0.0095	0.000	0.000	79.63							69.3	
0.178	193.5	0.043	75.1	0.329	367.8	0.111	129.4	0.000	0.000	0.000	109.1	0.000	67.9	0.0129	0.057	0.057	145.51							101.8	
0.290	239.1	0.108	116.1	0.516	315.8	0.074	175.0	0.068	0.068	0.194	133.1	0.261	92.2	0.0867	0.100	0.100	219.54							133.5	
0.328	298.2	0.134	163.8	0.681	386.5	0.144	194.8	0.000	0.000	0.000	157.7	0.239	117.4	0.1115	0.075	0.075	250.51							172.0	
0.517	350.8	0.246	216.3	1.043	452.3	0.069	222.8	0.100	0.100	0.276	197.1	0.457	150.3	0.1714	0.202	0.202	277.99							212.7	
0.612	407.7	0.391	282.4	1.207	532.4	0.215	275.7	0.195	0.195	0.186	260.2	0.436	183.8	0.2291	0.194	0.194	301.23							254.0	
0.735	467.0	0.424	271.1	1.526	546.5	0.246	303.6	0.338	0.338	0.415	294.3	0.668	218.6	0.0877	0.399	0.399	326.73							297.9	
0.966	517.4	0.651	326.0	1.669	654.9	0.395	363.4	0.540	0.540	0.575	325.5	0.648	253.4	0.2907	0.471	0.471	350.48							335.8	
1.223	579.1	0.873	380.9	1.789	621.8	0.369	397.1	0.610	0.610	0.749	352.2	0.973	288.3	0.234	0.547	0.547	375.01							379.9	
1.541	643.9	1.080	440.3	2.097	692.4	0.544	427.8	0.799	0.799	0.878	377.9	1.034	324.6	0.2153	0.840	0.840	400.98							419.1	
1.898	701.4	1.406	495.3	2.459	753.6	0.699	493.3	0.669	0.669	0.976	408.2	1.336	361.5	0.3433	0.787	0.787	424.31							463.3	
2.515	783.8	1.686	555.6	2.931	805.2	0.710	527.3	1.124	1.124	1.261	429.2	1.498	394.0	0.4037	1.003	1.003	447.91							508.1	
4.658	1,054.7	2.148	637.5	3.414	880.5	0.831	559.3	1.008	1.008	1.416	458.4	1.651	429.1	0.3459	1.217	1.217	473.88							546.4	
5.248	1,173.2	2.708	726.8	3.996	950.9	0.897	592.2	1.317	1.317	1.732	481.8	1.930	460.5	0.5184	1.475	1.475	496.82							584.4	
6.296	1,297.1	3.168	812.4	4.775	1,002.5	1.003	624.3	1.276	1.276	1.949	511.3	2.186	492.9	0.6193	1.608	1.608	518.57							622.7	
7.300	1,404.0	4.113	942.0	5.247	1,030.5	1.172	652.9	1.680	1.680	2.197	558.6	2.674	524.7	0.7079	1.740	1.740	565.4							665.4	
8.141	1,522.4	5.072	1,082.8	6.081	1,124.5	1.417	707.2	2.022	2.022	2.527	607.7	2.778	552.6	0.7299	2.062	2.062	593.41							700.8	
9.218	1,646.3	5.957	1,201.2	6.981	1,199.5	1.739	767.6	2.231	2.231	2.928	630.4	3.198	576.9	0.9174	2.371	2.371	613.63							730.9	
10.843	1,747.3	6.768	1,359.0	7.453	1,241.8	1.881	795.1	2.496	2.496	3.153	650.4	3.435	609.1	1.0186	2.580	2.580	634.67							768.3	
12.083	1,837.3	7.949	1,494.2	8.211	1,331.0	2.170	818.0	2.618	2.618	3.593	674.5	4.000	629.1	1.254	2.920	2.920	676.2							836.9	
13.102	1,910.3	9.071	1,629.4			2.424	869.6	2.998	2.998	3.804	704.6	4.338	662.3	1.3219	3.566	3.566	700.24							882.7	
		10.414	1,781.4			2.607	893.7	3.242	3.242	4.270	737.6	4.953	696.3	1.4084	4.291	4.291	723.25							913.2	
		11.638	1,956.1			3.051	951.0	3.527	3.527	4.727	768.6	5.550	726.1	1.5362	5.077	5.077	767.75							943.0	
		12.879	2,068.6			3.283	985.3	3.844	3.844	5.239	796.4	5.972	758.1	1.6655	5.607	5.607	816.24							981.8	
						3.606	1013.3	4.287	4.287	5.926	831.3	6.860	776.2	1.9785	6.598	6.598	850.88							1007.8	
						4.074	1091.5	4.748	4.748	6.477	862.0	7.590	797.6	2.3787	7.567	7.567	916.23							1015.3	
						4.389	1132.2	5.210	5.210	7.043	890.9	8.453	829.0	3.0668	8.795	8.795	952.42							989.3	
						4.684	1171.2	5.724	5.724	7.698	912.7	9.165	850.6	3.9274	9.619	9.619	977.38							1000.3	
						5.018	1204.4	6.142	6.142	8.211	937.9	9.849	876.7	5.3571	10.187	10.187	979.67							1031.1	
						5.364	1234.2	6.443	6.443	8.740	984.7	10.448	899.5	6.2778	10.610	10.610	1024.0							1074.4	
						5.885	1259.3	6.981	6.981	9.262	1010.8		918.4	7.4627			1038.1								
						6.215	1298.2	7.798	7.798	9.896	1018.8		922.6	8.7116			1036.5								
						6.613	1328.7	8.200	8.200	10.312	1053.6		939.2	9.8767			1063.7								
						6.893	1367.4	8.808	8.808	1071.0				10.798			1103.4								
						7.240	1398.3	9.272	9.272	1095.2															
						7.562	1426.9	10.183	10.183	1134.8															

Table B2. (Contd.)

Δa (mm)	J_d (kJ/m ²)																																
751-01T	25°C	751-03V	25°C	751-04T	25°C	752-08B	290°C	753-03V	290°C	753-05B	290°C	752-07T	290°C	752-03T	290°C	752-03T																	
400°C	10000 h	400°C	10000 h	450°C	2570 h	-	-	-	-	Annealed	-	320°C	30000 h	350°C	30000 h	350°C																	
0.000	16.12	0.000	21.0	0.000	11.4	0.000	17.7	0.031	18.9	0.000	31.7	0.000	19.3	0.106	41.5	0.074	45.26	0.066	18.4	0.018	63.4	0.004	0.004	0.004	0.014	79.2	0.027	71.2	0.014	61.0			
0.153	90.09	0.097	29.7	0.034	40.9	0.015	73.5	0.126	154.8	0.089	112.1	0.059	138.9	0.282	89.4	0.414	129.81	0.045	39.8	0.129	154.4	0.142	0.164	192.2	0.254	180.8	0.294	177.6	0.249	118.7			
0.501	146.14	0.050	55.6	0.348	204.3	0.119	72.3	0.080	210.6	0.270	217.0	0.338	216.2	0.408	150.9	0.511	161.56	0.146	82.1	0.700	233.7	0.105	92.6	0.000	176.5	0.294	254.2	0.505	256.0	0.412	183.3		
0.668	187.52	0.162	102.9	0.817	249.7	0.109	113.6	0.137	204.1	0.341	292.3	0.506	297.2	0.639	216.8	0.863	217.34	0.159	127.4	1.031	279.9	0.236	137.5	0.235	311.7	0.487	329.4	0.947	334.7	0.742	249.9		
1.078	252.14	0.288	153.3	1.342	307.3	0.295	161.7	0.052	253.6	0.173	332.2	0.516	368.6	1.141	282.5	1.208	267.63	0.388	179.2	1.517	335.1	0.269	196.3	0.236	374.6	0.619	407.6	1.334	411.0	1.157	316.0		
1.477	283.22	0.539	207.7	1.841	361.8	0.426	225.2	0.192	297.3	0.418	414.4	0.764	446.5	1.881	350.5	1.572	298.92	0.533	237.1	2.182	387.0	0.557	254.4	0.140	462.2	0.879	485.2	1.912	482.3	1.673	381.8		
1.856	319.16	0.759	267.9	2.488	411.0	0.746	283.7	0.162	343.1	0.634	473.3	1.061	523.2	2.256	417.4	2.113	334.31	0.887	296.8	2.780	435.1	0.847	314.3	0.287	501.9	1.158	561.9	2.449	553.7	2.245	444.1		
2.453	351.02	0.994	327.0	3.064	457.3	0.951	349.4	0.406	385.2	0.567	536.8	1.281	601.4	2.393	412.4	2.640	364.11	1.338	357.5	3.345	491.5	1.198	387.1	0.810	576.6	1.495	637.5	3.107	614.8	2.839	499.3		
2.784	380.68	1.636	384.1	3.744	523.0	1.477	424.5	0.615	423.7	1.041	621.4	1.557	678.0	3.663	533.7	3.011	400.37	2.095	418.3	4.245	544.2	1.924	470.4	0.595	442.7	1.161	715.3	3.913	662.2	3.537	574.6		
3.229	419.57	2.459	450.0	4.613	566.9	2.143	504.5	0.721	481.5	1.686	717.8	2.079	808.2	4.722	618.9	3.516	435.85	3.304	494.1	5.032	587.5	2.542	538.3	0.633	504.5	1.886	761.0	2.112	849.6	5.230	703.0	4.725	653.2
3.830	454.31	3.930	520.8	5.360	610.6	2.869	569.1	0.920	520.8	2.093	778.0	2.369	882.6	5.611	693.0	4.278	472.09	4.804	542.2	5.961	632.5	3.379	605.6	0.703	547.6	2.131	2.449	921.2	6.239	779.8	5.958	125.0	
4.571	487.03	5.490	568.4	6.636	642.1	3.756	639.7	0.934	589.6	2.630	888.4	2.714	954.2	6.726	768.5	5.377	498.36	6.102	594.1	7.182	661.1	4.315	669.4	1.148	610.2	3.527	924.3	2.908	991.1	7.616	839.0	7.251	777.9
5.853	503.19	6.606	624.1	7.885	670.8	5.013	693.9	1.274	659.3	4.097	984.6	3.300	1023.8	8.239	790.6	6.280	511.19	7.524	650.8	8.546	683.4	5.637	715.7	1.458	705.2	4.631	1063.8	3.794	1090.4	8.727	894.4	8.691	797.3
6.583	520.53	8.240	673.5	9.336	682.9	6.137	741.7	1.773	754.2	4.975	1106.6	4.164	1128.6	9.326	804.0	6.884	533.46	8.788	699.6	10.103	683.8	6.971	757.5	2.021	775.7	5.616	1116.4	4.532	1184.8	9.839	928.2	10.117	811.7
7.481	536.11	9.639	704.3	7.779	764.1	2.433	824.9	5.767	1162.6	5.087	1222.9	5.630	1254.1	10.436	936.1	7.861	535.41	10.356	708.0	8.513	773.6	6.194	1185.7	5.630	1254.1	10.436	936.1	10.436	936.1	10.436	936.1	10.436	936.1
8.584	550.54	11.026	717.2	9.370	772.7	3.676	950.3	6.956	1230.7	6.137	1285.7	6.137	1285.7	10.436	936.1	9.058	549.92	10.099	769.1	10.099	769.1	7.352	1248.4	6.861	1369.4	7.352	1248.4	6.861	1369.4	7.352	1248.4	6.861	1369.4
9.645	557.94	10.853	760.7	10.853	760.7	5.880	1173.6	8.323	1255.8	7.390	1387.2	7.390	1387.2	10.436	936.1	9.870	563.51	10.852	594.49	10.852	594.49	7.836	1265.0	8.661	1452.9	7.836	1265.0	8.661	1452.9	7.836	1265.0		
10.361	574.87	10.852	594.49	10.852	594.49	7.836	1265.0	8.661	1452.9	7.836	1265.0	8.661	1452.9	10.436	936.1	11.388	598.15	10.852	594.49	10.852	594.49	10.292	1449.5	10.292	1449.5	10.292	1449.5	10.292	1449.5	10.292	1449.5	10.292	1449.5

Table B2. (Contd.)

Δa (mm)	J_d (kJ/m ²)																		
752-05T	290°C	751-05T	290°C	751-02T	290°C	751-02V	290°C	751-03T	290°C										
350°C	30000 h	400°C	2570 h	400°C	10000 h	400°C	10000 h	450°C	2570 h										
0.083	16.6	0.017	13.7	0.229	17.7	0.000	14.4	0.000	14.6										
0.066	48.7	0.000	50.7	0.075	62.9	0.000	49.0	0.000	55.3										
0.241	67.6	0.231	83.6	0.264	91.2	0.000	74.8	0.119	86.1										
0.191	86.6	0.018	119.2	0.137	116.2	0.000	102.0	0.172	120.4										
0.360	107.3	0.295	157.1	0.443	143.1	0.011	130.8	0.603	156.7										
0.286	128.5	0.522	194.4	0.218	155.3	0.096	160.5	0.580	186.0										
0.506	158.5	0.595	226.1	0.525	184.1	0.049	192.0	0.944	216.4										
0.491	188.8	0.807	257.6	0.500	212.0	0.088	225.3	1.132	245.9										
0.792	219.1	0.894	290.8	0.841	240.1	0.285	253.9	1.342	276.7										
0.930	248.2	1.152	322.4	0.763	269.1	0.441	282.1	1.613	305.6										
1.210	278.5	1.227	355.2	1.277	295.4	0.694	309.3	1.821	335.0										
1.132	310.7	1.551	387.3	1.342	321.8	0.733	338.5	2.567	354.7										
1.485	342.1	1.881	412.9	1.833	346.1	0.988	366.7	3.083	373.3										
1.656	371.1	2.122	441.8	1.976	375.0	1.341	393.4	3.914	394.0										
1.968	397.1	2.495	467.5	2.488	400.1	1.511	419.2	4.288	418.4										
2.249	424.3	2.742	493.6	2.567	429.0	1.807	443.3	5.261	437.7										
2.595	448.2	3.139	517.0	3.121	451.5	1.971	468.4	5.772	458.7										
2.872	473.6	3.418	548.1	3.397	482.4	2.449	499.3	6.589	473.6										
3.188	496.7	3.814	570.0	3.828	511.7	2.786	522.6	7.239	486.6										
3.844	517.7	4.332	599.7	4.327	535.0	3.144	543.8	8.075	493.4										
4.284	548.6	4.929	632.6	4.809	555.8	3.478	572.3	8.635	505.3										
4.952	577.9	5.645	662.0	5.341	580.2	3.917	596.4	9.325	522.6										
5.634	610.1	6.191	693.5	5.901	600.3	4.569	617.6	10.060	533.7										
6.299	636.7	6.911	713.4	6.490	617.9	5.004	642.1												
7.003	657.7	7.472	735.5	7.170	641.0	5.447	666.8												
7.628	676.1	8.200	746.7	7.995	652.1	6.212	688.0												
8.326	686.6	8.734	763.2	8.698	661.4	6.931	703.7												
8.936	702.7	9.258	778.7	9.260	676.0	7.585	718.1												
9.421	712.7	9.789	791.1	9.808	690.6	8.073	739.4												
10.013	718.7	10.228	806.0	10.400	695.9	8.550	759.2												
						8.988	779.0												
						9.374	800.4												
						9.853	811.8												
						10.335	818.5												

Table B3. Results from fracture toughness J-R curves conducted at MEA on seven heats of CASS materials.

Specimen ID	Heat	Orientation	Test Temp. (°C)	Deformation J		Modified J		Flow Stress (MPa)	Time (h)	Temp. (°C)
				J _{IC} (kJ/m ²)	C	J _{IC} (kJ/m ²)	C			
I1S-03	I	C-L	25	508.4	781.5	498.0	796.0	411.2	Unaged	-
I1S-01	I	L-C	25	624.0	861.5	639.4	896.5	411.2	Unaged	-
I2S-01	I	L-C	25	544.7	811.6	551.3	840.7	411.2	Unaged	-
I1S-06	I	C-L	25	497.8	741.1	476.8	771.1	466.8	10000	350
I1S-04	I	L-C	25	455.7	705.8	409.7	733.9	466.8	10000	350
I2S-03	I	L-C	25	408.3	684.2	408.6	710.1	466.8	10000	350
I1S-02	I	L-C	290	386.2	512.6	364.5	534.3	284.2	Unaged	-
I2S-02	I	L-C	290	397.2	536.9	406.6	557.0	284.2	Unaged	-
I1S-05	I	L-C	290	250.1	385.5	223.4	402.2	303.7	10000	350
I2S-04	I	L-C	290	274.6	425.0	266.3	443.2	303.7	10000	350
P2B-03	P2	C-L	25	1,304.2	1,250.6	1,335.2	1,256.5	381.0	Unaged	-
P2B-01	P2	L-C	25	1,289.0	1,241.6	1,240.6	1,225.2	381.0	Unaged	-
P2T-01	P2	L-C	25	1,365.5	1,274.3	1,569.5	1,315.3	381.0	Unaged	-
P2T-06	P2	L-C	25	950.3	1,178.3	1,041.5	1,236.9	421.7	3000	350
P2B-07	P2	L-C	25	1,340.2	1,346.2	1,533.2	1,400.0	421.7	3000	350
P2T-08	P2	L-C	25	1,035.9	1,221.9	1,086.7	1,261.8	436.8	10000	350
P2T-10	P2	L-C	25	1,456.6	1,426.5	1,602.7	1,487.1	436.8	10000	350
P2B-06	P2	L-C	25	747.1	1,053.6	888.8	1,097.5	426.4	10000	400
P2T-04	P2	L-C	25	559.0	867.3	567.3	901.9	426.4	10000	400
P2B-02	P2	L-C	290	1,483.6	1,080.9	1,749.1	1,102.3	268.5	Unaged	-
P2T-02	P2	L-C	290	892.3	873.7	949.8	891.5	268.5	Unaged	-
P2T-07	P2	L-C	290	1,050.3	980.8	1,124.4	1,004.8	288.2	3000	350
P2T-09	P2	L-C	290	1,017.2	964.9	1,147.4	1,013.5	286.8	10000	350
P2T-05	P2	L-C	290	874.6	893.1	916.9	920.0	288.6	10000	400
692-08B	69	H-H	25	204.3	405.4	202.2	421.6	435.5	Unaged	-
692-08T	69	H-H	25	322.1	552.9	320.1	571.9	435.5	Unaged	-
691-04B	69	H-H	25	702.9	888.8	686.2	925.5	467.7	2570	350
691-03B	69	H-H	25	455.0	614.2	368.3	639.4	469.1	2570	400
691-05B	69	H-H	25	495.0	661.4	448.1	690.3	472.7	2570	450
693-07T	69	H-H	290	700.1	756.3	701.8	785.8	301.4	Unaged	-
693-01V	69	V-H	290	266.2	424.8	252.4	439.5	301.4	Unaged	-
691-06T	69	H-H	290	450.9	523.7	408.3	550.0	312.2	2570	350
691-05T	69	H-H	290	255.1	368.5	232.6	384.7	304.4	2570	400
691-03T	69	H-H	290	261.8	376.0	254.2	392.3	327.6	2570	450

Table B3. (Contd.)

Specimen ID	Heat	Orientation	Test Temp. (°C)	Deformation J		Modified J		Flow Stress (MPa)	Time (h)	Temp. (°C)
				J _{IC} (kJ/m ²)	C	J _{IC} (kJ/m ²)	C			
C1B-03	C1	C-L	25	347.3	549.0	349.8	569.8	356.2	Unaged	-
C1B-01	C1	L-C	25	291.9	404.6	276.3	422.5	356.2	Unaged	-
C1B-02	C1	L-C	25	220.4	416.5	217.3	431.3	356.2	Unaged	-
C1B-04	C1	L-C	290	-	-	238.0	384.5	241.1	Unaged	-
C1B-05	C1	L-C	290	236.5	362.4	221.6	380.3	241.4	Unaged	-
P1B-03	PI	C-L	25	605.9	866.5	617.2	898.0	413.8	Unaged	-
P1B-01	PI	L-C	25	499.8	776.1	502.6	803.4	416.5	Unaged	-
P1T-01	PI	L-C	25	734.3	1,017.4	740.6	1,045.3	416.5	Unaged	-
P1T-08	PI	C-L	25	210.3	526.3	202.0	546.4	439.8	10000	350
P1B-06	PI	L-C	25	716.8	945.8	737.7	982.0	458.1	10000	350
P1T-06	PI	L-C	25	521.3	837.6	521.6	866.5	458.1	10000	350
P1B-05	PI	L-C	25	242.8	445.0	241.2	482.2	481.8	10000	400
P1T-04	PI	L-C	25	203.7	368.0	203.0	382.7	481.8	10000	400
P1B-02	PI	L-C	290	554.5	664.1	557.8	691.7	295.8	Unaged	-
P1T-02	PI	L-C	290	630.6	733.8	646.2	771.2	295.8	Unaged	-
P1B-07	PI	L-C	290	400.7	529.9	389.2	559.7	315.8	10000	350
P1T-07	PI	L-C	290	542.3	663.3	526.4	691.7	315.8	10000	350
P1T-05	PI	L-C	290	293.7	451.7	298.6	470.0	324.2	10000	400
683-05B	68	H-H	25	334.4	552.8	334.4	572.9	400.2	Unaged	-
683-05T	68	H-H	25	282.6	485.5	243.2	504.1	400.2	Unaged	-
683-03V	68	V-H	25	312.1	526.0	294.7	546.3	400.2	Unaged	-
681-04B	68	H-H	25	798.0	1,037.7	832.0	1,075.5	444.3	2570	350
681-03B	68	H-H	25	408.4	648.6	412.6	673.6	467.8	2570	400
681-04T	68	H-H	25	294.5	467.7	283.1	486.1	471.7	2570	450
681-05B	68	H-H	25	293.0	532.9	290.1	551.9	471.7	2570	450
683-07T	68	H-H	290	753.4	783.0	740.5	795.3	282.2	Unaged	-
681-06T	68	H-H	290	446.1	592.8	459.4	617.0	318.8	2570	350
681-05T	68	H-H	290	335.3	464.9	323.4	487.9	312.2	2570	400
681-03T	68	H-H	290	312.5	454.9	316.6	475.1	338.5	2570	450
743-05B	74	H-H	25	610.3	795.4	573.4	826.1	405.1	Unaged	-
743-05T	74	H-H	25	577.1	710.6	584.4	746.0	405.1	Unaged	-
741-06T	74	H-H	25	692.1	852.6	725.0	895.6	410.5	2570	350
741-03B	74	H-H	25	389.0	556.5	374.0	578.7	429.6	2570	400
741-03T	74	H-H	25	238.8	404.0	210.2	418.0	438.5	2570	450
741-05B	74	H-H	25	312.9	502.9	308.6	514.8	438.5	2570	450

APPENDIX C: EXPERIMENTAL AND ESTIMATED CHARPY-IMPACT DATA FOR AGED CASS MATERIALS

The RT Charpy-impact energy of a specific heat of CASS materials as a function of aging time and temperature can be obtained from the estimated saturation RT Charpy-impact energy, C_{Vsat} , and the kinetics of embrittlement. The value of C_{Vsat} is estimated from Eqs. 18–26 described in Section 2.4.1 of the report and the kinetics of embrittlement are estimated from Eqs. 11–17 described in Section 2.3 of the report. Information regarding the initial RT Charpy-impact energy of the unaged material and the aging time and temperature is needed for these estimations. The RT Charpy-impact energy for a specific time and temperature condition is estimated in three steps. First, the aging time and temperature are converted to an equivalent value of Parameter P. Next, the tanh function of the term $[(P - \theta)/\alpha]$ is determined; two sets of tanh function values are obtained, one using the experimental value of θ and the second with an assumed value of 2.9 for θ . The C_V for the specific time and temperature is then calculated from Eq. 13 from Section 2.3 of the report. A single value of θ is assumed in this report. However, the existing data suggests that θ varies with the material composition.

A comparison of the estimated and experimental values of RT Charpy-impact energy for several heats of CF-3, CF-8, and CF-8M CASS materials are shown in Figs. C1 and C2. These figures are an updated version of Figs. 19 and 20 of NUREG/CR-4513 Rev. 1. The solid and dash lines represent the estimated values using, respectively, the experimental value or assumed value of θ .

The results indicate that the estimated values of RT C_{Vsat} are either accurate or slightly conservative for all grades and heats of CASS materials. The two exceptions are the static cast CF-3 Heat 47 and static cast CF-3M Heat FD. For these two heats, the estimated values are significantly higher than the experimental values. The reason for such a large difference for two heats out of more than 130 heats of materials is not known. The results also indicate that the estimates of the change in RT Charpy-impact energy for materials aged at low-temperature (i.e., 290-320°C) are in good agreement with the experimental values for most materials and are conservative for a few. The only exception is static cast CF-8M Heat 75. The estimates for high temperature (i.e., 350-400°C) aged materials show good agreement for most of the materials and are quite conservative for the rest. The exceptions are static cast CF-3 Heat 47 and the EPRI heat, centrifugally cast CF-8 Heat P1 and CF-8M heat P4, and the static cast CF-8M Heat FB. As discussed earlier, the agreement between the estimated and experimental values of RT Charpy-impact energy can be further improved by using a θ value that varies with the material composition and ferrite content, and activation energy for thermal embrittlement that varies with aging temperature.

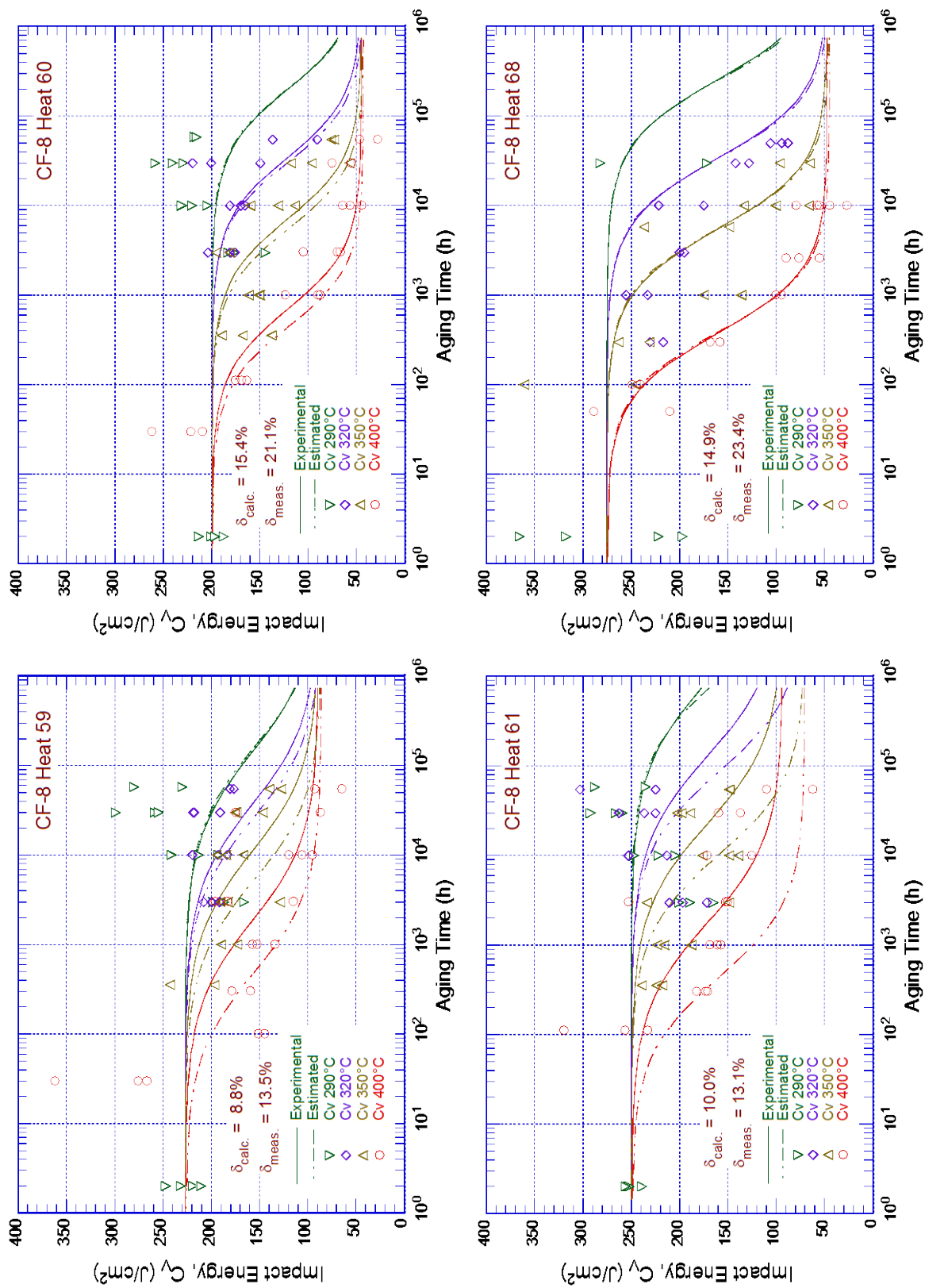


Figure C1. RT Charpy-impact energy for 16 ANL heats and 1 EPRI heat, observed experimentally (solid lines) and estimated (dashed lines) from the composition and initial impact energy of the materials aged at 290–400°C.

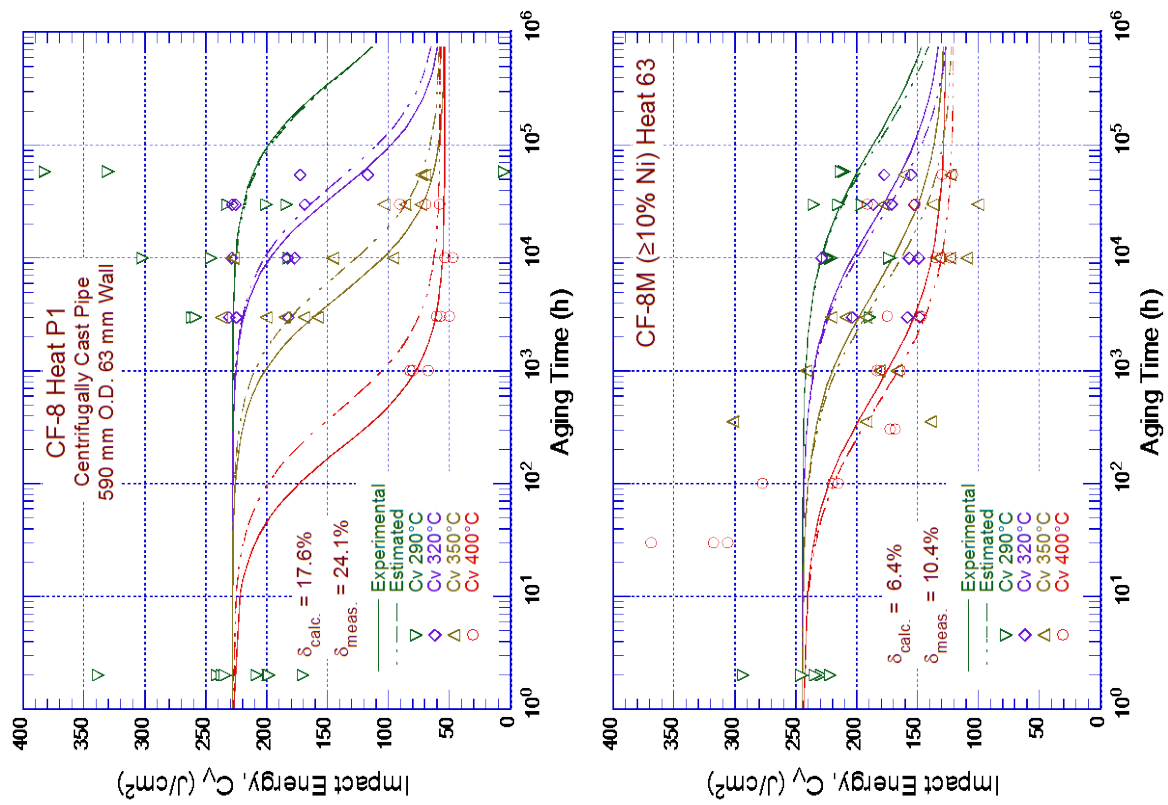
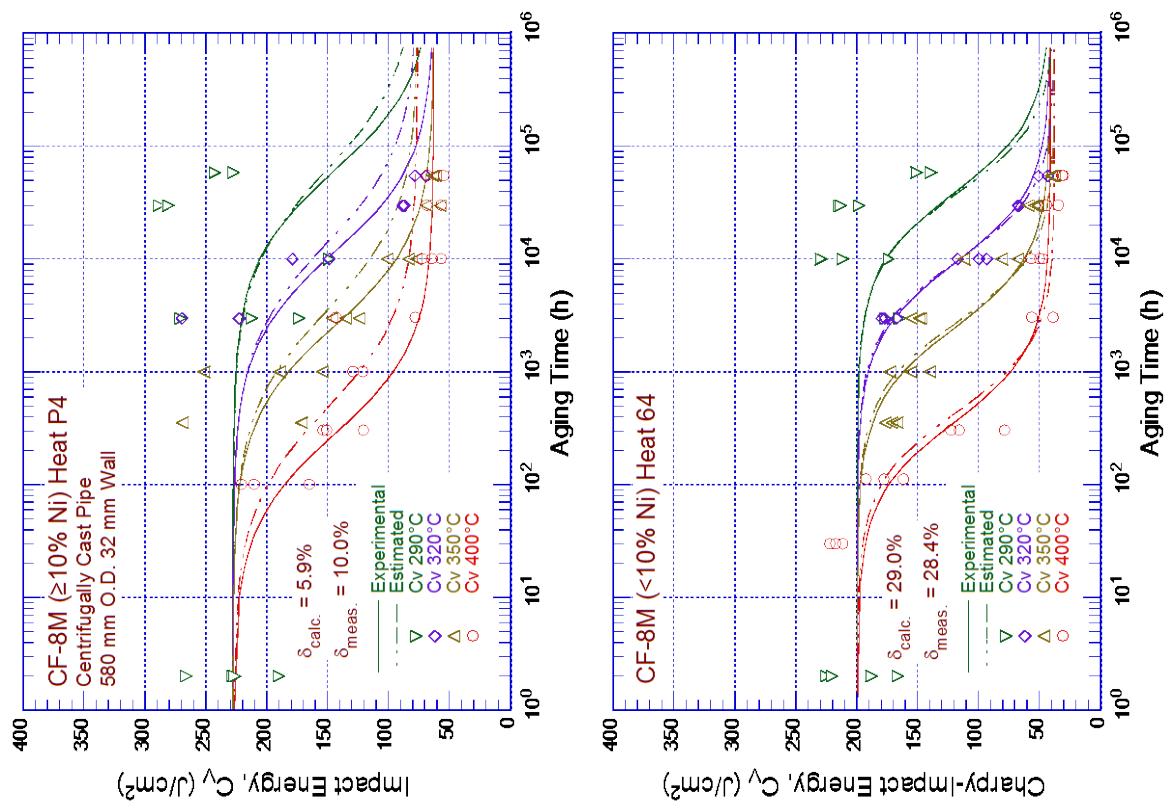


Figure C1. (Contd.)

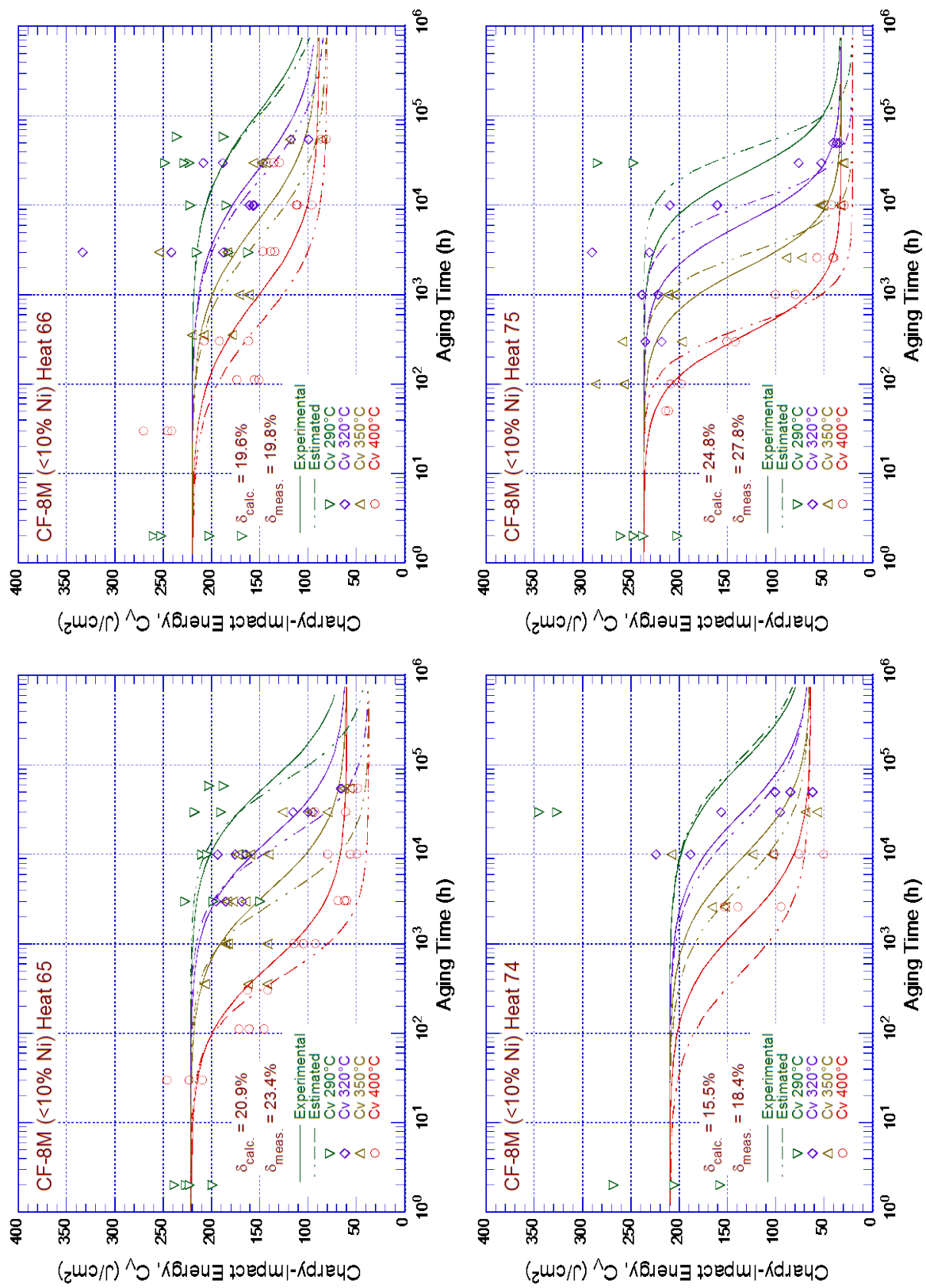


Figure C1. (Contd.)

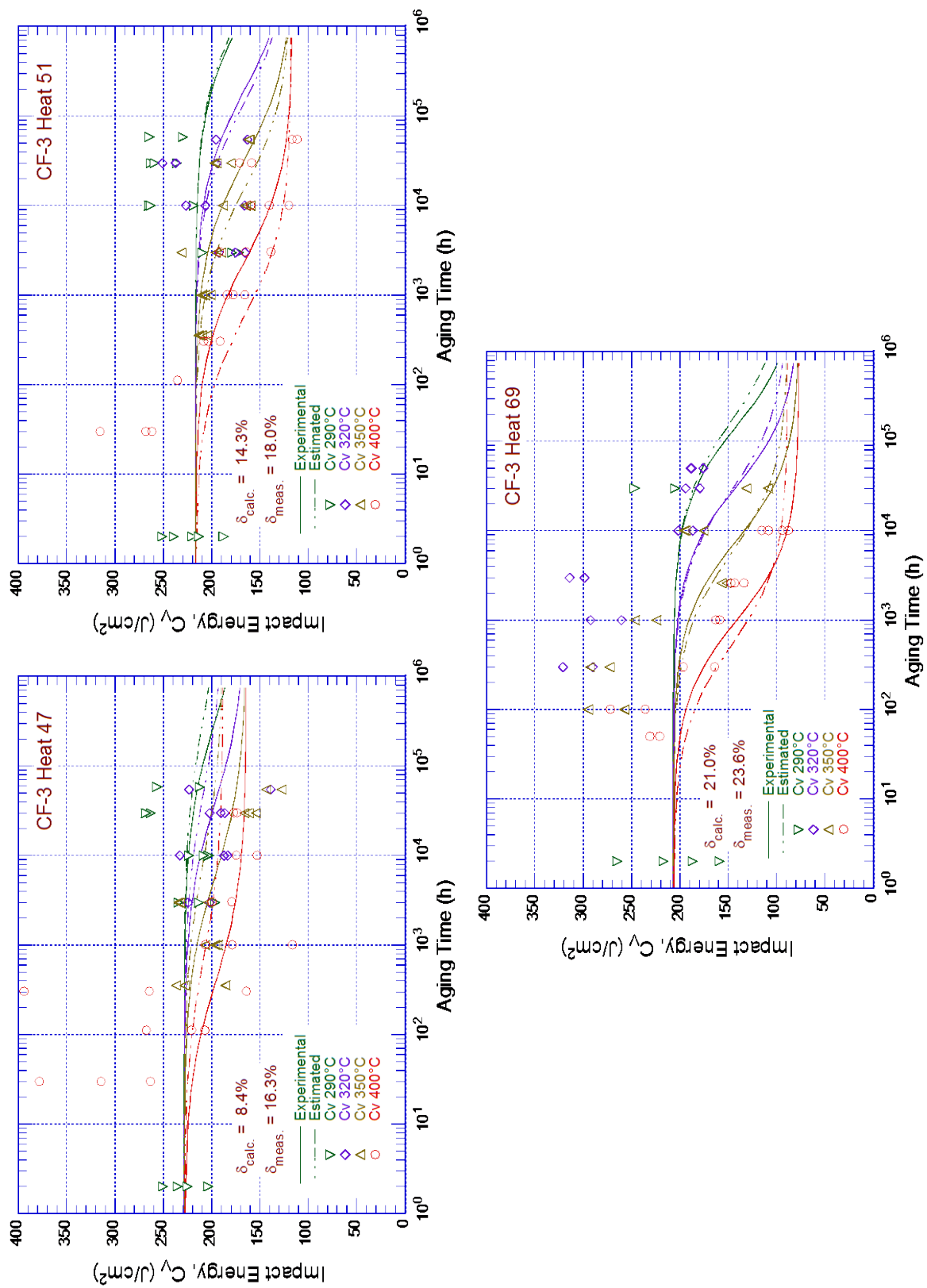


Figure C1. (Contd.)

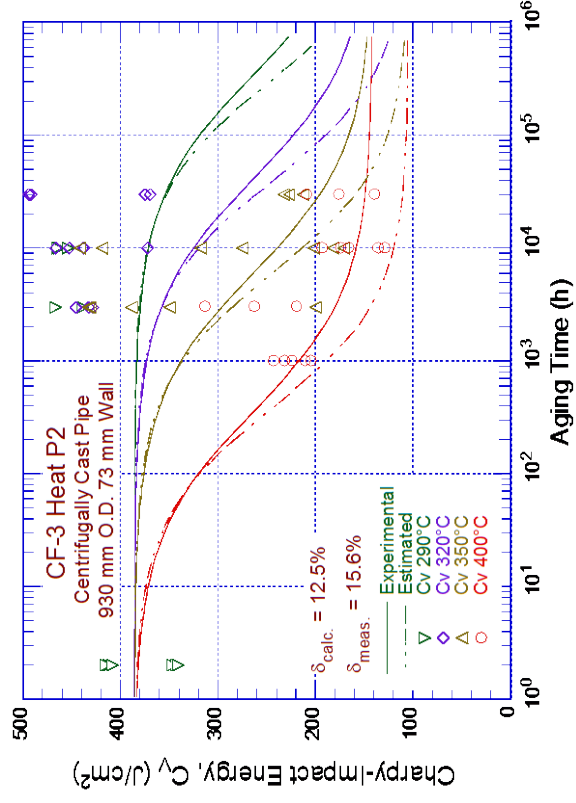
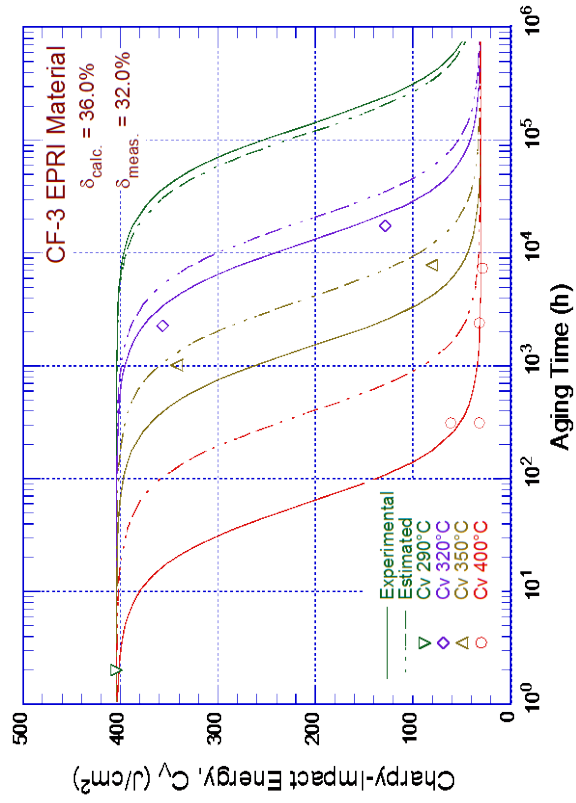


Figure C1. (Contd.)

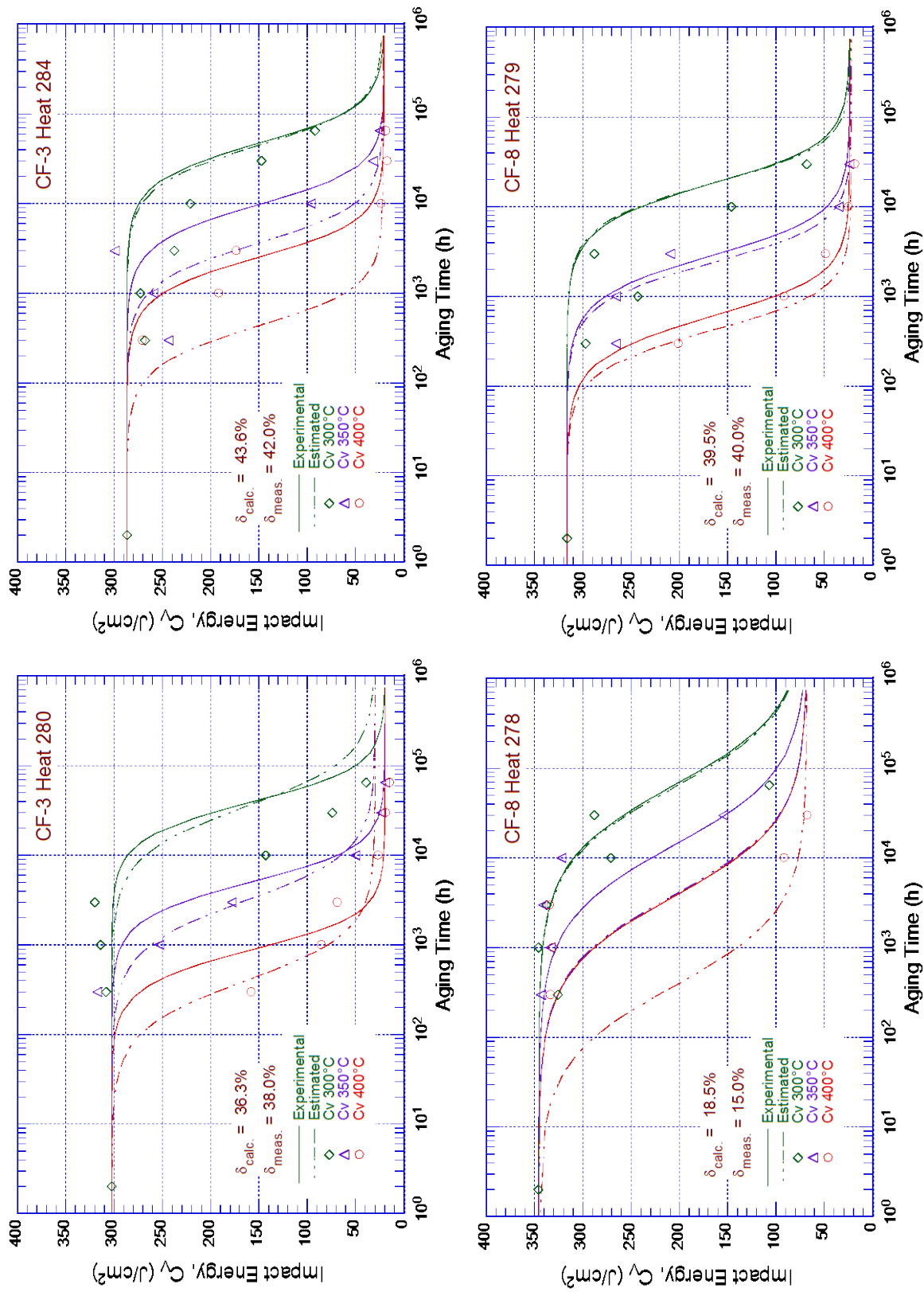


Figure C2. RT Charpy-impact energy for the GF, FRA and EdF heats, observed experimentally (solid lines) and estimated (dashed lines) from the composition and initial impact energy of the materials aged at 300–400°C.

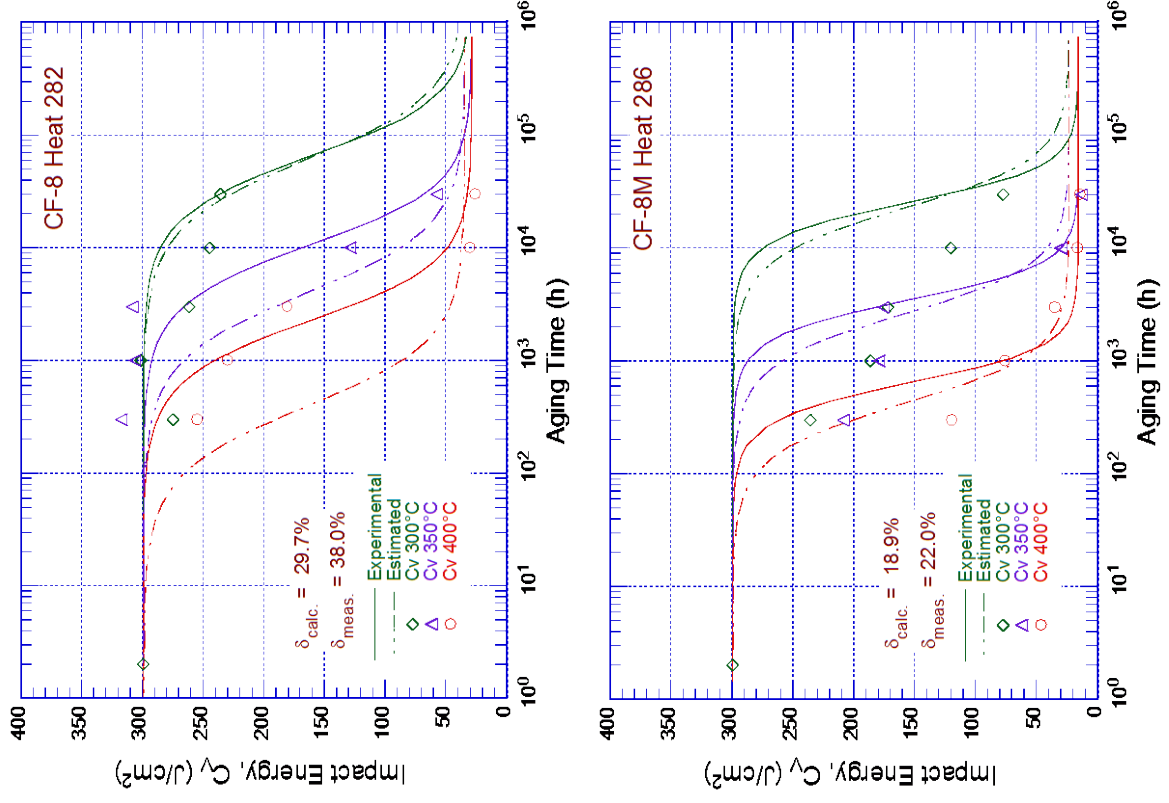
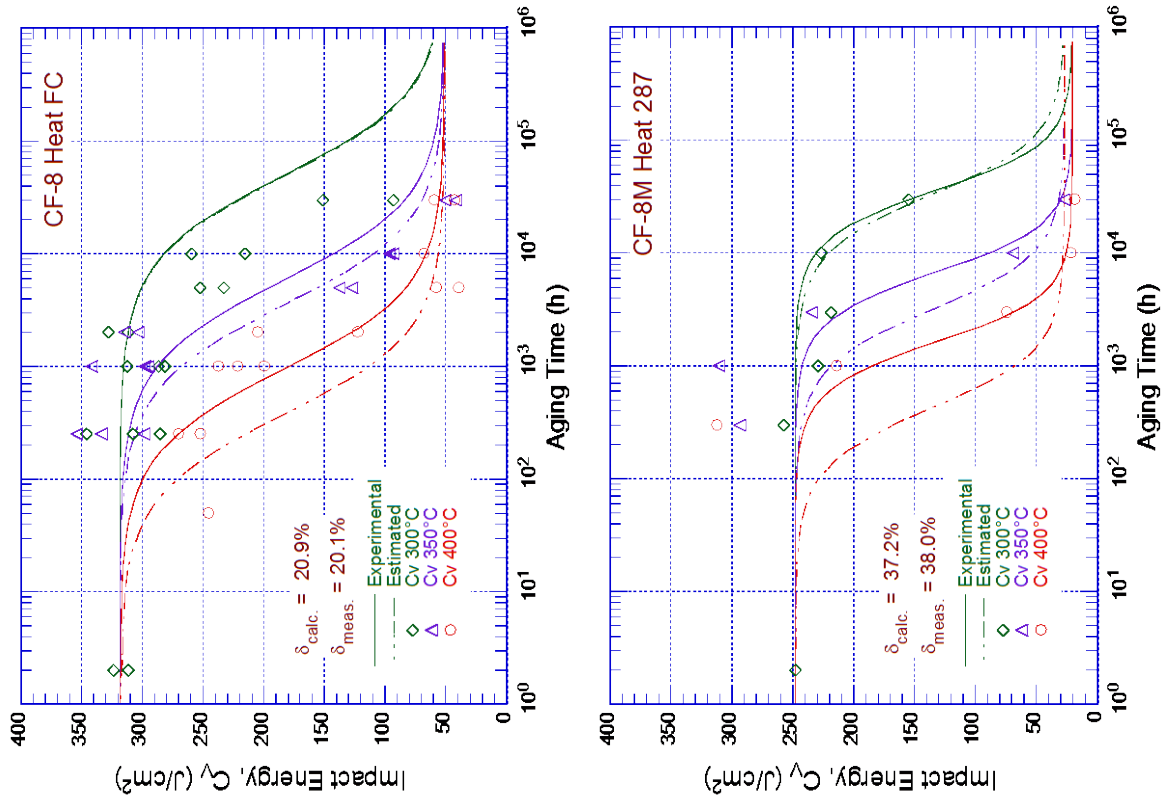


Figure C2. (Contd.)

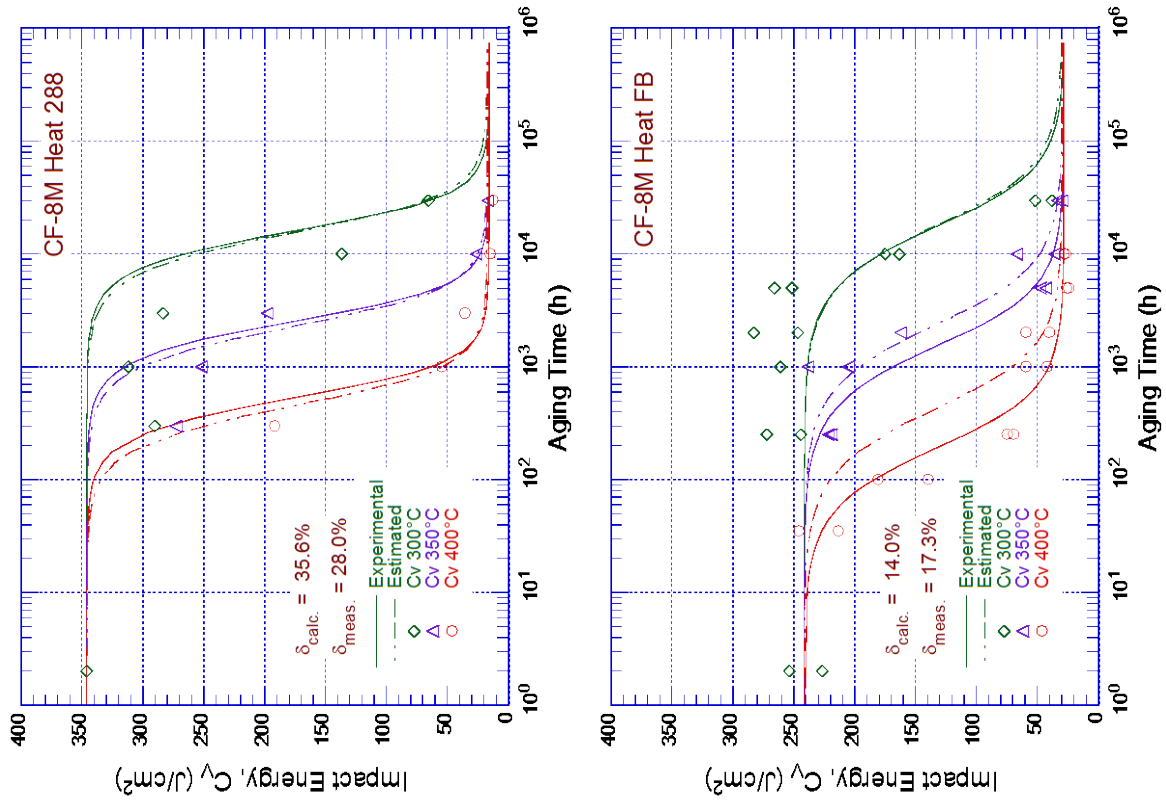
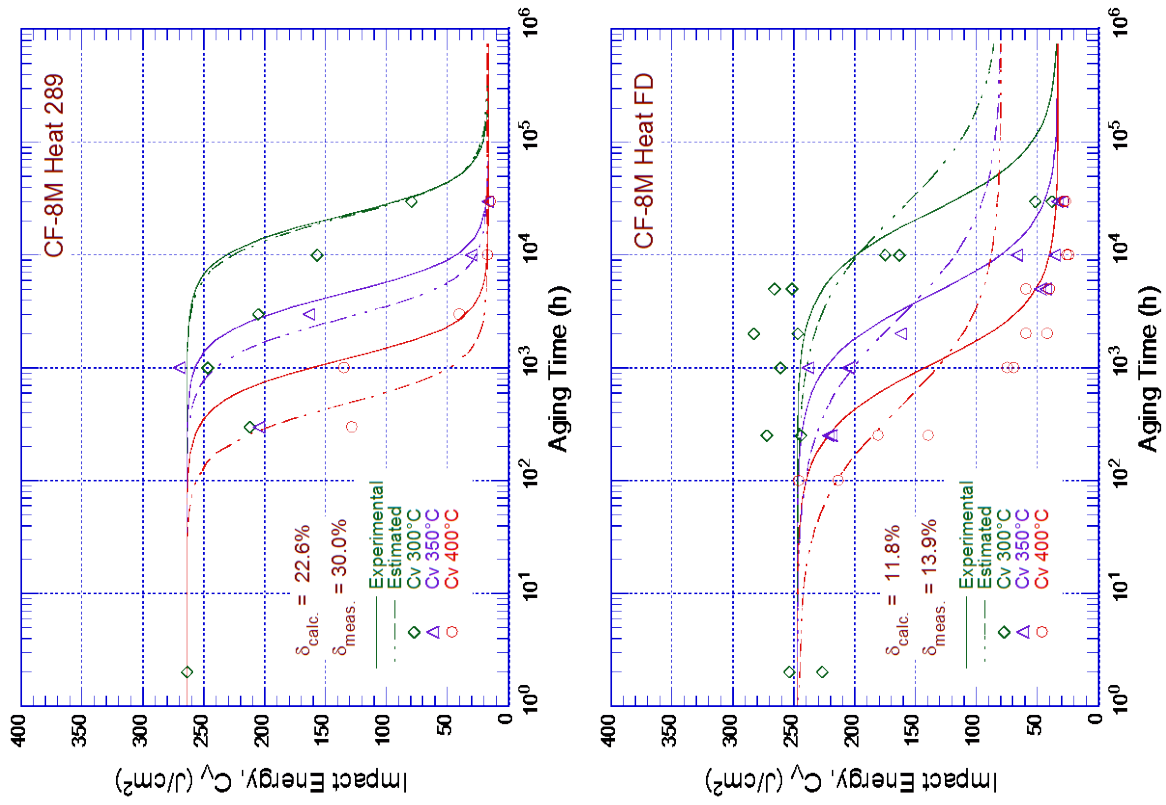


Figure C2. (Contd.)

APPENDIX D: REFERENCES

The source of the experimental data on Charpy-impact, tensile, and fracture toughness properties of unaged and aged but non-irradiated CASS materials are listed below according to the organization/institution where it was obtained.

Argonne National Laboratory, Argonne, IL, USA

- A1. Chopra, O.K., and A. Sather, Initial Assessment of the Mechanisms and Significance of Low-Temperature Embrittlement of Cast Stainless Steels in LWR Systems, NUREG/CR-5385, ANL-89/17, August 1990.
- A2. Chopra, O.K., A. Sather, and L.Y. Bush, "Long Term Embrittlement of Cast Stainless Steels in LWR Systems: Semiannual Report, April-September 1989," NUREG/CR-4744, Vol. 4, No. 2, ANL-90/49, June 1991.
- A3. Chopra, O.K., "Long-Term Embrittlement of Cast Duplex Stainless Steels in LWR Systems, Semiannual Report Oct. 1990 – March 1991, NUREG/CR-4744, Vol. 6, No. 1, ANL-91/22, August 1992.
- A4. Chopra, O.K., "Long-Term Embrittlement of Cast Duplex Stainless Steels in LWR Systems, Semiannual Report Oct. 1991 – March 1992, NUREG/CR-4744, Vol. 7, No. 1, ANL-92/42, May 1993.
- A5. Chopra, O.K., "Estimation of Fracture Toughness of Cast Stainless Steels during Thermal Aging in LWR Systems," NUREG/CR-4513, Rev. 1, ANL-93/22, August 1994.
- A6. Michaud, W.F., P.T. Toben, W.K. Soppet, and O.K. Chopra, "Tensile-Property Characterization of Thermally Aged Cast Stainless Steels," NUREG/CR-6142, ANL-93/35, February 1994.
- A7. Chopra, O.K. and W.J. Shack, "Mechanical Properties of Thermally Aged Cast Stainless Steels from Shippingport Reactor Components," NUREG/CR-6275, ANL-94/37, April 1995.

Central Electricity Generating Board, UK (The British Electricity Industry 1957-1990)

- A8. Pumphrey, P.H., and K.N. Akhurst, "Aging Kinetics of CF3 Cast Stainless Steel in Temperature Range 300-400°C," *Mater. Sci. Technol.* 6, 211–219, 1990.

Electricité de France (EdF), France

- A9. Bonnet, S., J. Bourgoïn, J. Champredonde, D. Guttman, and M. Guttman, "Relationship between Evolution of Mechanical Properties of Various Cast Duplex Stainless Steels and Metallurgical and Aging Parameters: An Outline of Current EDF Programmes," *Mater. Sci. Technol.* 6, 221–229, 1990.
- A10. Jayet-Gendrot, S., P. Ould, and T. Meylogan, "Fracture Toughness Assessment of In-Service Aged Primary Circuit Elbows Using Mini-CT Specimens Taken from Outer Skin," *Nucl. Eng. and Design* 184, 3–11, 1998.

- A11. Jayet-Gendrot, S., P. Ould, and P. Balladon, "Effect of Fabrication and Test Parameters on the Fracture Toughness of Aged Cast Duplex Stainless Steels," *Fonteveraud III*, Vol. 1, pp. 90–97, French Nuclear Energy Society, 1994.
- A12. Le Delliou, P., G. Bezdikian, P. Ould, and N. Safa, "Full-Scale Test on an Aged Cast Duplex Stainless Steel Lateral Connection: Results and Analysis," PVP2006-IVPVT-11-94005, in *Proc. of 2006 ASME Pressure Vessel and Piping Conf.*, July 23–27, 2006, Vancouver, BC, Canada, 2006.

Electric Power Research Institute

- A13. McConnell, P., and J.W. Sheckherd, "Fracture Toughness Characterization of Thermally Embrittled Cast Duplex Stainless Steel, Report NP-5439, Electric Power Research Institute, Palo Alto, CA, September 1987.

Framatome,

- A14. Meyzaud, Y., P. Ould, P. Balladon, M. Bethmont, and P. Soulat, "Tearing Resistance of Aged Cast Austenitic Stainless Steel," presented at *Int. Conf. on Thermal Reactor Safety (NUCSAFE 88)*, Avignon, France, October 1988.
- A15. Slama, G., P. Petrequin, and T. Mager, "Effect of Aging on Mechanical Properties of Austenitic Stainless Steel Castings and Welds," presented at SMIRT Post-Conference Seminar 6, *Assuring Structural Integrity of Steel Reactor Pressure Boundary Components*, Monterey, CA, Aug. 29–30, 1983.

General Electric Global Research, Niskayuna, NY, USA

- A16. Morra, M., "Program on Technology Innovation: Scoping Study of Low Temperature Crack Propagation for 182 Weld Metal in BWR Environments and for Cast Austenitic Stainless Steel in PWR Environments (Revision 1)," EPRI 1020957, Electric Power Research Institute, Palo Alto, CA, May 2010.

George Fischer, Switzerland

- A17. Trautwein, A., and W. Gysel, "Influence of Long Time Aging of CF-8 and CF-8M Cast Steel at Temperatures between 300 and 500°C on the Impact Toughness and the Structure Properties," in *Spectrum, Technische Mitteilungen aus dem+GF+Konzern*, No. 5, May 1981; also in *Stainless Steel Castings*, V.G. Behal and A.S. Melilli, eds., STP 756, pp. 165–189, 1982.

Japan Nuclear Energy Safety Organization, Japan

- A18. JNES (Japan Nuclear Energy Safety Organization), "Investigation Report on the Integrity of Thermally-Embrittled Cast Stainless Steel Pipe," JNES-SS-0602, Nuclear Energy System Safety Division, April 2006.

The Kansia Electric Power Co., Inc., Japan

- A19. Tanaka, T., S. Kawaguchi, N. Sakamoto, and K. Koyama, "Thermal Aging of Cast Duplex Stainless Steels," Joint ASME/JSME Pressure Vessel and Piping Conference – Structural Integrity of Pressure Vessels, Piping, and Components, Honolulu, HI, July 23–27, pp. 141–146, 1995.

Materials Engineering Associates, Inc.,

- A20. Hiser, A.L., "Tensile and J-R Curve Characterization of Thermally Aged Cast Stainless Steels," NUREG/CR-5024, MEA-2229, Nuclear Regulatory Commission, Washington DC, September 1988.

Mitsubishi Heavy Industry, Japan

- A21. Suzuki, I., M. Koyama, S. Kawaguchi, H. Mimaki, M. Akiyama, T. Okuba, Y. Mishima, and T.R. Mager, "Long Term Thermal Aging of Cast Duplex Stainless Steels," *Intl. Conf. on Nucl. Eng. (ICONE-4)*, American Society of Mechanical Engineers, New York, NY, pp. 253–257, 1996.
- A22. Kawaguchi, S., T. Nagasaki, and K. Koyama, "Prediction Method of Tensile Properties and Fracture Toughness of Thermally Aged Cast Duplex Stainless Steel Piping," *The 5th Intl. Conf. on Nucl. Eng. (ICONE-5)*, ICONE5-2379, May 26–30, American Society of Mechanical Engineers, New York, NY, 1997.

Ringhals Nuclear Power Plant, Sweden

- A23. Jansson, C., "Degradation of Cast Stainless Steel Elbows after 15 Years in Service," presented at *Fontevraud II Intl. Symp.*, Royal Abbey of Fontevraud, France, September 10–14, 1990.

The Welding Institute, UK

- A24. Hale, G.E., and S.J. Garwood, "The Effect of Aging on the Fracture Behaviour of Cast Stainless Steel and Weldments," *Mater. Sci. Technol.* 6, 230–235, 1990.

Westinghouse,

- A25. Landerman, E.I., and W.H. Bamford, "Fracture Toughness and Fatigue Characteristics of Centrifugally Cast Type 316 Stainless Steel Pipe after Simulated Thermal Service Conditions," in *Ductility and Toughness Considerations in Elevated-Temperature Service*, MPC 8, pp. 99–127, ASME, New York, NY, 1978.
- A26. Bamford, W. H., and A.J. Bush, "Fracture Behavior of Stainless Steels," *Elastic-Plastic Fracture*, STP-668, ASTM, Philadelphia, PA, pp. 553–577, 1979.

General References

- A27. Hiser, A.L., F.J. Loss, and B.H. Menke, "J-R Curve Characterization of Irradiated Low Upper Shelf Welds," NUREG/CR-3506, MEA-2028, Materials Engineering Associates Inc., April 1984.

- A28. Saxena, A., and S.J. Hudak, Jr., "Review and Extension of Compliance Information for Common crack Growth Specimen," *Int. J. Fracture* 5, Vol. 14, 453–468, 1978.
- A29. Loss, F.J., B.H. Menke, and R.A. Gray Jr., "Development of J-R Curve Procedures." *NRL-EPRI Research Program (RP 886-2). Evaluation and Prediction of Neutron Embrittlement in Reactor Pressure Vessel Materials Annual Progress Report for FY 1978*, J.R. Hawthorn. ed., NRL Report 8327, Naval Research Laboratory, August 1979.
- A30. Ernst, H.A. "Material Resistance and Instability Beyond J-Controlled Crack Growth," *Elastic-Plastic Fracture: Second Symp. Vol. I: Inelastic Crack Analysis*, ASTM STP 803, American Society for Testing and Materials, Philadelphia, PA, 1983.
- A31. Hutchinson, J.W., and P.C. Paris, "The Theory of Stability Analysis of J-Controlled Crack Growth," in *Elastic Plastic Fracture*, ASTM STP 668, pp. 37-64, American Society for Testing and Materials, Philadelphia, PA, 1983.

APPENDIX E: PREVIOUS DOCUMENTS OF SERIES

Initial Assessment of the Mechanisms and Significance of Low-Temperature Embrittlement of Cast Stainless Steels in LWR Systems, NUREG/CR-5385, ANL-89/17 (August 1990)

Estimation of Fracture Toughness of Cast Stainless Steels during Thermal Aging in LWR Systems, NUREG/CR-4513, ANL-90/42 (June 1991)

Estimation of Fracture Toughness of Cast Stainless Steels during Thermal Aging in LWR Systems, NUREG/CR-4513, Rev. 1, ANL-93/22 (August 1994)

Tensile-Property Characterization of Thermally Aged Cast Stainless Steels, NUREG/CR-6142, ANL-93/35 (February 1994)

Mechanical Properties of Thermally Aged Cast Stainless Steels from Shippingport Reactor Components, NUREG/CR-6275, ANL-94/37 (April 1995)

BIBLIOGRAPHIC DATA SHEET

(See instructions on the reverse)

1. REPORT NUMBER
(Assigned by NRC, Add Vol., Supp., Rev.,
and Addendum Numbers, if any.)
NUREG/CR-4513
Revision 2

2. TITLE AND SUBTITLE
Estimation of Fracture Toughness of Cast Stainless Steels during Thermal Aging in LWR
Systems

3. DATE REPORT PUBLISHED

MONTH	YEAR
May	2016

4. FIN OR GRANT NUMBER
NRC-HQ-60-13- D-0023

5. AUTHOR(S)
Omesh K. Chopra

6. TYPE OF REPORT
Technical

7. PERIOD COVERED (Inclusive Dates)

8. PERFORMING ORGANIZATION - NAME AND ADDRESS (If NRC, provide Division, Office or Region, U. S. Nuclear Regulatory Commission, and mailing address; if contractor, provide name and mailing address.)
Argonne National Laboratory,
9700 South Cass Avenue,
Argonne, IL 60439.

9. SPONSORING ORGANIZATION - NAME AND ADDRESS (If NRC, type "Same as above", if contractor, provide NRC Division, Office or Region, U. S. Nuclear Regulatory Commission, and mailing address.)
Division of Engineering,
Office of Nuclear Regulatory Research,
U. S. Nuclear Regulatory Commission,
Washington, DC 20555-0001.

10. SUPPLEMENTARY NOTES
Appajosula S. Rao, Contracting Officer Representative (COR)

11. ABSTRACT (200 words or less)
Cast austenitic stainless steel (CASS) materials are used extensively in reactor coolant pressure boundary systems as well as core support structure and reactor internals. However, they have a duplex structure consisting of austenite and ferrite phases and are susceptible to thermal aging embrittlement during reactor service. In addition, the prolonged exposure of these materials to neutron irradiation, changes their microstructure and microchemistry, which can degrade their fracture properties even further. This report is a revision of NUREG/CR-4513, Rev. 1, ANL-93/22 (August 1994); it revises the procedure and correlations used for predicting the change in fracture toughness and tensile properties of CASS components due to thermal aging during service in light water reactors at 280–330°C (535–625°F). The updated correlations are based on the current fracture toughness database for CASS materials aged up to 100,000 h at 290–350°C (554–633°F). The methodology for estimating fracture properties has been extended to cover CASS materials with a ferrite content of up to 40%. The fracture toughness J-R curve, tensile stress, and Charpy-impact energy of aged CASS materials are estimated from material composition. The mechanical properties of a specific CASS material are estimated from the extent and kinetics of thermal embrittlement. Embrittlement is characterized in terms of room-temperature Charpy-impact energy. The extent or degree of thermal embrittlement at “saturation” (i.e., the minimum impact energy that can be achieved for a material after long-term aging) is determined from the chemical composition of the material. A common “predicted lower-bound” J-R curve for CASS materials of unknown chemical composition is also defined for a given grade of steel, range of ferrite content, and temperature.

12. KEY WORDS/DESCRIPTORS (List words or phrases that will assist researchers in locating the report.)
Cast Stainless Steel (CASS), fracture properties, thermal embrittlement, thermal aging

13. AVAILABILITY STATEMENT
unlimited

14. SECURITY CLASSIFICATION
(This Page)
unclassified

(This Report)
unclassified

15. NUMBER OF PAGES

16. PRICE



Federal Recycling Program



**UNITED STATES
NUCLEAR REGULATORY COMMISSION**
WASHINGTON, DC 20555-0001

OFFICIAL BUSINESS



**NUREG/CR-4513
Revision 2**

**Estimation of Fracture Toughness of Cast Stainless Steels during Thermal
Aging in LWR Systems**

May 2016